UNIVERSITY OF OKLAHOMA

GRADUATE COLLEGE

PALEOENVIRONMENTAL INTERPRETATION OF THE WOODFORD SHALE, WYCHE FARM SHALE PIT, PONTOTOC COUNTY, ARKOMA BASIN, OKLAHOMA WITH PRIMARY FOCUS ON WATER COLUMN STRUCTURE

A THESIS

SUBMITTED TO THE GRADUATE FACULTY

in partial fulfillment of the requirements for the

Degree of

MASTER OF SCIENCE

By

GREGORY THOMAS CONNOCK
Norman, Oklahoma
2015

To Mandy, for her undying support, limitless patience and bountiful love... my dad and mom, who shaped me into the person I am today, supported me in every way imaginable and were always there for me, even if they were 2000 miles away... John, my brother and friend for life...and Uncle Bart, whose passion for science ignited my eternal flame of curiosity and inquisitiveness for the Universe and all its happenings

ACKNOWLEDGEMENTS

Many people over the past two years are responsible for the completion of my M.S. thesis, providing invaluable guidance and molding my academic career into something I am proud to have undertaken.

First, I would like to acknowledge Dr. Philp. I am indebted to him for introducing me to a field I did not anticipate coming to love. He has given me guidance, been a mentor and always welcomed my thoughts and ideas as if I was an esteemed organic geochemist like himself. Dr. Philp provided me with an excellent foundation of organic geochemistry, and I am forever grateful for his interest in me as a student, providing funding during my time at OU, and high expectations that helped me become the scientist I am today.

I would also like to thank Dr. Engel and Dr. Slatt for serving on my committee, providing great advice and suggestions for my thesis, and for taking the time to review this manuscript.

My appreciation extends to an extremely devoted post-doc, Dr. Thanh Nguyen, for his enthusiasm and passion for organic geochemistry has motivated me during this project and will continue to after I finish. The countless hours in lab helping me perfect laboratory techniques and multi-hour discussions on a wide range of topics have helped me immensely during this experience.

I want to thank Mr. Jon Allen for his tireless work maintaining all the laboratory instruments and ensuring everything was operating properly in lab. My gratitude goes out to all the members of the Organic Geochemistry Group, particularly Kirellos Sefein,

Damián Villalba, Dillon DeGarmo, Yue Ming Liu, Larry Hyde and everyone else that helped me during my time at OU.

I would like to extend my sincere gratitude to the entire Geology department at OU, helping me grow as a professional and individual. Additionally, I would like to thank the office staff on the 7th floor, especially Teresa Hackney, for her kindness and small talk always brightened up my day.

I am very appreciative of the constant support and interest shown by my family during this experience. I would not have reached this level of academia had it not been for them, and I am forever grateful.

Lastly, my fiancé, Mandy, has been amazing over these past two years. She always was understanding of my constant chatter about biomarkers and encouraged me every step of the way.

Thank you all for everything.

TABLE OF CONTENTS

LIST OF TABLES

LIST OF FIGURES

ABSTRACT

Twenty-nine Woodford Shale rock samples were acquired from the Wyche-1 core derived from the Wyche Farm Shale Pit, Pontotoc County, Arkoma Basin, Oklahoma. The TOC (total organic carbon) values ranged from 3.47-16.90 wt.%, with organic matter predominantly comprised of immature Type II kerogen with significant hydrocarbon potential. A sequence stratigraphic framework of the Wyche-1 core was integrated with biomarker data to reveal additional controls on compound distribution. Water column structure and chemistry were assessed following the identification of four novel C_{40} aromatic carotenoids; isorenieratane, paleorenieratane, renieratane and renierapurpurane, of which, only isorenieratane had been previously documented in the Woodford Shale. Paleorenieratane was measured via CSIA (compound specific isotope analysis) and was significantly enriched relative to algal biomass, ($\delta^{13}C$=-12‰ ± 1.5‰), suggesting carbon fixation via the reverse TCA (tricarboxylic acid) cycle utilized by the sulfur oxidizing bacteria *Chlorobiaceae*. The lower Woodford was characterized by isolated periods of photic zone euxinia, with the middle Woodford deposited during persistent photic zone euxinia as evinced by elevated concentrations of the C_{40} aromatic carotenoids. The upper member reflects 'normal' marine conditions characterized by bottom water anoxia. Periods of euxinia correlate with 3rd order HSTs (highstand systems tract) in the lower and middle Woodford, which likely caused cessation of upwelling and decreased circulation and vertical mixing leading to a stagnant, poorly ventilated water column permitting the development of a thick, well-defined chemocline in a restricted shelf environment.

CHAPTER I

1. Introduction

1.1. Evolution of Hydrocarbon Applications and the Role of the Woodford Shale

Hydrocarbons, the simplest organic molecules on Earth, comprise an industry worth approximately $1.5 trillion dollars[1] and deeply rooted in the fabric of human society. During the Neolithic period, hydrocarbons were used in the form of natural-occurring bitumen to provide seals for containers and jars (Binet et al., 2002; Connan, 1999), while today petroleum products find applications in almost all facets of everyday life. Despite the numerous complaints from environmentalists concerning global warming, hydrocarbons serve too integral of a role to simply vanish due to the advent of alternative propulsion mechanisms. In addition to fuel: adhesives, sealants, paints and plastics are formed from these organic compounds, which also are commonly used in crop protection, mining operations, industrial processes and household products (Moore et al., 2008). The wide-ranging applications of hydrocarbons may not have been realized had it not been for the efforts of Edwin Drake, who in 1859 drilled the first economically successful well in Titusville, PA (Binet et al., 2002). This resource was quickly relied upon as the heart of transportation was born and rapidly evolved in the late 1800s as both the internal combustion engine and internal compression engines were invented by Charles Duryea and Rudolf Diesel respectively (Smil, 1994; Totten, 2007). The success of any resource is reliant upon demand and adequate technology to

[1] Derived from a ~$50/barrel and total world production of 92.94 million barrels/day (http://www.eia.gov/forecasts/steo/report/global_oil.cfm;

recover and process the resource in an economic fashion. It was a similar set of circumstances which allowed for the 'shale revolution' to be realized in the United States of America.

The increased pursuit of shale as a source of oil was sparked and facilitated by the onset of several technological advancements in resource extraction methods. Shales are often laterally extensive units typified by unique physiochemical, geochemical and stratigraphic features while lacking thickness, porosity and permeability. This has led to the term 'unconventional' reservoir (although shales may also serve as the source and seal of hydrocarbons) relative to other lithologies, such as sandstones or carbonates termed 'conventional' reservoirs (Jarvie et al., 2007). According to Cardott (2005), an unconventional resource is defined as requiring elevated financial investment and heightened technological prowess to retrieve relative to conventional resources. Gas shales, oil shales, coal bed methane, methane clathrates, tight sands/carbonates and tar sands may be classified as unconventional (Cardott, 2005). The commercial application of horizontal wells integrated with hydraulic fracturing at multiple stages permitted the exploitation of unconventional reservoirs in an economical manner. In addition, the onset of 3D-seismic and microseismic fracture mapping spawned incredibly detailed subsurface mosaics assisting the navigation of the well bore, especially in faulted formations, such as the Woodford Shale in the Arkoma Basin (Aguilera et al., 2014).

The Woodford Shale was initially drilled in 1939 in southeastern Oklahoma and had only been completed 22 times by 2004 (Vulgamore et al., 2007). However, the success of the Barnett Shale in Texas reignited interest in the Woodford Shale, leading to 143 completions by late 2006 and nearly 350 wells drilled in 2007 (Haines, 2006;

Cardott, 2007; Vulgamore et al., 2007). The proliferation of advanced drilling techniques allowed the potential of this unconventional resource to be realized, earning the formation recognition as a member of the 'magnificent seven' (Figure 1; Cardott, 2012). The shale play has been estimated to contain 4 trillion ft^3 of gas (Kulkarni, 2011) and 250 million bbl of crude oil (Comer, 2005), as well as possessing favorable lithologic characteristics for hydrocarbon extraction, such as elevated amounts of biogenic silica and organic matter (Kirkland et al., 1992; Kuuskraa et al., 2011; Romero and Philp, 2012; Molinares, 2013). According to conodant biostratigraphy, the lithologic and geochemical features of the Woodford Shale are a result of 29 My. of deposition (Johnson et al., 1985), with other research concluding 33 My. were required (392-359 Mya.) to form this multi-billion dollar resource (Paxton et al., 2006). In that time span, the depositional environment likely experienced significant variations in redox conditions, sediment input, water chemistry, light intensity and many other components essential to support life. Fluctuations in the biological community will be recorded during deposition and reflected in the organic geochemical composition determined via biomarker analyses, yielding an enhanced conception of the paleoenvironment responsible for the formation of the Woodford Shale.

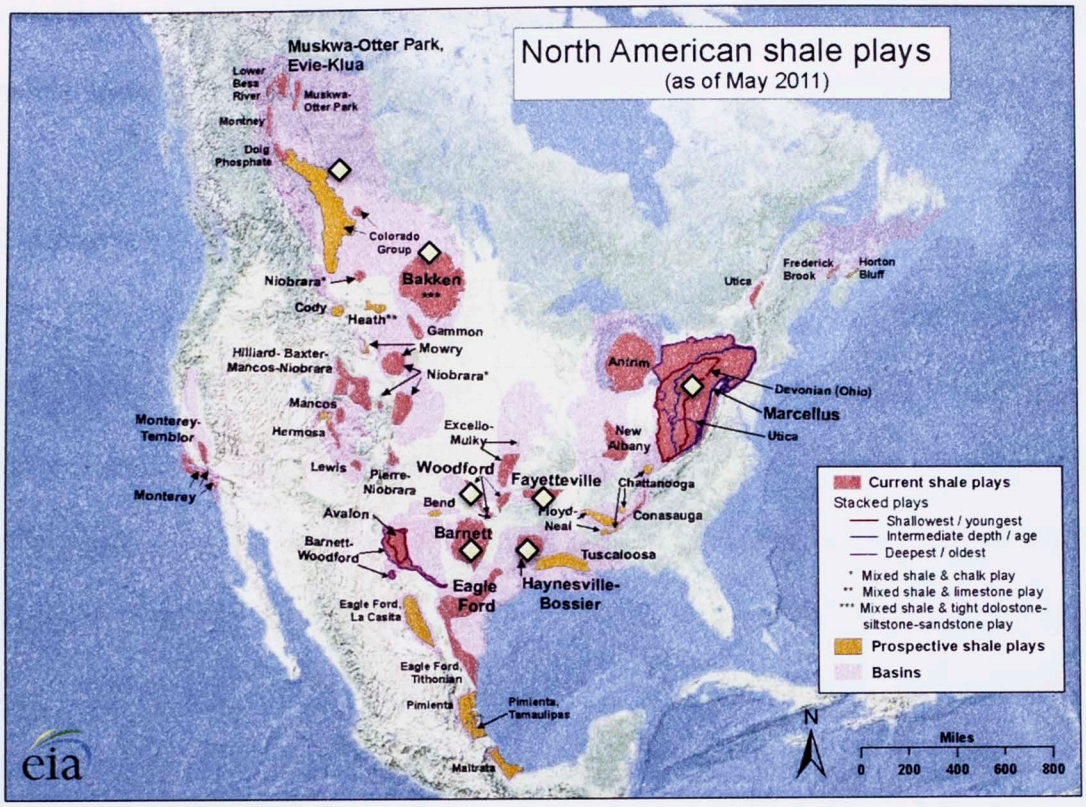

Figure 1. Primary North American shale plays as of 2011. Yellow diamonds indicate 'magnificent seven' (modified from EIA 2011).

This study utilizes an integrated geological and geochemical approach to enhance current knowledge of the depositional environment responsible for the formation of the Woodford Shale in the Arkoma basin. Previous work by Romero (2008) provided preliminary geochemical data, with significant findings related to potential photic zone euxinia during deposition. This has been elaborated upon here, and will be one of the primary foci throughout this discussion. Molinares (2013) outlines a detailed stratigraphic framework, accompanied by descriptions of nine different lithofacies in addition to palynological and trace element data. This project benefits from these previous studies by enabling highly specific geochemical analysis to

be assisted and constrained by sequence stratigraphy, permitting the construction of sensible applications and conclusions of both known and novel biomarkers.

1.2. Biomarkers

Biomarkers are molecular fossils preserved in sediments and hydrocarbon accumulations. It was the discovery of biologically derived organic components in preserved organic matter by Treibs (1936) which created the foundation of biomarker geochemistry. Following this breakthrough, scientists continued to push the limits of biomarker research in an attempt to understand ancient environments lacking 'observable' fossils (Eglinton and Calvin, 1967), eventually leading to the recognition of the biological composition of petroleum (Whitehead, 1973). These defunctionalized biological lipids, in the form of carbon skeletons, are capable of being traced to precursor structures derived from a specific suite of organisms or a vast array of biological ancestors (See Figure 2 for illustration of this principle; Philp, 1986; Volkman, 2005; Brocks and Summons, 2013). Essentially, these compounds represent a record of life from the time period in which they were synthesized. Life itself evolves and dies, flourishes and dwindles, and is inherently limited to external conditions governing its existence (i.e. environments). Therefore, biomarkers reflect temporal (Holba et al., 1998; Moldowan, 2000; Rampen et al., 2007) and environmental changes in the geologic past (Sinninghe Damste et al., 2003; Brocks and Schaeffer, 2008; Sousa Junior et al., 2013), but also possess the capacity to serve as proxies for determining the levels of thermal stress (Seifert et al., 1983; Mackenzie, 1984; Kolaczkowska et al., 1990) and biodegradation (of oils; Seifert and Moldowan, 1979; Moldowan and

McCaffrey, 1995; Mille et al., 1998) a source rock has experienced. These biogeochemical fossils can potentially highlight variations in the biosphere (e.g. biodiversity, trophic organizations), chemosphere (elemental cycling, temperature fluctuations, water column chemistry), geosphere (tectonic movement, clathrate destabilization) and indirectly the atmosphere (volcanic eruptions, methane injections). The following discussion will utilize one of the most implemented biomarker classes, hopanes (e.g. Philp and Mansuy, 1997; Peters et al., 2005), as well as a detailed discussion of the relatively underutilized C_{40} aromatic carotenoids (Summons and Powell, 1987; Requejo et al., 1992) to underline the value of these incredibly diverse compounds in paleoenvironmental reconstructions.

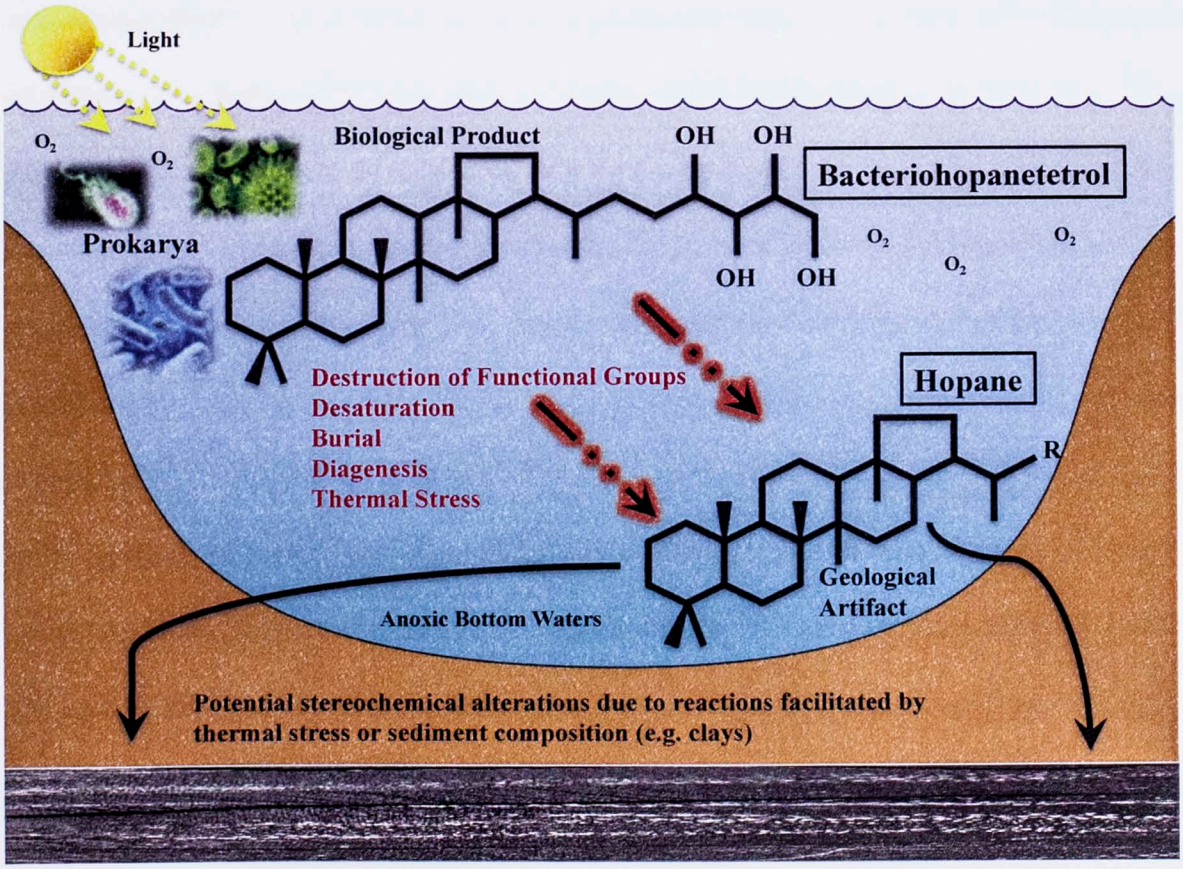

Figure 2. The biomarker theory, illustrated by the generation of bacteriohopanetetrol (biological) by prokarya and its subsequent degradation to a commonly used class of biomarkers, the hopanoids (geological).

Hopanoids represent 'the most abundant natural products on Earth' (Ourisson and Albrecht, 1992), demonstrated by the omnipresent temporal and spatial distribution characteristic of this compound class (Rohmer et al., 1979). Hopanes are most often associated with aerobic prokaryotic bacteria (Rohmer et al., 1984; Farrimond et al., 1998), derived from three derivatives of 3-deoxyhopane; diploterol (C_{30} derivatives), bacteriohopanetetrol (C_{35} derivatives), and bacteriohopanetetrol methylated at various positions of the ring system (Rohmer et al., 1979). The nonelongated hopanoids occur in less abundance (diploterol) relative to elongated hopanoids (bacteriohopanetetrol (BHP) in bacteria, which possess a polar side chain connected to C-29 of the hopane structure (Ourisson et al., 1987; Kannenberg and Paralla, 1999). These compounds, specifically BHPs, are postulated to serve analogous roles in bacterial cell membranes as sterols in eukarya (Ourisson and Albrecht, 1992; Kannenberg and Paralla, 1999). Due to the simple nature of prokarya, cell membranes serve a vital role in maintaining the organism's metabolic function throughout its existence, regulating the flux of components in and out of the cell itself. In order to fulfill this role properly cell membranes must be flexible, which is a function of fluidity. The fluidity of the membrane is dependent upon hopanoids to govern the flexibility. The BHPs tend to be more structurally sound than glycerol lipids, allowing for membrane fluidity to be kept within an ideal range for a variety of cell processes (Kannanberg and Paralla, 1999). The role of BHPs as membrane alterants assists in explaining their ubiquitous character in sediments and source rocks.

Hopanoids serve an equally integral role to the geochemist as in nature for bacteria. A great deal regarding depositional environments, redox conditions, maturity

and age can be discerned from observation of the distributions and presence of these compounds. For example, norhopane (C_{29}) predominance relative to the hopane (C_{30}) is typically a diagnostic marker for carbonate/evaporitic/marl environments. Low C_{24}/C_{23} and C_{26}/C_{25} accompanied by high C_{22}/C_{21} cheilanthane ratios and $C_{31}R/H$ (C_{31} homohopane/C_{30} hopane) ratios will further support this environmental interpretation (Peters et al., 2005). Elevated levels of gammacerane often suggest a stratified water column during the time of deposition, and in Type I kerogens or lacustrine source rocks may indicate hypersalinity (ten Haven et al., 1985; ten Haven et al., 1988; Sinninghe Damste et al., 1995b). Redox conditions can be illuminated through applications of the C_{35} homohopane index ($C_{35}S/C_{34}S$), which is extremely sensitive to oxic environments. In the presence of oxygen (high Eh), the side chain of the C_{35} homohopane will be rapidly degraded, resulting in lower abundances of this compound relative to the C_{34} homohopane (Peters and Moldowan, 1991). Simply the observation of certain compounds in a sample affords knowledge regarding the age in which these environmental conditions persisted. Recall, biomarkers are products of life and as a result reflect the extinction and proliferation of particular species. For example, oleanane (another pentacyclic triterpenoid) is a product of angiosperms (Whitehead, 1974; Grantham et al., 1983; ten Haven and Rullkötter, 1988), which did not prosper until the Cretaceous based on fossil evidence (Ge Sun et al., 1998). Therefore, source rocks containing oleanane may be inferred to be of Cretaceous age or younger although exceptions do exist (Peters et al., 2005). In addition to these environmental and temporal clues, the isomerization effects with increasing levels of thermal stress provide valuable insight to the level of maturity reached by a particular source rock. The S and

R isomers of the homohopanes undergo systematic changes as a result of increased thermal stress, with the less stable R isomer converting to the S stereoisomer. This ratio will eventually equilibrate (Figure 3) at the early oil window (0.55 for C_{31} homohopane isomers; Zumberge, 1987), but is useful in assessing the likelihood a source rock has reached thermal maturity (Seifert and Moldowan, 1980). Despite the diverse range of hopanoid applications to understanding paleoenvironments, these compounds lack a specific source (Brocks and Summons, 2013). Linkage to prokarya is not definitive relative to more powerful biomarkers with proven derivations from an explicit organism.

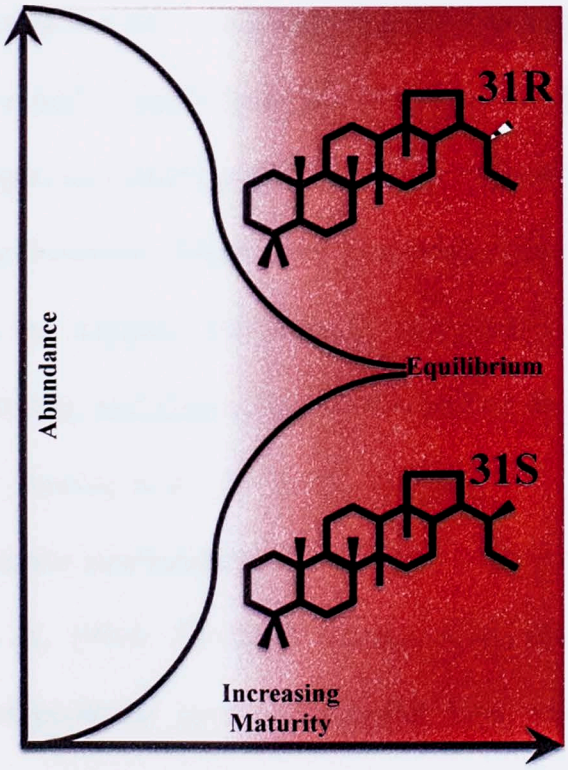

Figure 3. Stereochemical isomerization of the C_{31} homohopane S and R as a function of increasing thermal maturity.

The carotenoids in the scope of this study are derived from a clear source, organisms from the family *Chlorobiaceae* in the phylum *Chlorobi* (Imhoff, 1995). *Chlorobiaceae*, or green sulfur bacteria (GSB), are obligately phototrophic and obligately autotrophic anerobes (Frigaard and Dahl, 2008). The GSB exclusively produce the carotenoids isorenieratene (**I**; brown strain; see Appendix **I** for structures), chlorobactene (**VI**; green strain), paleorenieratane[2] (**II**; origin unknown) and possess a unique organelle, the chlorosome, composed of bacteriochlorophyll (BChl) *c, d,* and *e* (Hartgers et al., 1994; Bryant and Dahl, 2006; Frigaard and Dahl, 2008). Chlorosomes assist in the proliferation of GSB at extreme depths of the photic zone (>100m) characterized by low light intensities (Pfennig and Truper, 1989; Overmann et al., 1992), proving essential to GSB which lack flagella (characteristic of *Chromatiaceae,* purple sulfur bacteria) and instead utilize gas vacuoles for propulsion (Gorlenko, 1988). The GSB, capable light scavengers, require H_2S as an electron donor in addition to light to sustain metabolic function (Truper and Genovese, 1968; van Gemerden, 1983). Carbon is fixed via the reductive tricarboxylic acid cycle (i.e. reverse TCA, reverse citric acid cycle; Sirevag and Ormerod, 1970) resulting in biomass enriched in ^{13}C (Quandt et al., 1977; Sirevag et al., 1977; van der Meer et al., 2001) which retains this isotopic signature despite structural changes during burial and diagenesis (Grice et al., 1996; Koopmans et al., 1996b; Sinninghe Damste et al., 2001). This isotopic effect assists correlation of particular biomarkers to the GSB, which is beneficial from a paleoenvironmental perspective due to the specific and unique requirements of GSB.

[2] Paleorenieratane is a diaryl isoprenoid with a unique 2,3,6/3,4,5 substitution pattern proposed to be biosynthesized by *Chlorobiaceae* (Hartgers et al., 1994; French et al., 2015).

From an interpretative viewpoint, GSB provide powerful insight into the conditions characterizing past environments due to the unique settings in which they require to live and thrive. Euxinia (i.e. photic zone euxinia/photic zone anoxia; PZE) refers to invasion of the photic zone by hydrogen sulfide (H_2S), which causes anoxia throughout the affected section of the photic zone (Figure 4; Grice et al., 2005; Tulipani et al., 2015). Euxinic waters are a rarity in the modern world, with the Black Sea serving as a prime example (e.g. Overmann et al., 1992). The GSB require anoxia, being strict anerobes, as well as H_2S and light, as outlined previously. Therefore, the observation of carotenoids, such as isorenieratene and its derivatives, in sediments or source rocks provides substantial evidence PZE persisted in the geologic past.

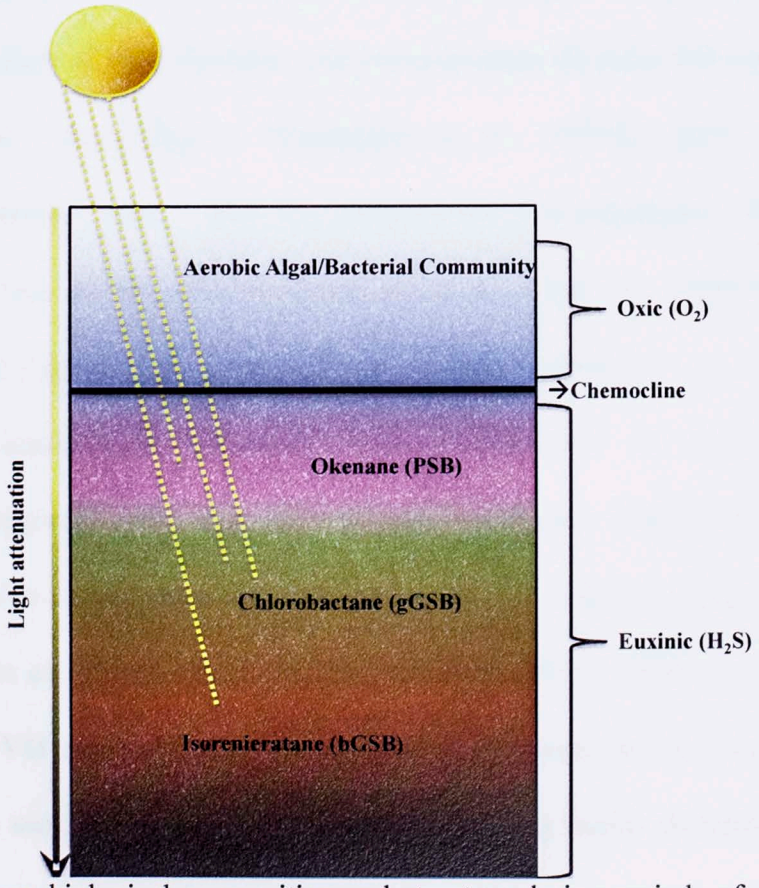

Figure 4. Water column biological composition and structure during periods of euxinia, i.e. invasion of photic zone by H_2S.

Isorenieratane (**I;** see Appendix **I** for structures) is produced via the hydrogenation of double bonds along the isorenieratene chain (Schaefle et al., 1977). Isorenieratene is a carotenoid specifically synthesized by the brown strains of GSB, or those comprising the deepest regions of the photic zone in euxinic systems. Occurrence of the biomarker, isorenieratane (**I**), in source rocks or oils will therefore suggest conditions existed which supported communities of GSB, yielding information regarding the position/depth of the chemocline, redox conditions and microbial community composition (Brocks and Schaeffer, 2008; French et al., 2015). This compound is particularly easy to identify due to both its prominent molecular ion (M^+=546) and the broadened peaks which typify many of the C_{40} compounds due to decomposition during analysis. If isorenieratane (**I**) is absent, it is important to realize other diagenetic products of isorenieratene and isorenieratane (**I**) exist that can evidence photic zone euxinia. According to Koopmans et al., (1996b), three groups of isorenieratene derivatives exist. The C_{40} compounds (isorenieratane) formed via hydrogenation reactions of the isorenieratene chain, C_{33} and C_{32} compounds from toluene/m-xylene expulsion of isorenieratene before reduction, or short-chain compounds (aryl isoprenoids) generated from continuation of diagenesis and catagenesis which degrades high molecular weight compounds (HMW) produced by inter- intramolecular reactions between isorenieratene and reduced inorganic sulfide species (Koopmans et al., 1996b; Sinninghe Damste et al., 2001). However, utilization of aryl isoprenoids (**VII** and **VIII**) as indicators of euxinia must be executed correctly, as these compounds may be formed from β-carotene during burial (Koopmans et al.,

1996a). Unlike isorenieratane[3](**I**), occurrence of aryl isoprenoids (**VII** and **VIII**) alone is not sufficient to claim euxinic conditions persisted. The aromatic carotenoids, such as isorenieratene, are restricted to a specific phylum whereas β-carotene, in contrast, is widespread throughout the entire plant kingdom (Liaeen-Jensen, 1979). In order to apply aryl isoprenoids (**VII** and **VIII**) in a similar fashion as isorenieratane (**I**) if it is absent, compound specific isotopic analysis (CSIA) must be conducted to ensure ^{13}C is enriched relative to algal biomass (Summons and Powell, 1987; Hartgers et al., 1994; Clifford et al., 1998). If this enrichment is not observed and β-carotane (**X**) is present, then it is likely aryl isoprenoids do not signify derivation solely from the isotopically enriched *Chlorobiaceae*.

The practice of biomarker application is limited, despite the vast array of information biomarkers provide. Increasing levels of thermal stress may degrade particular compounds relative to more stable structures (e.g. carotenoids degrade at T_{max} of 445°C, gammacerane and phytane are susceptible to thermal alteration as well), and microbial activity in the subsurface will selectively remove biomarkers in oils as biodegradation progressively increases (Peters et al., 2005). Also, biomarkers are inherently flawed due to preservation biases. Biomarkers are assumed to reflect the biosphere of the depositional environment, but it is possible other organisms existed whose biological products were unable to be preserved in the sediments. This means interpretation is tentative with respect to these limitations, requiring additional proxy

[3] Isorenieratane may be formed from β-carotene, in principal, if both cyclohexenyl functional groups are aromatized.

data to infer paleoenvironments. Geology, specifically sequence stratigraphy, can assist geochemical analyses through reinforcement of proxy observation and interpretations.

1.3. Sequence Stratigraphy

The cycles associated with accommodation are a vital element in the science of sequence stratigraphy. Sequence stratigraphy, according to Slatt (2013), "is the study of sedimentary rock relationships within a chronostratigraphic or geologic-time framework." This science hinges on the observation that the oceans rise and fall cyclically through geologic time (Slatt and Rodriguez, 2012). As a result of this rise and fall in sea level, sequences are generated by a diverse set of processes that occur over differing ranges of time. First order cycles, such as the global supercontinent cycle, can last 200-400 Myr., while fourth-order and fifth order cycles, which include Milankovitch cycles, are the shortest lived at 0.01-2 Myr (Eriksson et al., 2013). Table 1 highlights these stratigraphic cycles and the reasons these processes materialize.

Table 1. Various cycles operating over different temporal periods which influence the geologic record preserved today (Eriksson et al., 2013).

Sequence type	Duration (Myr)	Other terminology
A. Global supercontinent cycle	200–400	First-order cycle (Vail et al., 1977)
B. Cycles generated by continental-scale mantle thermal processes (dynamic topography), and by plate kinematics, including:	10–100	Second-order cycle (Vail et al., 1977), supercycle (Vail et al., 1977), sequence (Sloss, 1963).
1. Eustatic cycles induced by volume changes in global mid-oceanic spreading centres.		
2. Regional cycles of basement movement induced by extensional downwarp and crustal loading.		
C. Regional to local cycles of basement movement caused by regional plate kinematics, including changes in intraplate-stress regime.	0.01–10	3rd- to 5th order cycles (Vail et al., 1977). 3rd-order cycles also termed megacyclothem (Heckel, 1986), or mesothem (Ramsbottom, 1979).
D. Global cycles generated by orbital forcing, including glacio-eustasy, productivity cycles, etc.	0.01–2	4th- and 5th-order cycles (Vail et al., 1977). Milankovitch cycles, cyclothem (Wanless and Weller, 1932), major and minor cycles (Heckel, 1986).

An important cycle to realize in order to understand the context of this paper pertains to fluctuations in sea level. In general, a sea level cycle is composed of a fall, turnaround and rising stage. For a visual representation of the following information,

see Figure 5 below. During the falling and turnaround stage, the LST (Lowstand Systems Tract) is deposited. The rising stage results in two deposits, known as the TST (Transgressive Systems Tract) formed during the abrupt and fast rise in sea level, and the HST (Highstand Systems Tract) that is deposited at a later stage in sea level rise which is less rapid than that seen during the TST (Slatt and Rodriguez, 2012). The condensed section (usually a shale) and mfs (maximum flooding surface)[4] are typically the most organic-rich, since they represent periods of geologic time in which fine-grained sediment is deposited over a laterally extensive marine section. Through recognition of various system tracts within a core, gamma ray log, SP log, or other sources, the characteristics and processes responsible for creating the shale can be better understood (Figure 6). Also, sequence stratigraphy allows for correlation from a regional scale to a local scale and the focus to settle on the most conducive sections of the formation for hydrocarbon generation and storage.

[4] The mfs represents the maximum landward extent of the shoreline and is deposited atop the CS (Slatt, 2013).

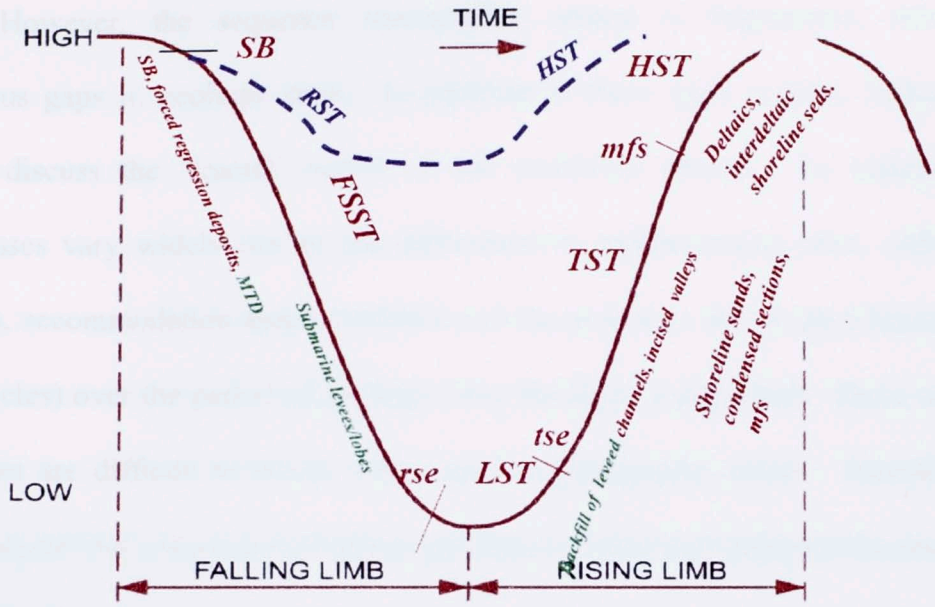

Figure 5. A visual representation of the sea level cyclicity recorded in shales, permitting sequence stratigraphic frameworks to be developed (Slatt, 2013).

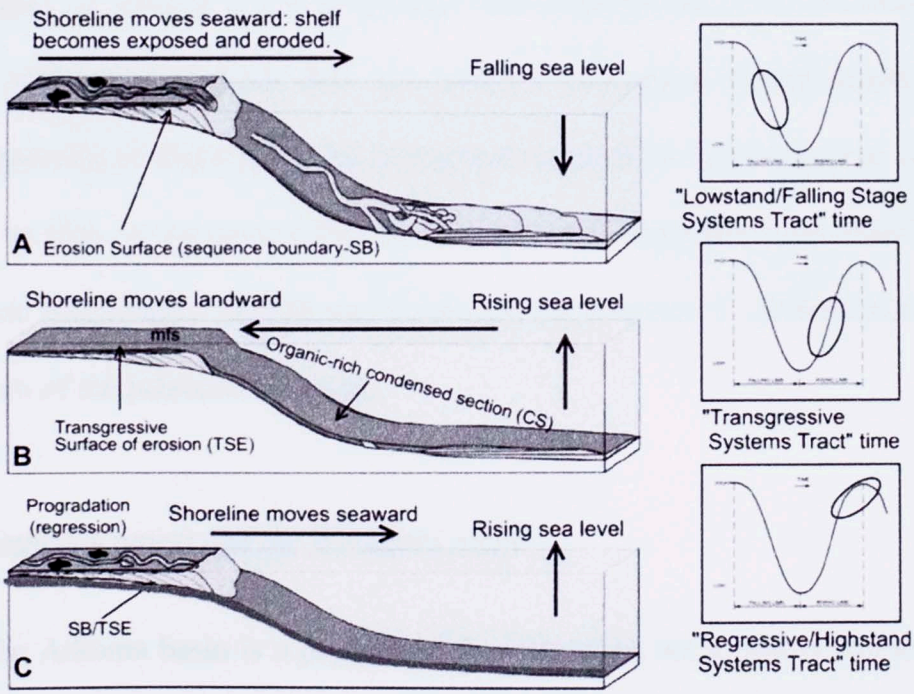

Figure 6. Geomorphic and depositional mechanisms as a function of fluctuating eustatic conditions (Slatt and Rodriguez, 2012).

However, the sequence stratigraphic record is fragmented, littered with numerous gaps in geologic time. In addition to these gaps in time, Eriksson et al. (2013) discuss the 'fractal' nature of the preserved record. To elaborate, layer thicknesses vary widely due to the differences in sedimentation rates, sedimentation hiatuses, accommodation space available and the processes active (as a function of sea level cycles) over the period of geologic time the layer is deposited. These small-scale variations are difficult to detect with sequence stratigraphy alone. Therefore, it has been realized that integration of select geochemical data may enhance the resolution of understanding ancient environments, as integration of geologic data will assist interpretations founded on biomarker proxies. Organic geochemistry utilizes a variety of techniques in order to better understand various properties of an oil, source rock or reservoir rock. Geochemical data can enhance assessment of stratigraphic models, either supporting or challenging the interpretations derived from sequence stratigraphy alone. The data, as mentioned before, may provide information not observed on the larger-scale stratigraphic models and it also has the potential to produce more accurate illustrations of the paleoenvironment.

1.4. Geological Context and the Woodford Shale

The Arkoma basin is a product of the Oklahoma basin, one of the three[5] major tectonic provinces that prevailed during Paleozoic time. Thin marine shales interbedded shallow marine carbonates and sands that composed the expansive, shelf-like region the

[5] In addition to the Oklahoma basin, the Oklahoma aulacogen to the south and Ouachita trough comprise the three major tectonic provinces (Johnson and Cardott, 1992; Northcutt et al., 2001).

Oklahoma basin covered (Johnson et al., 1989). The early Devonian deposits were then uplifted, vulnerable to erosion forming the pre-Woodford-Chattanooga unconformity which was subsequently overlain with organic-rich silts and clays in the late Middle to early Late Devonian. The hemipelagic rain (Slatt, 2013) and hyperpycnal flows were sourced by a westward advancing Woodford-Chattanooga sea characterized by anoxic bottom waters and clouded by high rates of sedimentation that populated most of the basin. In the Pennsylvanian, the Oklahoma basin was dissected by piercing uplifted crustal units to form the clearly bounded marine basins observed today (Figure 7 and 8; Johnson and Cardott,, 1992).

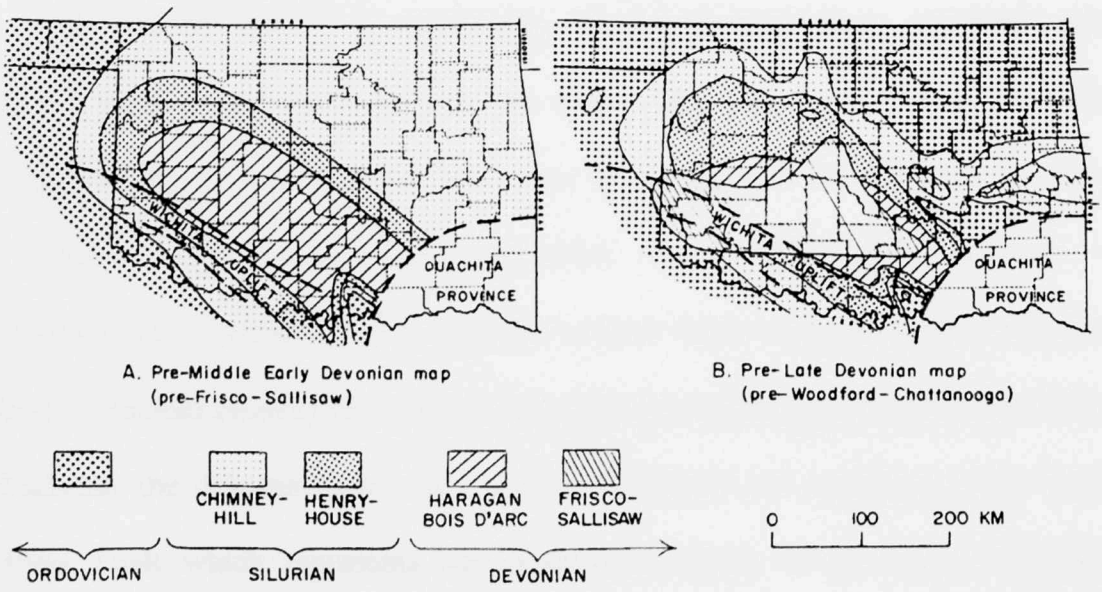

Figure 7. Paleogeographic maps of strata distribution in Oklahoma basin post-uplift in early Devonian (left) and Late Devonian (right) (Northcutt et al., 2001).

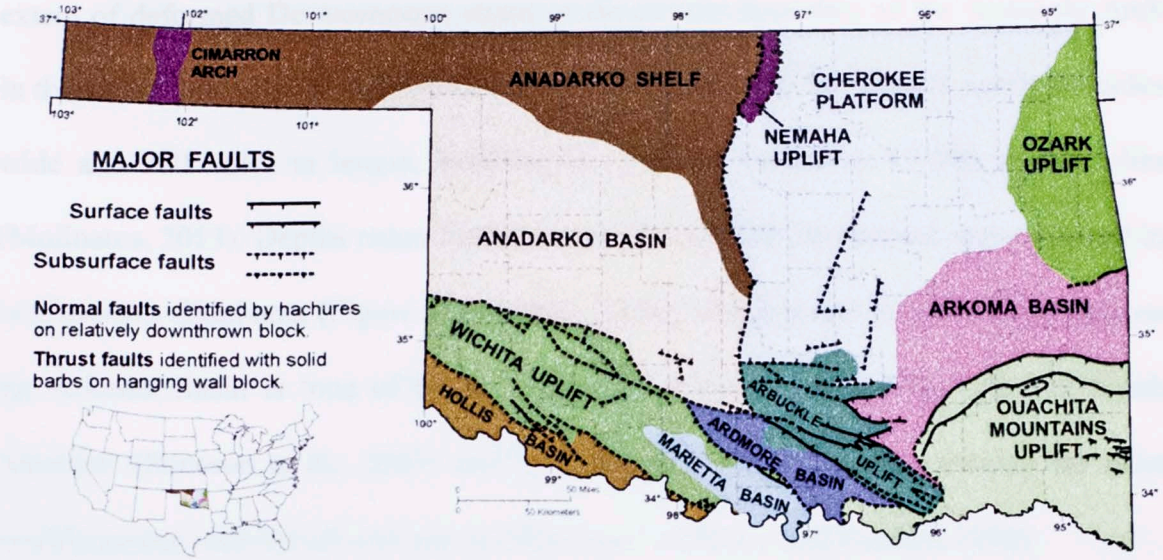

Figure 8. Primary geological provinces of Oklahoma in the modern (Cardott, 2012).

The Arkoma basin is a structurally warped foreland basin populated with significant quantities of hydrocarbons that strikes east-west as it extends from the Mississippi River and Reelfoot Rift fault zone in Arkansas to the Anadarko-Ardmore basin systems in the southeast of Oklahoma. The complexity of the basin is demonstrated by a multitude of high-angle normal faults formed syndepositionally during the Ouachita orogeny (Pennsylvanian) and acute angled basal detachment faults. In Oklahoma, the Arkoma basin and Ouachita Mountains are separated by the listric Chocktaw Fault which represents the easternmost thrust of the frontal Ouachita Mountains (Sahai and Çemen, 2008). This marks the southeastern boundary of the basin, with the southwestern extent terminating in the Arbuckle Mountains. The basin is separated from the Ozark Uplift by the south-dipping Mulberry Fault in the northeast, with the northwestern boundary slightly less apparent being marked by separation of folded and unfolded strata. In the west, the basin is bounded by either the western

extent of deformed Desmoinesian strata or the eastern boundary of the Seminole Arch in the subsurface (Figure 8; Suneson et al., 2005). Overall, the basin is nearly 40 miles wide and 260 miles in length, resulting in coverage of almost 13,000 square miles (Molinares, 2013). Depths range from 2 km to 10 km, with the deepest regions found in southeastern Oklahoma (Figure 9; Coleman, 2004), which is one of the primary reasons the Arkoma Basin is 'one of the most prolific petroleum-producing basins in North America' (Suneson et al., 2005) and '[the Woodford Shale] unquestionably the most prolific source rock for oil and gas in Oklahoma' (Johnson and Cardott, 1992).

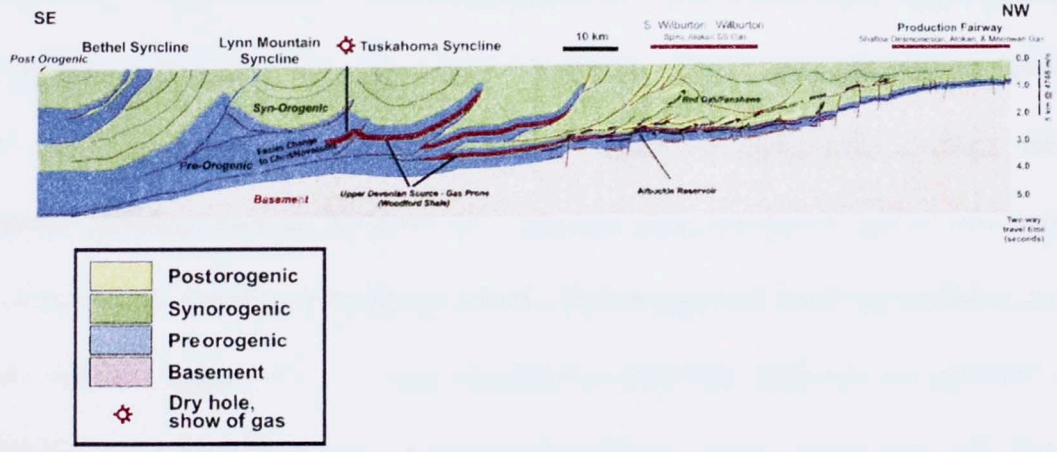

Figure 9. Simplified cross section of the Arkoma Basin in eastern Oklahoma displaying post-orogenic, syn-orogenic, preo-rogenenic and basement features. (Coleman, 2004).

The Woodford Shale was unconformably (SB/TSE; sequence boundary/transgressive surface of erosion) deposited during the Late Devonian-Early Mississippian (Frasnian-Tournaisian) on the shelf carbonates (Hunton Group) in the form of dark, fine-grained siliciclastic hemipelagic rain and/or hyperpycnites and turbidites (Slatt et al., 2012). In the Arkoma basin, the Woodford Shale ranges from 100-250 feet thick, thinning to less than 50 feet where it outcrops in the Lawrence

Uplift (Molinares, 2013). The Lawrence Uplift was one of the crustal blocks uplifted during Pennsylvania time, and is bounded in the north by the Ahloso Fault and to the south by the Stonewall Fault. Uplift was more severe in the west relative to the east, resulting in older strata being exposed in the west (Slatt et al., 2012). The Woodford Shale in the region of the study area, the Lawrence Uplift (see Figure 10), is approximately 120 feet thick and is described as a competent dark brown-black shale characterized by significant amounts of organic matter (Barrick et al., 1990; Over, 1992; Romero and Philp, 2012). Previous work on the study area yielded total organic carbon (TOC) values of 5.01-14.81% dominated by Type II and some Type I kerogen, with vitrinite reflectance (R_o) values of 0.29-0.63%. These data indicate an excellent source rock composed of marine organic matter of marginally mature nature. Biomarker proxies, such as pristane (Pr), phytane (Ph), sterane (C_{30}/C_{29}) and terpane (C_{23}Tri/H) values signify a mixture of marine and terrigenous input deposited in anoxic bottom waters (Figure 11). It was interpreted from the presence of gammacerane (**XXXVII**; see Appendix **I** for structures) that highly saline conditions and density-driven water column stratification persisted throughout deposition as well as periodic euxinia inferred from aryl isoprenoids (**VII** and **VIII**; Romero, 2008; Romero and Philp, 2012; Slatt and Rodriguez, 2012). These environmental conditions stabilized and fluctuated with depth (i.e. time) but, before further discussion of geochemical and geological data, a brief aside regarding Woodford terminology will be undertaken.

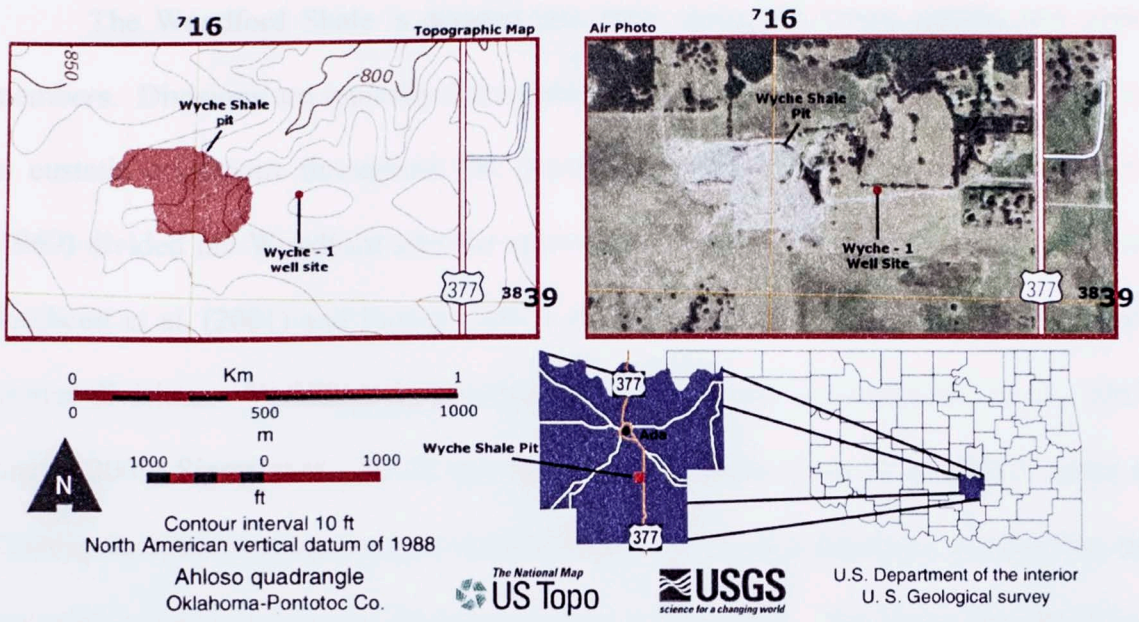

Figure 10. Location of study area, the Lawrence Uplift in the Arkoma Basin, Pontotoc County, OK. (Turner et al., 2015, modified from USGS 2012).

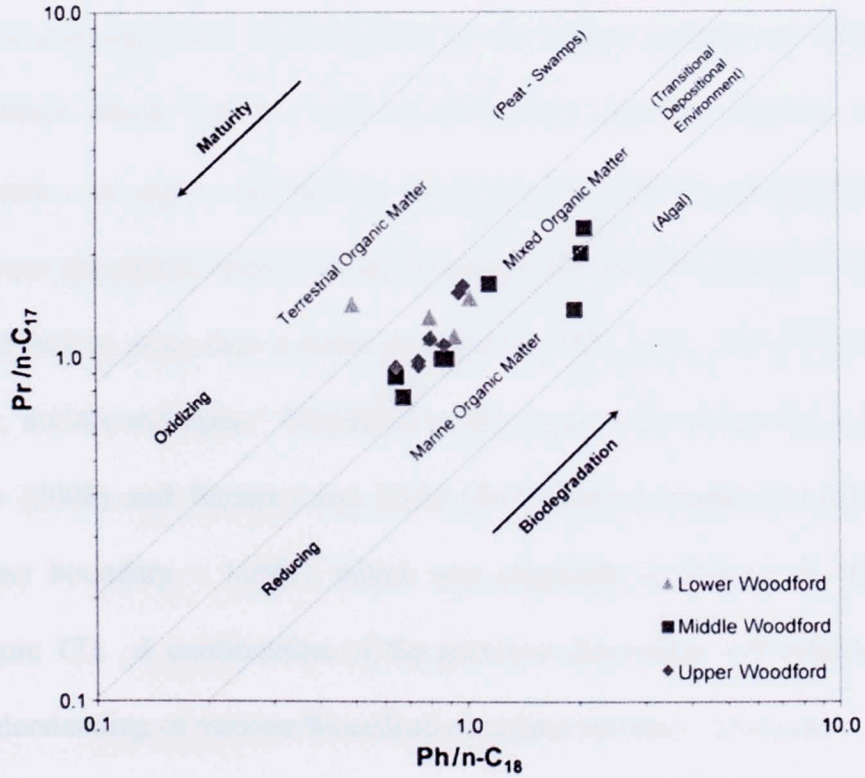

Figure 11. Redox and organic matter type as a function of specific isoprenoid ratios (Romero and Philp, 2012).

The Woodford Shale is divided into three units: the lower, middle and upper members. Divisions are typically formulated using some proxy to determine variations in eustatic conditions throughout the deposition of the shale. For example, Urban (1960) divided the Woodford into the appropriate members via palynological data and Northcutt et al. (2001) and Paxton (2007) utilized gamma ray spectroscopy to achieve similar divisions. Variations in geomechanical properties (Abousleiman et al., 2007; Portas, 2009; Sierra et al., 2010) and lithologic attributes (Slatt et al., 2012) assist in dividing the shale into appropriate members as well. From a lithologic perspective, the following is applicable to the Woodford Shale in this study. The lower Woodford is a black-gray, fissile, siliceous/carbonaceous shale and is distinguished from the upper by the absence of phosphate nodules and occurrence of silicified logs. The middle Woodford is a pyritic, black shale typified by the highest gamma ray values due to its organic-richness which may be a product of the late Devonian oceanic anoxic events (OAE). Lastly, the upper member is a quartzose, phosphatic gray-black shale littered with numerous phosphate lenses and phosphate/pyrite nodules ranging in size from less than half an inch to more than a meter in diameter (Slatt et al., 2012; Molinares, 2013). The 'lower, middle and upper' Woodford in this study is discussed in the same context as Romero (2008) and Romero and Philp (2012) (lower-middle boundary = 185ft., middle-upper boundary = 118ft.), which was originally developed by Buckner et al. (2009; Figure 12). A continuation of the previous discussion will resume now that a general understanding of various Woodford members has been achieved.

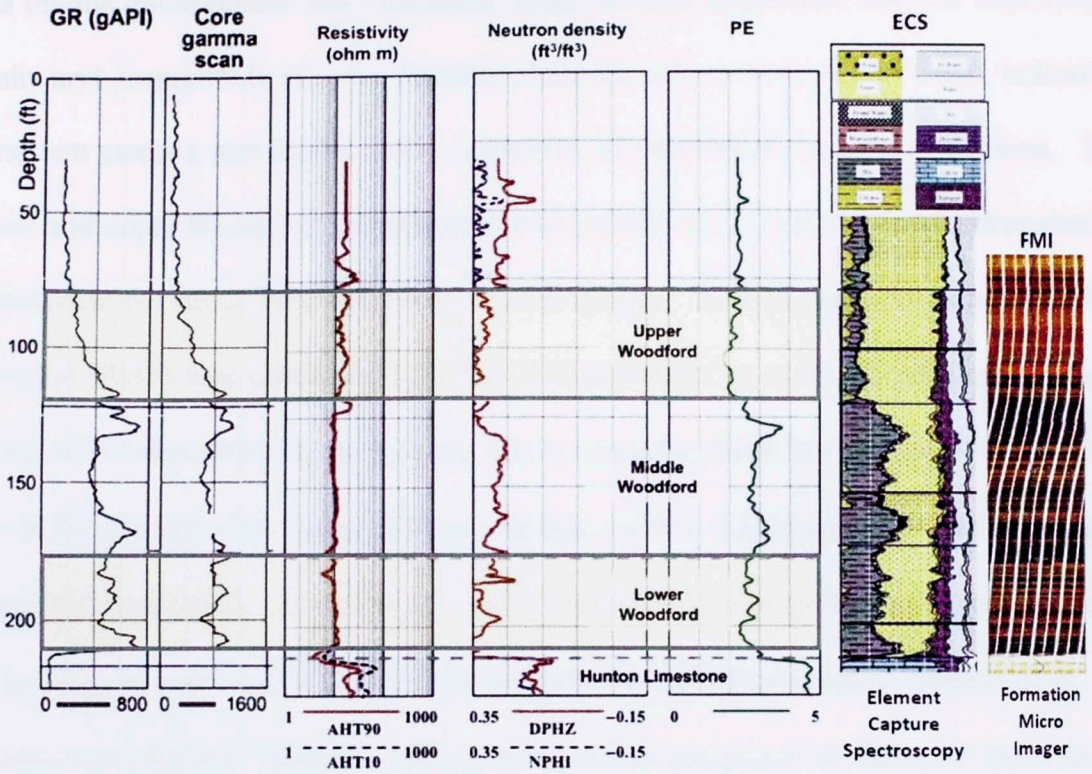

Figure 12. Wyche-1 borehole well log data compiled from Abousleiman et al. (2007); Buckner et al. (2009); Portas (2009); Sierra et al. (2010); Slatt et al. (2012); Romero and Philp (2012); in Molinares (2013).

Prior to discussing eustatic fluctuations coinciding with Woodford deposition, a discussion of geochemical studies (Romero, 2008; Romero and Philp, 2012) conducted on the Wyche-1 core from the Wyche Farm Shale Pit will be concluded. The lower and upper Woodford are characterized by dysoxic to suboxic deposition (Pr/Ph) in periodic euxinic conditions (inferred from the aryl isoprenoid ratio, AIR). Persistent euxinia and anoxia, coupled with elevated water salinity (relatively higher gammacerane indices), typify the middle Woodford. Chemocline depths varied, being shallower and more stable in the middle Woodford while fluctuating and deeper during formation of the lower and upper members. Euxinia, and the associated chemocline depth, was inferred from observation of the 2,3,6-aryl-isoprenoid (**VII**) configuration. The persistence of

this unique environment was calculated using the aryl isoprenoid ratio, or AIR (short-chain aryl isoprenoids (C_{13}-C_{17})/middle-chain (C_{18}-C_{22}), with lower ratios indicating persistent euxinia and higher ratios indicative of intermittent euxinic conditions. The lower and upper Woodford were deposited in episodic PZE, and the middle deposited in a persistent period of PZE according to AIR results. In addition, relative hydrocarbon potential (RHP) was calculated ((S_1+S_2)/TOC) in order to assess the temporal changes of Woodford deposition in the Arkoma Basin (Romero, 2008; Romero and Philp, 2012). The RHP consists of a rising-upward vertical organic facies sequence (VOFS) and a falling-upward VOFS. The former infers a transition from oxic to anoxia, representing an increase in sea level and enhanced preservation of organic matter illustrated by the transition to organic-rich facies. The latter indicates progressively leaner organic facies due to increasing oxic conditions in the water column due to the retreating sea (Fang et al., 1993). With proper application, the RHP can be utilized to discern differences in the stratigraphy to assist in identification of various system tracts.

From organic geochemistry alone, it was determined a total of five falling and rising stages of sea level comprise the Woodford data set to be used in this study (Romero, 2008). An appreciable transgression occurred at the base of the lower member, which was deposited throughout two transgressive-regressive cycles. The middle member was formed as a result of a significant transgression, or sea level rise, partially explaining the more stable and anoxic conditions observed. The upper Woodford was deposited during an overall regression (HST), characterized by high rates of deposition (Figure 13; Romero, 2008; Romero and Philp, 2012). This tentative sequence stratigraphic framework was developed through comparison of RHP data with

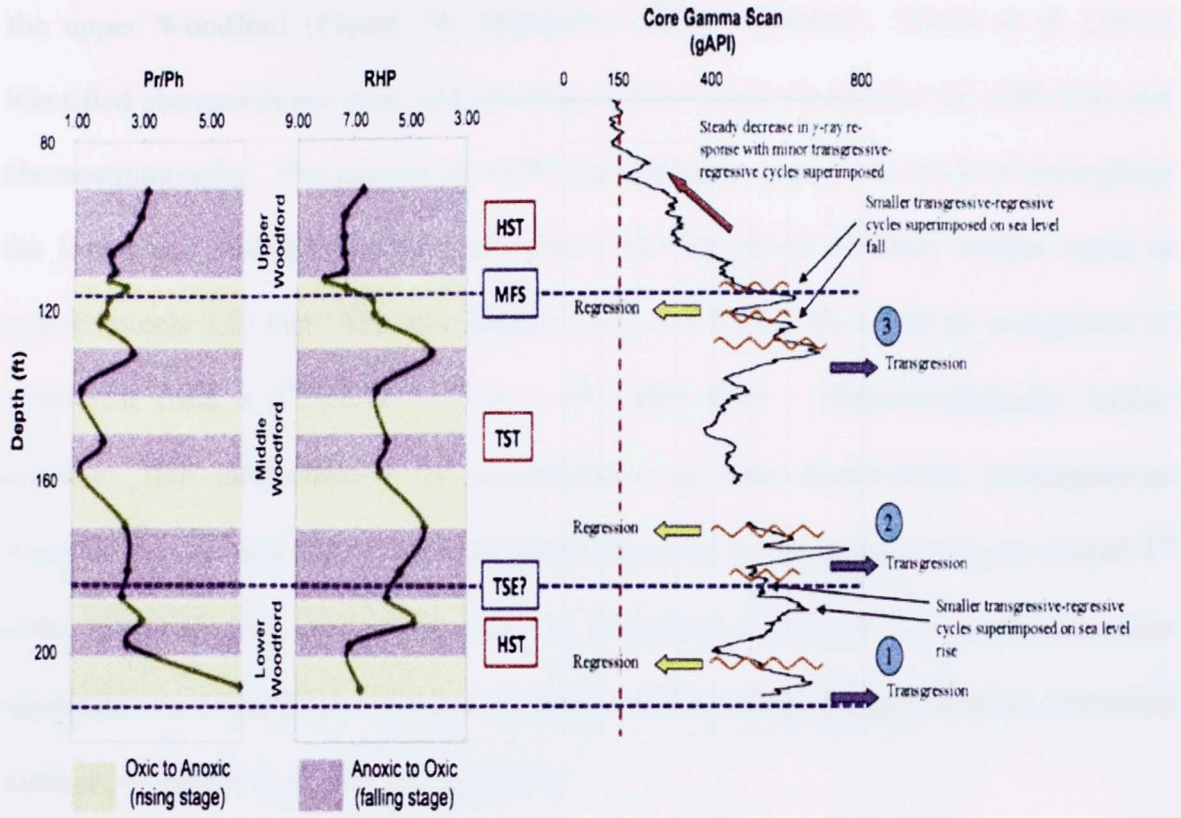

Figure 13. Sequence stratigraphic framework developed via RHP analysis and correlation to preexisting characterizations of the Woodford (Romero and Philp 2012).

existing sequence stratigraphic framework by Buckner et al. (2009) and Slatt et al. (2011). Years later, Molinares (2013) conducted extensive lithologic and sequence stratigraphic research to produce a framework specifically for the Wyche-1 core researched in this current study. Nine different lithofacies were identified, in addition to a detailed sequence stratigraphic framework which will be integrated into the findings from this study. The lower and middle Woodford represent a 2nd order TST and the upper signifies a 2nd order HST. 3rd Order cycles were then recognized via observation of stacking patterns in the Woodford derived from correlation of detailed lithofacies descriptions and gamma ray log measurements. The lower and middle Woodford are characterized by five 3rd order cycles, with six 3rd order cycles found in

the upper Woodford (Figure 14; Molinares, 2013). Recently, Turner et al. (2015) identified changes in sea level and resulting system tracts via gamma ray (GR) logs and chemostratigraphy. The gamma ray (GR) data infers an increase in sea level throughout the lower and middle members, and places the maximum flooding surface (mfs) at approximately 130 feet. The mfs divides rising and falling sea levels by recognition of a reversal from a 2^{nd} order TST to a 2^{nd} order HST. Chemostratigraphy further enhances this interpretation by identification of four fourth-order parasequences representing retreat and advancement of the shoreline which occur during an overall 3^{rd} order sea level rise (TST). The HST is composed of four 4^{th} order parasequences identified via recognition of clay, biogenic quartz, carbonate and detritus elemental surrogates (Turner et al., 2015; Figure 15).

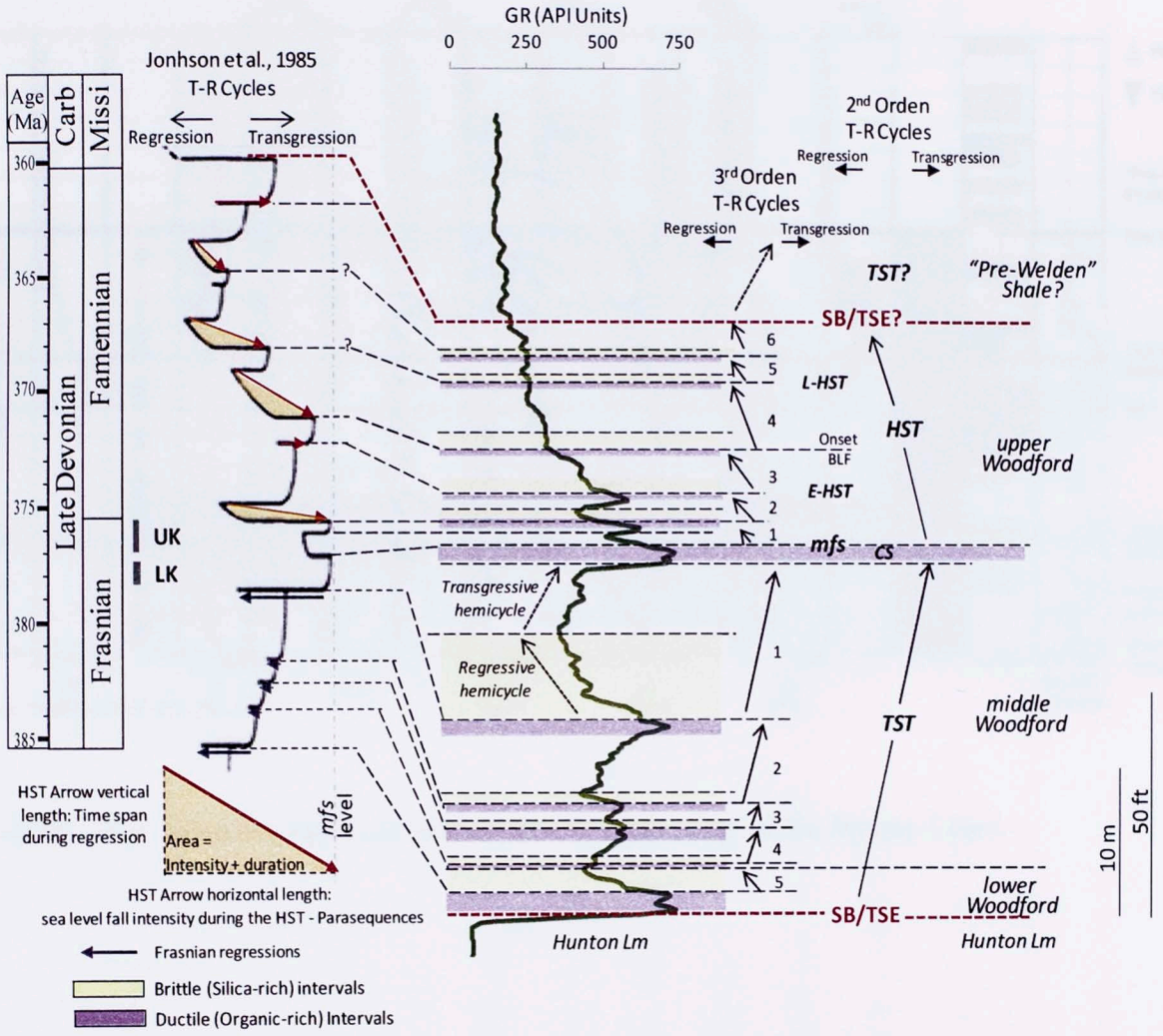

Figure 14. Sequence stratigraphic framework generated for the Wyche-1 core by Molinares (2013).

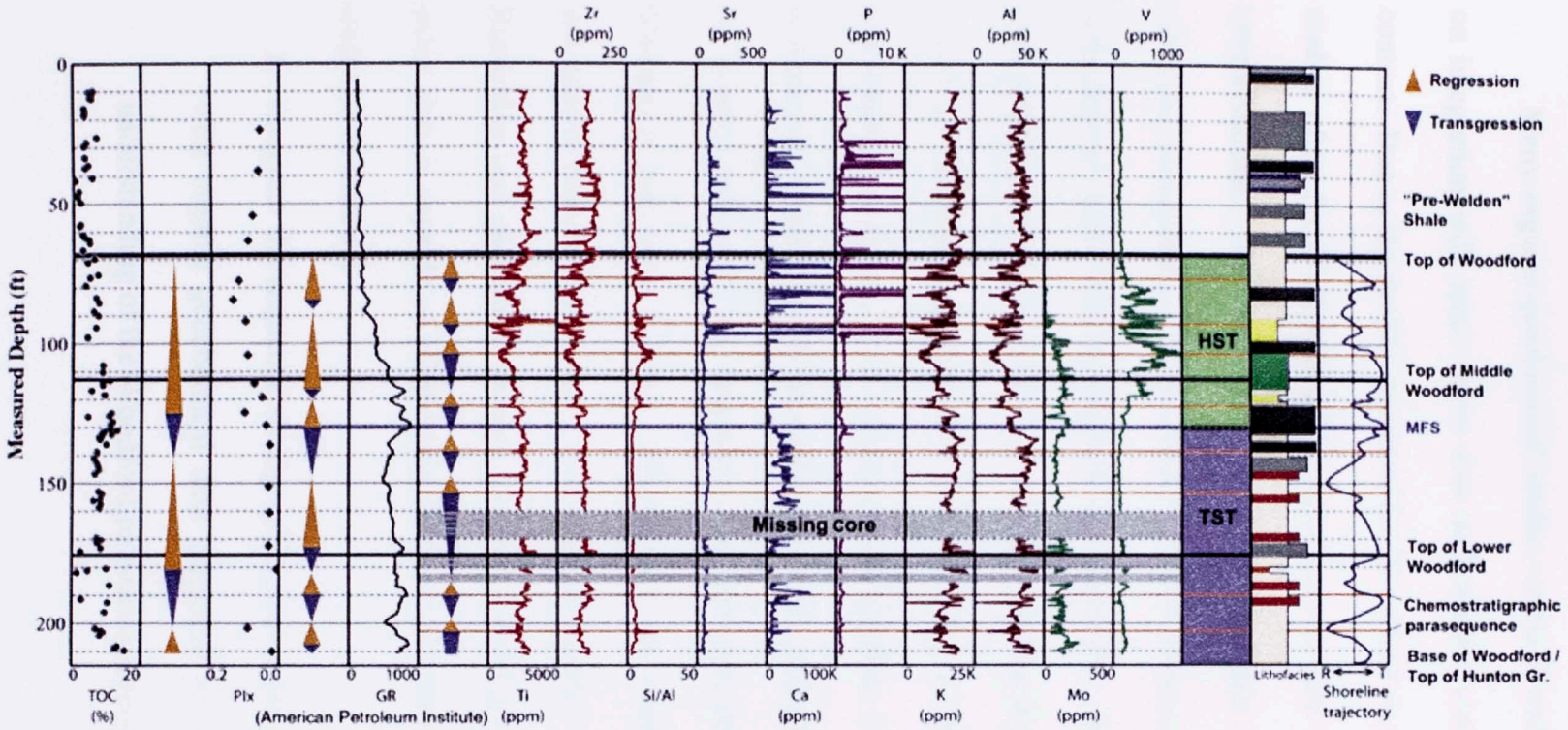

Figure 15. Gamma ray, trace element, organic richness and pollen index logs of the Wyche-1 core.

1.5. Objectives

Many organic geochemical studies on the Woodford Shale exist, but lack focus on integration with other proxy data and seldom constrain results in a stratigraphic context. Due to the prolific nature of the Woodford as a source rock and resource play, studies often focus on industrial applications in lieu of detailed paleoenvironmental interpretations. The identification of C_{40} aromatic carotenoids will allow for an enhanced conception of the Woodford paleoenvironment to be constructed, specifically pertaining to water column structure and chemistry. Romero (2008) and Romero and Philp (2012) produced excellent initial results on the Wyche-1 core, but were limited by a lack of sequence stratigraphic data specific to the studied data set and some experimental novelties. The sequence stratigraphic framework by Molinares (2013) provides an overall view of temporal variations throughout the Wyche-1 core, but can be further enhanced via integration of detailed biomarker data. For example, biomarkers may assist in better understanding the mechanisms governing productivity and preservation during fourth-order parasequences and third-order system tracts. Biomarker and geological proxies possess individual deficiencies, but integration of proxy data is capable of eliminating some of the pitfalls. Therefore, the goals of this study are as follows:

1. Integrate the sequence stratigraphic framework developed by Molinares (2013) with organic geochemical data generated in this study to provide enhanced understanding of the Woodford paleoenvironment.

2. Specifically, develop a foundation supported by C_{40} aromatic carotenoids, carotenoid derivatives, benzohopanes, hopenes, and other novel biomarkers, which may then be utilized to construct paleoenvironmental interpretations.
3. Investigate the paleowater column structure and chemistry using preexisting applications of select biomarkers and attempt to propose, augment or refine these applications to enhance the current understanding of the Woodford paleoenvironment.
4. Perform CSIA on the C_{40} aromatic carotenoid, paleorenieratane, to gain greater source specificity and resolution of formerly interpreted data to clarify conclusions. In particular, infuse the occurrence of paleorenieratane with significance via determination of its origin.
5. Assess the temporal flux of the microbial community to supplement the core interpretation of the Woodford paleoenvironment.

CHAPTER II

2. Methods

2.1. Area of Study

Twenty-nine rock samples (Table 2) were collected from Dr. Roger Slatt's core lab in Sarkey's Energy Center located on the main University of Oklahoma campus. The Wyche-1 core was taken from the Wyche Shale Pit located at UTM: 14S X=716339 Y=3839956 (34.67875°N, -96.63864°E; Figure 16). Wyche-1 was drilled as a research well, producing core and log data for the OU-Devon-Schlumberger enterprise. The drilled core is approximately 200 ft. long and is comprised of Woodford and pre-Welden formations with portions missing due to previous research projects/analyses and remnant sections placed in plastic wrap in cardboard boxes. Samples were removed from the core as either whole pieces, or as chips in the event unique features (e.g. radiolarian tests, phosphate nodules) were present.

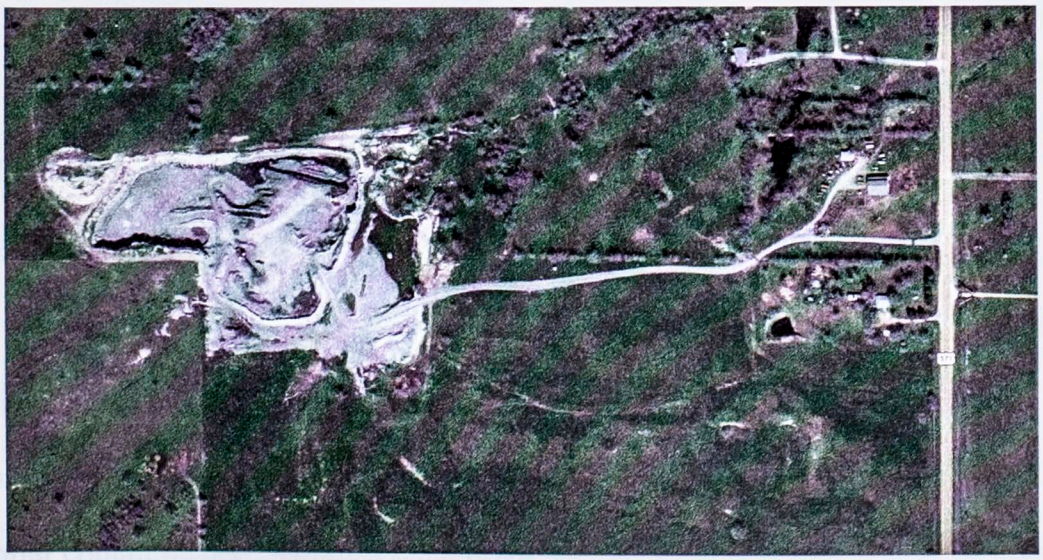

Figure 16. Aerial satellite view of the Wyche-1 quarry in Pontotoc County, OK.

Table 2. Woodford samples with associated depths and locations obtained from the Wyche-1 core for geochemical analyses.

Sample	Depth	County	Global Position	Member
WSLU-1	93.83	Pontotoc	2N 6E S2	Upper
WSLU-2	109.17	Pontotoc	2N 6E S2	Upper
WSLU-3	112.5	Pontotoc	2N 6E S2	Upper
WSLU-4	126.17	Pontotoc	2N 6E S2	Middle
WSLU-5	131.75	Pontotoc	2N 6E S2	Middle
WSLU-6	132.75	Pontotoc	2N 6E S2	Middle
WSLU-7	134	Pontotoc	2N 6E S2	Middle
WSLU-8	145.17	Pontotoc	2N 6E S2	Middle
WSLU-9	153.58	Pontotoc	2N 6E S2	Middle
WSLU-10	160.17	Pontotoc	2N 6E S2	Middle
WSLU-11	160.83	Pontotoc	2N 6E S2	Middle
WSLU-12	169.33	Pontotoc	2N 6E S2	Middle
WSLU-13	170.92	Pontotoc	2N 6E S2	Middle
WSLU-14	172	Pontotoc	2N 6E S2	Middle
WSLU-15	172.42	Pontotoc	2N 6E S2	Middle
WSLU-16	173.83	Pontotoc	2N 6E S2	Middle
WSLU-17	174.42	Pontotoc	2N 6E S2	Middle
WSLU-18	181.92	Pontotoc	2N 6E S2	Lower
WSLU-19	185.92	Pontotoc	2N 6E S2	Lower
WSLU-20	186.42	Pontotoc	2N 6E S2	Lower
WSLU-21	187.75	Pontotoc	2N 6E S2	Lower
WSLU-22	191.08	Pontotoc	2N 6E S2	Lower
WSLU-23	191.33	Pontotoc	2N 6E S2	Lower
WSLU-24	192.75	Pontotoc	2N 6E S2	Lower
WSLU-25	193.75	Pontotoc	2N 6E S2	Lower
WSLU-26	195.42	Pontotoc	2N 6E S2	Lower
WSLU-27	203.08	Pontotoc	2N 6E S2	Lower
WSLU-28	207	Pontotoc	2N 6E S2	Lower
WSLU-29	209.92	Pontotoc	2N 6E S2	Lower

2.2. Experimental Procedure

2.2.1. Preliminary Sample Treatment

Rock samples were scraped with a razor blade and dipped in an azeotropic solution of 1:1 CH_2Cl_2 (dichloromethane) and methanol (CH_3OH) with sterilized metal tongs to minimize experimental bias from handling, plastics, drilling mud and other potential contaminants. Samples were dried for 24 hours in a hood to ensure complete solvent evaporation before being crushed to < US Standard mesh No. 40 (0.425mm) in

a cleaned (soap+water→ DCM→ MeOH→clean) porcelain mortar and pestle. Samples were crushed until adequate powder was acquired for bulk geochemical analyses and extraction/fractionation procedures. Samples for Rock Eval/TOC were stored and transported in glass vials, while samples awaiting solvent extraction were preserved in several wraps of aluminum foil.

2.2.2. Rock Eval 6 Pyrolysis and Total Organic Carbon

Approximately 1g of each sample were sent to the Research and Technology Center at Chesapeake Energy Corporation located in Oklahoma City, OK for bulk geochemical evaluations. The TOC analysis was performed on a LECO-C144 Carbon series and pyrolysis data were generated by a Vinci Technologies Rock Eval 6 analyser.

2.2.3. Extraction of Soluble Organic Matter

Prior to sample extraction, the respective Soxhlet extraction system (Soxhlet apparatus, thimble and glass wool) was preextracted for 24 hours with a 1:1 mixture of DCM and MeOH. Cellulose thimbles were weighed prior to extraction in the event kerogen data was required. Powdered sample was introduced to the thimble by carefully pouring crushed rock from an aluminum foil funnel to avoid powder adherence to the wall of the thimble. After sample introduction, glass wool was inserted to assist in repressing sample overflow during peak levels of solvent while cycling. Activated copper (treated with concentrated HCl) was placed in each 500mL round-bottom flask after approximately 375-400mL of solvent was added. Round-bottoms were attached to the solvent extractor and samples were subjected to 24 hours

of cycling with mild heat applied to avoid unintentional alteration of extracted organic matter.

2.2.4. Bitumen Fractionation

After 24 hours, samples were allowed to cool before rotary evaporation to remove excess solvent and facilitate transfer to 20mL vials necessary for quantifying the bitumen. Prior to transfer, bitumen was passed through three layers of thoroughly packed glass wool using DCM initially, followed by MeOH to ensure total transfer of extracted organic matter was accomplished. Samples were dried using a Meyer Organomation N-evap analytical evaporator under a gentle nitrogen stream before obtaining sample mass. Variable amounts of bitumen were transferred to 40mL centrifuge tubes and deasphaltened (50-80mg) using an unconventional method due to the immature nature of many samples in this study. A 300µL mixture of 1:1 DCM and MeOH was added to samples prior to *n*-pentane introduction. A glass burette was filled with *n*-pentane for controlled administration of nonpolar solvent to the samples. Drop by drop, *n*-pentane was added to samples in an ice bath subjected to sonication via a Branson B2510 ultrasonic cleaner. A notable 'critical point' was observed, where *n*-pentane could be introduced rapidly without premature precipitation of organic material. After successful introduction of excess *n*-pentane, samples were placed in a freezer (~ -2°C) overnight to allow adequate time for deasphaltation. The following day, samples were centrifuged in a Daman IEC Model K centrifuge for 15 minutes to ensure asphaltenes and other polar components remained in the pellet while the supernatant was decanted off using a pipet. The supernatant (maltene) was transferred

to 250mL round-bottom flasks and subjected to rotary evaporation to facilitate transfer to 4mL vials using DCM as the carrier solvent.

2.2.5. Maltene Fractionation: Gas Chromatography and High Performance Liquid Chromatography

All samples were diluted to 3mg/mL in *n*-hexane prior to screening via an Agilent Technologies 6890 Gas Chromatograph. A splitless capillary injection system and 60m J&W Scientific DB-1 122-0162 fused silica column (0.250 mm i.d. and 0.25 μm liquid filmed coating). An initial temperature was set to 40°C and held for 1.5 min after sample injection, followed by a temperature ramp of 4°C/min. At 310°C, the oven became isothermal for 24 min. until method completion. Helium was utilized as the carrier gas, with a flow rate of 1.4mL/min. Post-screening, maltene fractions were filtered through glass wool with DCM to ensure fraction purity prior to HPLC fractionation. Samples were diluted to a concentration of 10mg/60μL in preparation for injection into an Agilent Technologies 1050 series HPLC. An external standard (*n*-C_{20} + *n*-C_{24} + toluene + xylene + dimethylnapthalene + phenanthrene + chrysene) injected before the initial analysis and every 5 analyses after that. Saturate, aromatic and polar (resin/NSO) components of the maltene were collected and analyzed in a similar fashion as the maltene fraction discussed above.

2.2.6. Gas Chromatography-Mass Spectrometry

Twenty-nine saturate and aromatic fractions were concentrated to 3mg/mL in 2,2,4-trimethylpentane (iso-octane) and spiked with tetracosane (saturates) or deuterated

phenanthrene (aromatics) in preparation for GCMS analysis. An Agilent Technologies 7890A Gas Chromatograph (column: J&W Scientific DB-5MS 122-5562 fused silica column; injector: type=splitless, T=310°C carrier gas: He; transfer line: T=310°C)) was integrated with an Agilent Technologies 5975 XL Mass Selective Detector (ion source: T=250°C, EI @ 70eV; quadrapole analyzer: T=200°C). Single-ion monitoring (SIM) or multiple ion detection (MID) was employed to evaluate the distributions and concentrations of hydrocarbons in each sample, with full scan used to assist with different identifications. The GC temperature program initialized at 40°C and held for 1.5 min. before a temperature ramp to 315°C preceded an isothermal period of 50 min. Important note: it appears C_{40}+ compounds (e.g. aromatic carotenoids) do not fully elute at 310°C or in a timely manner, explaining the absence of these compounds from previous studies (Romero 2008; Romero and Philp 2012). At 315°C, elution occurs between 105-115 minutes with the outlined temperature program and instrument settings, but greater amounts elute relative to an internal standard at 320°C. However, this temperature may prematurely degrade and damage instrument components, so 315°C seems an appropriate compromise experimentally and instrumentally.

2.2.7 Gas Chromatography-Mass Spectrometry-Mass Spectrometry

Select saturate and aromatic fractions requiring compound verification were analyzed by a Thermo Scientific TRACE 1310 GC coupled with an 8000 triple stage quadrupole (TSQ) operating in splitless injection mode. A 60m by 0.25mm i.d. J&W scientific DB-5MS fused silica capillary column coated with a 0.25μm liquid film. Single reaction monitoring was used to facilitate identification of compounds coeluting

(e.g. gammacerane) with others to ensure the integrity of the quantified data. The temperature program involved an initial 40°C isothermal stage for 1.5 min before ramping to 300°C at 4°C/min with a final hold time of 34 min with helium as the carrier gas with a flow rate of 1.4mL/min.

2.2.8. Compound Specific Isotope Analysis (Gas Chromatography-Isotope Ratio Mass Spectrometry)

Compound specific isotope analysis (CSIA) was performed on WSLU-8, which contained the highest concentrations of paleorenieratane. High concentrations were needed to yield accurate data, and until further concentrates are generated, only WSLU-8 will be analyzed. Stable carbon isotope values were obtained using an Agilent 6890 series GC system with a split/splitless capillary injection system equipped with a 25m by 0.25mm i.d. J&W scientific fused silica capillary column with a 0.25μm liquid film interfaced to a Finnigan GC combustion III reactor and Finnigan Delta plus XL. The temperature program began at 280°C and was held for 1.5 min before increasing at 4°C/min to 300°C before being held isothermal for 34 min. Helium was used as the carrier gas flowing at 1.4mL/min. The high injection temperature and short column were used to enhance the peak height of paleorenieratane for easier, more accurate measurement.

2.2.9. Identification

Hydrocarbons were identified using preexisting literature; ion scans (50-600) of appropriate elution windows, comparison of parent ions (M+) with published reports

and parent-daughter analyses via a GC-MS-MS. A visual aid was created to assist in understanding the methods workflow in this study (Figure 17).

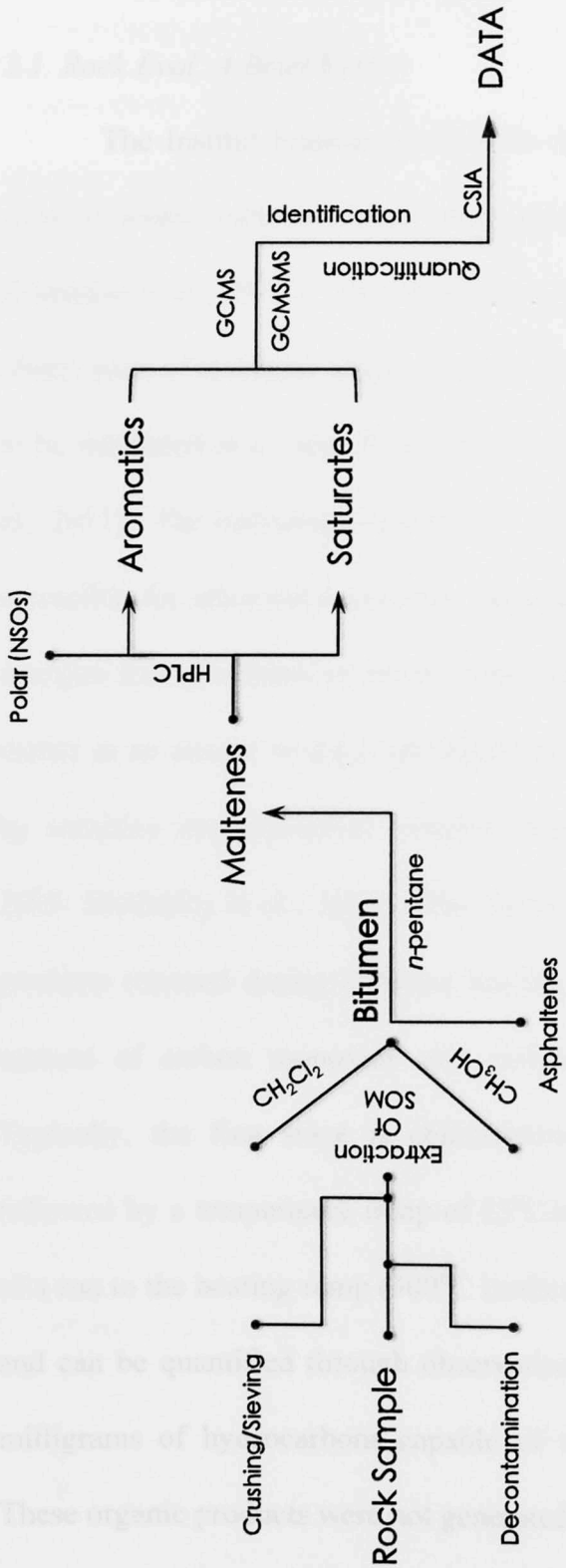

Figure 17. Illustration of laboratory workflow responsible for the production and subsequent observation of geochemical data in this study.

CHAPTER III

3. Results and Discussion: Bulk Geochemical Data

3.1. Rock Eval: A Brief Review

The Institut Francais du Petrole developed the pyrolysis procedure commonly used to assess various crucial characteristics of a source rock, Rock Eval, in 1977 (Espitalie et al., 1977). This temperature-programmed pyrolysis instrument allows for observation of reactions which take hundreds to millions of years in a sedimentary basin to be simulated in a mere 20 minutes (Espitalie et al., 1977; Peters, 1986; McCarthy et al., 2011). The instrument requires 50-100 mg of pulverized rock, which is loaded into a crucible for automated analysis. Samples are introduced into an atmosphere of inert nitrogen for subsequent pyrolysis (generation of organic products from heating organic matter in an anoxic system) and oxidation via a series of temperature ramps controlled by sensitive thermocouples, ranging from 100°C-850°C (Peters, 1986; Behar et al., 2001; McCarthy et al., 2011). The flame ionization detector (FID) records the organic products released during different heating stages, while infrared detectors quantify the amount of carbon monoxide and carbon dioxide produced from crushed samples. Typically, the first stage is characterized by an isotherm 300°C for 2-4 minutes, followed by a temperature ramp of 25°C/min to an apex of 850°C. From the initiation of a run to the heating ramp (300°C isotherm), free hydrocarbons (bitumen) are released and can be quantified through observation of the corresponding S_1 peak, measured as milligrams of hydrocarbons capable of thermal distillation from one gram of rock. These organic products were not generated by the pyrolysis, but in the subsurface due to

natural processes. Expulsion, however, was facilitated by pyrolysis. As the temperature rapidly increases to 850°C, pyrolitic products begin to be released and detected due to decomposition reactions occurring in the kerogen. The increased temperatures are able to provide the necessary thermodynamic conditions to generate hydrocarbons from the insoluble organic matter, reaching the required activation energies causing a spike in organic components during this stage of the experiment. This spike is called the S_2 peak, and it grants knowledge regarding the remaining potential of a source rock if maturation continues, reported as milligrams of remaining hydrocarbons (i.e. hydrocarbons generated by thermal breakdown of kerogen) per gram of rock. The apex of the S_2 peak represents T_{max}, the pyrolysis temperature at which peak hydrocarbon generation occurs. This is often used to assess the maturity of the sample, and lends knowledge of the optimal temperature for hydrocarbon generation from that particular specimen. The S_3 peak signifies the carbon dioxide produced during thermal cracking of kerogen, and is reported as milligrams of CO_2 per gram of rock (up to 390°C; Peters, 1986; Behar et al., 2001). The S_4 is comprised of carbon dioxide (S_4CO_2) and carbon monoxide (S_4CO), representing the residual organic carbon and the S_5 (CO_2) is produced from carbonate decomposition (McCarthy et al., 2011). The pyrolysis peaks are utilized in the form of several indices used in source rock characterization, such as kerogen typing and maturity assessment. Figure 18 provides a visual representation for reference of the previous discussion and Table 3 signifies acronyms used throughout this section.

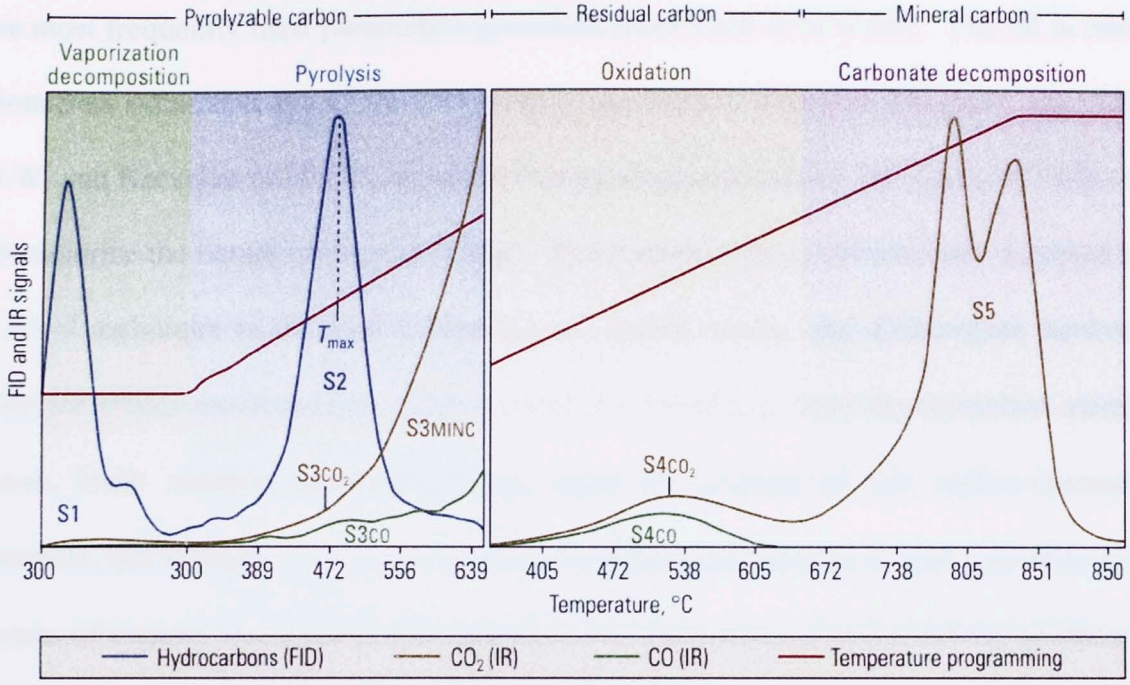

Figure 18. Temperature programmed Rock Eval 6 pyrolysis results and associated products and heating ramps (McCarthy et al., 2011).

Table 3. Legend of bulk geochemical abbreviations and associated units used throughout this section.

Rock Eval Nomenclature		
Parameter	**Meaning**	**Unit**
TOC	Total Organic Content	wt.%
S1	Free Hydrocarbons	mg HC/g rock
S2	Hydrocarbon Potential	mg HC/g rock
S3	Gas from Kerogen Cracking	mg CO2/g rock
HI	S_2/TOC	mg HC/g OC
OI	S_3/TOC	mg CO2/g OC
TMAX	Apex of S_2	°C
NOC	Normalized Oil Content (S_1/TOC)	mg HC/g rock

The hydrogen index (HI; S_2/TOC)) and oxygen index (OI; S_3/TOC) are two of the most frequently used parameters generated from Rock Eval 6 data. The HI is often plotted as a function (y) of the OI (x) on a pseudo-van Krevelen Diagram. In 1950, D.W. van Krevelen published success of using elemental atomic H/C and O/C ratios to characterize the nature of organic matter. This method was instantaneously accepted as a novel technique to observe differences in organic matter and differentiate between multiple source environments. The original plot benefitted from dimensionless atomic ratios, basic reaction mechanisms and rapid illustrations of the coal's chemical structure, not kerogen. From an exploration perspective, the plot is used primarily as a means of organic matter type determination and the nature of hydrocarbons produced. Organic matter type is ultimately controlled by the persisting environmental conditions during the time of deposition, with different environments contributing organic matter of varying compositions. As a result of compositional variances, organic matter type can be discerned via a van Krevelen Diagram. (van Krevelen, 1984). Integration of van Krevelen (1950) atomic ratio method and Espitalie et al. (1977) pyrolitic indicies is problematic (Orr, 1981; Katz, 1983; Jones, 1987), with almost a 70% difference in HI values for H/C ratios between 1.2-1.4 (Type II marine; Grabowski, 1984). Also, the van Krevelen diagram was initially designed for integration of atomic data, not pyrolitic data, which lacks the ability to define organic matter quality and maturity as efficiently (Baskin, 1997). Therefore, these discrepancies should be in mind during interpretation of pseudo-van Krevelen diagrams and Rock Eval data, as is utilized in this study. The premise of these interpretations is based on the assumption hydrogen-rich (high HI) source material is more prone to production of oil, since oil is hydrogen-rich. In

addition, hydrogen facilitates hydrocarbon production from kerogen, so a higher HI enables greater and prolonged generative capacity. When there is no longer any hydrogen, despite large amounts of remaining carbon, hydrocarbon genesis will cease (Waples, 1981; Hunt, 1996). The HI and OI of a pseudo-van Krevlen diagram (Figure 19) are functions of biological contribution, which is governed by environmental conditions and features. Marine and lacustrine environments are typified by biological compositions rich in lipids and proteins, where H>>C (high HI). Terrestrial organic matter is relatively depleted in these components (lower HI), but enriched in carbohydrate and polysaccharides where O>>C (high OI; McCarthy et al., 2011). In addition to HI and OI, other indices and cross plots have been developed that utilize the pyrolysis results from Rock Eval. These applications fall into three broad categories; organic richness, which may be determined via Rock Eval, but was generated using a Leco SC-444 in this study, organic matter type and thermal maturity. The results will be reported for each of these categories, with brief introductions elaborating on the indices and cross plots employed to decipher the nature of the organic matter in the studied dataset.

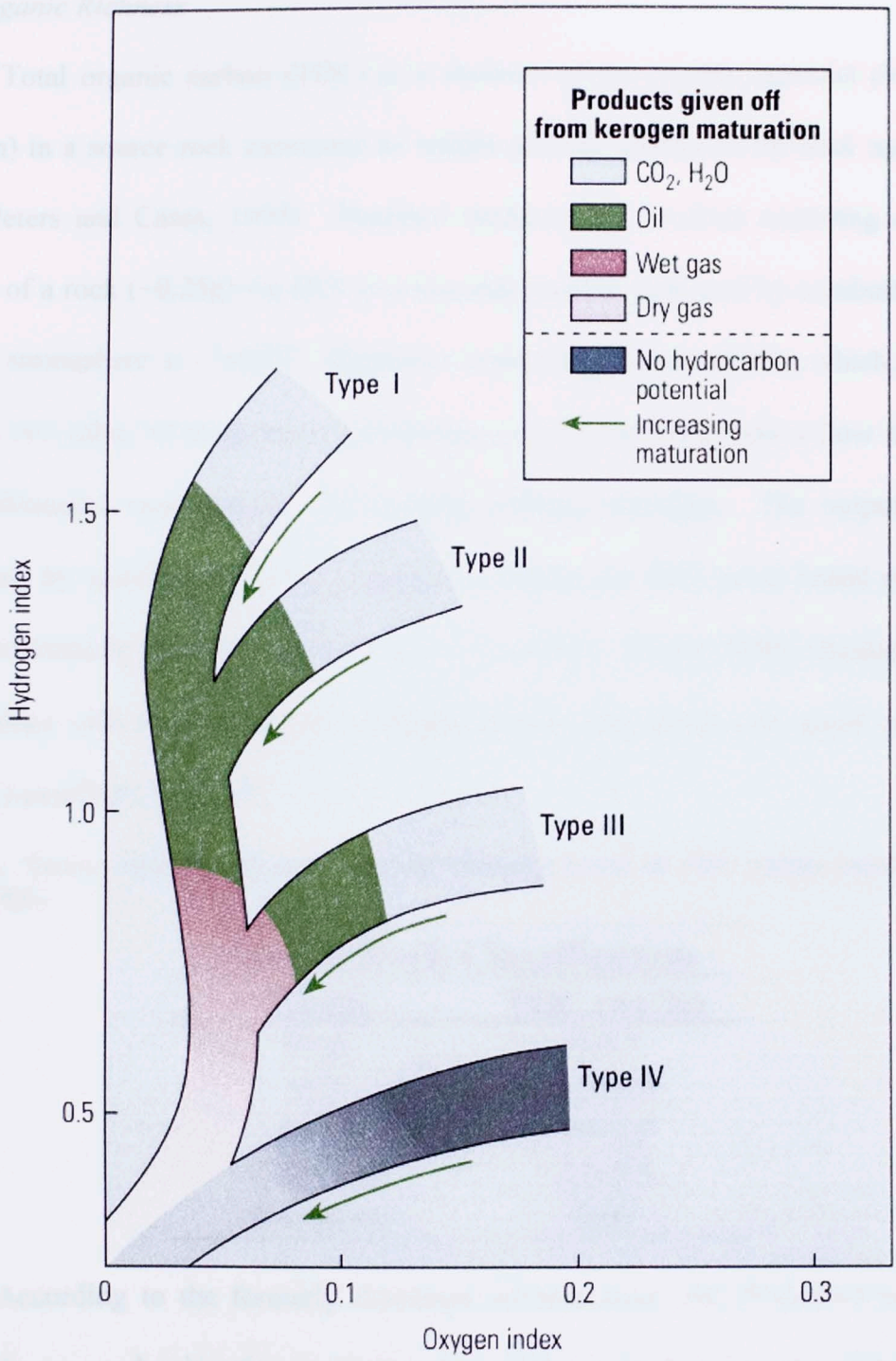

Figure 19. Pseudo-Van Krevlen Diagram displaying the regions of various kerogen types as a function of HI and OI (McCarthy et al., 2011).

3.2. Organic Richness

Total organic carbon (TOC) is a measure of the organic material (bitumen + kerogen) in a source rock expressed as weight percent relative to the total mass of the rock (Peters and Cassa, 1994). Standard methodology involves removing carbonate content of a rock (~0.25g) via HCl in a filtering crucible, followed by combustion in an oxygen atmosphere at ~1000°C. Oxidation leads to formation of CO_2, which is carried through two tubes of magnesium perchlorate (retains humidity) and a flow controller, with subsequent measurement via sensitive infrared detectors. The output TOC is calculated by specific algorithms designed to adjust the final result based on sample mass and humidity measurements (Behar et al., 2001). Peters (1986) standardized the TOC values with the classification scheme of poor, fair, good, very good, and (more recently) excellent (Table 4).

Table 4. Source rock classification naming scheming based on TOC values (modified from Peters 1986).

Source Rock Classification	
Grade	**TOC (wt.%)**
Poor	0-0.5
Fair	0.5-1.0
Good	1.0-2.0
Very Good	2.0-5.0
Excellent	5.0+

According to the formerly discussed nomenclature, the Woodford samples in this study are predominantly excellent source rocks, with four samples plotting in the very good range (Figure 20). Values range from a minimum of 3.47% at 126.17ft. in the UW to a maximum of 16.90% at 207ft. in the LW (Table 5; Figure 20). If means are calculated for individual members, the lower, middle and upper members possess average TOC values of 9.66%, 7.46% and 8.19%; respectively. This is contrary to

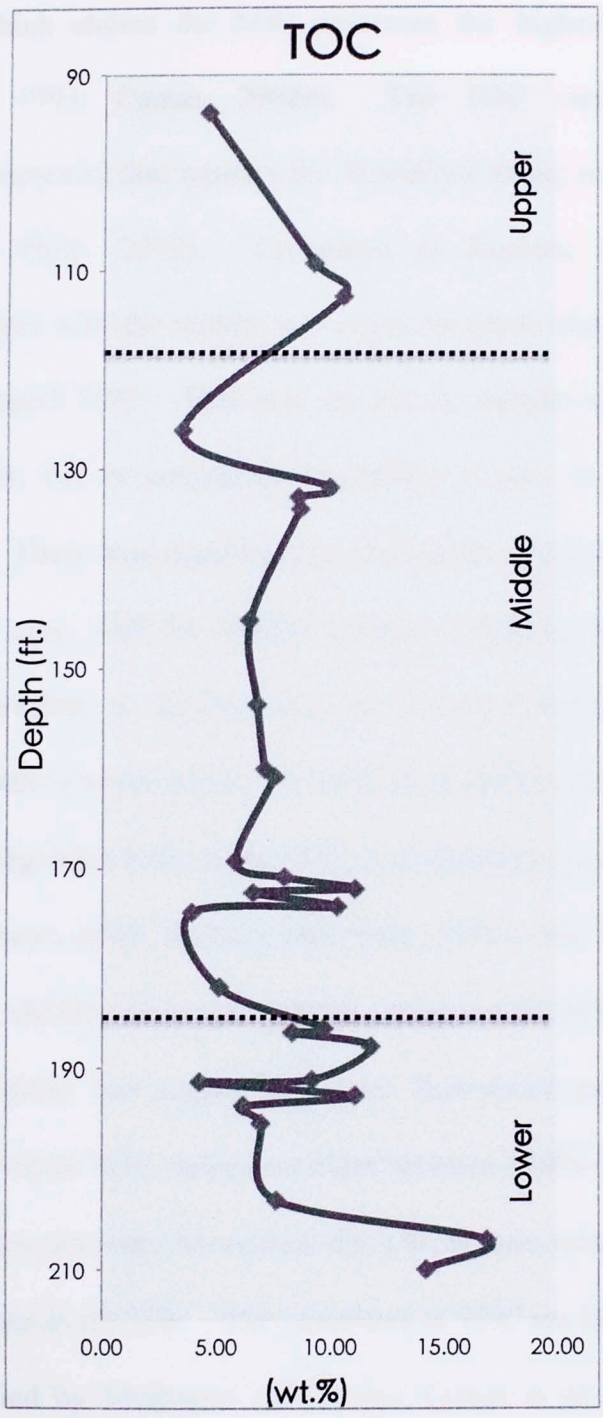

Figure 20. TOC log of the Wyche-1 core displaying the variable nature of organic richness, underlining the complexity and heterogeneity of the Woodford Shale.

preexisting work, which claims the MW possesses the highest TOC of the three members (Lambert, 1993; Comer, 2008a). The TOC variance illustrates the heterogeneity and complexity that typifies the Woodford Shale, recognized in previous work (Romero and Philp, 2012). Compared to Romero (2008), the UW is approximately the same, with the middle and lower members characterized by about a 1% decrease in averaged TOC. This may be due to sample selection, or different laboratory calibrations, but is considered negligible relative to the overall organic richness of this core. There was significant variation from a mean of 8.29% of ±3.04% throughout the entire core, with the middle member exhibiting the most stable TOC values (standard deviation ± 2.23%) and the lower member displaying values fluctuating ±3.86% relative to the mean. This may be an artifact of enhanced stability of the water column during deposition of the MW, as evinced by persistent euxinia during this time period (Romero, 2008; Romero and Philp, 2012). The TOC log (Figure 20) illustrates the relative stability of organic matter content in the MW. Greater sampling intensity in select regions has highlighted some fine-scaled perturbations, such as between 175ft.-170ft where TOC values oscillate between ~10%-5% in less than 1.5ft. Overall, the TOC values decrease throughout the LW, remain relatively constant in the MW, and decrease again in the UW. The variations in TOC are likely explained by the parasequences identified by Molinares (2013) and Turner et al. (2015), and may be linked to extinction horizons throughout the Woodford as well.

Table 5. Bulk geochemical data of the Wyche-1 core, including S_1, S_2, S_3, HI, OI, PI, T_{max}, R_c, TOC, and NOC of the samples with associated depths.

Sample	Depth (ft.)	S_1 (mg/g)	S_2 (mg/g)	S_3 (mg/g)	T_{max} (°C)	Calc. R_o	TOC (wt. %)	HI	OI	PI	NOC
WSLU-1	93.83	0.51	26.31	0.50	428.0	0.54	4.66	550.93	15.90	0.043	24.54
WSLU-2	109.17	1.64	57.02	0.89	426.0	0.51	9.32	539.18	14.58	0.043	24.15
WSLU-3	112.5	2.74	66.29	1.00	427.0	0.53	10.60	555.69	14.26	0.038	22.00
WSLU-4	126.17	0.94	20.40	0.45	424.0	0.47	3.47	494.17	14.47	0.032	16.50
WSLU-5	131.75	1.45	45.05	1.64	416.0	0.33	10.00	450.50	16.40	0.031	14.50
WSLU-6	132.75	1.60	49.74	1.47	420.0	0.40	8.63	576.36	17.03	0.031	18.54
WSLU-7	134	1.80	49.51	1.29	424.0	0.47	8.66	589.74	13.85	0.024	14.36
WSLU-8	145.17	1.59	35.70	1.03	421.0	0.42	6.48	500.00	14.92	0.030	15.38
WSLU-9	153.58	1.64	36.61	0.99	416.0	0.33	6.79	618.53	12.75	0.036	23.39
WSLU-10	160.17	1.58	40.52	1.18	419.0	0.38	7.14	582.70	13.51	0.036	22.07
WSLU-11	160.83	1.70	40.32	1.21	418.0	0.36	7.55	572.68	13.33	0.031	18.37
WSLU-12	169.33	1.32	30.50	1.01	419.0	0.38	5.86	561.44	14.39	0.037	21.29
WSLU-13	170.92	1.39	31.98	1.33	410.0	0.22	8.02	564.59	10.73	0.019	10.94
WSLU-14	172	2.21	59.96	1.53	421.0	0.42	11.10	611.80	9.55	0.028	17.60
WSLU-15	172.42	1.45	36.62	0.94	422.0	0.44	6.59	567.51	16.53	0.038	22.13
WSLU-16	173.83	1.70	50.90	1.49	418.0	0.36	10.30	534.04	16.03	0.040	22.52
WSLU-17	174.42	0.56	23.00	0.54	426.0	0.51	3.90	520.48	17.24	0.041	22.53
WSLU-18	181.92	0.83	28.39	0.67	427.0	0.53	5.12	554.49	13.09	0.028	16.21
WSLU-19	185.92	1.79	55.22	1.33	423.0	0.45	9.72	568.11	13.68	0.031	18.42
WSLU-20	186.42	1.44	48.53	1.13	424.0	0.47	8.35	581.20	13.53	0.029	17.25
WSLU-21	187.75	2.41	64.73	1.55	420.0	0.40	11.80	548.56	13.14	0.036	20.42
WSLU-22	191.08	1.69	50.52	1.36	421.0	0.42	9.20	549.13	14.78	0.032	18.37
WSLU-23	191.33	0.66	21.45	0.64	424.0	0.47	4.29	398.75	16.58	0.042	17.33
WSLU-24	192.75	2.45	64.68	1.50	421.0	0.42	11.10	625.38	9.43	0.040	25.85
WSLU-25	193.75	1.13	35.22	0.82	423.0	0.45	6.15	587.90	12.97	0.044	27.09
WSLU-26	195.42	1.48	39.02	1.00	420.0	0.40	6.95	571.71	14.90	0.035	20.79
WSLU-27	203.08	1.78	47.07	0.97	424.0	0.47	7.61	540.18	13.78	0.036	19.91
WSLU-28	207	3.28	86.62	2.09	419.0	0.38	16.90	512.54	12.37	0.036	19.41
WSLU-29	209.92	2.90	76.99	1.84	419.0	0.38	14.20	542.18	12.96	0.036	20.42

One of the highest TOC values in the MW at 131.75ft. appears to correspond with the maximum flooding surface (mfs) identified by Turner et al. (2015) and Molinares (2013) (Figure 21). The highest TOC values in the LW provide initial

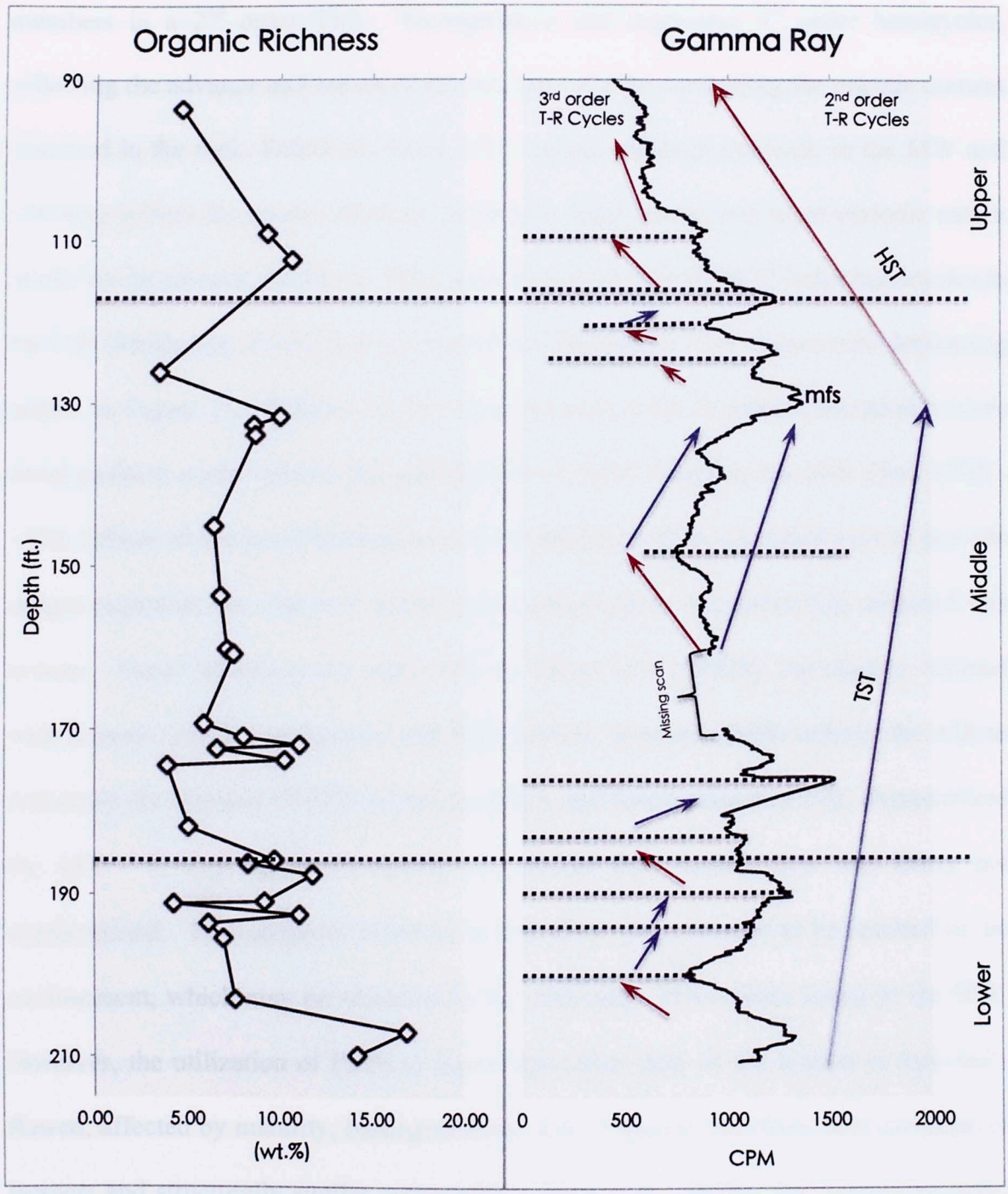

Figure 21. Integration of gamma ray log and sequence stratigraphic data with TOC data generated in this study.

evidence for highly reducing conditions characterizing this member, with perturbations in the TOC abundance explained by increased circulation possibly influenced by the progressive deepening of the water column during deposition of the lower and middle members in a 2nd order TST. Transgressive and regressive 3rd order hemicycles, reflecting the advance and retreat of the sea, may also be controlling the organic content observed in the rock. Relatively lower TOC values, although minimal, in the MW and UW may reflect the general decrease in bottom water anoxia and more periodic nature of this environmental condition. The predominance of regressive 3rd order hemicycles in the UW (Molinares, 2013) likely produced the attenuating TOC values with decreasing depths in Figure 21. Stability of the water column as the Woodford assumed a more distal position could explain the stabilization of TOC values in the MW from 170ft.-135ft. Effects of sea level fluctuation on the biosphere will be discussed later to provide insight regarding the extent to which either preservation or productivity affected this system. These inferences are supported by Turner et al. (2015), but slightly contrast with Romero (2008) and Romero and Philp (2012). Romero (2008) utilized the AIR to determine the duration of PZE in each member, and found persistent PZE characterized the MW. If PZE stabilized during this period then stratification was likely not compromised. This temporal cohesion would allow for a balance to be reached in the environment, which may be recorded by the consistent TOC values found in the MW. However, the utilization of Pr/Ph to assess the redox state of the bottom is reportedly flawed, affected by maturity, biodegradation, lack of source-specificity and coelution of isomers and structurally similar compounds (Didyk et al., 1978). The lower and upper members were deposited in dysoxic-suboxic conditions and the middle deposited in

predominantly anoxic bottom waters, interpreted by Pr/Ph (Romero, 2008; Romero and Philp, 2012). However, discussion later in this study will provide evidence displaying potential pitfalls of this ratio due to coelution with other compounds, such as crocetane, which yield misleading data. For example, heightened abundance of crocetane will cause lower Pr/Ph ratios due to coelution with phytane (Huang and Armstrong, 2009). It is known from previous work (Romero and Philp, 2012) euxinia dominated MW deposition. Crocetane is a possible diagenetic product of paleorenieratane, which is found in greatest abundance during the MW, leading to potential misinterpretation of Pr/Ph ratios and the water column redox state (Greenwood and Summons, 2003). In addition, productivity reflects the overall biomass generated by the biosphere, indirectly controlling TOC. Certain organisms are capable of generating thick mats, which may cause increased competition for light beneath the mats. Proliferation of one species may negatively impact the overall generation of biomass throughout the water column, leading to slightly lower TOC values, as observed in the MW. Analysis of biomarker data will permit the evaluation of the microbial community composition and assist in refining interpretations derived from bulk geochemical data.

3.3. Kerogen Characterization

As briefly discussed before, the primary means of assessing the kerogen type comprising a source rock is through construction of a van Krevelen Diagram. However, from HI alone, some interesting conclusions can be formulated (Figure 22). HI values ranged from 400 to 625 mgHC/gTOC, with an average of 550 mgHC/gTOC for the entire core. These data plot in the marine (oil-prone) region of an HI geochemical log,

consistent with previous data of Woodford kerogen types (Romero and Philp, 2012; Slatt and Rodriguez, 2012). The variability between different members is negligible, with the LW, MW and UW characterized by average HIs of 545, 554, and 548,

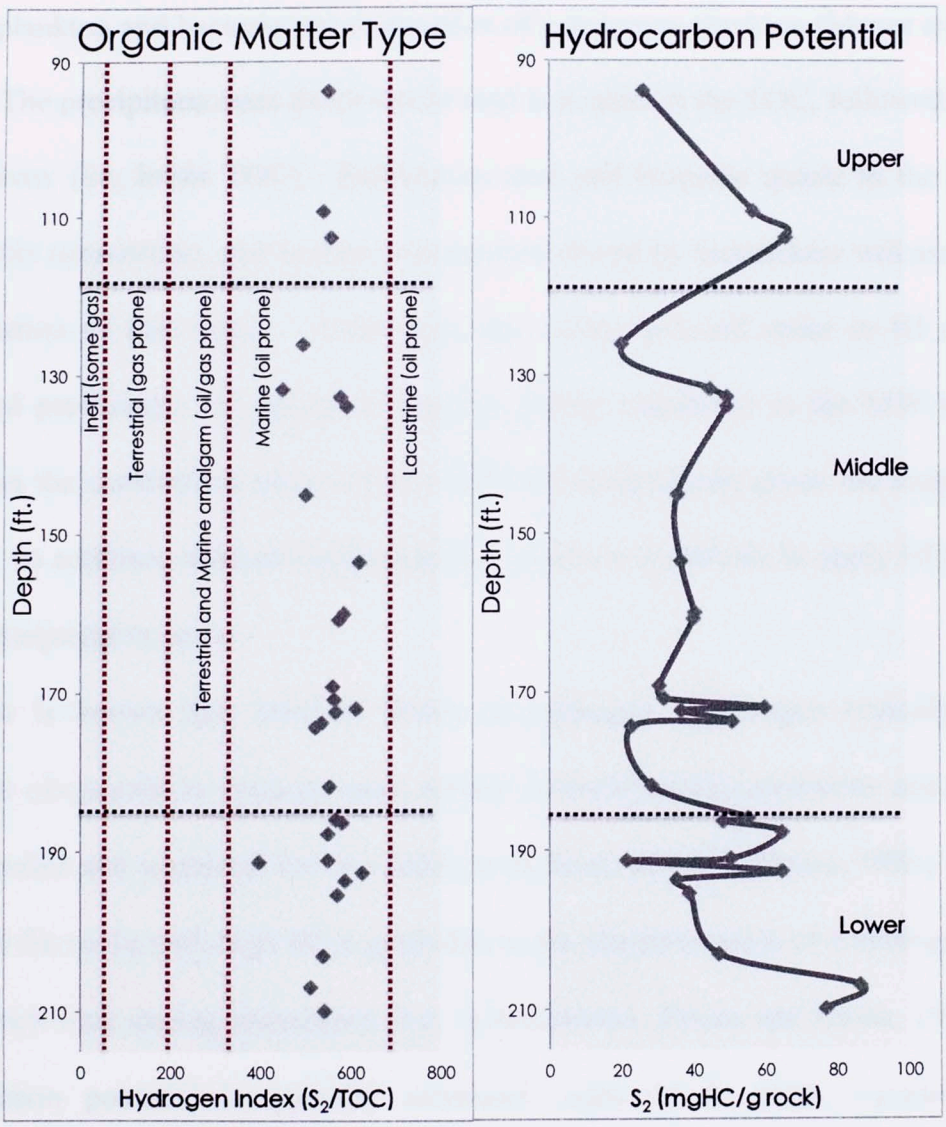

Figure 22. Hydrogen index and S_2 variability with depth in the Woodford Shale of the Wyche-1 core. HI is employed to evaluate the nature of the organic matter comprising a source rock and S_2 to assess its hydrocarbon potential.

respectively. The minimum and maximum HI values (400 and 625) were separated by only ~1 ft., which corresponds with a 7% difference in TOC as well. This highlights the variability shale can exhibit and may be explained by an abrupt, short regression during

the overall TST in the LW. Alternatively, a biotic crisis may have occurred, affecting productivity and subsequent influx of organic carbon to the sediments. An upwelling event has the potential to cause temporary hypoxia, leading to proliferation of organic-walled plankton and bacteria and decimation of calcareous plankton (Meyer and Kump, 2008). The precipitous mass death would lead to a spike in the TOC, followed by lower productivity (i.e. lower TOC). Radiolarian tests and biogenic quartz in the LW may reflect this supposition, and further investigation driven by biomarkers will assist in the confirmation of this theory. Other than the severe inversed spike in HI and TOC discussed previously, HI appears to display greater variability in the MW than does TOC, but the oscillations observed are relatively insignificant given the magnitude of change. In addition, without supplemental evidence it is difficult to apply HI in a more direct interpretative sense.

It is known that elevated levels of hydrogen in kerogen typically signify excellent oil-generative capacity once certain thermodynamic conditions and pressures are exceeded and sustained for thousands to millions of years (Peters, 1986). The oil-potential for rocks with high HI is great due to the transformation of a hydrogen-rich to carbon-rich rock during maturation (i.e. hydrocarbons; Peters and Cassa, 1994). The hydrocarbon potential is typically measured using the S_2 peak, representing the remaining generative capacity of the source rock if favorable thermodynamic conditions are reached or sustained. The Wyche-1 core appears to possess very good hydrocarbon potential, with a similar distribution shown by the TOC values in Figure 20 (Figure 22). If the potential were to be attained, then the source rock would likely generate a mixture of oil and gas. This was inferred from the location of the data points on a pseudo-Van

Krevelen Diagram (Figure 23). The Woodford plots as a Type II kerogen according to HI and OI values. However, Cornford et al. (1998) suggest using alternative typing methods for immature to early mature source rocks via a S_2 v TOC scatterplot, partly due to erroneous OI values obtained in carbonate-rich samples (Figure 24). The slope of this plot is essentially the HI, representing the kerogen quality as previously discussed. This method is affected by maturity however, and should be used with caution (if at all) with mature samples due to the diminishment of HI with increasing maturity. According to this method, the samples still plot as Type II (marine) oil-prone source rocks (Figure 24). The mineral matrix likely had no effect on kerogen characterization, with only organic lean samples (S_2=0-3 mgHC/g rock) predisposed to measurement error (Dahl et al., 2004). The calibration results of the standard from the lab that conducted the TOC and Rock Eval were accurate as well. Therefore, any flaws associated with kerogen typing were likely caused by the immaturity of the samples.

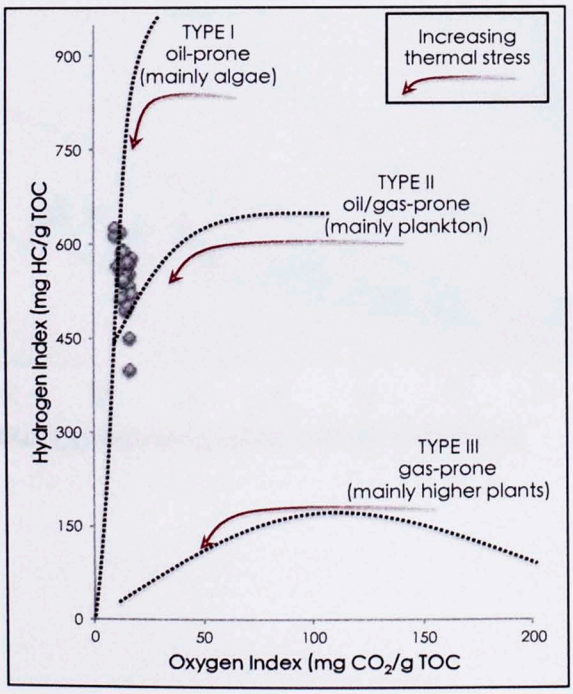

Figure 23. Pseudo-Van Krevelen Diagram plotting HI (y) and OI (x) to assess the kerogen type of the Woodford samples. Most samples plot as Type II, with potential mixing from Type I and Type III in some samples characterized by predominantly Type II.

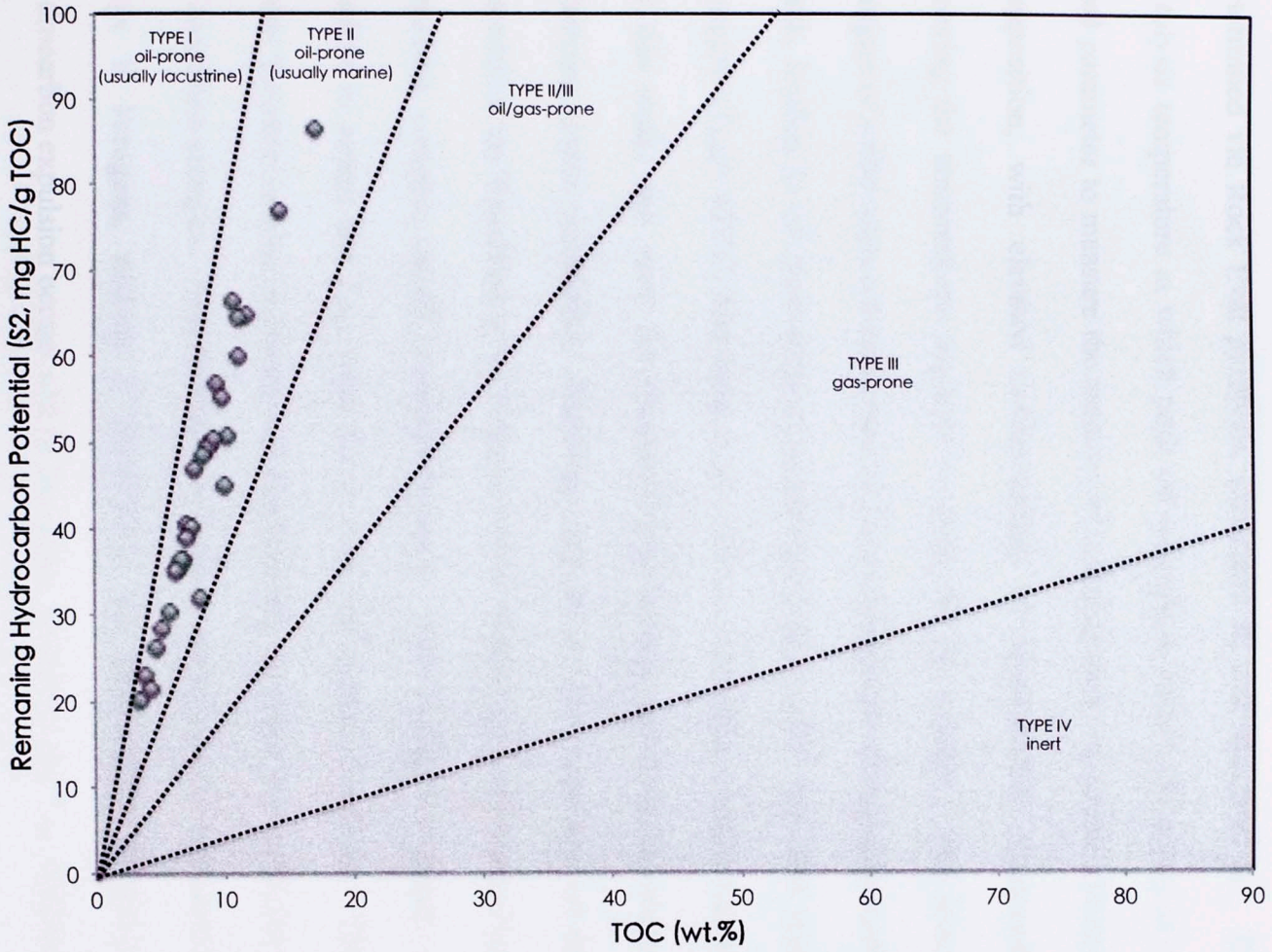

Figure 24. S_2 v TOC plot proposed by Cornford et al. (1998) to determine the kerogen type of the Woodford samples. Specific for immature to early mature source rocks.

3.4. Thermal Maturity

The levels of thermal stress imposed on the Woodford Shale in this study were determined via Rock Eval pyrolysis, calculated R_o and measured R_o. The T_{max}, the pyrolysis temperature at which peak oil generation occurs (S_2 apex), is a commonly used parameter to measure the maturity of a source rock. It can be affected by sample composition, with elevated concentrations of organosulfur compounds typically lowering the temperatures required to reach the oil window. The lower activation energies of sulfur-carbon bonds require lower temperatures than carbon-carbon bonds to break, leading to oil generation at temperatures up to 30°C less than typical Type II kerogens (T_{max}= 435°C; McCarthy et al., 2011). The sulfur content was not measured for this study, nor were the required multi-heating rate experiments conducted to determine kinetic parameters. Therefore, any effect sulfur may have on the generation potential of the Woodford is not discussed here. Additionally, kerogen (Figure 25) is an incredibly complex, poorly understood matrix. Each kerogen is unique, and it is not possible to assign one T_{max} value for a 'class' of source rock types. The number of bonds between various elements will be different, resulting in a particular distribution of activation energies. This distribution is highly unlikely to be replicated between two Type II kerogens, making it improbable the temperature at which maximum hydrocarbon expulsion occurs will be the same. However, the T_{max} temperatures for the samples ranged from 410-428°C, with a mean of 421°C (Table 5). These data indicate a thermally immature rock throughout the core, with potentially the highest measurements in the early oil window (Figure 26). Calculated vitrinite reflectance, from T_{max}, provided a similar conclusion regarding maturity. Samples plot in the

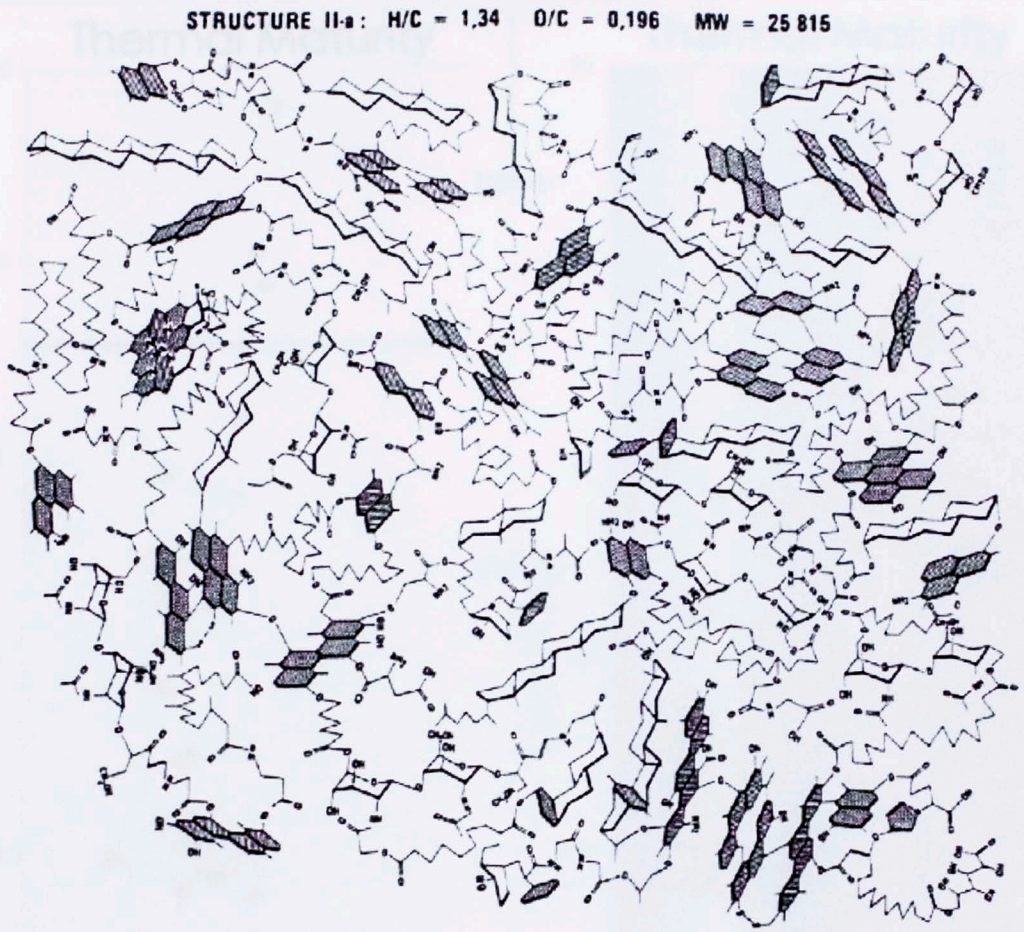

Figure 25. Illustration of the structural complexity associated with a Type II kerogen, underlining the uncertainty with which T_{max} is so loosely applied (Vandenbroucke and Largeau 2007).

immature zone (Figure 26), minimally changing with depth. Romero (2008) obtained similar results for calculated R_o, shown in Table 6. In addition, vitrinite was measured in the previous study, with an average of 0.55% R_o for the three samples observed. This is slightly higher than the average calculated R_o, but can be explained by inherent flaws associated when transforming values from one parameter to another. The calculated values in this study also closely resemble vitrinite reflectance maps constructed by Cardott (2012). The area marked LH (Lawrence Horst = Lawrence Uplift) is the location of the study area (indicated by red arrow), and is characterized by R_o of ~0.50

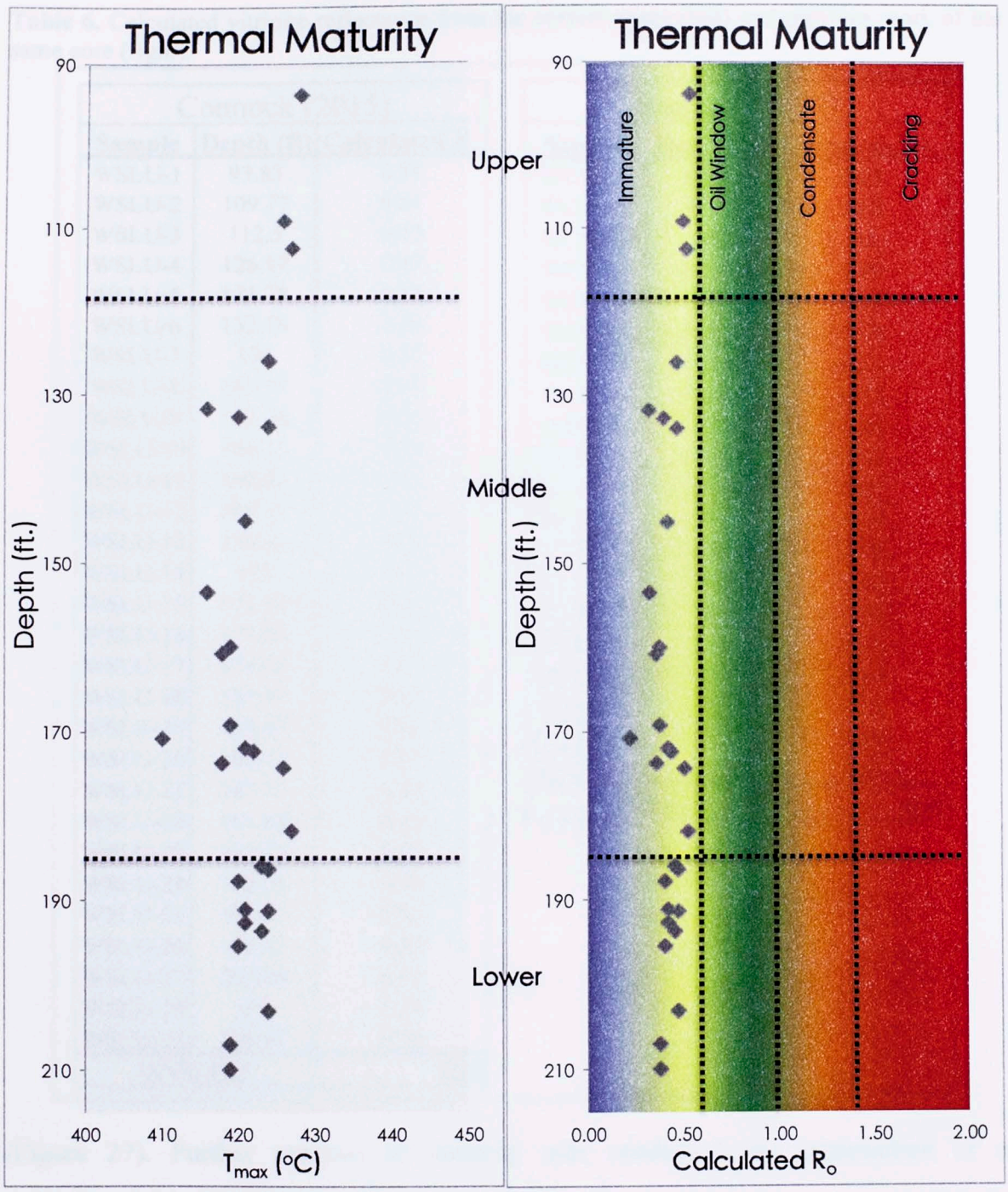

Figure 26. Geochemical logs of T_{max} (left) and calculated R_o(right), with the latter color shaded to assist in illustration of various parts of the maturation process. Data points are derived from the data in this study, with Romero (2008) not included due to potential discrepancies between maturity data.

Table 6. Calculated vitrinite reflectance from the current study (left) and previous work of the same core (right).

Connock (2015)		
Sample	**Depth (ft)**	**Calculated R_o**
WSLU-1	93.83	0.54
WSLU-2	109.17	0.51
WSLU-3	112.5	0.53
WSLU-4	126.17	0.47
WSLU-5	131.75	0.33
WSLU-6	132.75	0.40
WSLU-7	134	0.47
WSLU-8	145.17	0.42
WSLU-9	153.58	0.33
WSLU-10	160.17	0.38
WSLU-11	160.83	0.36
WSLU-12	169.33	0.38
WSLU-13	170.92	0.22
WSLU-14	172	0.42
WSLU-15	172.42	0.44
WSLU-16	173.83	0.36
WSLU-17	174.42	0.51
WSLU-18	181.92	0.53
WSLU-19	185.92	0.45
WSLU-20	186.42	0.47
WSLU-21	187.75	0.40
WSLU-22	191.08	0.42
WSLU-23	191.33	0.47
WSLU-24	192.75	0.42
WSLU-25	193.75	0.45
WSLU-26	195.42	0.40
WSLU-27	203.08	0.47
WSLU-28	207	0.38
WSLU-29	209.92	0.38
AVERAGE		0.42

Romero (2008)		
Sample	**Depth (ft)**	**Calculated R_o**
WCWF 1	92.21	0.63
WCWF 2	97.92	0.62
WCWF 3	103	0.6
WCWF 4	107.08	0.49
WCWF 5	111	0.47
WCWF 6	113.08	0.69
WCWF 7	115.13	0.53
WCWF 8	118.04	0.45
WCWF 9	121.17	0.53
WCWF 10	123.13	0.47
WCWF 11	130.41	0.31
WCWF 12	139.15	0.49
WCWF 13	151.08	0.38
WCWF 14	157.83	0.42
WCWF 15	170.45	0.26
WCWF 16	181.04	0.36
WCWF 17	186.9	0.49
WCWF 18	192.35	0.33
WCWF 19	198.21	0.29
WCWF 20	208.08	0.42
AVERAGE		0.46

(Figure 27). Further analysis of maturity was conducted via construction of a normalized oil content (NOC) log (Figure 28). NOC is a function of the S_1 peak normalized to TOC, or the free hydrocarbons normalized to the TOC. If the organic content is sufficient, the rock will begin to expel hydrocarbons at maturity, with more hydrocarbons being generated as the correct conditions are maintained. A low NOC is explained by either lack of hydrocarbon genesis due to immaturity, or thermal

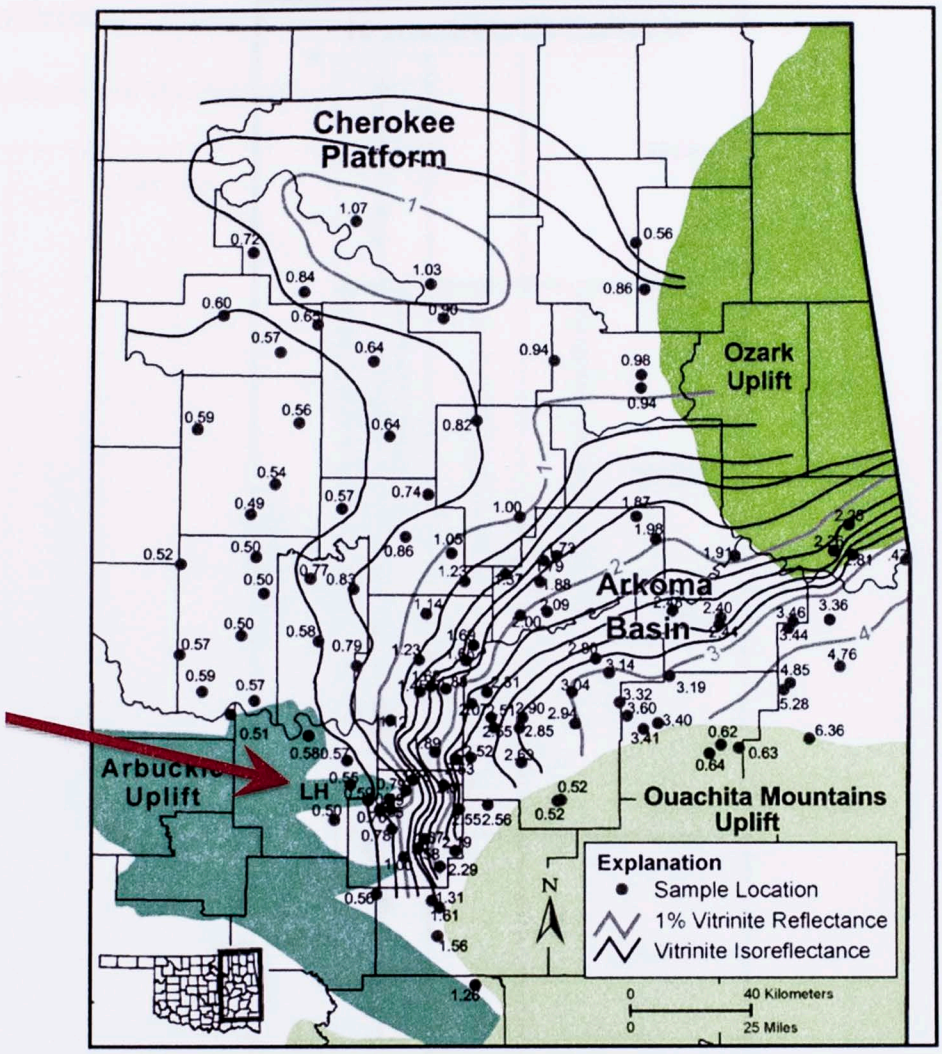

Figure 27. Contoured map of vitrinite reflectance of the Woodford Shale in eastern Oklahoma (modified from Cardott 2012). Red arrow indicates the relative location of the Wyche-1 shale pit in the Lawrence Uplift/Horst.

destruction of hydrocarbons as in overmature source rocks. Figure 28 indicates this scenario, with previous maturity data ruling out the possibility of hydrocarbon degradation, leaving immaturity, or volatilization of hydrocarbons prior to analysis, as the correct explanation. Of the three members, the LW and UW appear to contain certain sections nearing the low maturity window, but the probability of any significant hydrocarbon generation is very low. Lastly, HI and T_{max} were integrated as a cross plot

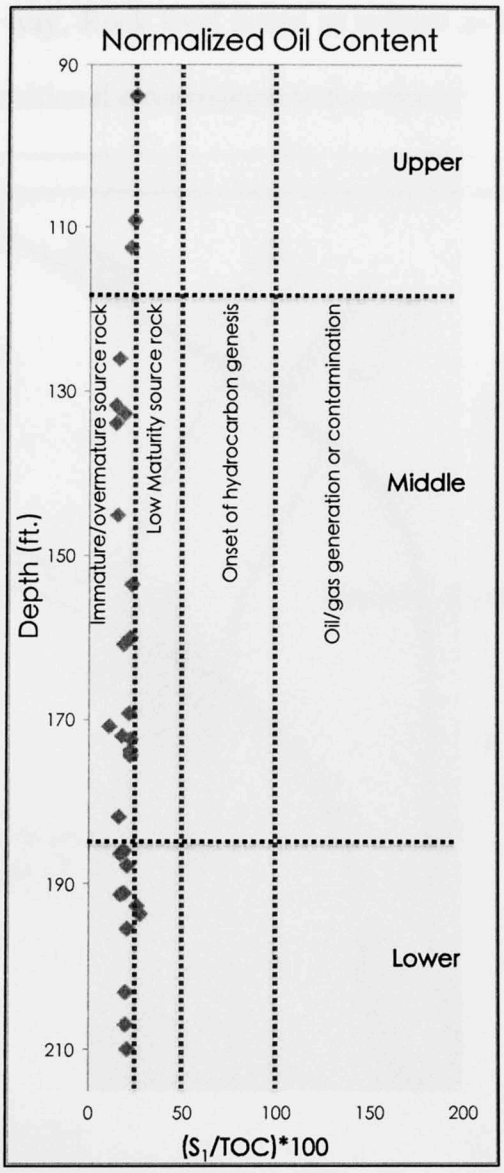

Figure 28. Geochemical log of normalized oil content displaying the immature nature of the studied core. NOC was likely not affected by overmaturity due to geovalidation with T_{max}, S_1 and S_2 data.

to assess the kerogen type (HI) and maturity (T_{max}) simultaneously. Results confirm the source rock is immature, but indicates some potentially mixed Type II kerogen (Figure 29). However, this observation can be accounted for as the placement of the Type II vector, or the fact the data points predominantly plot along the Type II line meaning this

is an aberration. Either way, Rock Eval is not as refined as biomarker analyses when determination of the depositional environment is the objective.

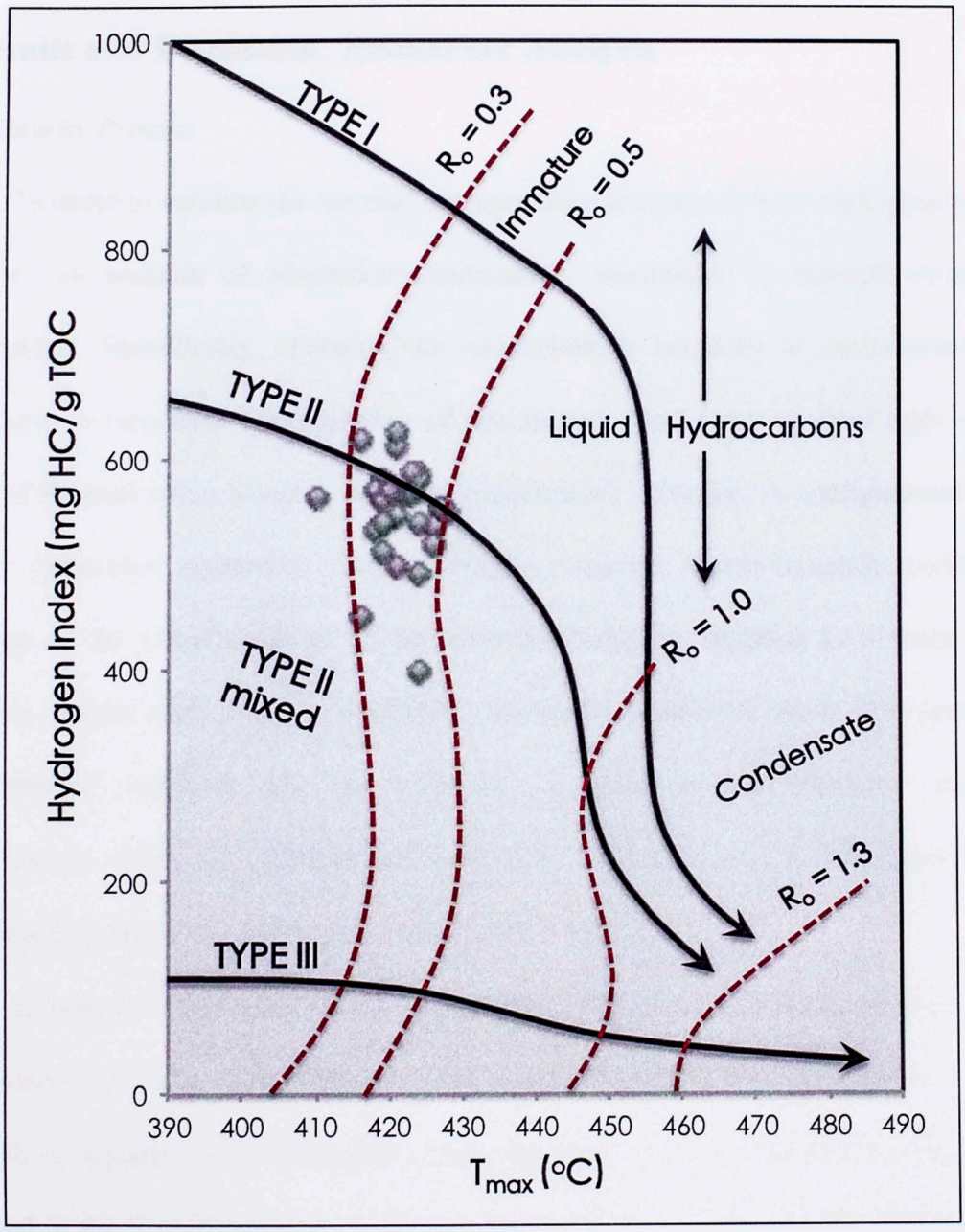

Figure 29. Kerogen classification and maturity assessment via integration of HI and T_{max} data. This plot depicts the kerogen type and maturity level simultaneously, allowing for a convenient composite of the primary interpretations from Rock Eval data.

CHAPTER IV

4. Results and Discussion: Biomarker Analysis

4.1. Maturity Proxies

In order to validate the thermal maturity data determined from bulk geochemical methods, an analysis of biomarkers particularly susceptible to thermal stress was undertaken. Specifically, characteristic isomerization reactions at stereocenters and alterations to structural configuration of the steranes and hopanes shed light on the levels of thermal stress a source rock has experienced. Changes in configuration occur due to molecular adaptation to increasingly energetic thermodynamic conditions, resulting in the transformation of the molecule from an unstable to a more stable structure (Peters et al., 2005). In addition, two novel maturation ratios were developed and assessed explicitly for the immature to early mature windows involving isomerization of the C_{21} cheilanthanes (tricyclic terpanes) and the hydrogenation of unsaturated pentacyclic terpanes to saturated derivatives.

In nature, there is no known organism capable of synthesizing sterols in the S configuration at C-20. Therefore, all sterols and subsequent steroid derivatives can be assumed to initially have undergone some diagenetic and/or catagenetic effect when observed in the S configuration (Volkman, 2005; Brocks and Summons, 2013). When assessing maturity, the isomerization of C-20 in the C_{29} 5α, 14α, 17α(H)-steranes is highly applicable from the immature to mature range due to the gradual thermal evolution of the S/R ratio until it reaches equilibirum at ~0.55 (Mackenzie et al., 1980; Seifert and Moldowan, 1986; Peters et al., 1990). Intially, the biological 20R

configuration is degraded, producing a mixture of the two isomers (Requejo, 1994). Continued elevation of thermal stress will eventually begin to degrade both isomers, underlining thermal degradation as the primary control mechanism of this ratio. In certain cases, biased generation of the 20S (Dzou et al., 1995) or organic matter composition (Strachan et al., 1989) may effect this ratio as well. Isomerization of the C-14 and C-17 positions of the C_{29} 20S and 20R steranes produces an additional sterane maturity parameter slightly less susceptible to organofacies differences and more appropriate at differentiating higher maturities due to a higher equilibirum ratio of ~0.7 than 20S/20R (Seifert and Moldowan, 1986; Peters et al., 1990). This ratio utilizes the enhanced thermal resistance of the αββ steranes relative to the less stable ααα biologically-produced configuration. This parameter is still susceptible to particular pitfalls, such as contribution of the αββ steranes from kerogen as thermal stress increases and organofacies effects. Despite these shortcomings, sterane ratios are among the most heavily employed maturity parameters in biomarker geochemistry (Farrimond et al., 1998). Isomerization reactions involving the pentacyclic triterpanes (hopanes, **XXXV**) and tricyclic terpanes (cheilanthanes, **XXXIII**) are capable of assessing source rock maturity based on similar premises as those above, but excel in different regions of the oil window. The C_{31}-C_{35} 17α-homohopanes undergo steroechemical changes at C-22 earlier than most biomarkers applied to maturity assessment (Ensminger et al., 1977). This allows for better characterization of source rocks in the earlier stages of the oil window, making the 22S/(22S+R) ratio possibly the most utilized hopane maturity parameter in petroleum geochemistry (Farrimond et al., 1998). As maturity increases, the S/R ratio increases until equilibrium at ~0.55. Similar

to the C_{31} 22R, the biologically produced 17β, 21α(H)-moretanes (**XL**) are less resistant to thermal degradation compared to the corresponding 17α, 21β(H)-hopanes (**XXXV**). Unlike previous ratios where isomer mixtures increase to equilibria, the moretanes (**XL**) should be absent in mature source rocks and oils, unless contaminated. Farrimond et al. (1998) found the ratio to decline from 0.6 (moretane/hopane) to 0, whereas Seifert and Moldowan (1980) observed a decrease from 0.8 to 0.05. The initial ratio will vary between samples due to variations between depositional environments, with hypersaline source rocks containing elevated concentrations of moretane/hopane relative to interbedded shales (Rullkotter and Marzi 1988).

The Woodford in the Wyche Farm Shale Pit was found to be thermally immature based on low (< 435°C) T_{max} values (AVG=421°C). Biomarker parameters (see Appendix **II** for specific formulae and Appendix **III** for identification) reveals a similar conclusion (averaged values for Wyche-1 core in parentheses), with the C_{29} ααα 20S/20R (0.17), C_{29} αββ/ααα (0.35), C_{31} 22S/22R (0.37), and C_{30} moretane/hopane (0.42) ratios yet to reach equilibrium (Table 7). When compared to T_{max} data, no relationships appear between the bulk geochemical data and biomarker data (e.g. Figure 30). The lack of a strong trend between the maturity parameters and the T_{max} values is unsurprising given the immature state of the Woodford in this study. This is likely explained by depositional effects imposed on the source rock that lead to various genetic differences in biomarker composition and distribution throughout the core yet to be normalized by thermal effects. Overall, the entire core is immature with minimal variations in maturity with depth (Figure 31). Due to the very low maturities characterizing the samples, an attempt was made to exploit the vast array of unsaturated

Table 7. Biomarker parameters utilized to assess the levels of thermal stress the Woodford was subjected to in the study area. Sterane, hopane, cheilanthane, moretane, and hopene ratios assist in evaluating the amount of thermal stress each sample experienced.

Sample	T_{max} (°C)	C_{29} ααα 20S/(20S +20R)	C_{29} αββ/(ααα +αββ)	C_{31} 22S/(22S +22R)	C_{30} Moretane/ C_{30} Hopane	C_{21} Tri ββ/ (βα+αα)	Σ C_{30}-C_{35} Hop-(17)21-enes / ΣC_{30}-C_{35} Hopanes
WSLU-1	428.00	0.13	0.25	0.36	0.36	0.19	0.15
WSLU-2	426.00	0.19	0.47	0.43	0.36	0.25	0.22
WSLU-3	427.00	0.20	0.33	0.44	0.39	0.25	0.25
WSLU-4	424.00	0.19	0.31	0.42	0.30	0.16	0.17
WSLU-5	416.00	0.17	0.29	0.30	0.56	0.21	0.29
WSLU-6	420.00	0.17	0.30	0.31	0.42	0.23	0.20
WSLU-7	424.00	0.15	0.39	0.32	0.34	0.21	0.16
WSLU-8	421.00	0.15	0.28	0.34	0.33	0.21	0.12
WSLU-9	416.00	0.15	0.29	0.33	0.46	0.22	0.16
WSLU-10	419.00	0.16	0.29	0.34	0.47	0.22	0.18
WSLU-11	418.00	0.17	0.30	0.36	0.42	0.20	0.17
WSLU-12	419.00	0.16	0.29	0.36	0.36	0.20	0.17
WSLU-13	410.00	0.17	0.30	0.34	0.42	0.22	0.21
WSLU-14	421.00	0.18	0.31	0.35	0.44	0.20	0.27
WSLU-15	422.00	0.18	0.31	0.36	0.50	0.18	0.31
WSLU-16	418.00	0.18	0.31	0.35	0.44	0.21	0.28
WSLU-17	426.00	0.17	0.43	0.36	0.46	0.17	0.28
WSLU-18	427.00	0.16	0.45	0.38	0.38	0.17	0.13
WSLU-19	423.00	0.18	0.48	0.37	0.45	0.23	0.19
WSLU-20	424.00	0.17	0.46	0.38	0.41	0.22	0.19
WSLU-21	420.00	0.17	0.47	0.37	0.42	0.22	0.18
WSLU-22	421.00	0.17	0.47	0.37	0.38	0.21	0.19
WSLU-23	424.00	0.18	0.31	0.38	0.43	0.18	0.26
WSLU-24	421.00	0.18	0.32	0.38	0.41	0.20	0.23
WSLU-25	423.00	0.18	0.31	0.39	0.40	0.18	0.26
WSLU-26	420.00	0.18	0.31	0.38	0.38	0.20	0.22
WSLU-27	424.00	0.18	0.33	0.39	0.43	0.21	0.23
WSLU-28	419.00	0.20	0.35	0.37	0.49	0.21	0.31
WSLU-29	419.00	0.21	0.35	0.38	0.56	0.20	0.40
Average	421.38	0.17	0.35	0.37	0.42	0.21	0.22

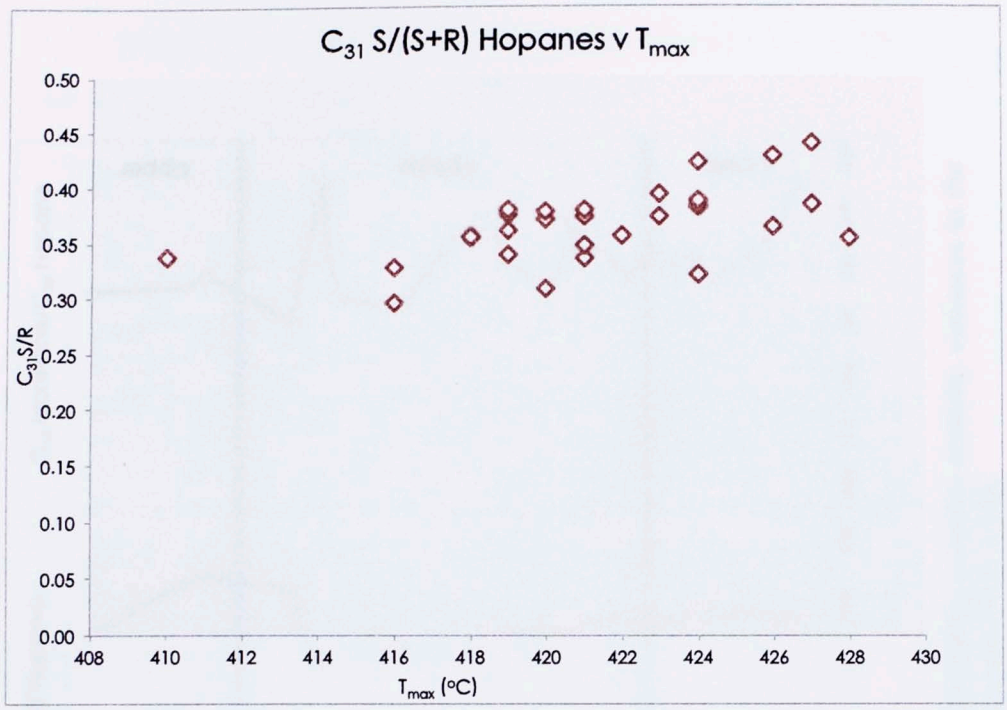

Figure 30. Cross-plot displaying the relationship between the hopane isomerization ratio and T_{max}. No other conventional maturity parameters correlated with bulk geochemical data.

compounds typically not detected in such abundance in a source rock. Similar to Aquino Neto et al. (1986), the thermally unstable C_{21} ββ cheilanthane comprise the numerator and the diagenetic βα and αα products the denominator of a ratio suited to qualitatively describe source rocks from the immature-early mature window. Unfortunately, the minimal maturity differences throughout the sample set likely explained the lack of trend observed. Additionally, the C_{30}-C_{35} hop-17(21)-enes (**XLI**) were normalized by the corresponding hopanes (**XXXV**), but little relationship was observed with depth. However, the sum of the C_{30}-C_{35} hopenes/ C_{30}-C_{35} hopanes plotted against the C_{29} sterane S and R isomers produces a subtle relationship (Figure 32). Despite the sterane isomers lack of agreement with the T_{max} values, this is an

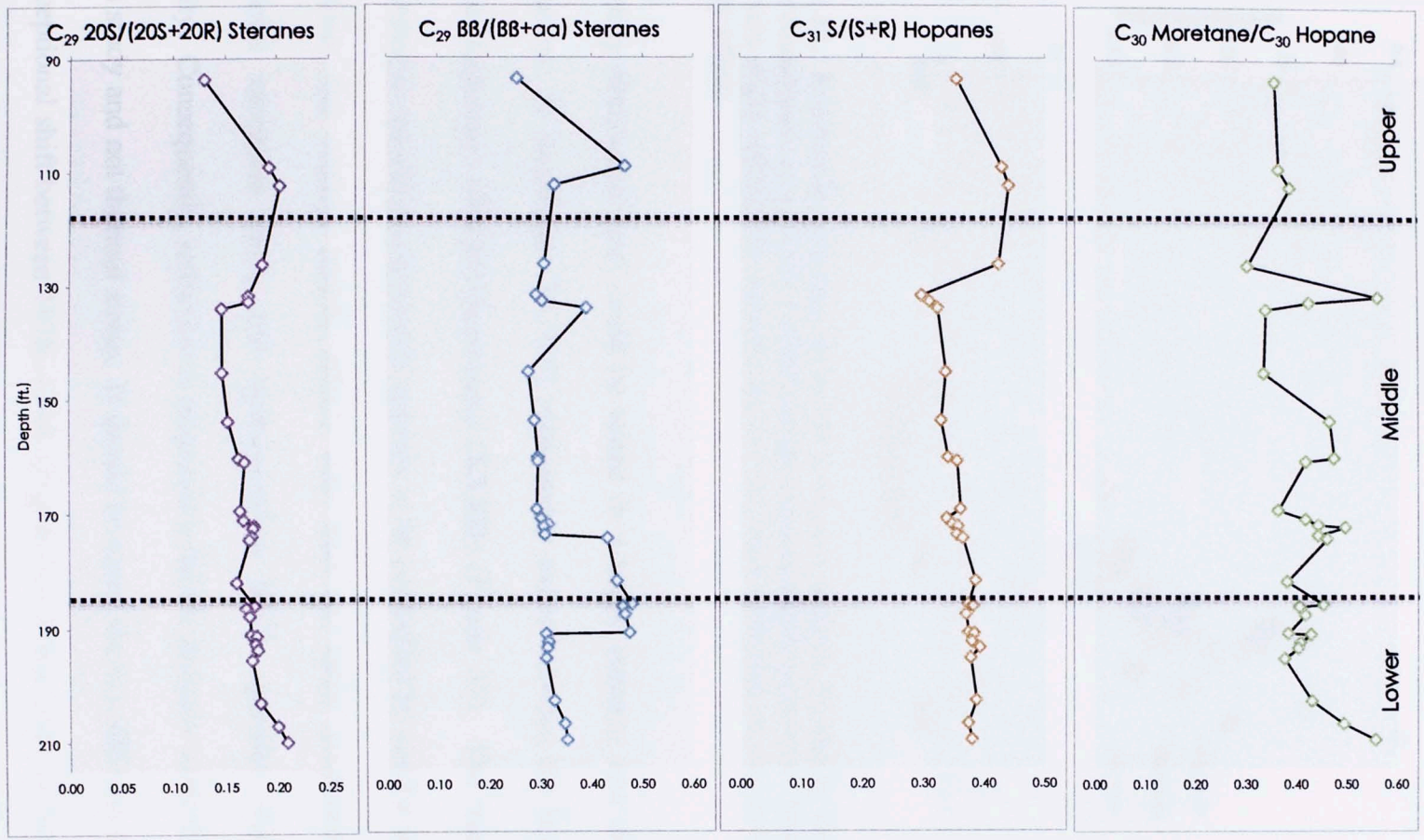

Figure 31. Geochemical logs of sterane and hopane isomerization ratios illustrating potential maturity variances in the Wyche-1 core. Note the pronounced shift in the C_{29} $\beta\beta/(\beta\beta+\alpha\alpha)$ steranes between 191ft.-174ft.

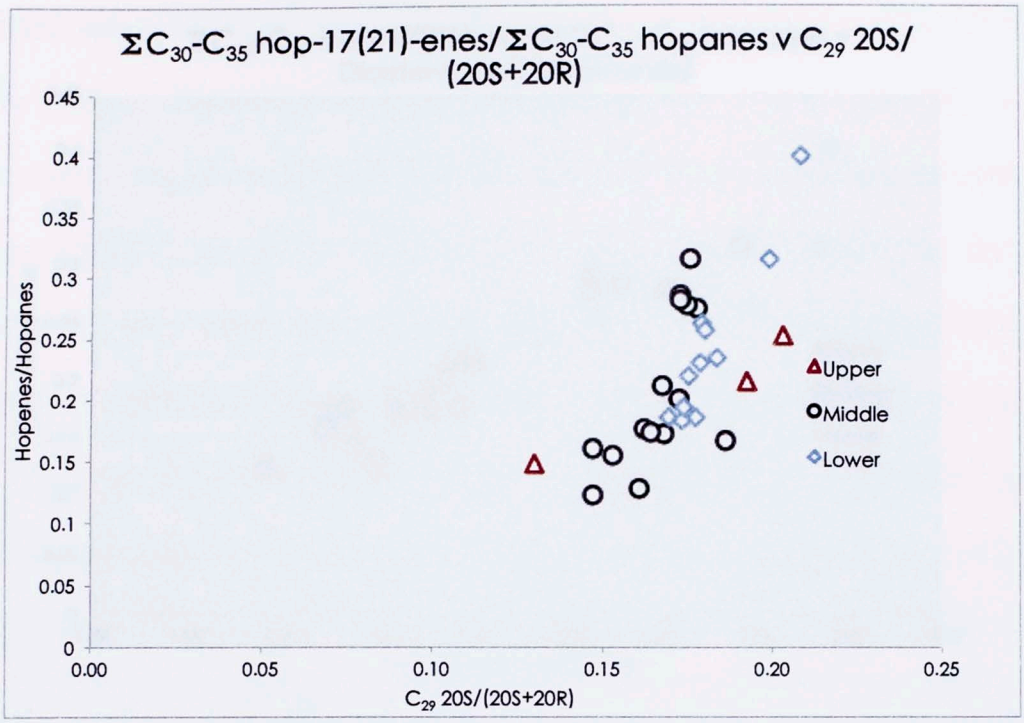

Figure 32. Relationship between the series of C_{30}-C_{35} hopenes divided by the corresponding hopane counterparts as a function of the sterane isomer maturity parameter. Note the axis scale, as the very slight relationship between the two are likely reflecting environmental features, not maturity effects.

interesting observation and could be tested in a larger maturity and depth range for application. A significant (R_2>0.9) relationship exists between the hopenes/hopanes and the diasterenes (**XXXI**)/diasteranes (**XXXII**) (Figure 33). The transformation of unsaturated to saturated compounds appears to be controlled by similar thermodynamic conditions, but mineral matrix effects may bias the latter proposed parameter if lithofacies variations exist, and hydrogenation likely operates independently of maturity. Consequently, reduction is proposed to be the primary control on these ratios in this study and not thermal stress. It should be noted the C_{29} αββ/ααα steranes exhibit an exceptional shift between 191ft.-174ft. (Figure 31) where none of the other maturity ratios display a similar shift. It is difficult to explain this in the scope of maturity alone, since neither the T_{max} or biomarkers reflect this trend. Instrumentation error, incorrect

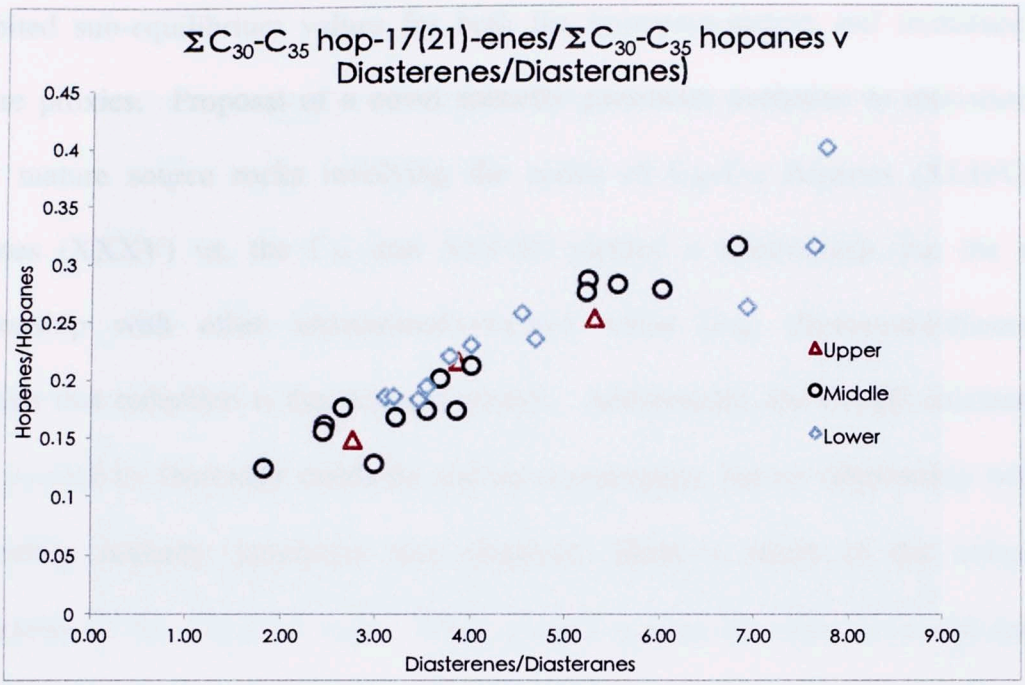

Figure 33. Assessment of additional maturity parameters specific to immature-early mature. The hopenes and diasterenes are divided by the hopanes and diasteranes, respectively. Hydrogenation in immature-early mature source rocks is probably genetic function, unrelated to maturity.

calculation of standard concentration, or other experimental errors could be responsible, but this shift is confined to a specific depth interval by six points with elevated ββ steranes, making error unlikely. Barring experimental issues, it could be a function of abrupt changes in the depositional environment, especially if conditions became more restricted leading to hypersalinity (ten Haven et al., 1986), resulting in the observed predominance of ββ steranes. These six data points (191ft.-174ft.; Figure 31) may be affected by various organofacies within the Woodford or delineate environmental changes.

The biomarker maturation proxies supported inferences from T_{max} data, indicating a thermally immature source rock with minimal depth variation. Well established maturity parameters reliant on thermally-induced isomerization reactions

exhibited sub-equilibrium values for both the immature-mature and immature-early mature proxies. Proposal of a novel maturity parameter exclusive to immature-very early mature source rocks involving the series of C_{30}-C_{35} hopenes (**XLI**)/C_{30}-C_{35} hopanes (**XXXV**) vs. the C_{29} ααα S/(S+R) yielded a relationship, but the strong relationship with other unsaturated/saturated ratios (e.g. diasterenes/diasteranes) suggests that reduction is the primary control. Additionally, the C_{21} ββ chielanthanes were divided by thermally stable βα and αα counterparts, but no relationship with any preexisting maturity parameter was observed, likely a result of the ubiquitious immaturity of the Wyche-1 core. When plotted against the other proposed maturity parameter (hopenes/hopanes), no trend was depicted (Figure 34). Genetic differences and lack of a specific source (e.g. prokaryotes→hopanes) likely compound any thermal effects imposed on cheilanthane sterochemistry. Other than the inability to test the proposed maturity indicators adequately, the immature nature of the samples ensures subsequent biomarker analyses will reflect genetic environmental artifacts and not secondary products of thermal alteration.

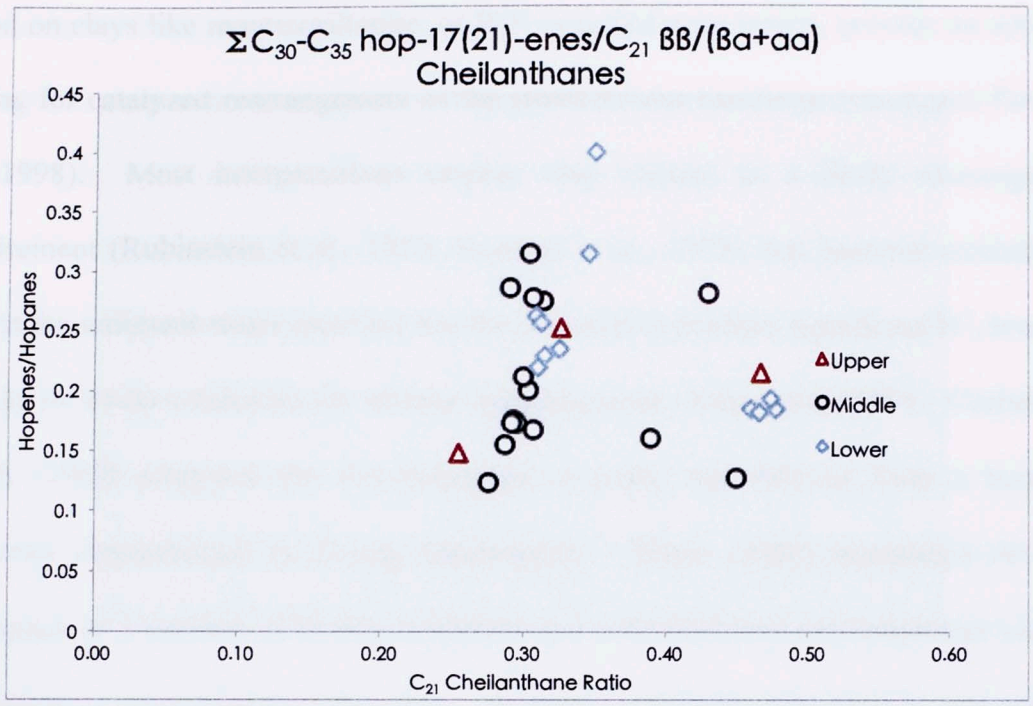

Figure 34. Cross plot of the two proposed maturity parameters, the sum of the C_{30-35} hopenes/the sum of the C_{30-35} hopanes vs. the C_{21} ββ cheilanthane/ C_{21} βα+αα cheilanthane.

4.2. Lithologic Proxies

The diasteranes (**XXXII**), diasterenes (**XXXI**), C_{30} diahopane, neohop-13(18)-enes (**XXXIX**), and benzohopanes (**XLII** and **XLIII**) comprise a unique suite of biomarkers capable of characterizing the lithology of a source rock. This application is constructed upon a foundation of previous research outlining the effects of mineral matrices on rearrangement reactions required to produce these compounds, or correlations between distinct environments/lithologies and the occurrence of particular biomarkers (e.g. benzohopanes).

Diasteranes (**XXXII**), diasterenes (**XXXI**), diahopane and neohop-13(18)-enes (**XXXIX**) signify acidic and potentially oxic-suboxic (low pH and high Eh) conditions prevailed during diagenesis (Moldowan et al., 1986; Brincat and Abbott., 2001). These acidic conditions may be present in the form of clays or water chemistry. Acid sites

found on clays like montmorillonite, or H_2S saturated pore waters, provide an adequate setting for catalyzed rearrangement of the sterol/sterene backbone (van Kaam-Peters et al., 1998). Most interpretations employ clay content as a likely rearrangement requirement (Rubinstein et al., 1975; Sieskind et al., 1979), but bacterial oxidation of H_2S at the sediment-water interface has the potential to produce significant H^+, lowering the pH to levels conducive for sterene rearrangement (Jorgensen, 1989). Corbett and Smith (1969) proposed the 17α-diahopane structure was derived from a hopanoid precursor characterized by D-ring functionality. Peters (2005) interpreted the 17α-diahopane as a product of D-ring oxidation and acid catalyzed rearrangement via clay mediation of some hopanoid precursor. Prokaryotic bacteria deposited in oxic-suboxic waters and clay-rich sediments appear to correlate with the interpreted environments where these rearranged hopanes are found in the highest concentrations (Philp and Gilbert, 1986). Neohop-13(18)-enes (**XXXIX**) are structural clones of the hopane carbon skeleton (**XXXV**), excluding the methyl shift from C-18 to C-17 (Sinninghe Damste et al., 2014). These unique rearranged hopanes are suggested to be formed by dehydration and isomerization of the hopanols or hop-17(21)-enes (**XLI**) (Moldowan et al., 1991), but earlier work by Berti and Bottari (1968) found hop-17(21)-enes (**XLI**) subjected to substantial acidic environments during isomerization formed neo-13(18)-enes (**XXXIX**). Sinninghe Damste et al. (2014) infers from Ensminger (1977) that the formation of neohop-13(18)-enes (**XXXIX**) requires more aggressive reaction parameters or lengthened reaction times to form relative to hop-17(21)-enes (**XLI**). This is based on the observation by Ensminger (1977) who noted the lack of neohop-13(18)-ene (**XXXIX**) formation from diplotene exposed to montmorillonite at room

temperature for one hour. Therefore, neohop-13(18)-enes (**XXXIX**) may be indicative of harsher, more acidic conditions during diagenesis, but isotopic data is conflicting regarding the proposed hop-17(21)-ene precursor (Sinninghe Damste et al., 2014).

Neohop-13(18)-enes (**XXXIX**) were found to be enriched by 3.5 $^{o}/_{oo}$ to 5.5 $^{o}/_{oo}$ relative to hop-17(21)-enes (**XLI**) (Sinninghe Damste et al., 2014), indicating an alternative source as suggested by Farrimond and Telnaes (1996). However, this contrasts with other research reporting depleted values for both biomarkers (Koster et al., 1998). Similarly, ratios of diasteranes (**XXXII**) vary significantly within similar lithologies, explained by variations in acidity and oxicity of a particular environment (Moldowan et al., 1986). This may be correct, but further study suggests clay mineral availability (not absolute percentage, but relative to TOC) may impact these ratios as well. The sensitive nature of formation explains the surprisingly high concentrations of diasteranes (**XXXII**) relative to steranes (**XXVII, XXVIII, XXIX, XXX**) in some carbonate/marls, and the varying amounts of these biomarkers in samples of similar lithology (van Kaam-Peters et al., 1998). To account for this effect, benzohopanes (**XLII, XLIII**) could be employed to assess any potential aberrations of the diasterenes (**XXXI**) or diasteranes (**XXXII**).

Benzohopanes (hexacyclic hopanes; **XLII, XLIII**) are postulated to form via dehydration reactions of bacteriohopantetrol (BHP; **XXXIV**) very early in diagenesis with subsequent cyclization forming the aromatic ring and side-chain degradation forming the lower homologs (Hussler et al., 1984). However, Rinaldi et al. (1988) proposed homologs of lower carbon numbers were formed from biological oxidation prior to diagenetic effects while others believe mineral matrices mediate acid-catalysis

due to the occurrence of these compounds in immature source rocks (Hussler et al., 1984). Despite conflicting belief on formation, the association of benzohopanes (**XLII, XLIII**) with sulfur-rich carbonate and evaporite lithologies provides these compounds with interpretative powers to the geochemist. Connan and Dessort (1987) found the C_{32}-C_{36} homologs to occur predominantly in carbonates and evaporites characterized by extremely anoxic conditions (determined via Pr/Ph). Benzohopanes (**XLII, XLIII**) are not necessarily limited to carbonate or evaporite source rocks though, with noted occurrences in many oils and source rocks in low abundance (Hussler et al., 1984).

In this study, the diasterane/sterane and diasterene/sterane ratios (for all formulae and biomarker identifications discussed in this section, refer to Appendices **II** and **III**; Appendix **IV** contains a biomarker reference table to assist in following the discussion) are conflicting (Figure 35), likely a result of early diagenetic effects imposed by mild thermal stress. In order to address this discrepancy, ratios were compared with the diahopane/hopane parameter to evaluate governing mechanisms. It was found the diasterenes/steranes paralleled the rearranged hopane ratio (Figure 36), and the diasterane/sterane ratio failed to display any relationship (Figure 35). This may be a result of the low diasterane abundances relative to the diasterenes, with the ratio of diasterenes/diasteranes ranging from 1.83-7.78 throughout the entire core and an average value of 4.29 (Table 8). The lack of diasterene conversion to diasteranes potentially destabilizes the use of diasteranes as lithologic proxies, resulting in primary use of the unsaturated precursors. The diasterenes/steranes (DSE/S), diahopane/hopane (C_{30}^{*}/H) and neo-13(18)-enes/hopane (NeoH/H) ratios (clay proxies) will be discussed

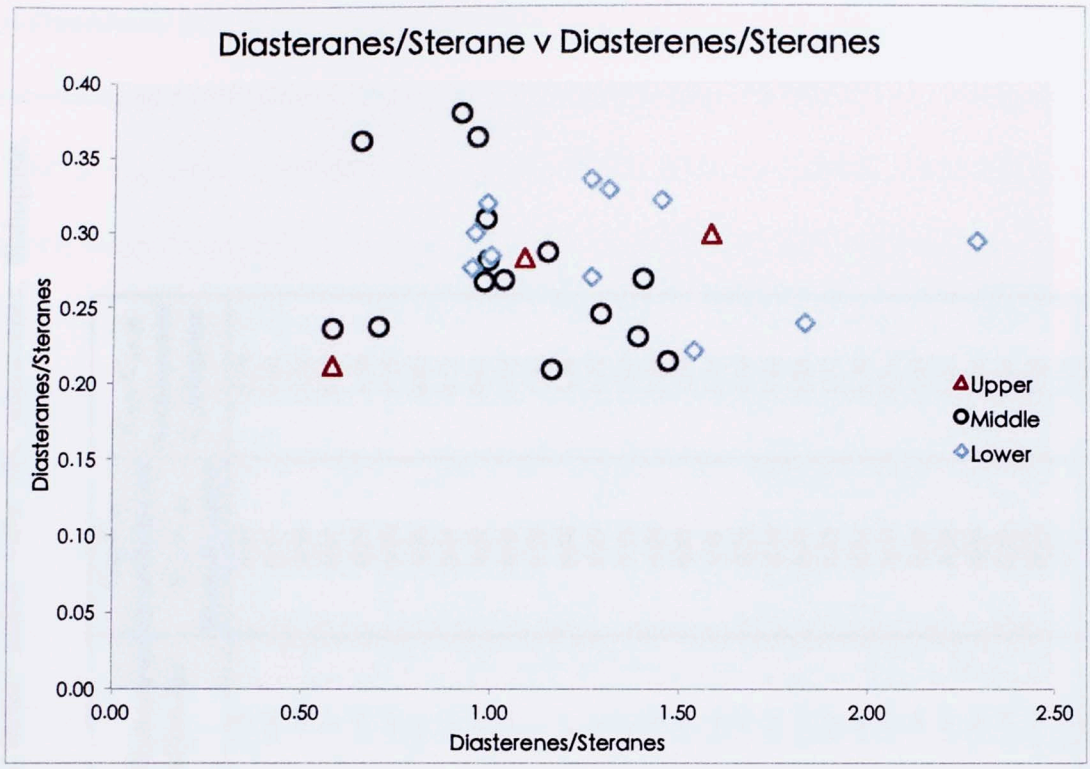

Figure 35. Relationship analysis of diasteranes and the unsaturated precursors, diasterenes. Both rearranged steranes are divided by the regular steranes (C_{27}-C_{29}).

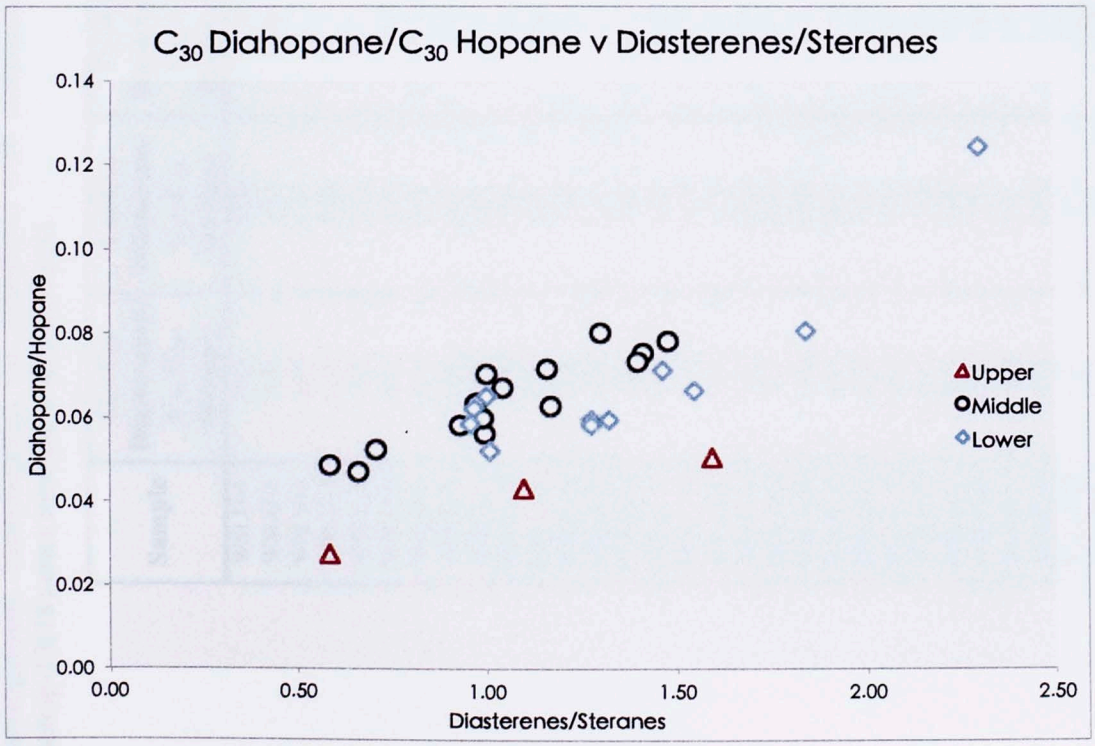

Figure 36. Display of rearranged compounds and potential relationships, indicating a common governing mechanism. The LW data point with the greatest ratios is likely an experimental outlier.

Table 8. Biomarkers affected by lithology (diasteranes, diasterenes, diahopane, neohop-13(18)-enes via clay-induced rearrangement; benzohopanes via correlation with carbonate/evaporite facies) and/or water pH (diasterenes, diahopane, neohop-13(18)-enes increase with lower pH).

Sample	C_{27}-C_{29} Diasteranes/ C_{27}-C_{29} Steranes	C_{27}-C_{29} Diasterene/ C_{27}-C_{29} Steranes	C_{27}-C_{30} Diasterenes/ C_{27}-C_{30} Diasteranes	C_{30}Diahopane/ C_{30}Hopane	C_{32}-C_{35} Benzohopanes /C_{32}-C_{35} Homohopanes	C_{27}, $C_{29\text{-}30}$ Neohopenes/ C_{30}Hopane
WSLU-1	0.21	0.58	2.76	0.03	0.48	0.74
WSLU-2	0.28	1.10	3.88	0.04	0.51	1.04
WSLU-3	0.30	1.59	5.33	0.05	0.50	1.20
WSLU-4	0.31	0.99	3.21	0.06	0.42	0.70
WSLU-5	0.25	1.29	5.25	0.08	0.29	1.76
WSLU-6	0.27	0.99	3.69	0.06	0.29	1.39
WSLU-7	0.24	0.58	2.47	0.05	0.36	0.99
WSLU-8	0.36	0.66	1.83	0.05	0.36	0.71
WSLU-9	0.38	0.93	2.45	0.06	0.42	0.93
WSLU-10	0.36	0.96	2.66	0.06	0.43	1.07
WSLU-11	0.27	1.03	3.86	0.07	0.32	1.13
WSLU-12	0.28	1.00	3.55	0.07	0.38	1.07
WSLU-13	0.29	1.15	4.01	0.07	0.49	1.27
WSLU-14	0.27	1.41	5.23	0.07	0.32	1.62
WSLU-15	0.21	1.47	6.84	0.08	0.39	1.74
WSLU-16	0.23	1.39	6.04	0.07	0.42	1.57
WSLU-17	0.21	1.16	5.57	0.06	0.42	1.27
WSLU-18	0.24	0.70	2.98	0.05	0.26	1.04
WSLU-19	0.32	0.99	3.12	0.06	0.34	1.44
WSLU-20	0.30	0.96	3.21	0.06	0.41	1.26
WSLU-21	0.28	0.95	3.46	0.06	0.42	1.31
WSLU-22	0.28	1.01	3.54	0.05	0.41	1.29
WSLU-23	0.22	1.54	6.94	0.07	0.39	1.31
WSLU-24	0.33	1.32	4.01	0.06	0.36	1.49
WSLU-25	0.32	1.46	4.55	0.07	0.50	1.62
WSLU-26	0.33	1.27	3.80	0.06	0.40	1.36
WSLU-27	0.27	1.27	4.70	0.06	0.37	1.24
WSLU-28	0.24	1.84	7.65	0.08	0.39	1.73
WSLU-29	0.29	2.29	7.78	0.12	0.51	2.24
Average	0.28	1.17	4.29	0.06	0.40	1.29

simultaneously due to the similar behaviors of each proxy with depth, and the apparent relationship between them (Figure 37). The LW is characterized by an overall decrease in DSE/S, C_{30}^{*}/H and NeoH/H continuing until 181.92 ft. in the MW. The MW exhibits a subtle decrease following a sharp increase just after the first minimum at 181.92ft before another excursion extending into the UW. The UW displays diminishing diasterenes, diahopanes and neo-13(18)-enes relatively, with DSE/S appearing more sensitive to potential controls than the C_{30}^{*}/H. The benzohopanes/homohopanes (carbonate/evaporite proxy) exhibit a cyclic pattern from the base of the core to the MW at 160.83ft., where the ratio stabilizes somewhat until an abrupt decrease at 131.75ft. at which the clay proxies increase acutely. After this deviation, the carbonate proxy increases into the UW and stabilizes again (Figure 38). In the context of this discussion, the assumption is made biomarker parameters are controlled by lithology (i.e. clay content) alone, and not water acidity. Potential effects from pH/Eh variations will be addressed, with incorporation of the interpretations from this section, in the discussion on water chemistry.

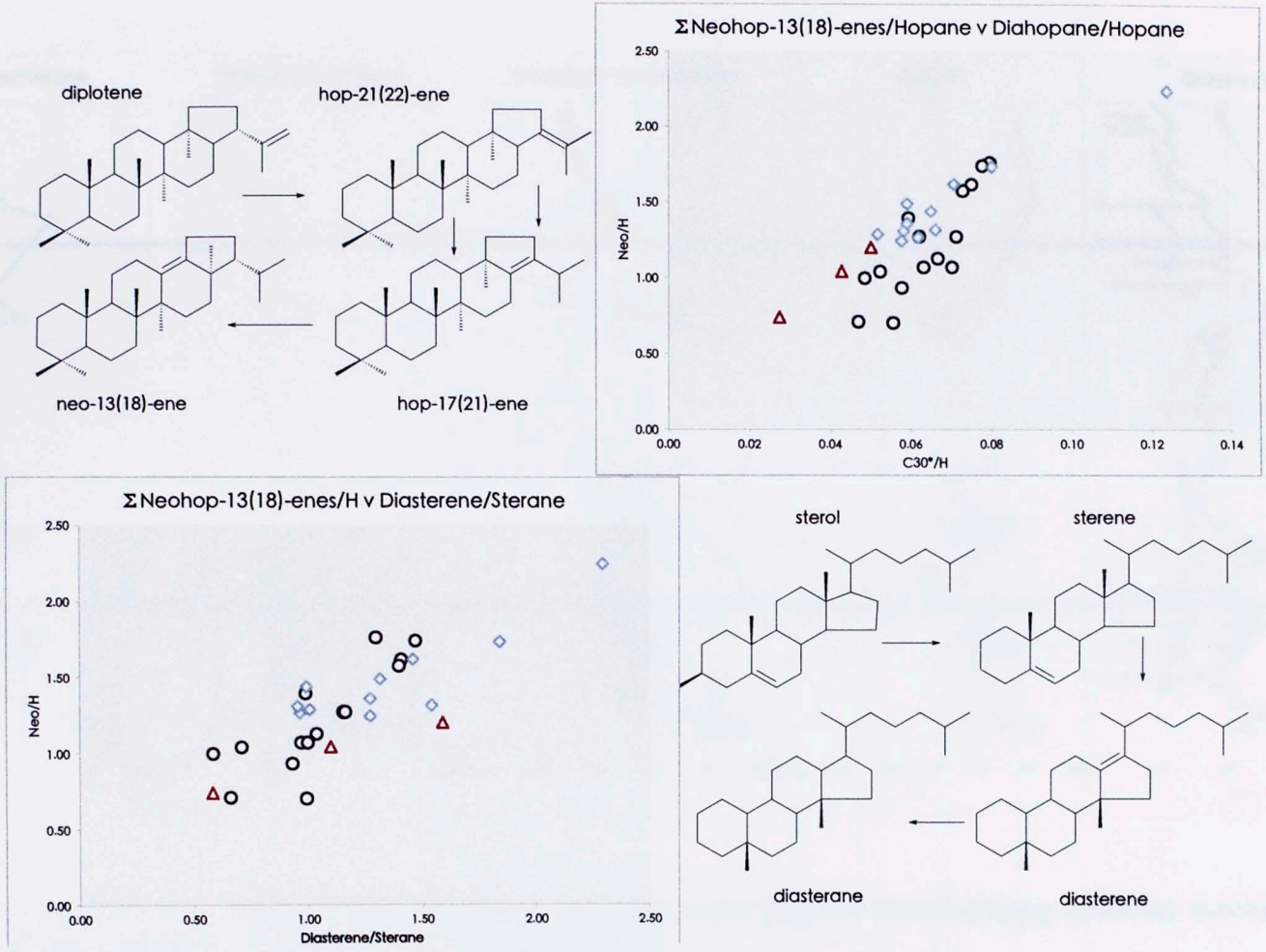

Figure 37. Relationship between well-established clay-catalyzed rearranged biomarkers and the neohop-13(18)-enes with associated reaction pathways adjacent to each figure. The correlation of the nehop-13(18)-enes with both ratios is interpreted as either a clay-catalyzed effect or a product of water acidity.

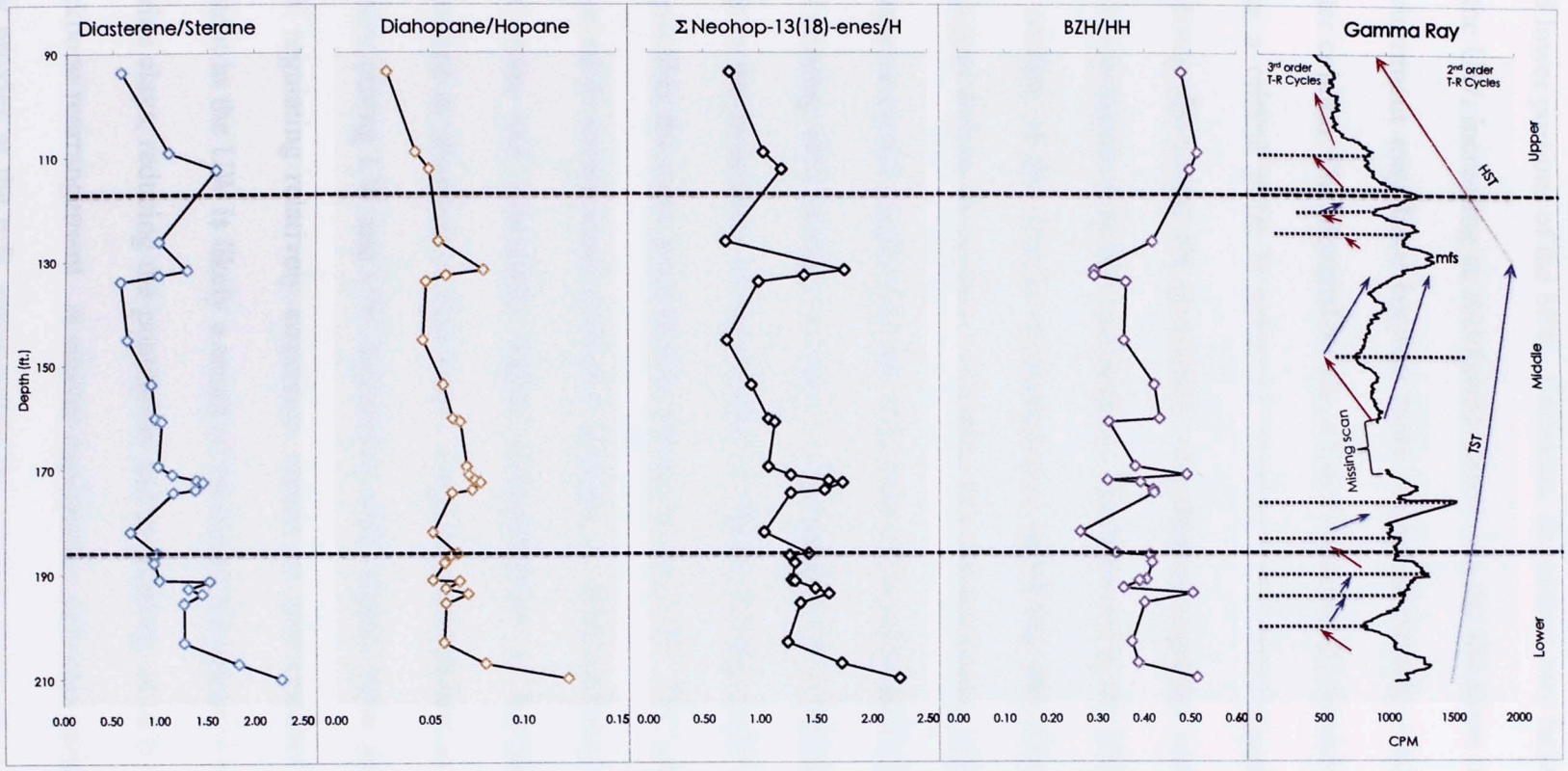

Figure 38. Geochemical and gamma ray logs of lithologic indicators in the Wyche-1 core displaying variability between the three members; sequence stratigraphic framework from Molinares (2013).

The carbonate proxy is difficult to interpret due to rapid fluctuations in the LW and lower portions of the MW. Carbonate deposition may have been more predominant in the UW, increasing as mentioned above. As the shoreline retreated, the depositional environment may have become more restricted causing $CaCO_3$ to supersaturate the water column. The elevated levels of $CaCO_3$ eventually would precipitate from solution once a critical point is achieved, forming carbonate/evaporitie lithologies. Further evidence discussing the possibility of subaerial exposure can be found in DeGarmo (2015) to supplement this explanation. The behavior in the LW and lower MW may be an artifact of the shorter parasequences involving the advance and retreat of the shoreline. Figure 38 appears to confirm this interpretation, with 3rd order transgressive-regressive cycles controlling the abundance of benzohopanes (**XLII, XLIII**). The mfs and ensuing HST portray a clearer relationship with inferred carbonate lithology. A drop in the abundance of benzohopanes (**XLII, XLIII**) at the mfs is logical, explained by possibly the most open marine settings in the MW. The superceding HST would be expected to create more restricted settings, as discussed above, with more carbonate-rich strata and potentially higher concentrations of benzohopanes (**XLII, XLIII**) deposited as observed in this study. Clay proxies indicate an overall decrease in clay content during LW and UW deposition, with slightly more persistent conditions in the MW regulating relatively consistent values for this member. The decrease in clay content in the UW is likely a result of increased terrigenously-source sediment diluting marine clays, reducing the population and availability of acid sites available to catalyze backbone rearrangement. A similar explanation provides insight regarding the spike in clay proxies at the mfs, representing the greatest stand of eustatic sea level. The mfs

marks the base of the condensed section, an interval characterized by condensation. Geologically, condensation describes the incorporation of large temporal intervals into a comparatively thin unit, a result of slow deposition caused by sediment starvation during the maximum landward extent of the shoreline. Prolonged depositional rates theoretically permit a greater period of time for diagenetic reactions to occur in a given interval of sediment, allowing for more rearrangement to occur resulting in elevated levels of these rearranged biomarkers to 'normal' biomarkers. This possibility reveals an alternative mechanism controlling the concentration of rearranged steranes and hopanes in sediments. Shales are, by definition, clay-rich. The concentrations of diasterenes/steranes, diahopane/hopane and neo-13(18)-enes/hopane may not necessarily be subject to the availability or abundance of clays in shales, but rather the rate of deposition. Assuming acidic site availability is the rate-limiting factor, many shales can be considered excellent environments facilitating rearrangement reactions. The governor of the extent to which these reactions occur may be depositional rate, evinced by the sharp rise in these ratios at the mfs as previously mentioned. Slower depositional rates may allow for more rearrangement to occur in one layer of sediment than if sediment was rapidly deposited, potentially hindering the extent of rearrangement in that same layer. It is difficult to extrapolate this logic beyond the mfs, with other regions of the core exhibiting contrasting trends (e.g. increase of diasterene/sterane at the onset of the HST), which instill uncertainty to this proposed application of rearranged biomarkers.

Lithologic proxies in this study show greatest application potential at the mfs, with an inverse relationship between clay proxies (diasterenes (**XXXI**) , diahopane, and

neohop-13(18)-enes (**XXXIX**)) and indicators for carbonate/evaporite lithologies (benzohopanes (**XLII, XLIII**)). In other regions of the core fluctuations can be explained by 3rd order transgressive-regressive cycles, especially in regards to the benzohopanes (**XLII, XLIII**). The UW exhibits the expected behavior of these proxies during an HST, with the influx of terrigenous material diluting fine silicates (clays) causing a drop in diasterene (**XXXI**), diahopane and neohop-13(18)ene (**XXXIX**) concentration and an increase in benzohopanes (**XLII, XLIII**), possibly explained by shallowing and subaerial exposure of the marine environment during this period (for more on subaerial exposure of the UW, refer to DeGarmo, 2015). Alternatively, the decrease in these biomarkers may result from an elevated rate of deposition, regulating the amount of time for diagenetic reactions to affect the arrangement of specific biomarkers. It is proposed, in shales, that rearrangement reactions are inversely proportional to depositional rates. The spike of diasterenes (**XXXI**), diahopanes and nehop-13(18)-enes (**XXXIX**) in the condensed section lend support to this claim, due to the slow deposition characterizing this interval. Further experiments are necessary to elevate this proposal beyond pure conjecture, but the sequence stratigraphic model supports the possibility of this occurrence.

4.3. Age Dating the Woodford Shale

Biomarkers comprise a sliver of the biogeochemical record of life through geologic time, reflecting temporal changes of the biosphere. The Cambrian explosion 540 Mya. marked the rapid diversification of preexisting organisms and the introduction of most phyla present in modern ecosystems (Maloof et al., 2010). Since that period, organisms have evolved, flourished, or perished. These changes through time have been well documented and certain organisms are known to be limited to defined regions of geologic time due to extinction or proliferation. As a result, biomarkers, the geological fossils of biological products, possess the potential to be used as tentative to excellent age-dating tools to ensure analyzed hydrocarbons are genetic features and not secondary contaminants.

Initially, the C_{28}/C_{29} sterane ratio was used in order to establish a general understanding of the age-range of the samples. The steranes are comprised of the cholestanes (C_{27}; **XXVII**), ergostanes (C_{28}; **XXVIII**) and stigmastanes (C_{29}; **XXIX**), which are biosynthesized by no particular eukaryotic group. Despite the lack of source-specificity beyond linkage to eukarya, the ergostanes (**XXVIII**) and stigmastanes (**XXIX**) display a methodical evolution during the Phanerozoic, with the C_{28}/C_{29} ratio increasing in marine samples through geologic time. This increase in abundance of the ergostanes (**XXVIII**) is a result of marine diversification from simple phytoplankton assemblages to more complex organisms, such as dinoflagellates, diatoms and coccolithophores, which began to thrive in the Mesozoic (Grantham and Wakefield, 1988). An alignment with the geological sterane record was observed in this study. Samples from the Wyche Farm Shale Pit plotted between 0.38 and 0.65, with most data

points plotting within the error of the chart (Figure 39) developed by Grantham and Wakefield (1988). The distribution of C_{28}/C_{29} falls nicely into the 0.5-0.7 range typical of Devonian-Triassic source rocks, providing insight regarding the general age of the Woodford in this study. However, the Devonian was recently observed to contain fluctuating C_{28}/C_{29} ratios, with the early Devonian and Devonian-Carboniferous boundary exhibiting significantly higher values which would initially be interpreted as Triassic (Schwark and Empt, 2006). The middle-late Devonian is more consistent with Grantham and Wakefield (1988), but the higher values in this study may be explained by this oscillating biological behavior of the sterane precursors (Schwark and Empt, 2006). Further analysis was required in order to refine interpretations and ensure the integrity of the age-dating interpretations.

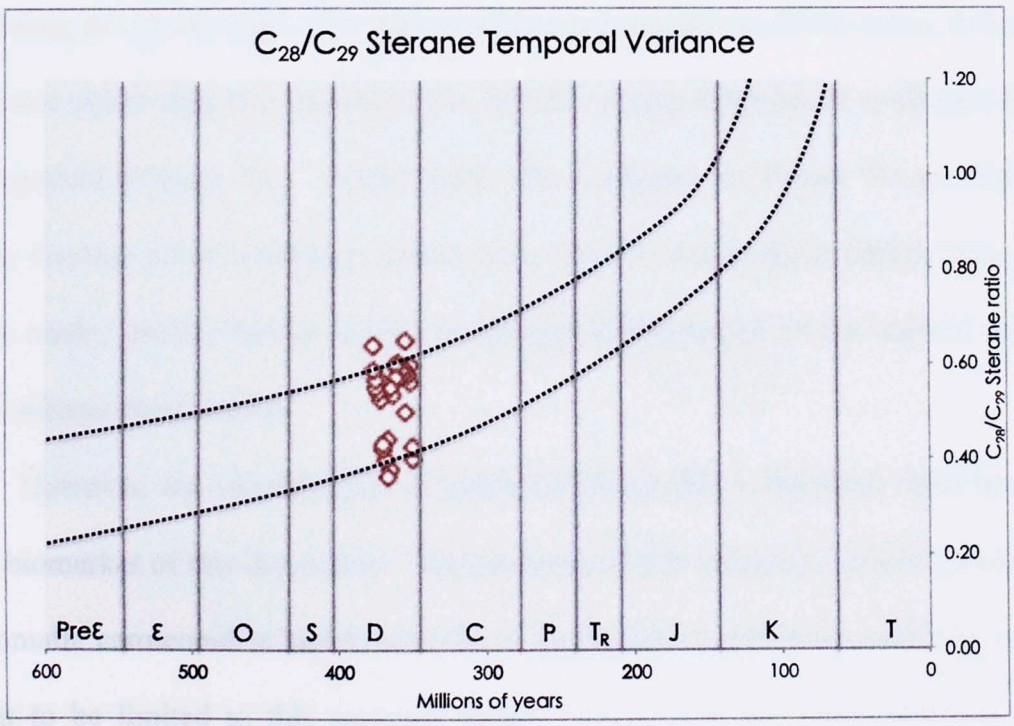

Figure 39. Sample distribution based on C_{28}/C_{29} sterane ratios to infer general age window of data. (from Grantham and Wakefield 1988). Dotted black lines account for variation within each geological period.

The lack of triaromatic 23,24-dimethylcholesteroids and triaromatic dinosteroids confirms the samples are Paleozoic and not Mesozoic in age (Barbanti et al., 2011). Due to the difficulties of detecting the saturated analogues, the triaromatic cholesteroids were used to great effect in differentiating Mesozoic and younger oils from Paleozoic samples by Barbanti et al. (2011). With a Paleozoic age established for hydrocarbon mixtures, the *n*-alkane predominance was assessed to further constrain the geologic period in which deposition occurred.

The slight odd-even predominance between the *n*-C_{15}-*n*-C_{17} in most of the samples and *n*-C_{17}-*n*-C_{22} in one sample may indicate a slight contribution from the cyanobacteria *Gleocapsomorpha prisca* (Reed et al., 1986; Fowler, 1992). This species of cyanobacteria flourished from the Cambrian to the Devonian, reaching a biological peak during the Ordovician. The lack of higher concentrations of the *n*-C_{15}, n-C_{17}, and *n*-C_{19} casts doubt onto this interpretation, but the unique behavior of *n*-alkanes should be recognized (Figure 40). Additionally, the *n*-alkanes in Figure 40 are from the saturate fraction of an immature source rock, not oil, where these observations were initially made, casting further doubt on the age determination of the studied samples using *n*-alkane distributions.

However, the identification of paleorenieratane (**II**) is the most important age-dating biomarker of this discussion. The presence of this unique 2,3,6/3,4,5 substituted C_{40} aromatic carotenoid is highly specific to Devonian source rocks, and was initially thought to be limited to this geologic period (Requejo et al., 1992; Hartgers et al., 1994). Further investigation has expanded the occurrence window to span from the Neoproterozoic to the early Triassic, but relatively high concentrations, as found in this

study, appear to be limited to the Devonian (French et al., 2015). Devonian oil from the Canning basin in Australia exhibits a very similar distribution of aromatic carotenoids as observed in this study. With more data, especially during the Devonian, carotenoid distribution could be used as a timely molecular clock. In all, these results align nicely with preexisting age dating work on the Woodford that determined a late Devonian-early Mississippian age (Paxton et al., 2006). The lack of aromatic dinosteroids, appropriate sterane ratios and the occurrence of paleorenieratane in high abundance suggest the analyzed fractions in this study were derived from the Devonian period.

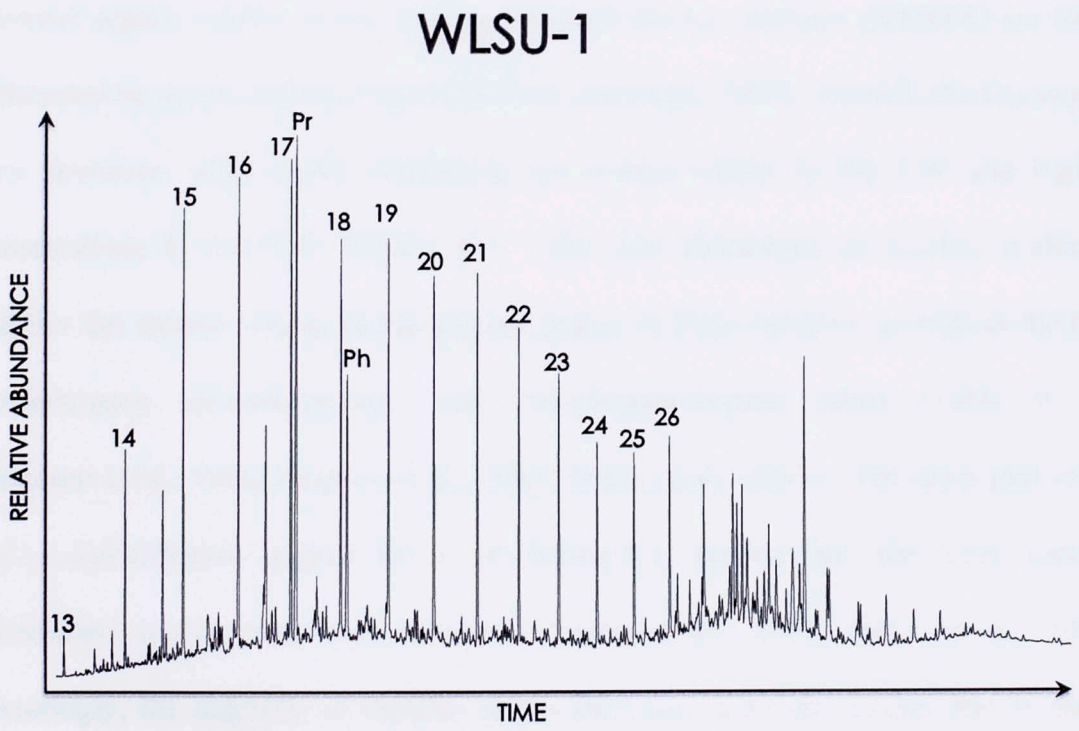

Figure 40. GC chromatogram of the saturate fraction from WSLU-1, located at 93.8 ft.

4.4. Depositional Environment

The C_{30} sterane index ($C_{30}/\Sigma C_{27}$-C_{30} regular steranes) is a strong indicator of marine depositional environments (Moldowan et al., 1985; Peters et al., 1986). The C_{30} steranes (i.e. 24-*n*-propylcholestanes; **XXX**) are biosynthesized exclusively by

Sarcinochrysidales which comprise an order of marine pelagophyte/chrysophyte algae (Raederstorff and Rohmer, 1984; Moldowan et al., 1990). Typically, a C_{30} sterane index exceeding 4% is interpreted as an input of marine organic matter to the source rock (Hays et al., 2012). The samples in this study ranged from 2.39%-5.74%, with an average of 3.55%, somewhat low for a marine depositional environment (Table 9; for all formulae and biomarker identifications discussed in this section, refer to Appendices **II** and **III**). This is possibly due to the relatively high abundance of C_{29} steranes (**XXXIX**) relative to the C_{27} steranes (**XXVII**), suggesting a potential contribution of terrestrial organic matter to the system, although the C_{29} steranes (**XXXIX**) are likely synthesized by primitive green algae (Scwark and Empt, 2006). Overall, the C_{30} sterane index decreases with depth, displaying the lowest values in the LW and highest concentrations in the UW (Figure 41). The low abundance of C_{21}-C_{35} *n*-alkanes solidifies the marine origins of the organic matter in these samples, as well as the high sterane/hopane, pristane/phytane and dinorhopane/hopane ratios (Table 9, 10; Moldowan et al., 1985; Hughes et al., 1995; Peters et al., 2005). The cross plot of the C_{26}/C_{25} cheilanthanes against the C_{31}R hopane/C_{30} hopane has also been used to differentiate source rock environments (Peters et al., 2005; Hays et al., 2012). Interestingly, the majority of samples plot within the carbonate section due to higher ratios of the C_{31} homohopane/hopane than reported for most marine shales (Figure 42). Marine source rocks often display C_{26}/C_{25} cheilanthane ratios <1.2, and higher C_{31}R hopane/C_{30} hopane ratios (>0.2). The higher C_{31}R hopane/C_{30} hopane parameter may be explained by the immature nature of this core, with thermal degradation yet to affect the homohopanes or due to the initial application of this cross plot for oils, not source

Table 9. Biomarker proxies capable of characterizing ancient environments and organic matter origin.

Sample	Pr/Ph	Sterane Index (%)	C_{27}/C_{29} Steranes	C_{26}/C_{25} Cheilanthanes	$C_{31}R/C_{30}$Hopane	C_{29} Norhopane/ C_{30} Hopane	MATH (µg/g OC)
WSLU-1	2.06	4.95	0.70	0.88	0.58	0.67	0.33
WSLU-2	1.58	5.74	0.57	0.91	0.46	0.64	0.17
WSLU-3	1.48	5.57	0.81	0.99	0.49	0.73	0.05
WSLU-4	1.61	4.53	0.82	0.81	0.41	0.74	0.09
WSLU-5	1.52	3.38	0.90	0.93	0.72	0.82	0.12
WSLU-6	1.23	3.13	1.14	0.90	0.66	0.73	0.26
WSLU-7	1.19	3.14	0.76	0.77	0.62	0.69	0.06
WSLU-8	1.23	4.22	0.85	0.78	0.49	0.55	0.24
WSLU-9	1.42	3.97	0.83	0.76	0.51	0.56	0.19
WSLU-10	1.43	4.10	0.85	0.89	0.51	0.63	0.16
WSLU-11	1.55	4.05	0.87	0.84	0.55	0.70	0.32
WSLU-12	1.58	3.56	0.87	0.83	0.51	0.67	0.36
WSLU-13	1.58	3.64	0.87	0.84	0.53	0.68	0.31
WSLU-14	1.72	3.13	0.81	1.07	0.63	0.82	0.09
WSLU-15	1.77	2.85	0.76	1.07	0.68	0.96	0.16
WSLU-16	1.91	2.97	0.79	1.11	0.62	0.81	0.17
WSLU-17	2.12	2.39	0.54	1.25	0.63	0.84	0.10
WSLU-18	1.89	2.70	0.53	1.04	0.53	0.69	0.10
WSLU-19	1.61	3.68	0.68	0.99	0.61	0.68	0.08
WSLU-20	1.95	3.22	0.62	0.92	0.53	0.64	0.06
WSLU-21	1.81	3.45	0.63	0.99	0.61	0.63	0.04
WSLU-22	1.65	3.34	0.67	0.95	0.59	0.67	0.08
WSLU-23	1.91	2.69	0.74	1.21	0.59	0.85	0.08
WSLU-24	1.80	3.08	0.89	0.98	0.57	0.72	0.02
WSLU-25	1.84	2.76	0.85	1.03	0.55	0.78	0.34
WSLU-26	1.87	3.49	0.74	0.97	0.53	0.74	0.01
WSLU-27	1.92	3.22	0.96	1.03	0.53	0.74	0.04
WSLU-28	1.81	3.17	1.01	1.01	0.58	0.80	0.22
WSLU-29	1.70	2.80	0.97	1.05	0.62	1.14	0.05
Average	1.68	3.55	0.79	0.96	0.57	0.74	0.15

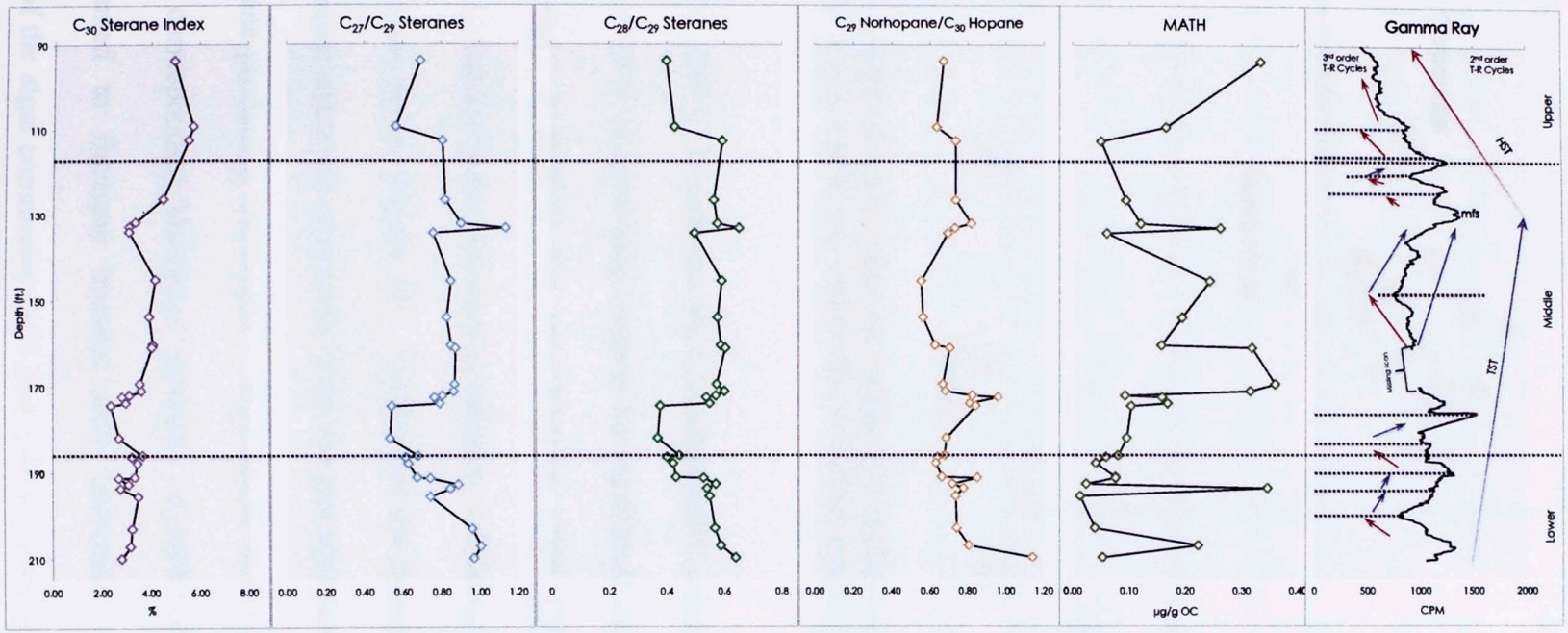

Figure 41. Geochemical logs representing the environmental fluctuations controlling the type of organic matter input into the system and organisms occupying the water column.

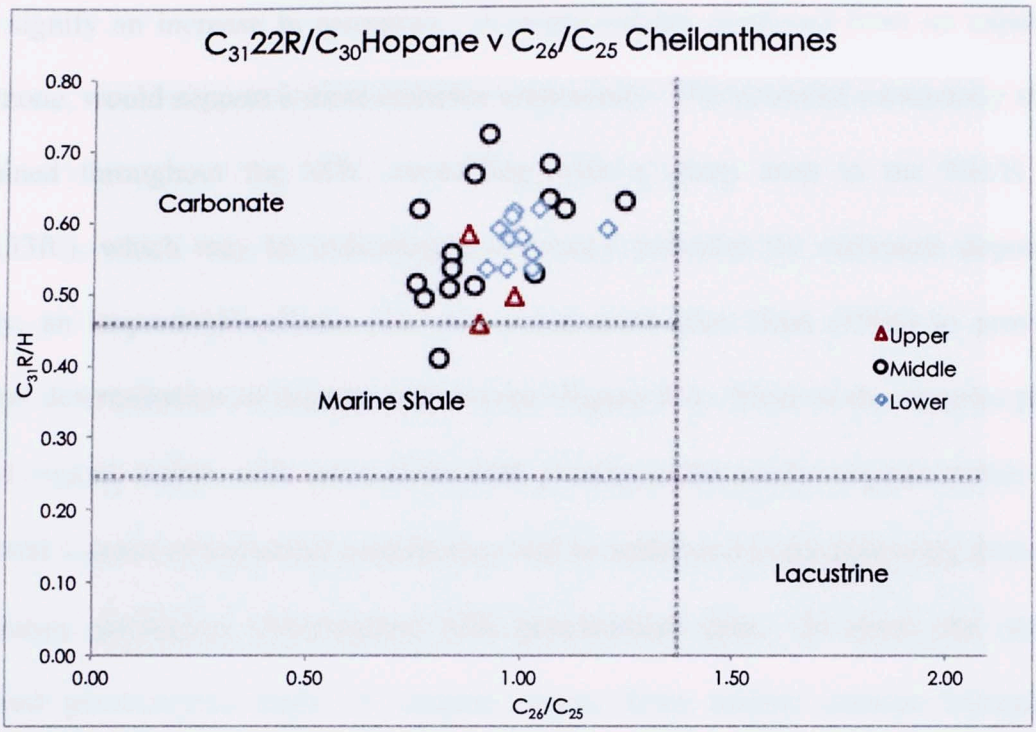

Figure 42. Differentiation of source input via hopane and cheilanthanes. This cross plot was initially developed for oils, which may explain the Woodford samples plotting in the carbonate region.

rocks (Peters et al., 2005). In addition, the C_{29} norhopane/C_{30} hopane ratios are elevated (Wyche-1 core AVG=0.74) providing support for significant carbonate contribution to the source material. A drop in this ratio between 170ft.-130ft. coincides with an increase in the C_{30} sterane index and C_{28}/C_{29} steranes, validating the use of this ratio as a tentative carbonate proxy (Figure 41). Carbonates are typically deposited in more anoxic environments where the expansion of the oxygen minimum zone may invade the habitats of sterane-producing autotrophs. This would lead to an increase in these organisms, and corresponding biological products, as carbonate content decreases if oxicity is assumed to fluctuate linearly with carbonate production. A rapid diversification of the algal community (173.83ft.) from a predominantly primitive algal community to a heterogeneous group of red, brown (modern) and green (ancient) algae

may signify an increase in resources. A larger habitat, produced from an expanding oxic zone, would support a more complex community. This potential community shift is sustained throughout the MW, coinciding with a sharp drop in the NH/H ratio (169.33ft.), which may be indicating a decreased potential for carbonate deposition. Lastly, an isoprenoid/*n*-alkane plot was constructed after Hunt (1996) to provide a general determination of organic matter type (Figure 43). Most of the samples plot as mixed organic matter, with some of the MW plotting in the marine organic matter zone. Potential sources of terrestrial contribution will be addressed in the following discussion integrating geological observations with geochemical data. In short, the samples received predominant input of organic matter from marine sources enriched in carbonaceous material and secondary input from terrigenous sources. Integration of these proxies with sequence stratigraphic data will assist in better understanding the controls governing the depth fluctuations previously discussed.

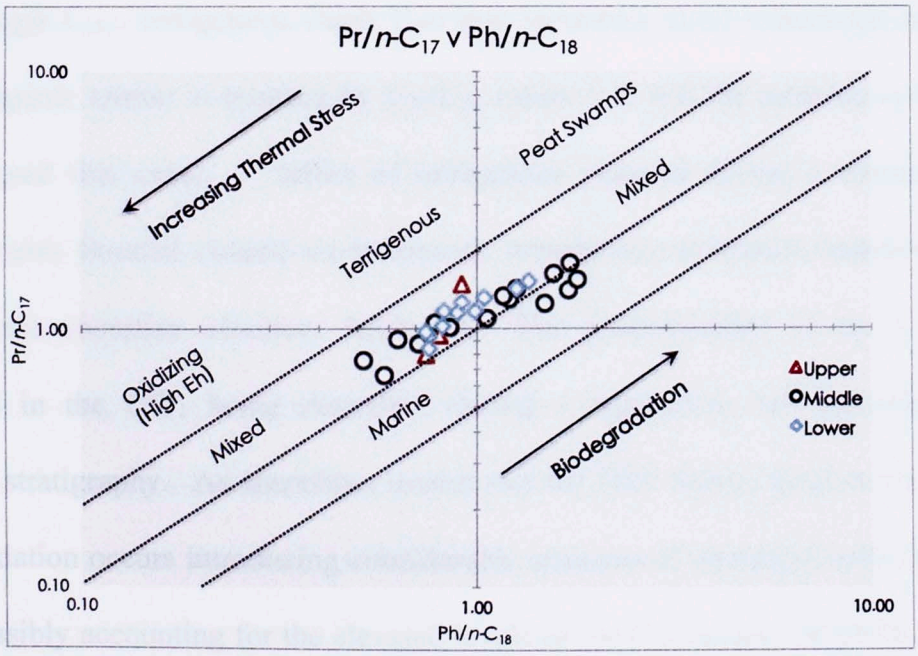

Figure 43. Determination of organic matter type after Hunt (1996). This diagram was used to tentatively understand the source of organic matter in this study. More specific plots/relationships are necessary to accurately define the depositional environment.

The 2nd order TST (transgression) extending from the base of the LW to the boundary between the MW/UW reflects deepening of the water column, allowing for open marine settings to predominate over terrestrial influxes which may be affecting the LW. Pelagophytes (marine algae) would be able to stabilize and flourish, possibly resulting in the observed increasing C_{30} sterane index upsection. The C_{27}/C_{29} and C_{28}/C_{29} ratios do not appear to align with this interpretation, declining from the LW to approximately 174 ft. This is followed by a sharp increase in the C_{27}/C_{29} and C_{28}/C_{29} ratios followed by an apparent stabilization throughout much of the MW. An isolated spike at 131.75ft. in the MW disrupts the stable algal community composition, indicating rapid diversification at this depth. The C_{29} sterane (**XXXIX**) begins to overwhelm the other steranes in the UW, reflected by a decline in the C_{27} (**XXVII**) and C_{28} (**XXVIII**) relative to the C_{29}. Recall, the steranes possess little source specificity to an exclusive species, but are preferentially synthesized in different proportions by marine (high C_{28}), terrigenous (high C_{29}) and lacustrine (C_{27}) eukaryotic organisms. Marine organic matter is typified by C_{27}/C_{29} ratios > 1, but the samples in this study rarely exceed this value. Influx of terrigenous material during a transgression is possible, with flooded coastal environments introducing terrestrial sediments to the basin as the shoreline advances landward. The predominance of the C_{29} sterane (**XXXIX**) in the UW, being deposited during a regression, can be explained by sequence stratigraphy. As shorelines retreat and the HST forms, erosion will increase as progradation occurs introducing considerable amounts of terrestrial material into the basin, possibly accounting for the elevated levels of the C_{29} sterane (**XXXIX**, assuming it is not derived from algae) and decrease in the C_{30} sterane index within this member.

The 3rd order regression in the LW may explain the decrease in the C_{27} (**XXVII**) and C_{28} steranes (**XXVIII**) relative to the C_{29} sterane (**XXXIX**), but still does not explain the overall increase of the C_{30} sterane index in the LW. The superceding 2nd order TST likely exerted influence on the smaller parasequences discussed previously, resulting in an overall increase in marine algae over time. The 4th order sequences recognized by Turner et al. (2015) appear to exert little control on the sterane distributions. Alternatively, the C_{29} sterane predominance may be an artifact imposed by the time in which these samples were deposited. Recall in the earlier discussion on age-dating tools that the C_{28}/C_{29} sterane ratio increases throughout geologic time (Grantham and Wakefield, 1988), and was based on marine samples in that study. The gradual evolution of algae is reflected in the geologic record by a decrease in the more primitive green algae (C_{29}) relative to the modern brown algae (C_{28}). As a result, the interpretations assuming the C_{29} sterane is terrestrial in origin may be flawed based on the temporal evolution of the sterane distribution. Due to the lack of angiosperms and other terrigenous contributors which just began to blossom during the Devonian, it is difficult to evaluate the potential story of terrestrial input in this system and cross examine the significance of the C_{29} sterane. In addition, it was inferred by Comer (1991) the low concentrations of terrestrial organic matter to the Woodford might be a result of barren land, not a distal position. Other markers for higher plants, such as tricyclic and tetracyclic diterpanes, were not detected while bicyclic sesquiterpanes were in low abundance. However, 5-methyl-10-(4-methylpentyl)-des-*A*-25-norabora(ferna)-5,7,9-triene (MATH; **XLIV**) was detected, which is a marker for certain plant communities (e.g. early gymnosperms and coniferophytes). This

compound is supposedly derived from a fernane/arborane precursor subjected to strong, acidic conditions responsible for the methyl shift and cleavage rearrangement to occur (Vliex et al., 1994). The MATH (**XLIV**) log in Figure 41 exhibits erratic behavior, with numerous spikes in the concentration. The UW displays the clearest trend, possibly due to lack of sampling intensity, but is in agreement with previous interpretation of the UW in this discussion. The increase in MATH (**XLIV**) in the UW is likely a product of the increased input of eroded terrigenous matter being deposited into the basin, as reflected by increased amounts of the C_{29} sterane (assuming its derivation from terrestrial plants, but this is highly unlikely). Lack of clear relationships throughout other members could be explained simply by assuming the samples were deposited in a much more proximal location than currently believed. This would explain the seemingly random control over the MATH (**XLIV**) abundance. The presence of MATH (**XLIV**) indicates a shallow shelf setting (<300m) because transport of this material to a distal position in the basin seems unlikely. Additionally, when discussing 'deep water' in North American epicontinental seas the depth is inferred to be no greater than several hundred meters (e.g. Potter et al., 1982; Algeo and Maynard, 1997; Jaminski et al., 1998). MATH (**XLIV**) may be a more sensitive proxy for terrestrial input than 3rd order cycles detected by Molinares (2013), with the spike at 194ft. appearing to correlate with one of the 4th order parasequences identified chemostratigraphically by Turner et al. (2015). Positive MATH excursions appear to correlate with the apex (most landward extent of shoreline) of the 4th order parasequences at approximately 190ft., 175ft., and 130ft. (mfs), counter to expectations. MATH, a terrestrially-sourced biomarker, should be found in HSTs during regressions,

not in transgressions when a more distal position is assumed. Flooding of the shoreline may lead to greater riverine influx from continental runoff, introducing terrestrial material during a TST. This could also be explained by enhanced preservation during these periods due to bottom water anoxia, resulting in a preservation bias controlling the MATH concentrations more than the influx of terrestrial organic matter into the basin.

Several biomarker proxies discussed in this section appear to correlate strongly with the maximum flooding surface found at the top of the condensed section (Figure 41). The C_{27}/C_{29} sterane ratio and MATH (**XLIV**) exhibit a sharp increase at 132.75 ft., with a slightly less noticeable spike in the C_{28}/C_{29} ratio. From a geologic perspective, the maximum flooding surface represents the maximum landward extent of the shoreline. Therefore, it is surprising to see the abrupt positive excursion of MATH, a supposed terrestrial indicator, peak during this time. Instead of invoking some farfetched transport mechanism to specifically deliver one terrestrial biomarker to the marine sediments, a chemical approach is much more efficient at explaining this phenomena. The low benzohopanes/homohopanes, and high diasterenes/steranes diahopane/hopane, and neohop-13(18)-enes/hopane ratios mentioned previously may indicate more than solely lithologic variations. Increasing acidity (likely between 6.5-7.3; see *Temporal Evolution of the Water Column with focus on Carotenoid Applications* for more detail) of the ocean water during this time explains the abrupt changes observed in the geochemical logs of these biomarkers. MATH (**XLIV**) was suggested to form in strongly acidic conditions from fernane/arbornane precursors (Vliex et al., 1994), the same conditions facilitating the rearrangement of sterenes and hopenes to diasterenes and diahopane, respectively. A lower pH may be a product of

CO_2 adsorption from the atmosphere, impeding the formation of $CaCO_3$ through bicarbonate production and hindering the formation of carbonate material, potentially impacting the generation of benzohopanes as well. Consequently, MATH (**XLIV**) may be controlled by both terrestrial input and water chemistry in this system, but the detection of the precursor fernanes and arbornanes was unsuccessful. The overall increase in MATH concentration and significant spikes during the 2nd order TST challenges previous work (e.g. Over, 2002) suggesting a reduction in terrestrial influx coinciding with sea level rise. Depending on the degree to which water chemistry affects MATH, this may be of further interest in reassessing the extent of terrigenous input during the 2nd order TST in which the lower and middle members were deposited. Assuming terrestrial input retains partial governance of this biomarker, the sharp increase in MATH concentration challenges the assumption the C_{29} sterane is derived solely from vascular plants, due to the decrease in abundance observed relative to other steranes. If it was biosynthesized by a terrestrial source, then the ratios normalized by the C_{29} sterane (**XXIX**) should exhibit a decrease, not increase, where the MATH spikes. In this study it seems the C_{29} sterane (**XXIX**) is sourced by additional organisms, such as green algae (e.g. *Chlorophyceae*; Volkman, 1986; Brocks and Summons, 2013), and is unable to serve as a marker for terrigenous input. However, the sterane distributions still remain relevant as indicators of potential source material if analyzed as a whole according to Volkman (1986). The marine organisms responsible for biosynthesizing the C_{27} (**XXVII**) and C_{28} (**XXVIII**) steranes may explain the rapid rise in abundance of these steroids in the condensed section. Marine unicellular green (eustigmatophytes and prasinophytes) and multicellular red algae (rhodophytes) likely

thrived during the eustatically stable time interval, allowing for dense colonies to saturate the oxic layers of the water column. The lack of organic matter from other sources in this quiescent period would allow for minimal dilution of the marine signal, resulting in the steroids from marine algae to dominate the sedimentary record.

The Woodford samples are composed of a mixture of carbonaceous marine and terrestrial organic matter, as evinced by isoprenoid/alkane distributions, the presence of 24-*n*-propylcholestane, MATH, relatively high C_{29} norhopane/hopane ratios and the absence of abundant C_{21}-C_{35} *n*-alkanes. High concentrations of MATH and high ratios of C_{27} and C_{28} normalized by stigmastane appear to serve as potential markers for the maximum flooding surface in the sedimentary record. MATH may be governed by both the abundance of source material and conducive conditions in the water column, with its presence indicating a shallow shelf setting (<300m). The likelihood of stigmastane derivation from more than vascular plants is high, with other marine inputs, such as green algae, probable candidates. The chemical status of the water column will be evaluated in depth in the following section, with focus on the variability of biomarker distributions relative to system tracts providing additional evidence and explanation surrounding these proposed biogeochemical eustatic proxies.

4.5. Temporal Evolution of the Water Column with focus on Carotenoid Applications

C_{40} Aromatic carotenoids, unlike the hopanes or steranes, are biosynthesized solely by purple (PSB) and green (GSB) photosynthetic sulfur bacteria in marine sedimentary environments (Brocks and Summons, 2013). Paleoenvironmental reconstructions commonly utilize the occurrence of these compounds as markers for

photic-zone euxinia (PZE) in the paleowater column due to the PSB/GSB's adapted ability to thrive in H_2S-saturated waters. (Summons and Powell, 1987; Requejo et al., 1992; Koopmans et al., 1996a; Sinninghe Damste et al., 2001; Maresca et al., 2008; Melendez et al., 2013; Sousa Junior et al., 2013; Tulipani et al., 2015). Specifically, the presence and distributions of the C_{40} aromatic carotenoids allow for general estimation of chemocline position and thickness. For example, the occurrence of okenane (**V**) implies a shallow (12-25m) anoxic/oxic boundary depth and severe penetration of H_2S into the photic zone (Guerrero et al., 1985; Brocks and Schaeffer, 2008). However, unique physiological characteristics of sulfur oxidizing bacteria remain untapped. The rationale on which chemocline depth is inferred relies on multiple variables controlling the presence of PSB/GSB in the photic zone. Few studies investigate alternative governing mechanisms other than the fact H_2S invaded the photic zone (exceptions include Brocks and Schaeffer, 2008; French et al., 2015). Light availability, dependent on the depth of the anoxic/oxic boundary and water turbidity, sulfide concentration, pH and competition from organisms in the oxic layer all will impact the ability of PSB/GSB to flourish. Consequently, this intricate relationship between the anoxic- and oxic-dwelling organisms with the persisting water state can provide the geochemist with a means to tentatively glean environmental information at a resolution unmatched by other biomarkers. This powerful tool relies on the fact only two organisms, the PSB and GSB, synthesize C_{40} aromatic carotenoids in marine environments (Brocks and Summons, 2013). Of the two, GSB are more resilient than the PSB, tolerating larger variations in light availability, sulfide concentration, and pH. Initially, the primary application (estimation of chemocline position) of carotenoids and

associated derivatives will be discussed in the scope of this study, with additional sections evaluating secondary applications of these unique aromatic biomarkers.

Paleorenieratane (**II**), isorenieratane (**I**), renieratane (**III,** rare) and renierapurpurane (**IV,** rare) were detected in variable concentrations throughout the Woodford Shale (Figure 44; Table 10, see page 105). Okenane and chlorobactane were tentatively identified, but in unquantifiable amounts to be of interpretative significance. Other than Nowaczewski (2011), who detected isorenieratane in low abundances in the I-35 Woodford outcrop, this is the first reported occurrence of four C_{40} aromatic carotenoids in the Woodford Shale, with two (paleorenieratane and isorenieratane) observed in high concentrations. Identification was achieved by comparison with preexisting chromatograms and similar mass spectra published in the literature (see Appendix **III** for identified fragmentograms; Schaefle et al., 1977; Requejo et al., 1992; Hartgers et al., 1994; Brocks and Schaeffer, 2008). Numerous carotenoid derivatives outlined by Koopmans et al. (1996b) were detected as well, with potential applications and significance beyond the scope of the current study, but will be reported in future publications (see Appendix **III** m/z 237 for preliminary results). Paleorenieratane (**II**) was the dominant C_{40} carotenoid in most samples, with isorenieratane (**I**) the second most abundant. It appears the concentrations of these two carotenoids parallel each other, lending a clue as to where the former C_{40} carotenoid may be sourced (further discussion in section: *Evolution of the Microbial Community and Possible Source Organisms for Disputed Biomarker Origins).* For the following discussion, it is assumed that paleorenieratane (**II**) precursors occupy a slightly shallower niche of the water column than isorenieratane (**I**), derived from the brown strain of GSB (bGSB).

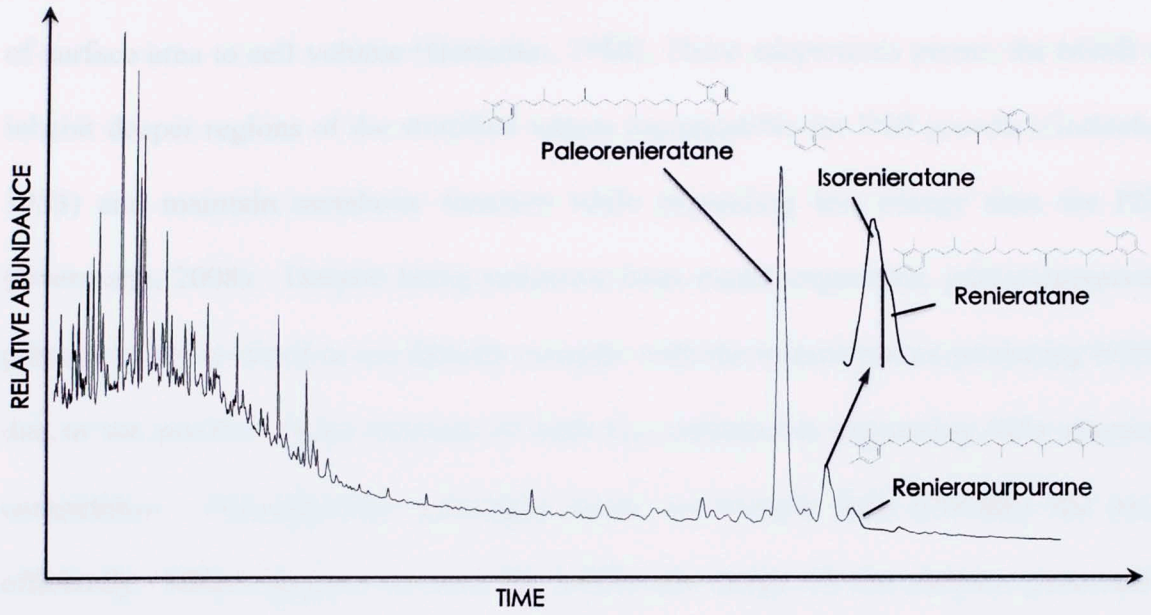

Figure 44. Aromatic TIC depicting C_{40} aromatic carotenoid distribution and abundance with carotenoids labeled accordingly. Note the coelution of isorenieratane and renieratane. Additional peaks are identified as predominantly C_{40} carotenoid derivatives and can be found in Appendix **III**).

The brown strain is characterized by the chlorosome (a specialized light-harvesting organelle) and photoadaptism, or the ability to alter the homolog composition in response to changing light conditions (Borrego et al., 1997). The bGSB are more efficient sulfide oxidizers at low light (found to survive as low as 20 lux (Biebl and Pfennig 1978)), and have ~175% more light harvesting pigments than green and purple strains (Overmann et al., 1992). Phototrophic bacteria found in regions of low light often increase the size of photosynthetic units (Drews and Golecki 1995; Overmann 2008), with PSB possessing 20-2000 bacteriochlorophyll (BChl) *a* molecules/reaction center (Zuber and Codgell 1995) and the specialized chlorosomes of the bGSB containing 5000-8000 BChl *c* molecules/reaction center (Frigaard et al.,

2003). PSB also require more CO_2 (8-10.5 mol quanta/mol CO_2) than GSB (3.5-4.5 mol quanta/mol CO_2; Brune 1989), which also possess prosthecae that increase the ratio of surface area to cell volume (Gorlenko, 1988). These adaptations permit the bGSB to inhabit deeper regions of the stratified waters incompatible for PSB growth (Gorlenko, 1988) and maintain metabolic function while expending less energy than the PSB (Overmann, 2008). Despite being unknown from extant organisms, paleorenieratane-precursors are assumed to not directly compete with the isorenieratene-producing bGSB due to the positive linear increase of both C_{40} carotenoids suggesting little resource competition. Isorenieratene scavenges lower wavelength light (460mμ) the most efficiently, which happens to also be within the range of the deepest penetrating daylight wavelengths of 450-470mμ, meaning paleorenieratane is likely produced from an organism occupying a shallower region of the chemocline to avoid direct competiton with the highly specialized bGSB. Okenone (okenane precursor) is derived from the PSB *(Chromaticeum)*, which are limited to the upper regions of the chemocline. These bacteria are highly mobile (flagella) and are capable of utilizing multiple carbon sources (e.g. pyruvate, propionate, lactate, fructose, malate, bicarbonate, acetate), but are ultimately limited by the absorption spectra (peak at 850mμ) despite these advantages over the less motile and more restricted (carbon-source) GSB (Truper and Genovese, 1968). The first 25m of the water column absorbs all λ above 640mμ (Jerlov 1951; Yentsch 1962), meaning the PSB require the chemocline (being strict anaerobes and requiring sulfide as the electron donor) to be shallower than 25m. Lack of okenane[6] in the samples is interpreted as a chemocline depth greater than 25m, intense equatorial

[6] Detected(?) in negligible amounts of samples containing the highest concentrations of paleorenieratane and isorenieratane.

winds causing intermixing of the oxic-anoxic interface, murky waters, or the lesser possibility of *Chromaticeum* outcompeted by some unknown organism. Alternatively, absence of the okenane pigment may not imply the absence of PSB or a chemocline deeper than 25m.

Paleorenieratane (**II**) and isorenieratane (**I**) are employed to infer the extent of photic zone euxinia (PZE) during Woodford deposition. This is based on the assumption the GSB were a planktonic community not restricted to benthic algal mats. French et al. (2014) attributed the presence of GSB and PSB to benthic microbial mats, not a planktonic source due to the correlation observed between wavy laminations and algal mats. The lithofacies described by Molinares (2013) characterized by wavy laminations is limited primarily to the UW, where the aromatic carotenoids are in lowest concentration. Lack of lycopane, a carotenoid produced by the hydrogenation of lycopene synthesized by all mat species (Brocks and Schaeffer, 2008) and wavy laminations permit interpretation of paleorenieratane (**II**) and isorenieratane (**I**) as biological products of planktonic GSB in this study. On average (Wyche-1 core average), paleorenieratane (**II**) is three times more abundant than isorenieratane (**I**) (12.13 µg/g OC to 3.70 µg/g OC), with both carotenoids displaying very similar changes throughout the core (Table 10; for any formulae see Appendix **II**, and refer to Appendix **IV** for a biomarker reference guide outlining the primary applications of the compounds discussed in this section). These C_{40} aromatic carotenoids exhibit isolated spikes in the LW, followed by an overwhelming rise to prominence in the middle MW where paleorenieratane (**II**) abundance reaches 92.84 µg/g OC at 145.17ft. and

Table 10. Biomarkers as indicators for water structure and chemistry in the Wyche-1 core. Paleorenieratane, isorenieratane and potential derivatives (aryl isoprenoids) signify H_2S-saturation of portions of the photic zone, gammacerane assists in inferring water stratification, and 28,30-dinorhopane, HHI and Pr/Ph provide insight into the redox state of the Woodford paleoenvironment.

Sample	Paleorenieratane (µg/g OC)	Isorenieratane (µg/g OC)	Σ C_{15}-C_{31} 2,3,6 Aryl Isoprenoids (µg/g OC)	Σ C_{15}-C_{31} 3,4,5 Aryl Isoprenoids (µg/g OC)	28, 30 Dinhorhopane /C_{30} Hopane	Gammacerane Index	Homohopane Index (%)	C_{35}/C_{34} Homohopanes	Pr/Ph
WSLU-1	1.77	0.70	13.63	3.61	0.16	0.18	12.61	1.36	2.06
WSLU-2	1.08	0.97	37.32	6.34	0.28	0.22	12.01	1.33	1.58
WSLU-3	0.58	1.08	29.91	5.62	0.31	0.12	11.39	1.27	1.48
WSLU-4	3.79	1.10	58.07	25.38	0.17	0.13	8.89	1.04	1.61
WSLU-5	5.76	1.47	75.02	36.66	0.35	0.28	6.42	1.12	1.52
WSLU-6	17.72	2.76	80.51	49.38	0.32	0.32	7.37	1.24	1.23
WSLU-7	33.09	6.60	174.96	86.58	0.26	0.32	7.68	1.20	1.19
WSLU-8	92.84	13.82	240.55	142.17	0.37	0.43	6.72	1.03	1.23
WSLU-9	59.28	14.37	226.65	126.97	0.56	0.43	7.60	1.13	1.42
WSLU-10	37.07	10.63	216.85	109.72	0.48	0.43	6.51	1.04	1.43
WSLU-11	20.66	7.17	179.90	85.07	0.54	0.39	7.33	1.07	1.55
WSLU-12	23.71	7.76	200.89	92.90	0.47	0.38	7.37	1.04	1.58
WSLU-13	15.16	5.69	163.40	71.04	0.56	0.36	7.20	1.16	1.58
WSLU-14	2.68	1.32	61.79	23.37	0.38	0.28	7.03	0.99	1.72
WSLU-15	0.97	0.63	61.63	16.52	0.36	0.23	6.99	1.07	1.77
WSLU-16	1.76	2.09	64.52	16.22	0.33	0.27	7.46	1.08	1.91
WSLU-17	0.82	0.81	44.60	10.91	0.23	0.15	7.13	1.10	2.12
WSLU-18	0.57	0.88	25.50	6.07	0.21	0.18	6.54	1.06	1.89
WSLU-19	7.05	4.47	84.33	28.68	0.31	0.35	7.51	1.06	1.61
WSLU-20	2.35	3.35	64.31	14.51	0.29	0.28	7.24	1.11	1.95
WSLU-21	2.96	2.25	51.23	15.82	0.29	0.27	6.57	1.02	1.81
WSLU-22	8.32	5.06	85.34	31.94	0.28	0.26	6.93	1.04	1.65
WSLU-23	1.13	1.13	50.25	13.71	0.26	0.16	6.87	1.03	1.91
WSLU-24	2.59	1.45	55.81	16.50	0.31	0.26	6.92	1.06	1.80
WSLU-25	1.49	2.37	92.80	20.39	0.33	0.21	6.54	0.97	1.84
WSLU-26	1.43	1.60	30.25	7.73	0.35	0.26	7.22	0.99	1.87
WSLU-27	3.40	3.81	86.22	20.30	0.33	0.26	8.02	1.01	1.92
WSLU-28	1.52	1.84	68.00	14.62	0.38	0.22	6.33	0.93	1.81
WSLU-29	0.12	0.20	46.85	12.57	0.44	0.18	4.29	1.08	1.70
Average	12.13	3.70	92.11	38.32	0.34	0.27	7.54	1.09	1.68

isorenieratane (**I**) reaches its maximum of 14.37 µg/g OC at 153.58 ft. The second half of MW deposition records a rapid cessation of carotenoid dominance, with minimal concentrations observed from latter sections of the MW into the UW (Figure 45). Based on these observations, it can be inferred the LW was characterized by isolated episodes of PZE. During these periods, chemocline depth likely did not exceed 25-50m, allowing for the brief proliferation of GSB before interruption of well-stratified waters led to temporary collapse of the marine GSB community. Upwelling of deep waters may have disturbed the chemocline, causing a flooding of O_2-rich waters that would result in the decimation of the sulfur-oxidizing bacteria. In the Oklahoman Woodford, upwelling is postulated to originate from the southwestern ocean with cold waters transported along the seafloor of NW Texas before upwelling in the epicontinental seas (Comer, 1991; Roberts and Mitterrer, 1992). However, the interpreted shallow shelf position of the samples (<300m.) limits the transfer of significant amounts of deep water to the shelf via major ocean currents (Shaw, 1964; Kirkland et al., 1992), challenging the extent of upwelling as a control in the MW. This shallow, shelf basin interpretation was initially suggested in this study from the presence of the terrigenously sourced MATH. Isorenieratane (**I**), detected in high concentrations in this study, is reported to be indicative of upper Devonian shelf environments for source rocks found in the Holy Cross Mountains, Poland (Marynowski et al., 2000; Brown and Kenig, 2004; Hartkopf-Froder et al., 2007). Therefore, the presence of isorenieratane (**I**) in this study is proposed to be indicative of a similar position relative to the shoreline due to the observation of other biomarkers, such as MATH, supporting this interpretation. A recent study also documented the lack of PZE in basinal settings, with deposition of

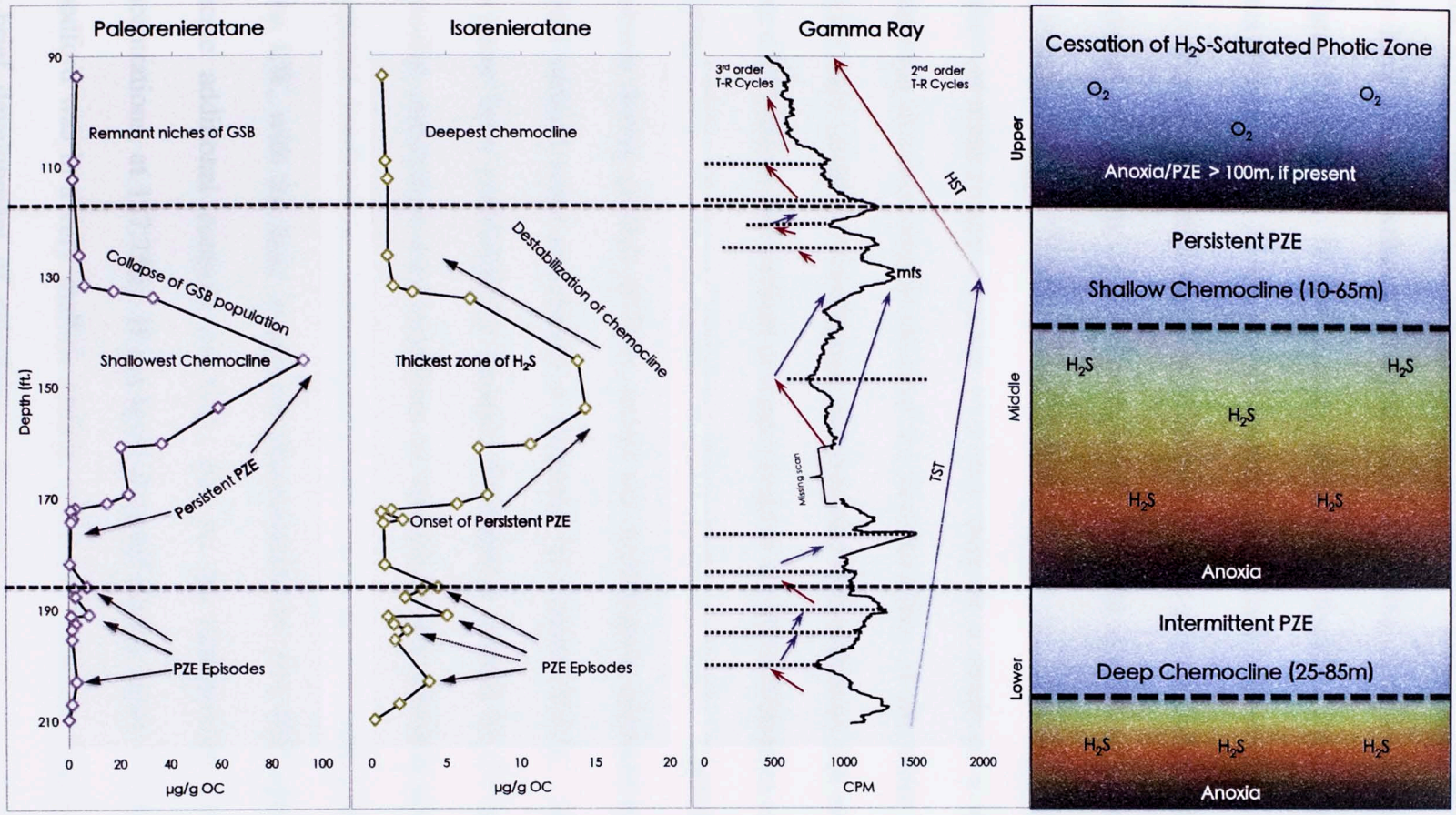

Figure 45. Evolution of the chemocline throughout Woodford deposition as inferred by C_{40} aromatic carotenoid distributions. The LW exhibits isolated PZE episodes with a protracted period of PZE in the MW, with all periods of PZE correlating with 3rd order HSTs.

Chlorobiaceae biomass restricted to shelf and slope facies (Slowakiewicz et al., 2015). If the Appalachian Basin cratonic basins are used as analogs, the development of sills may have limited exchange of deep water, impeding the development of upwelling (Algeo et al., 2007). In the modern, GSB are not found in marine sulfidic upwelling zones (French et al., 2014), further supporting the lack of upwelling during periods of PZE. Strong equatorial winds may still have been present during MW deposition, as suggested by Roberts and Mitterer (1992), but did not create upwelling of bottom waters and instead affected the microbial community. The lack of okenane (**V**), a product of PSB (found between 10-25m.), may be a result of a wind mixed layer comprising chemical stratification of the first 80-100m. of the water column. Models typically are unable to incorporate okenane and chlorobactane due to the oxygenation created by wind-driven vertical mixing (Ozaki et al., 2011; Monteiro et al., 2012) unless the atmospheric effects are adjusted to affect shallower depths. Upwelling is inferred to be absent during periods of PZE, unless the stratification imposed by the chemocline limited vertical water circulation as proposed by Comer (2012). Alternatively, PZE may have been controlled by eustatic fluctuations caused by 3rd order T-R cycles. Typically, regressions may contribute to vertical mixing which is not reflected by the carotenoid distributions. Isolated periods of PZE in the LW reflect the two regressions in the LW, with the later regression characterized by two PZE episodes. This may indicate additional controls on PZE, due to the unexplained drop in carotenoid concentrations, at 187.75ft. If sea level dropped during these 3rd order HSTs and the Woodford was in a very shallow setting, carotenoid abundances may be explained by the brief development of paleolakes. Paleolakes would resolve the 'no analogue'

problem termed by French et al. (2014), noting the lack of PSB/GSB in the modern sulfidic marine environments. The MW marks the onset of persistent PZE, which was preceded by a miniature depression in the GSB community from the last episode of PZE in the LW (185.92-172.42ft.). Persistence of such conditions is underlined by the continued increase in carotenoid concentration from 172-145.17ft., reflecting the stable and well-defined chemocline marking the boundary between the sulfur-rich waters below and the oxygen-rich waters above. Strong stratification invokes the stagnant circulation model (Molinares, 2013), rather than the upwelling circulation model, in this region of the MW. This stability would allow for the GSB to proliferate, potentially forming dense microbial mats at the oxic-anoxic interface, much more resistant to periodic environmental threats than isolated, free-floating communities of bacteria in the LW. Hydrographic restriction has been previously documented to exert controls on sediment geochemistry (e.g. Algeo et al., 2007), and is suggested to control the distribution of C_{40} aromatic carotenoids in this study. Contrary to previous claims, upwelling may have facilitated the sustained PZE in the MW by providing essential nutrients to aerobic organisms. Precipitation of large amounts of organic matter would facilitate the persistence of anoxic waters below the chemocline reflected by the expanding oxygen minimum zone (OMZ). Chemocline depth and thickness is interpreted to be the shallowest and greatest (10-25m from the surface) at 145.17ft., the same point which corresponds to the paleorenieratane (**II**) maximum. This is assuming the extent of a wind mixing was minimal. As previously mentioned, the lack of PSB derivatives may be a result of the initial 50-80m of the water column being mixed and oxygenated by atmospheric forces. If this occurred, the chemocline depth is adjusted

approximately 50m (60-85m. from surface) to permit the survival of sulfidic organisms below the deepened oxic-anoxic interface. These deeper depths parallel work in the Black Sea, which found the chemocline at 80-120m., with seasonal fluctuations of 20-50m. (Sinninghe Damste et al., 1993; Meyer et al., 2008). It is difficult to give a more refined estimate due to the uncertainty associated with the origins of paleorenieratane (**II**). If paleorenieratane (**II**) was isotopically depleted, it likely occupied the same position as the PSB-produced okenane. However, Hartgers et al. (1994) reported $\delta^{13}C$=-12‰, similar to isorenieratane (**I**), meaning carbon is fixed via the reverse TCA cycle utilized by *Chlorobiaceae* (GSB). Compound specific isotopic analysis of paloernieratane (**II**) in this study yielded identical results, with paleorenieratane (**II**) significantly enriched ($\delta^{13}C$=-12‰ ± 1.5‰) relative to marine algal biomass ($\delta^{13}C \approx$ -30‰; Peters, 2005). The enriched carbon relative to algal biomass signifies derivation from a potentially extinct strain of *Chlorobiaceae*, based on the more positive carbon isotope delta values typical of GSB utilizing the reverse TCA cycle. Paleorenieratane-producing bacteria are assumed to not directly compete with bGSB-producing isorenieratane for the same region of the water column. This assumption is based on the fact bGSB are so well adapted to low light other organisms would be outcompeted for this niche. This means that paleorenieratane-producing bacteria occupy a shallower region of the water column to avoid resource competition. The increased abundance in paleorenieratane signifies the likely increase in habitat volume interpreted as the shallowing and expansion of the chemocline and OMZ to grant greater area for these bacteria to thrive. Analysis of the evolution of the microbial community throughout the Woodford in the following section reveals the increase of carotenoid concentration

coincides with a decrease in the sterane/hopane ratio, providing further evidence for expansion of GSB habitat. Also, Truper and Genovese (1968) noted the three-fold increase in sulfur oxidation by GSB when optimal light conditions were present. These bacteria, specifically the bGSB, are adapted to survive in low light, but when light is not a limiting factor metabolic activity is greatly enhanced. A shallower and thicker chemocline would allow for the migration of GSB communities to better lit regions of the water column, with elevated productivity levels resulting in greater amounts of *Chlorobiaceae* biomass deposited in sediments. The high concentrations of C_{40} aromatic carotenoids reported from ~170-135ft. is strong evidence for a very shallow, expanding and well-defined chemocline developing in the beginning of the MW. Approximately halfway through the MW, destabilization and deepening/thinning of the chemocline is marked by the rapid decrease in C_{40} carotenoid concentration. The prolonged period of PZE in the MW strongly corresponds to eustatic changes experienced during MW deposition. Persistent PZE commenced under a relatively long (longest 3rd order parasequence in the core) 3rd order regression and subsided during the subsequent 3rd order transgression. Isolated periods of PZE in the LW were connected to 3rd order cycles, but correlation of PZE over a longer time period with sequence stratigraphy provides strong evidence for development of euxinic conditions during regressions. The following transgression may have reestablished ocean circulation patterns, currents and vertical mixing present in the LW, limiting stratification from developing. The 2nd order TST may provide additional explanation for the GSB behavior in the LW and MW, assisting in the expansion of the OMZ on the shelf with brief periods of PZE in the LW coinciding with the beginning of pronounced water

stratification in the Woodford Sea. Further sea level rise on a 2nd order scale, with lesser 3rd order regressions providing hydrographic restriction, created an expansive, well developed OMZ saturated with H_2S supporting large populations of GSB in the MW. Restriction and water stagnation in the depositional environment would buffer external disturbances capable of dismantling the well-defined chemocline. Development of sills as sediment supply exceeds the rate of erosion in the 3rd order HSTs could assist in restricting and isolating a body of water from the total system, allowing for unique environmental conditions to develop, such as PZE. If progradation during the HSTs created a barrier between the epicontinental Woodford Sea and the ocean in the south, circulation likely was impeded and stagnant water developed. Isolated periods of PZE in the LW may be a result of sill development (Figure 46), foreshadowing the construction of a more resilient restrictive feature during the 3rd order HST in the MW that allowed for significant stratification to occur. This could explain the relationship between 3rd order regressions and PZE, with PZE indirectly controlled by the restrictive features created during progradation that permit a long period of chemical stratification in a poorly ventilated sea. These bathymetric features would be destroyed during eustatic turnaround as the 3rd order transgression (and ongoing 2nd order TST) imposed greater volumes of water capable exceeding sediment supply, eroding the sills and causing intermixing of waters. The sill would be eroded relatively quickly, explaining the rapid demise of PZE in the MW as intermixing disturbed the chemocline. Sill erosion is not necessary, but would assist in establishing extensive vertical mixing required to disturb the chemocline. Comer (1991) outlines the irregular seafloor topography characterizing the Woodford Sea. Local bathymetric lows with little

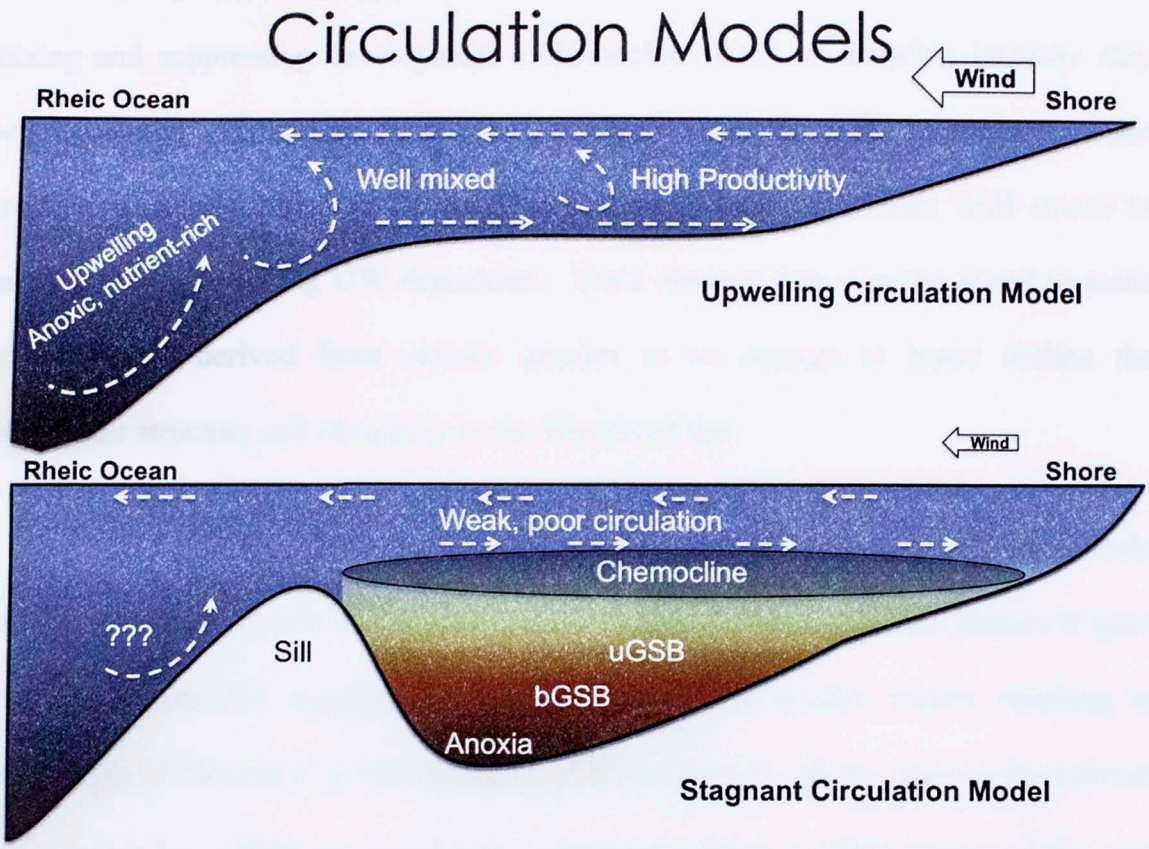

Figure 46. Theoretical circulation models explaining the development of restricted conditions conducive to the development of PZE or well-mixed periods detrimental to the proliferation of *Chlorobiaceae.*

circulation could develop unique conditions permitting GSB proliferation, similar to the sill example. The extent of persistent PZE is marked by the return to 'baseline' of the carotenoids in Figure 45 at ~130ft. Chemocline deepening (80-100m.) and stratification breakdown resulted in constriction of the GSB habitat and subsequent decimation of well-established GSB communities. Following this significant environmental change, the UW possesses minimal concentrations of these carotenoids, but appears to sustain a relatively stable population of the deepest-dwelling GSB. Wavy laminations observed in the UW suggest a shallower water column, possibly too shallow to develop stratification necessary for large GSB communities to thrive. The protracted 2nd order

HST likely deposited large amounts of sediment into the environment, facilitating water mixing and suppressing development a chemocline. Lack of sampling intensity may belie potential chemocline excursions as observed in the LW, or limited sulfide production and light availability could only sustain the most tolerant GSB strains in small populations during UW deposition. Trace element data was integrated to assist interpretations derived from organic proxies in an attempt to better outline the paleowater structure and chemistry in the Woodford Sea.

Trace element data were aligned with aforementioned PZE proxies to help validate and enhance previous interpretations, but little relationship was present (Figure 47). Vanadium and molybdenum become insoluble in euxinic waters, resulting in enrichment of Mo and V in the sediments (Takahashi et al., 2014). During the inferred PZE, V and Mo exhibit no significant enrichment relative to other regions of the core interpreted as non-euxinic. The UW, which was likely the least euxinic of the three members, reveals a critical flaw in the application of trace elements to understanding water column chemistry. V increases, and Mo decreases, indicating additional processes were controlling the deposition of these trace elements to the sediments. The MW was very likely deposited in a sustained period of PZE as inferred from *Chlorobiaceae* biomass, but V and Mo are relatively depleted. Mo spikes during the onset of PZE, as indicated by isorenieratane (**I**) and paleorenieratane (**II**) concentrations increasing, but does not exhibit elevated values during peak PZE. This may be a result of the trace element input to the system, or the utilization of a significant portion of these bioessential elements by organisms in the oxic layer (Takahashi et al., 2014). The fact *Chlorobiaceae* require sulfide-rich waters for electron donors, similar to

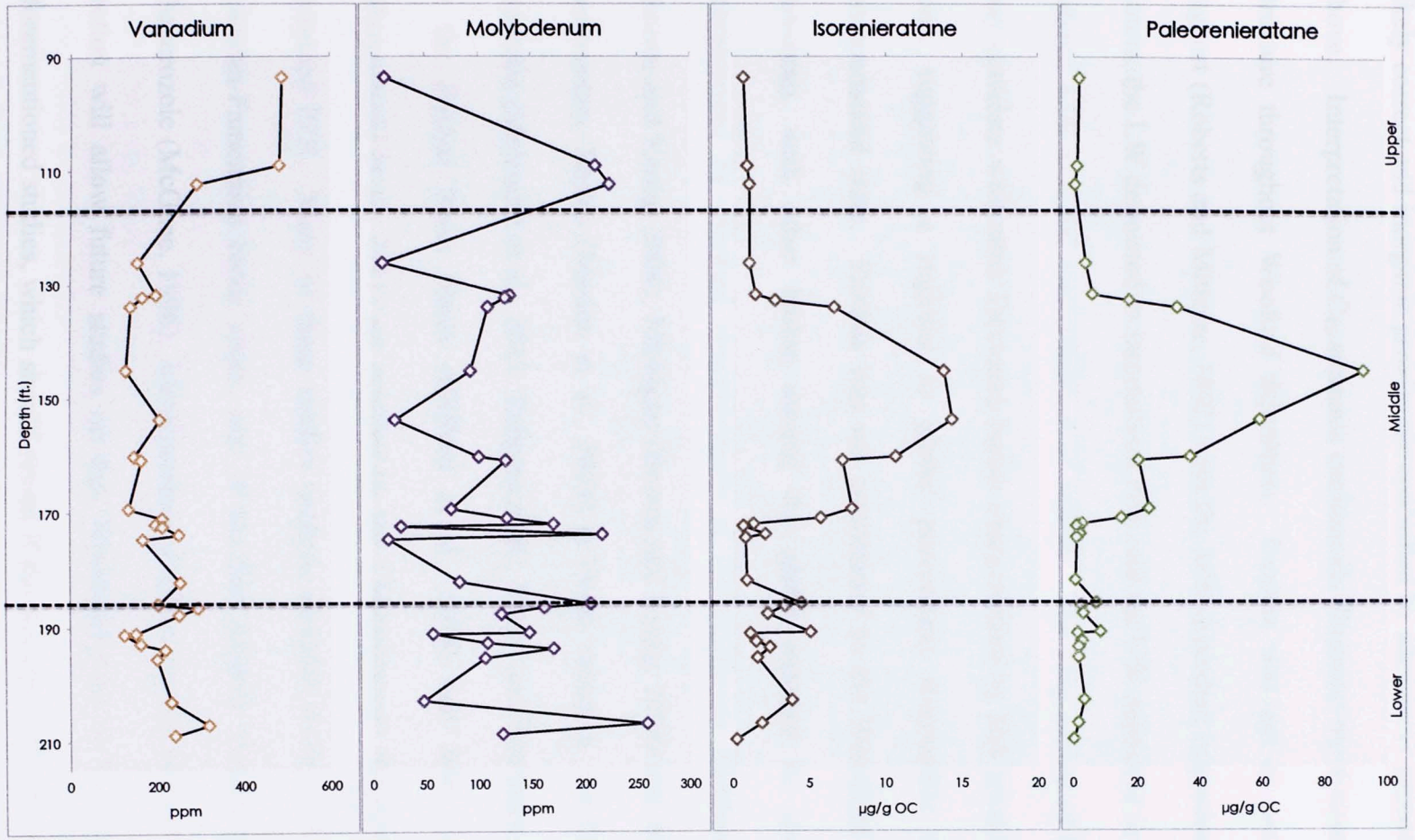

Figure 47. Assessment of organic (isorenieratane and paleorenieratane) and inorganic (vanadium and molybdenum) proxies of PZE. The unique synthesis of C_{40} aromatic carotenoids serves as a more direct indicator of PZE, challenging interpretations based on trace element data.

cyanobacteria which oxidize water for the same purpose, means the organic data is likely correct and inorganic proxies are controlled by alternative processes as discussed above. Interpretation of C_{40} aromatic carotenoids illustrates the dynamic water column structure throughout Wooford deposition. Euxinia was not as persistent as some suggest (Roberts and Mitterer, 1992) with the MW deposited in predominantly euxinic waters, the LW deposited in intermittent PZE and the UW deposited in an anoxic water column with minimal concentrations of sulfide. The long period of PZE in the MW may correlate with other Devonian basins characterized by H_2S invasion of the photic zone, suggesting a regional to global process(es) responsible for this unique environmental state. Euxinia was not constrained to the Woodford Sea during the Devonian, with other basins around the globe reported to contain sediments characterized by elevated concentrations of *Chlorobiaceae* biomass. The Illinois (Brown and Kenig, 2004), Michigan (Brown and Kenig, 2004) and Western Canadian Sedimentary Basins (Maslen et al., 2009) in North America, the Canning Basin in Australia (Melendez et al., 2013; Tulipani et al., 2015), and European sediments found in the Pripyat River Basin (Clifford et al., 1998) and Holy Cross Mountains (Marynowski et al., 2011) are typified by the *Chlorobiaceae* fingerprint indicative of sustained PZE. Many of these studies propose elevated levels of H_2S preceded the Frasnian-Famennian biotic crisis, one of the five greatest biodiversity losses in the Phanerozoic (McGhee, 1996). Identification of this extinction horizon in the following section will allow future studies on this Woodford core to be integrated with the aforementioned studies, which should reveal if the euxinia in the Woodford aligns with global events or is independent of these, controlled by processes operating on a regional

to local scale. In order to properly integrate studies utilizing C_{40} aromatic carotenoid derivatives, such as the aryl isoprenoids, ratios (e.g. AIR) employing these derivatives need to be evaluated as indicators for PZE.

PZE determined by carotenoids in this study parallels previous work done on this core by Romero (2008) and Romero and Philp (2012), which utilized the 2,3,6-aryl isoprenoids (**VII**) in the form of AIR (aryl isoprenoid ratio). This ratio is comprised of the C_{13}-C_{17}/C_{18}-C_{22} 2,3,6-aryl isoprenoids originally proposed by Schwark and Frimmel (2004) to evaluate the persistence of PZE in the geological record. It was found that the upper and lower members were characterized by episodic PZE, with the MW subjected to persistent PZE. This is in agreement with results for this study determined by aromatic carotenoids, but the UW may have experienced minimal H_2S invasion of the photic zone (not as episodic as Romero and Philp 2012 imply) relative to the LW (Figure 45). Use of aryl isoprenoids to infer PZE is unsound unless carbon is isotopically enriched relative to algal biomass, similar to the precursor isorenieratane/paleorenieratane (Summons and Powell 1987; Koopmans et al., 1996a). For those reasons, the AIR was not used to assess PZE in this study due to the detection of precursors permitting direct interpretation of the depositional environment (Figure 44). However, the aryl isoprenoids were evaluated with depth and plotted against potential precursors to assess the potential origins of these compounds. Geochemical logs of both the 2,3,6- (**VII**) and 3,4,5- (**VIII**) aryl isoprenoids reveal markedly similar depth trends as isorenieratane (**I**) and paleorenieratane (**II**). When plotted against these carotenoids, a relatively linear relationship appears for isorenieratane (**I**) and a more logarithmic relationship for paleorenieratane (**II**) (Figure 48). The 2,3,6-aryl

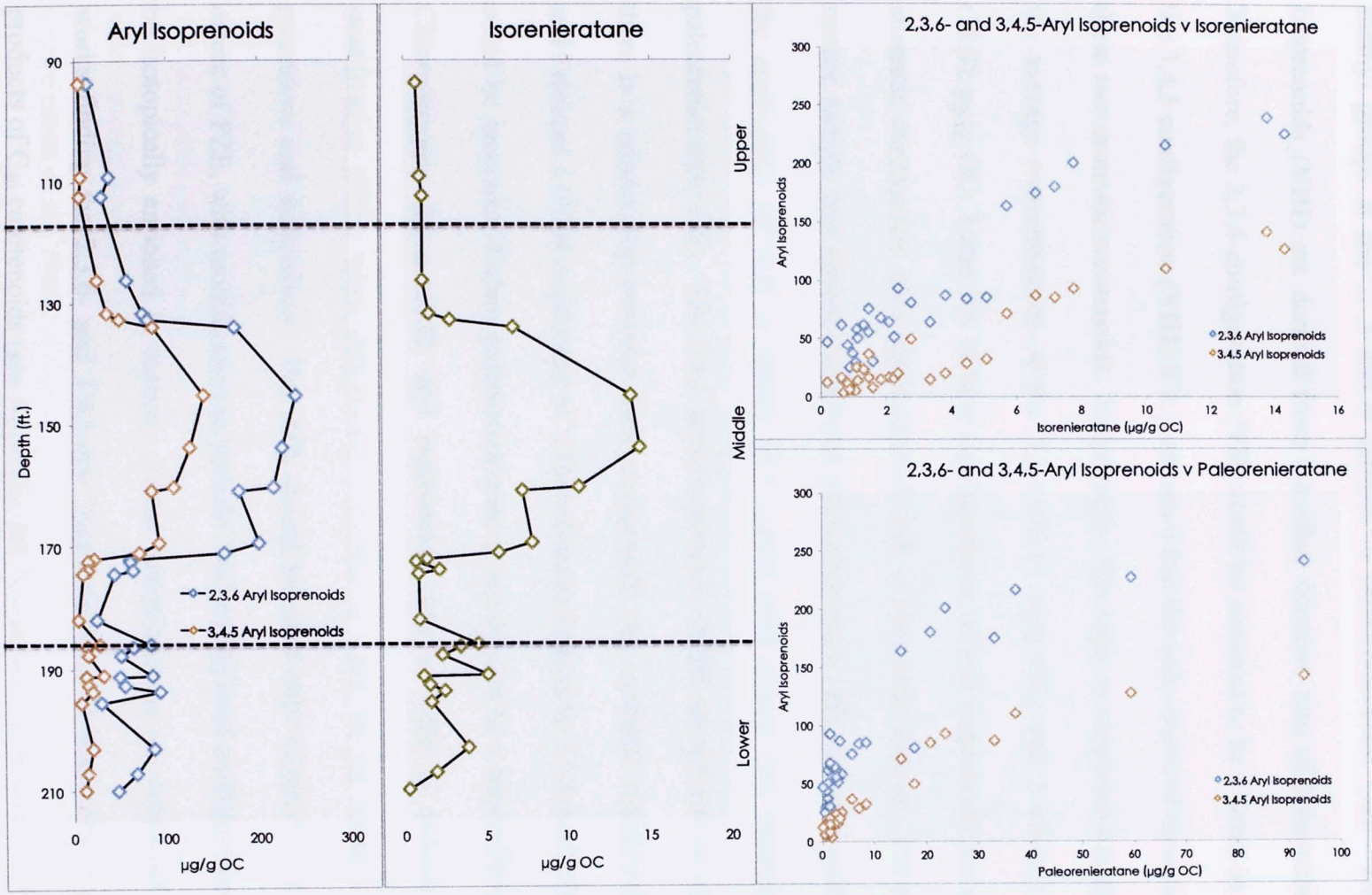

Figure 48. Geochemical log of aryl isoprenoids in the Wyche-1 core and plots evaluating potential relationships between probable C_{40} aromatic carotenoid precursors. This challenges work by Schwark and Frimmel (2004), specifically if the oil/source rock is of Devonian age with possible diagenetic products of paleorenieratane in the 3,4,5-configuration.

isoprenoids (**VII**) are likely sourced from isorenieratane (**I**) and the benzene ring with methyl groups at the 2, 3 and 6 carbons in paleorenieratane (**II**). The 3,4,5 aryl isoprenoids (**VIII**) are derived from the other benzene ring of paleorenieratane (**II**). Therefore, the 2,3,6-configuration (**VII**) could be assumed to be 3 times as abundant as the 3,4,5 configuration (**VIII**) if it is assumed that the sole source of these isoprenoids is these two aromatic carotenoids. Surprisingly, this logic is supported extremely well by the average concentrations of the 2,3,6-(92.11 μg/g OC) and 3,4,5-aryl isoprenoids (38.32 μg/g OC; Table 10). If both configurations of aryl isoprenoids are derived from aromatic carotenoids, then application of AIR is inherently flawed. For example, if a mature sample had initially contained paleorenieratane (**II**) and no isorenieratane (**I**), the application of AIR to assess PZE would only reflect one benzene ring from paleorenieratane (**II**). The 3,4,5 aryl isoprenoids (**VIII**) should not be discounted, as there is a relationship between these compounds and aromatic carotenoids. Schwark and Frimmel's (2004) statement of 'Chlorobiaceae-indicative 2,3,6-methylation pattern' could be incorrect if/when paleorenieratane is recognized as a biosynthetic product of *Chlorobiaceae.* As a result, aryl isoprenoids may be used as indicators of water stratification (PZE) when isotopically enriched or when strong trends exist between precursors and derivatives. The AIR should be used only tentatively to evaluate the extent of PZE, with modification to include 3,4,5-methylated configurations if found to be isotopically enriched in carbon. These interpretations are supported by previous works finding the 2,3,6- and 3,4,5-aryl isoprenoids to be diagenetic and catagenetic products of C_{40} carotenoids (see Appendix **III**; Summons and Powell, 1987; Hartgers et al., 1994). In addition, the tentative detection of β-carotane (**X**; lacking any taxonomic

specificity) in minor quantities suggests potential contribution to the 2,3,6-aryl isoprenoids (**VII**) as well. Any aryl isoprenoids that are products of this carotenoid are not indicative of euxinic conditions, weakening conclusions based on these compounds alone.

Gammacerane (**XXXVII**; Damste et al., 1995b), and to a lesser extent, 28, 30-dinorhopane (i.e. bisnorhopane, **XXXVIII**; DNH; Damste et al., 2014) signify water stratification characterized the depositional environment during deposition. However, gammacerane (**XXXVII**) has been utilized as a marker for hypersaline, highly reducing conditions (Moldowan et al., 1985; Fu Jiamo et al., 1986) and DNH as an indicator of anoxia in clay-poor sediments (Katz and Elrod, 1983; Curiale and Odermatt, 1989). Hypersalinity and anoxia are both capable of creating stratified waters either through density-gradients (hypersalinity) or an oxic-anoxic interface, but in this system the presence of each is likely a function of the chemocline separating H_2S-rich waters from shallower oxic waters. The co-occurrence of DNH (**XXXVIII**) and interpreted euxinia is well-recognized (Grantham et al., 1980; Schoell et al., 1992), as the relationship between DNH (**XXXVIII**) and sulfur-rich water columns is very strong. Interpretations of DNH (**XXXVIII**) should be used with caution in mature samples, as this compound is not bound in the kerogen. This was confirmed by numerous pyrolysis experiments on kerogens associated with bitumens containing DNH (**XXXVIII**), but the compound was never recognized in pyrolysates (Moldowan et al., 1984; Noble et al., 1985; Tannenbaum et al., 1986). This absence from the sulfur-bound fraction (Kohnen et al., 1992; Schoell et al., 1992), confirms the biological origins of DNH (**XXXVIII**), and explains the dilution effect observed as samples mature and additional hydrocarbons are

released into the bitumen from the kerogen. Gammacerane (**XXXVII**) and DNH (**XXXVIII**), despite lacking source-specificity (although gammacerane (**XXXVII**) is likely sourced from tetrahymanol (**XXXVI**)), are proven markers for stratified water columns, and this will be assumed to be the primary application of these compounds throughout this discussion.

The gammacerane index (see Appendix **II** for all formulae) reaches significant levels (GI>0.2) in the lower and middle members, but falls below 0.2 for most of the UW (Table 10; Figure 49). Unexceptional GIs (as observed in lacustrine/hypersaline environments) contrast with Comer's model (2008b), which claims hypersaline brines promoted density stratification restricting vertical water exchange. As discussed previously, the likely cause of stratification was the development of a chemocline separating oxic waters above and sulfidic waters below, independent of density differences produced by salinity variations. The LW exhibits periodic negative excursions of the GI, with a positive excursion marking the lower-middle boundary. It appears to reflect a similar behavior as isorenieratane in the MW, increasing and decreasing in the same samples. In the UW, there is a subtle increase in the GI followed by a gentle decrease. The dinorhopane index is of appreciable amount (Wyche-1 core AVG_{DNHI}=0.34), with peak values approximately 60% of the C_{30} hopane in the MW. The DNHI consistently decreases from the LW into the MW before increasing along with the GI and aromatic carotenoids at 174.42 ft. Unlike the GI, the DNHI continues to oscillate in the MW, before a rapid decline premature to the GI decrease. There is a more pronounced spike at 131.75ft. than in the GI, with an increase from the MW into the UW where it steadily declines (Figure 49). Despite these

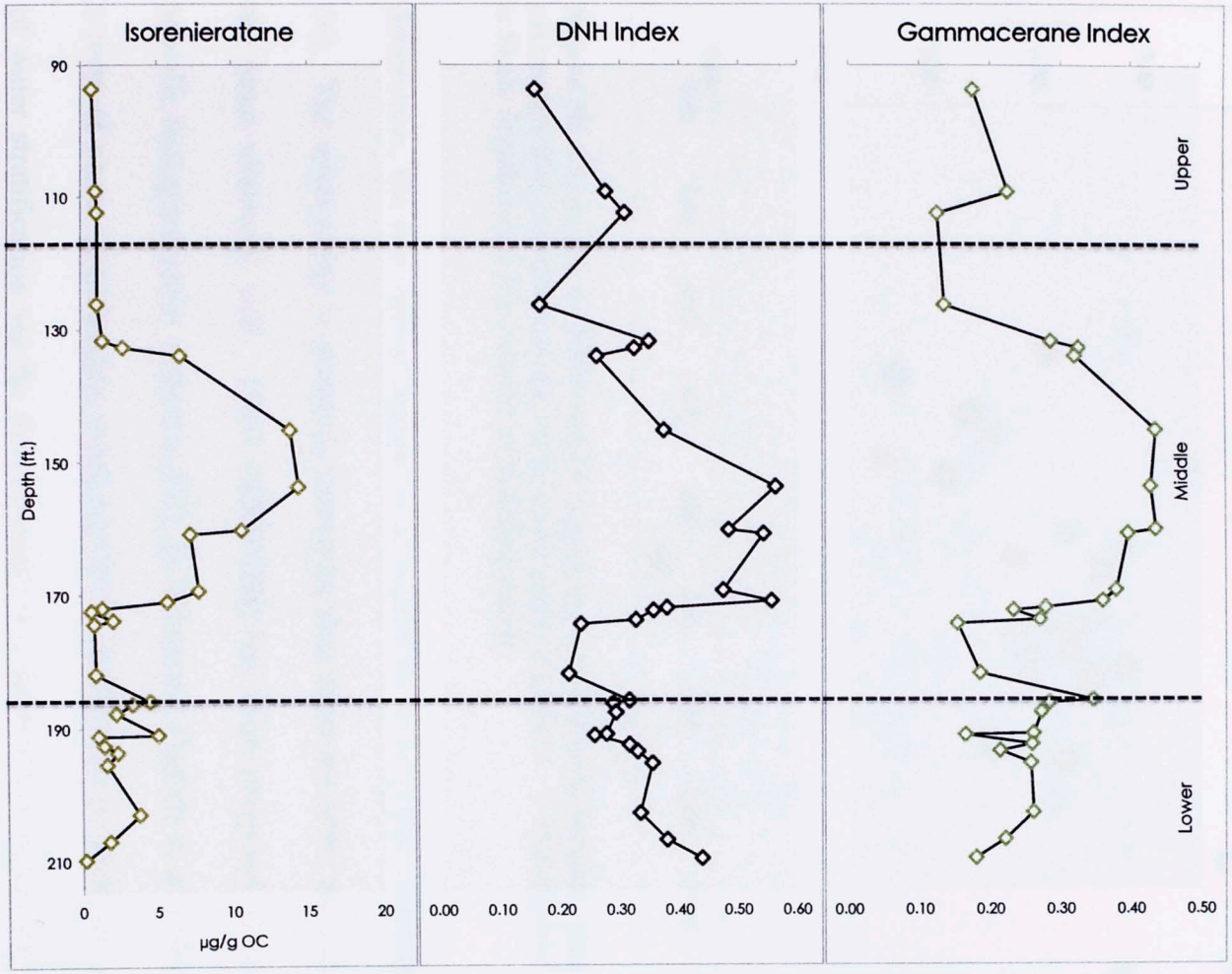

Figure 49. Geochemical logs of stratification proxies (GI and DNHI) compared to the PZE indicator, isorenieratane for the Wyche-1 core. The GI is relatively similar to the PZE log, with the DNHI apparently affected by additional processes, such as direct competition with the GSB for sulfur species.

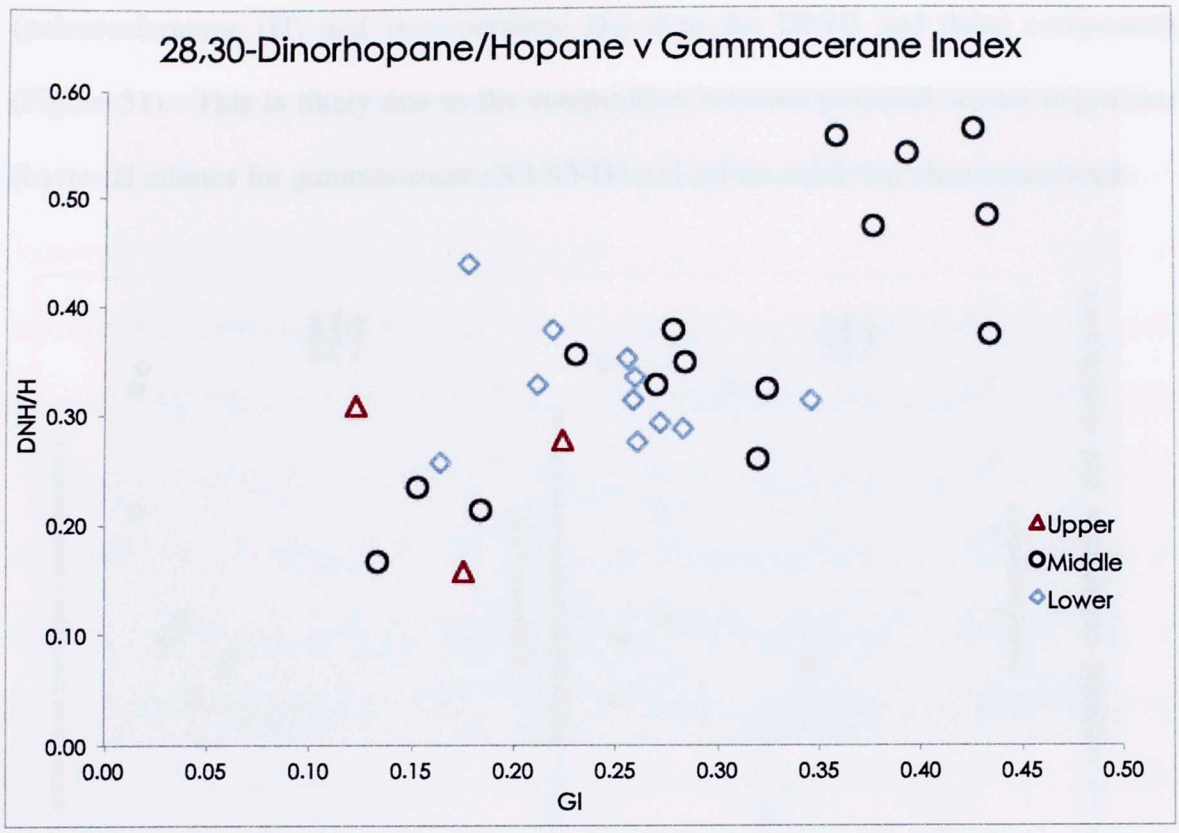

Figure 50. Cross plot of DNHI and GI displaying a relationship between these two biomarker parameters that extends from the lower to the upper members. A relationship between the two is likely founded on a requirement of stratified waters.

differences, the two indices appear to be related by a cross plot of DNHI v GI (Figure 50). The relationship is primarily driven by data from the MW, but other members fit the trend relatively well. DNH (**XXXVIII**) has been proposed to originate from a specific biological entity related to PZE by Sinninghe Damste et al. (2014). The PZE is a form of ocean stratification, implying DNH (**XXXVIII**) is likely an indirect product of water stratification via the development of a chemocline separating sulfidic waters and oxic waters. A correlation was found between sulfur-bound isorenieratane (**I**) and DNH (**XXXVIII**), substantiating the evidence for the relationship between DNH (**XXXVIII**) and PZE (Kuypers et al., 2002; Sinninghe Damste et al., 2014). In this study, a stronger relationship exists between the GI and C_{40} aromatic carotenoids

(paleorenieratane (**II**) and isorenieratane (**I**)) than the DNHI and these compounds (Figure 51). This is likely due to the competition between potential source organisms (bacterial ciliates for gammacerane (**XXXVII**) and sulfur-oxidizing chemoautotropic

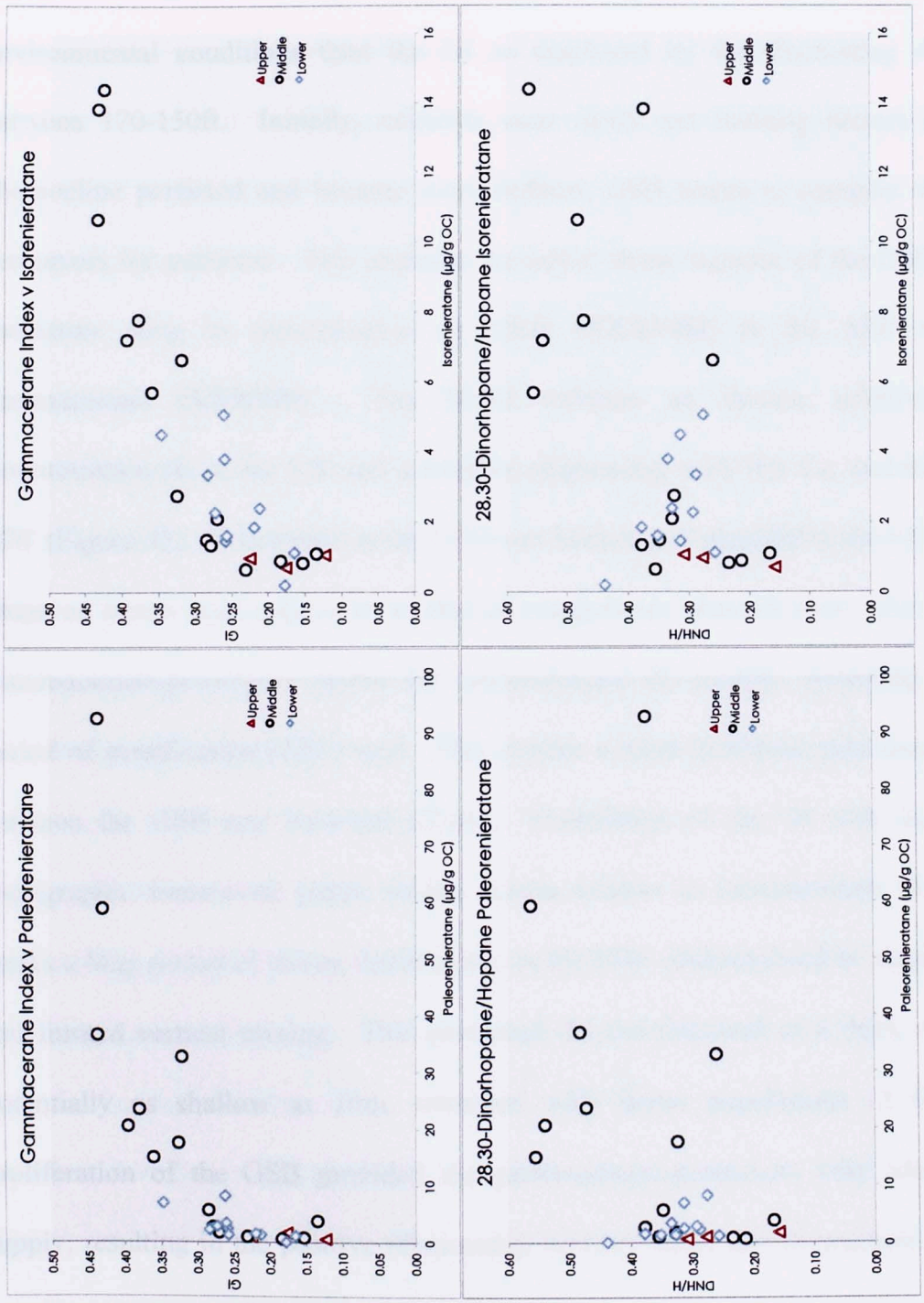

Figure 51. Cross plots depicting the potential correlation between C_{40} aromatic carotenoids and stratification proxies (GI and DNHI).

bacteria for DNH[7] (**XXXVIII**)) in the water column throughout deposition. Bacterial ciliates feeding off bacteria (e.g. GSB) may be more resistant to poor-nutrient concentrations (e.g. sulfur) required by chemoautotrophic bacteria. The DNHI increases along with the GI in the MW, but appears to be more sensitive to environmental conditions than the GI as displayed by the fluctuating data points between 170-150ft. Initially, nutrients were likely not limiting factors but as the chemocline persisted and became more defined, GSB began to compete with DNH-precursors for nutrients. This explains the initial sharp increase of the DNHI and the premature drop in concentration of DNH (**XXXVIII**) in the MW relative to gammacerane (**XXXVII**). The DNHI exhibits an inverse relationship with isorenieratane (**I**) in the LW and a positive relationship with this C_{40} carotenoid in the MW (Figure 51). If nutrients in the LW were limited and plentiful in the MW, then the observed trends lend support to claims of competition between these two organisms. Gammacerane-precursors mirror the isorenieratane (**I**) closely, reflecting the entire period of stratification (PZE) well. This implies a more symbiotic relationship existed between the GSB and bacterial ciliates. Correlation of the GI with the sequence stratigraphic framework yields similar results relative to isorenieratane (**I**). The GI marks a long period of strong stratification in the MW, characterized by stagnant waters and limited vertical mixing. This permitted the development of a thick chemocline, potentially as shallow as 10m, saturated with dense populations of GSB. The proliferation of the GSB provided the gammacerane-precursors with adequate food supply, resulting in the positive relationship between these two biomarkers. A similar

[7] These compounds will be the focal point of the discussion on potential sources for disputed biomarker origins to avoid digression of the current context.

relationship exists between the GI and paleorenieratane (**II**), but this trend is not as apparent as the relationship between the GI and isorenieratane (Figure 51). The DNH-precursors appear to undergo stress in the initial stages of PZE (oscillations) and the latter parts of PZE, suggesting competition between some other organisms. Alternatively, DNH (**XXXVIII**) may be sourced from a species yet to be recognized, invalidating the prior reasoning. This study does not imply gammacerane (**XXXVII**) or DNH (**XXXVIII**) are derived from a specific species, as more evidence (i.e. isotopic data) is required to suggest these origins, but in the scope of this study strong empirical evidence (Figure 51) exists relating the proliferation of GSB and PZE with the development of gammacerane (**XXXVII**), and to a lesser extent, DNH (**XXXVIII**). These findings are in agreement with previous studies that found gammacerane (**XXXVII**) and DNH (**XXXVIII**) to be markers of water stratification (Sinninghe Damste et al., 1995b; Sinninghe Damste et al., 2014).

Evaluation of the DNHI as a marker for anoxia is troublesome in this study due to the relatively unchanged redox state (highly reducing) observed in the Woodford (Figure 52). Previous work has claimed this biomarker to be a marker for anoxia in high concentrations, but that concentration is not well defined (Katz and Elrod, 1983; Dahl, 2004). Others report the presence of DNH (**XXXVIII**) is sufficient to infer anoxia, in any concentrations (Slowakiewicz et al., 2015). Little relationship exists between the slight changes in the homohopane index, which has been used to discern highly reducing conditions persisted in the depositional environment (Peters and Moldowan, 1991), and the DNHI. The homohopane index exceeds 10% (marker for anoxia) only in the UW, with values below 10% characterizing the lower and middle

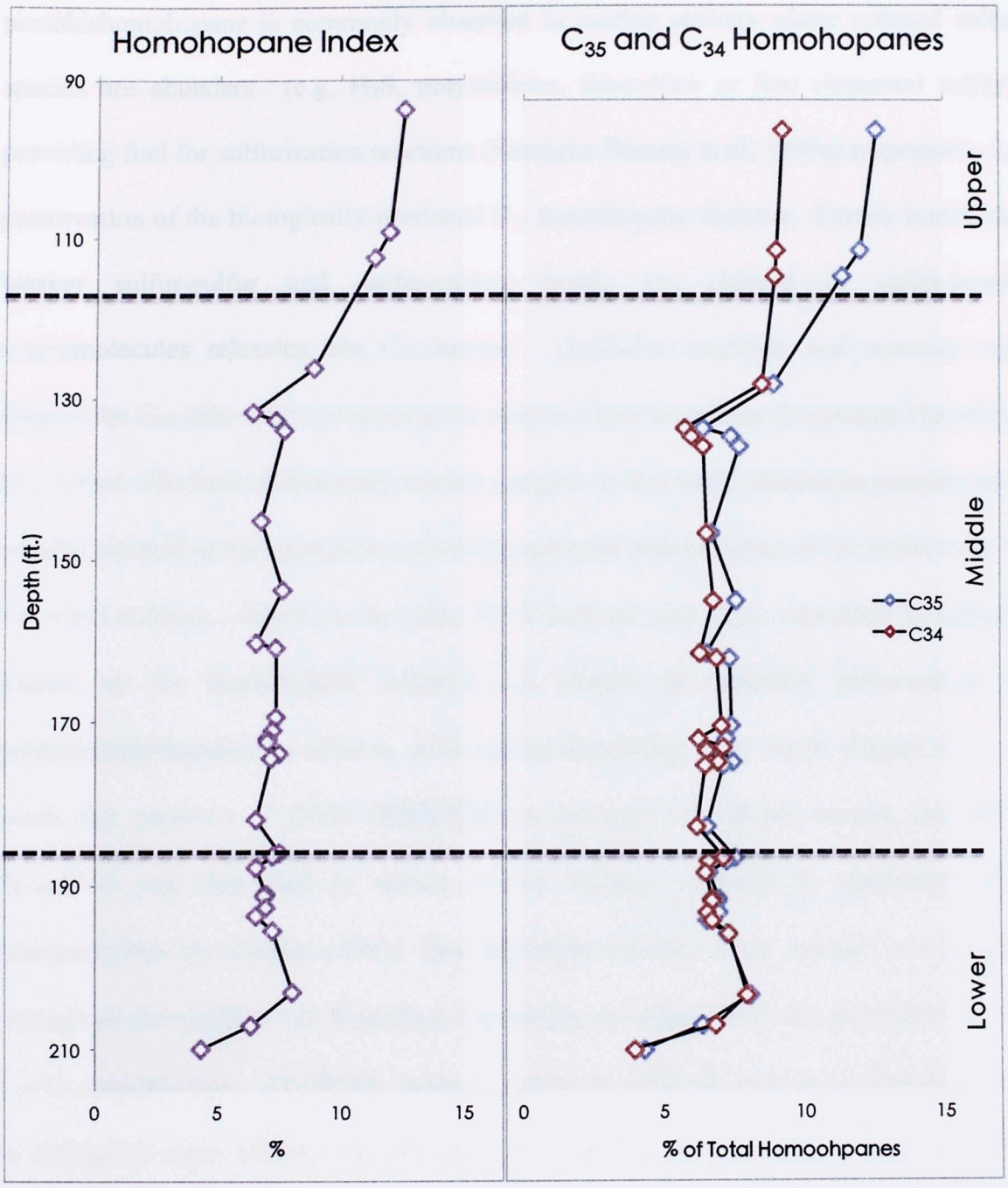

Figure 52. Redox variations in the Wyche-1 core indicated by the homohopane index (see appendix **II**) and relative percent of the C_{34} and C_{35} homohopanes to the sum of the C_{30}-C_{35} hopanes.

members (Table 10). However, the C_{35}/C_{34} αβ(S+R) homohopane ratio exceeds 1 in many of the samples (Table 10; Figure 52), noted to characterize marine anoxic environments (Bishop and Farrimond 1995). This selective preservation of

pentakishomohopane is commonly observed in marine settings where reduced sulfur species are abundant (e.g. H_2S, polysulfides, thiosulfate or free elemental sulfur), providing fuel for sulfurization reactions (Sinnighe Damste et al, 1995a) responsible for preservation of the biologically-produced C_{35} homohopane skeleton. During burial, the weaker sulfur-sulfur and sulfur-carbon bonds are cleaved in sulfur-bound macromolecules releasing the C_{35} hopane. Oxidative reactions and maturity will destroy the C_{35} side-chain, producing the shorter-chain homologs (Sinninghe Damste et al., 1995a). The lack of thermally mature samples in this study eliminates maturity as a possible control on this parameter, allowing unbiased interpretation of the redox state in the water column. Based on the data, the Woodford was likely deposited in suboxic (based on the homohopane index)/anoxic (based on selective preservation of pentakishomohopane) conditions, with anoxia decreasing with depth (Figure 52). If solely the presence of DNH (**XXXVIII**) is assumed to indicate anoxia, the entire Woodford was deposited in anoxic bottom waters. This is in agreement with interpretations by Comer (1991) that persistent bottom water anoxia was present throughout the majority of Woodford deposition and agrees with the predominance of C_{35}/C_{34} hopane ratio. The Pr/Ph values are given in Table 10, but are not discussed due to biological input effects (ten Haven et al., 1987) and the immature nature of the samples (Peters et al., 2005). The subtle change in the homohopane redox parameters makes it difficult to attribute DNH (**XXXVIII**) fluctuations to redox variations, with the more likely control being water stratification. Similar to proposed maturity parameters, the hop-17(21)-enes were used in the numerator of a ratio to assess the redox state of recent-ancient water columns. The C_{35}/C_{34} hop-17(21)-enes (**XLI**) plotted against the

C_{35}/C_{34} hopanes reveals the potential application of these homohopane precursors as a redox proxy (Figure 53). Conversion of the hop-17(21)-enes (**XLI**) to neohop-13(18)-enes (**XXXIX**) via clay mediated rearrangement may affect this ratio in certain cases, but it appears to exert little effect on the applicability of this proposed redox proxy in this study. Despite the detection of neohop-13(18)-enes (**XXXIX**) in appreciable abundance (Table 8), the ratio remains comparable to the standard application of the saturated homologs. The limited maturity range of the Woodford in this study limits the evaluation of this ratio beyond observation of correlations, but this proposed redox proxy may find application in immature-early mature source rocks elsewhere.

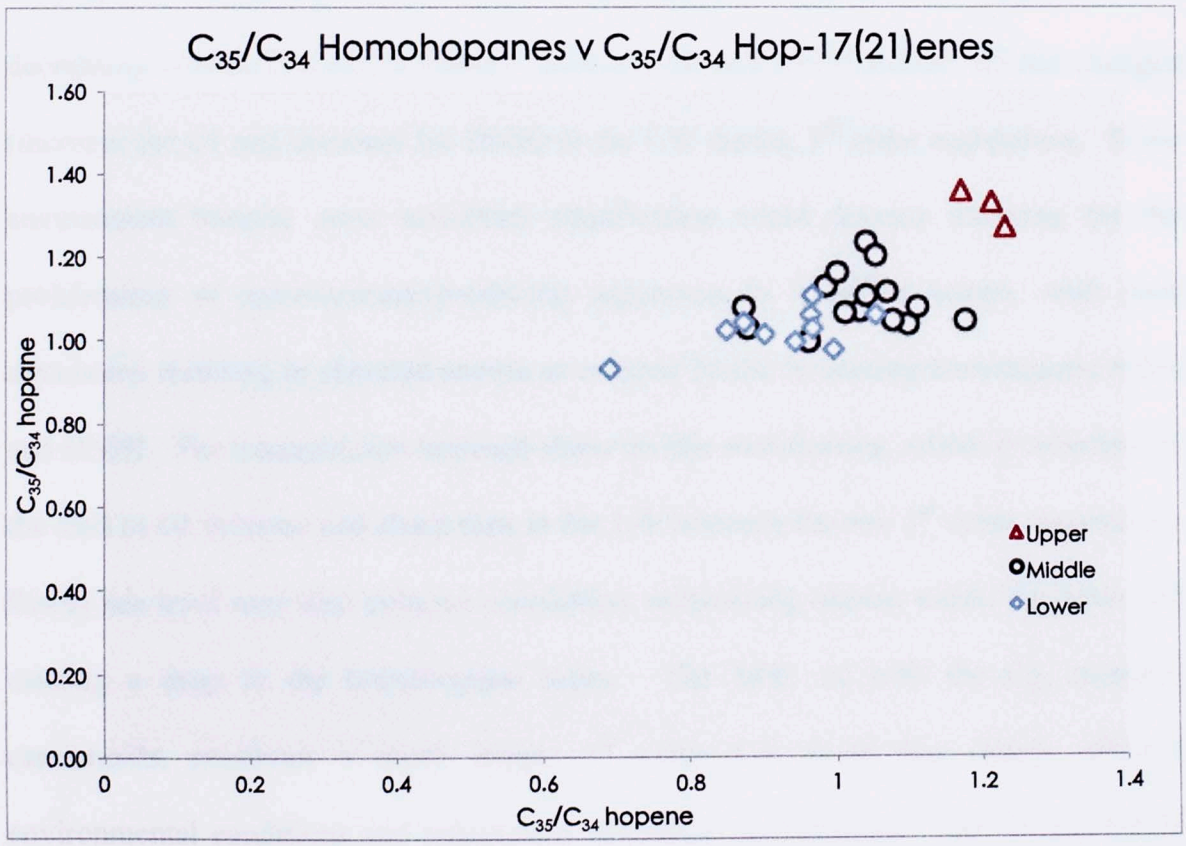

Figure 53. Cross plot of hop-17(21)-enes and homohopanes to assess the ability to utilize the hop-17(21)-enes as redox proxies due to the selective preservation of the C_{35} skeleton in highly reducing conditions.

Eustatic fluctuations could be influencing the observed changes in redox and stratification indicators utilized in the previous discussion. In the LW during the first 3rd order regression, the GI increases and the DNHI decrease (Figure 54) which corresponds to the first PZE episode in the LW (Figure 45). The inverse nature of the two indices reflects the possible competition between GSB and the biological source of DNH (**XXXVIII**) previously outlined. Initial bursts of H_2S into the photic zone in the LW were not sustainable, likely due to limited nutrients and environmental factors. The GSB were much more capable of scavenging sulfur compounds, assisting in the development of a defined chemocline where bacterial ciliates (gammacerane, **XXXVII**) were able to temporally thrive. The GI increases overall in the LW, with the DNHI decreasing overall in a cyclic pattern. Both the GI and DNHI exhibit similar changes (increase for GI and decrease for DNH) in the LW during 3rd order regressions. If the environment became more restricted, stratification could develop allowing for the proliferation of gammacerane-producing organisms in stratified waters, with poor circulation resulting in elevated anoxia as evinced by the increasing homohopane index and DNHI. The transgression imposed stress on this stratification, which is reflected by the stall in GI increase and sharp dips in the LW between the two 3rd order regressions. Rising sea level may also enhance circulation, minimizing anoxia within the basin and causing a drop in the homohopane index. The MW, as with the C_{40} aromatic carotenoids, possesses a much longer 3rd order T-R cycle that clearly affected environmental conditions and subsequent biomarker distributions. The GI and DNHI increase in the MW at 172 ft., marking the onset of chemically induced stratification by PZE. The GI is more stable throughout the persistent PZE interval, with a strong

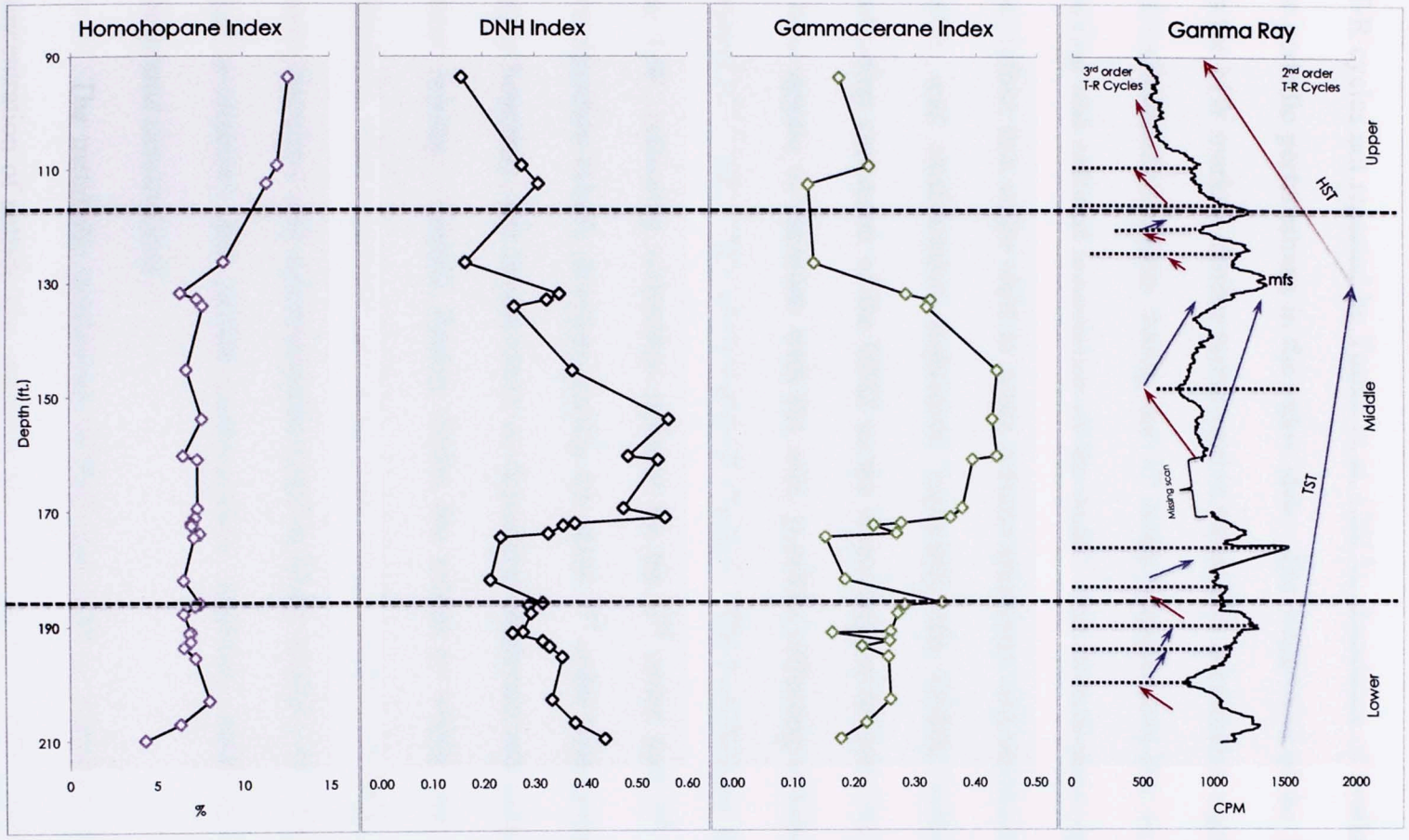

Figure 54. Assessing sequence stratigraphic controls on the redox (HHI and DNHI) and stratification (GI and DNHI) proxies in the Wyche-1 core.

relationship with the carotenoid distribution during this time (Figure 51). The DNHI begins to oscillate, indicating this stratification proxy may be more sensitive to 4th order T-R cycles not reported by Turner et al. (2015), abundance of available sulfide species or periodic perturbations in the redox state. The turnaround of the 3rd order T-R cycle in the MW marks a similar turnaround in biomarker parameters, signifying the collapse of well-stratified waters during the 3rd order transgression due to enhanced vertical mixing and reduced constriction of the basin. The homohopane redox indicator does not reflect this major shift in water column chemistry and structure. At 131.75ft. the redox and stratification indicators, especially the DNHI, exhibit sharp changes indicating expansion of the OMZ as the water column became increasingly stratified. These appear to correlate with the mfs, possibly reflecting enhanced and prolonged preservation rather than environmental changes. The homohopane index increases into the UW, reflecting restriction induced by the 3rd order and 2nd order regressions. Stratification briefly develops during the short 3rd order transgression at the middle-upper boundary, but breaks down as deposition continued and progradation facilitated water mixing. Sample density limits the extent to which this can be explained, especially when regression facilitates water stratification in the MW. The differences in water chemistry and environmental controls likely explain this discrepancy, with pH, light availability and sulfide concentration imposing additional controls on these compound distributions.

The metabolic persistence of PSB and GSB is a function of the presence and concentration of sulfide (i.e. electron donor; Gorlenko, 1988), light availability (Biebl and Pfennig, 1978; French et al., 2014) pH (Gorlenko, 1988; Madigan, 2002) and

salinity (Gorlenko, 1988; Frigaard and Dahl, 2008). Primary application of these organisms to understanding the geologic record relies on the characteristic stratification, PZE, typifying environments sustaining populations of sulfur bacteria. An understanding of the chemocline depth and persistence has been established employing these sulfur oxidizing bacteria, with an attempt to extend applications of these biomarkers beyond PZE to be proposed. There are few studies, if any, which have attempted to utilize the physiological requirements of these organisms to characterize paleoenvironmental conditions operating in conjunction with, or in isolation from, PZE.

Light availability is a function of water clarity, latitude (angle at which light penetrates the water), and obstructions (e.g. algal/bacterial mats) in the depositional environment. Fluctuations in the amount of light penetration could mislead interpretations of chemocline depth. For example, murky waters inhibit light infiltration, stressing organisms poorly adapted to low light conditions while clear waters allow for maximum light penetration. Fluctuations in the C_{40} aromatic carotenoid distribution may not solely reflect the shallowing or deepening of the chemocline, but water clarity as well. Chemocline depth may have been less than 25m during Woodford deposition, but was littered with sediments perturbing light from reaching adequate intensities to support the PSB population. Thick algal mats in the oxic zone may have prevented light of the appropriate wavelength penetrating the chemocline, denying PSB of necessary resources to sustain a population large enough to be recorded in the sedimentary record. Latitude was likely not a factor in the absence of PSB, with subtropical to tropical latitudes ideal for the proliferation of *Chromatiaceae.* The 3rd order regressions in the Woodford that appear to partially control PZE likely

introduced considerable amounts of sediment and humic material into the environment. Humic substances have been reported to absorb a significant portion of blue and ultraviolet wavelengths, giving the bGSB an adaptive advantage over the GSB and PSB (Parkin and Brock, 1980). This would explain the predominant occurrence of paleorenieratane (**II**) and isorenieratane (**I**), and the lack of okenane (**V**; PSB) and chlorobactane (**VI**; GSB) during periods of PZE. Chlorobactane (**VI**), produced by the green strain (GSB) of sulfur bacteria, was found to thrive in water columns shaded by PSB. Despite being specialized to absorb light of the blue-green spectra, green strains are outcompeted by brown strains when exposed to blue-green wavelengths and the opposite occurs when exposed to red-white wavelengths. Parkin and Brock (1980) interpreted this to be a result of the shading effect by PSB, increasing the proportion of long wavelengths comprising the spectra and complimenting the pigment tactics of the green strain (Vila and Abella 1994). The deeper chemocline, or cloudy water, prevented the development of PSB, causing the GSB to be outcompeted by the energy- and light-efficient bGSB. A deeper chemocline is an acceptable interpretation, as bGSB are enriched with carotenoids (isorenieratane **I**) and bacteriochlorophylls not found in other strains (Gorlenko, 1988). This would enable survival of bGSB in poorly lit waters over the less resistant green and purple strains. Light alone is not the ultimate control on sulfur oxidizing bacteria distribution and concentrations, with the inversely proportional sulfide gradient (relative to light) equally as important.

The existence of the brown strain and an unknown (paleorenieratane **II**) strain of GSB in the Woodford samples implies sulfide concentrations were relatively high. According to Gorlenko (1988), hydrogen sulfide is the primary control on the

establishment of one species over another. The GSB have been reported to possess a greater affinity for sulfide in experiments with PSB of similar growth rates and subjected to identical light conditions. *Chlorobiaceae* deposit sulfur as extracellular globules that can be utilized as an electron donor at a later time and only by that particular cell, whereas *Chromaticeae* disperse the sulfur throughout growth media rendering it useless for immediate donor-ship (van Gemerden, 1983). The affinity for sulfide in GSB is underlined by the preferential use of this substrate over other sulfur substrates (i.e. polysulfides), even if in greater abundance (Brune, 1989). Guerrero et al. (1985) reported similar results supporting the greater affinity and toleration of high sulfide levels in the water by GSB. It is of no surprise that sulfur affinities have developed inversely proportional to light requirements in sulfur oxidizing bacteria. The PSB require the least incisive light spectra, but tolerate lower concentrations of sulfide, especially in the inhibitory, toxic form H_2S; while bGSB tolerate much higher concentrations of H_2S, are sulfide-inclined, and require the least amount of light to sustain metabolic activity. However, even bGSB require sulfur substrates for bacterial photosynthesis, which are often provided by sulfur-reducing bacteria in marine environments. If light is thought of as a top-down control on sulfur-oxidizing bacterial communities, then the availability/concentration of sulfide species may be considered a bottom-up control on these bacteria. Sulfur-reducing bacteria typically inhabit near or at the bottom of the water column, with a secondary community existing in the upper regions occupied by sulfur-oxidizing bacteria. Sulfide diffuses upward, where it is utilized by the PSB/GSB in the photic zone. Cessation of sulfur reduction due to collapse of the sulfur-reducing community could occur if extracellular sulfur is

competed for by the GSB and the sulfur-reducers, which may halt the sulfur recycling in the system. Some species of sulfur-reducing bacteria are unable to utilize sulfide as an electron donor and require sulfur for this reaction. If GSB oxidize extracellular sulfur, generating sulfate, then the recycling of sulfur will terminate and eventually the sulfur-oxidizing bacteria will be elementally starved. This scenario is unlikely though, with experiments by Biebl and Pfenning (1978) indicating that minimal amounts of sulfur are necessary to sustain these populations, implying sulfur recycling is considerably efficient in nature. Additionally, the affinity of GSB/PSB for sulfide assists in regulating this sulfur balance, permitting the majority of extracellular sulfur to be incorporated by sulfur-reducing bacteria. This demonstrates the importance of sulfide, and presence of a source (e.g. sulfur-reducing bacteria), to the development of a chemocline and recognition of PZE in ancient environments. From a chemical perspective, sulfide production may have been inefficient to diffuse to shallower depths required by okenane- and chlorobactane-producing bacteria. Alternatively, formation of dense bGSB mats may have inhibited the transport of sulfur species to these better-lit depths, or the sulfur-reducing bacterial population was not sufficient to produce the amount of sulfide necessary to diffuse hundreds of meters through the water column. In contrast, sulfur-reducing bacteria may have been prolific in sulfide production to the extent that high concentrations proved toxic to other strains of GSB/PSB. This is especially true at low pH values (Gorlenko, 1988), suggesting tolerance to sulfide may have been a key factor controlling phototrophic sulfur-oxidizing bacterial populations.

The importance of pH hinges on the ability for these values to influence the velocity at which a reaction proceeds. Low pH values are optimum for H_2S retention in

water as undissociated hydrogen sulfide molecules build up and produce inhibiting effects on surrounding organisms. This will cause the selective growth of more tolerant organisms (e.g. GSB relative to PSB) to capitalize on these stressful conditions as discussed previously. It has been reported that a large variety of GSB species require pH values in the range of 6.4-7.8 (Gorlenko, 1988) in lacustrine environments and 4-6 in hot springs (Madigan, 2002), so an attempt was made to observe any relationship between biomarkers affected by water acidity and C_{40} aromatic carotenoid abundance (Figure 55). The primary assumption regarding this discussion pertains to the rearranged biomarkers diasterene (**XXXI**), diahopane (C_{30}^{*}/H) and neohop-13(18)-enes (**XXXIX**) reflecting predominantly chemical, not lithologic, variations mediating backbone rearrangement. Diasterenes (normalized to regular steranes) and neohop-13(18)-enes (normalized to C_{30} hopane) display similar relationships overall and in individual members of the Woodford Shale with the aromatic carotenoids isorenieratane (**I**) and paleorenieratane (**II**). Overall, isorenieratane (**I**) and paleorenieratane (**II**) increase with decreasing pH proxy ratios, with carotenoid abundances exhibiting elevated values beginning between 0.96-1.27 DSE/S and 1.31-1.62 NeoH/H. Peak carotenoid abundance narrows to a range of 0.66-0.96 DSE/S and 0.71-0.93 NeoH/H (pH equivalents 6.4-7.8; Gorlenko, 1988), but several issues are likely already noted. The ranges are strictly controlled by the overwhelming abundance of carotenoids in the lower-middle MW, with values from all three members falling within the above ranges, but producing no elevated concentrations of GSB derivatives. This is strong evidence pH was secondary to a principle control(s) governing the proliferation of GSB in the MW. Therefore, the following discussion does not imply pH was a serious control

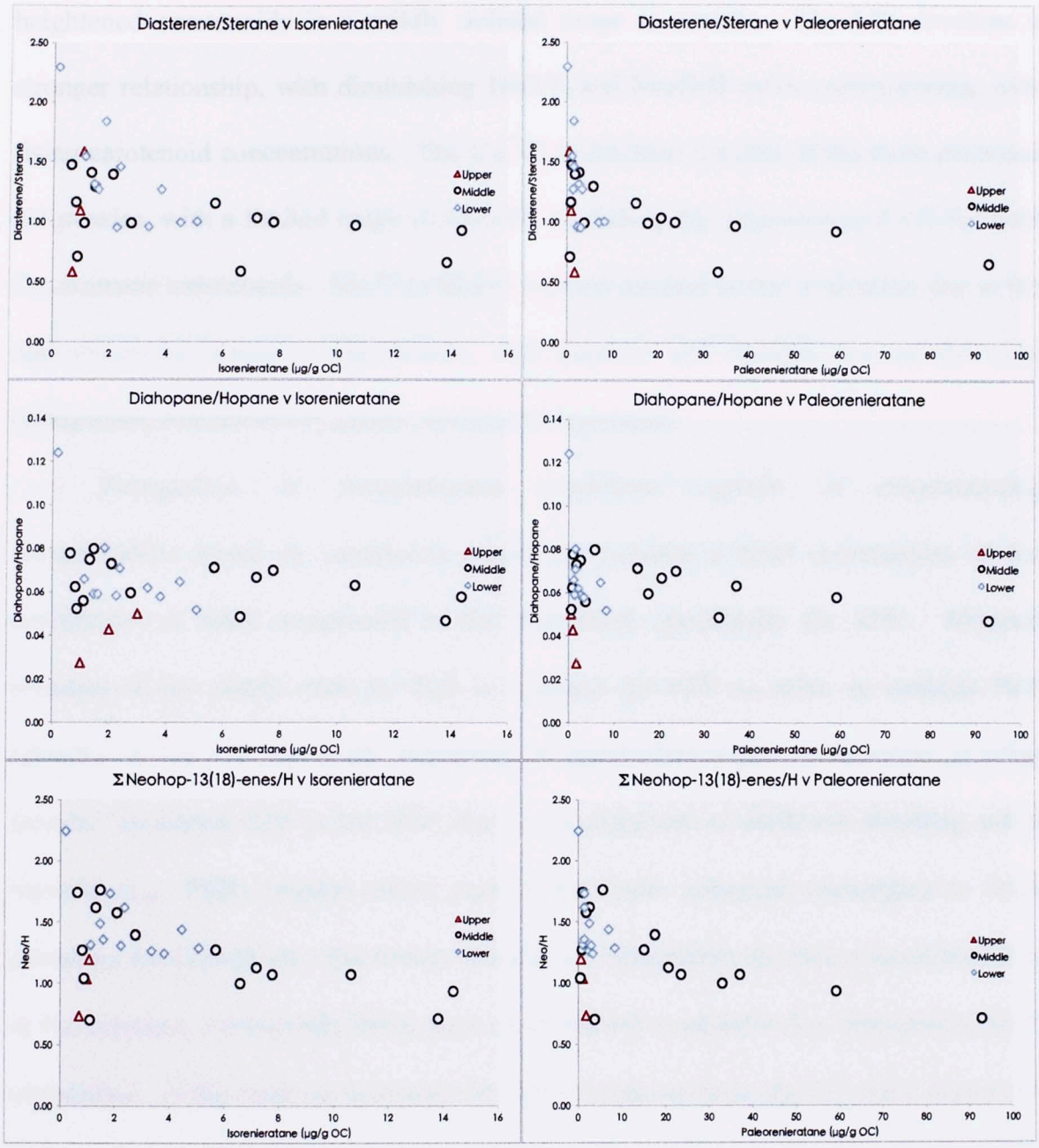

Figure 55. Cross plots of select rearranged biomarkers and C_{40} aromatic carotenoids geared towards interpretation of pH effects on GSB metabolic function.

mechanism on the GSB, but implies a certain range of pH values assisted in the advancement of GSB up the biological ladder. Variations in clay content may impact these ratios as well, resulting in the apparent similarities between samples characterized by different pH values at the time of deposition. Regardless, the observation of

heightened carotenoids in a mildly defined range is notable. The LW develops a stronger relationship, with diminishing DSE/S and NeoH/H ratios corresponding with rising carotenoid concentrations. The C_{30}^{*}/H is the least specific of the three proposed pH proxies, with a limited range (0.03-0.08, excluding the aberration at 0.12) for both C_{40} aromatic carotenoids. MATH (**XLIV**) was not applied to this evaluation due to the non-ubiquitous nature of distribution, with hopanes and steranes two of the most omnipresent biomarkers in aquatic marine environments.

Recognition of environmental conditions capable of misconstruing interpretations based on carotenoid abundance requires a brief reevaluation of the distribution of these compounds in the Woodford, specifically the MW. Minimal invasion of the photic zone by H_2S is required for PZE to exist, so isolated PZE episodes in the LW are likely explained by chemocline depth independent of other factors. Sustained PZE in the MW, but no development of shallower-dwelling sulfur bacteria (e.g. PSB), implies either chemocline depth remained unchanged or other processes were involved. The former is unlikely, reflected by the pronounced increases in C_{40} aromatic carotenoids likely as a result habitat expansion (i.e. chemocline/OMZ expansion). If the latter is assumed, the relationship between the 3rd order regression and persistent PZE in the MW may have been induced by humic input during progradation. Increased concentration of particulate matter in the water, especially humic sediments, would inhibit the penetration of light regardless of the absorption spectra. Chemocline depth likely did rise, but the selective absorption by humic material could have impeded the growth of okenane- and chlorobactane-producing bacteria. The rapid increase observed in these biomarkers implies a bountiful supply of

sulfide became available for use, possibly proving toxic (dependent on pH and concentration) to other bacterial strains such as the PSB. A deepening of the chemocline is less complex, but may have been controlled by other processes. Decline in isorenieratane (**I**) and paleorenieratane (**II**) may have been due to cessation of sulfide production by sulfur reducing bacteria, resulting in lessened amounts of sulfide diffusing upward, diminishing the photic extent of the chemocline. The 3rd order transgression likely increased the water depth, which may have impacted light availability to sub-chemocline depths as the oxic zone expanded due to vertical mixing.

The Woodford was deposited in a dynamic water column as evinced by aromatic carotenoids, gammacerane, 28,30-dinorhopane and aryl isoprenoids. Lack of okenane and chlorobactane suggests the chemocline was deeper than 25m during episodic PZE in the LW and between 10-25m in the MW; but light availability, sulfide concentration and pH may affect this interpretation. Thick algal mats in the oxic zone or turbid, murky waters littered with humic matter would adversely impact the sulfur oxidizing bacteria immediately below the chemocline. An abundance of sulfide or low pH would prove toxic to less tolerant organisms, causing the observed carotenoid distributions in this study. *Chlorobiaceae* were dominated by the brown strain (paleorenieratane excluded), which is well adapted to low light conditions provided by a deeper chemocline, turbid waters or dense communities of oxygenic phototrophs. The LW exhibits periodic PZE and an overall increase in water stratification. Isolated spikes of carotenoid concentrations reflect brief expansion of the chemocline in this member. The MW was deposited during a lasting episode of PZE, evinced by exceptional *Chlorobiaceae* biomass input reflecting a thicker and shallower chemocline.

Stratification was marked by enhanced amounts of gammacerane as well, which closely mimicked carotenoid distributions. Redox state remained relatively constant throughout LW and MW deposition, with the greatest increase leading up and into the UW characterized by the formation of a 2nd order HST. The AIR should be used with caution to assess the extent of PZE, as contribution from paleorenieratane to the 3,4,5-aryl isoprenoids is a possibility overlooked by this ratio. The DNH is suggested as a marker for anoxia and tentatively, stratification, with unidentified processes controlling its abundance in this study.

4.6. Evolution of the Microbial Community and Possible Source Organisms for Disputed Biomarker Origins

The entire discussion of the Woodford paleoenvironment extensively used biomarkers as proxies for a variety of environmental conditions. Lithology, water acidity, organic matter source, water column structure, and more are inferred from these hydrocarbon skeletons preserved in the geologic record. These proxies are founded upon intricate competition for resources between biosynthesizers, with the preserved molecular fossils reflecting the suite of organisms able to most efficiently withstand the dynamic environmental conditions. For example, H_2S invasion of the photic zone resulted in the proliferation of one type of organic (GSB) and the decimation of aerobic organisms unable to tolerate the toxic H_2S. This section will focus on the evolution of the biosphere between 392-359 Mya (time of Woodford deposition according to Paxton et al., 2006), with an initial discussion attempting to tentatively assign origins for biomarkers with disputed or unknown beginnings based on empirical evidence.

Paleorenieratane (**II**), renieratane (**III**) and renierapurpurane (**IV**) are three of the four detected C_{40} aromatic carotenoids present in the Woodford samples evaluated in this study. The source of paleorenieratane (**II**) has previously been discussed, likely a sulfur oxidizing bacteria occupying a slightly shallower region than the bGSB responsible for isorenieratane (**I**). Reported carbon enrichment of paleorenieratane ($\delta^{13}C$=-12‰, Hartgers et al., 1994) and in this study ($\delta^{13}C$=-12‰ ± 1.5‰) indicates derivation from an extinct or uncharacterized species of extant *Chlorobiaceae* (GSB). Carbon fixation via the reversed TCA cycle (inferred from enriched carbon delta values) suggests a deeper environment of the paleorenieratane-producing GSB relative to the PSB utilizing depleted carbon sources via the Calvin Cycle. As a result, paleorenieratane (**II**) is assumed to supplant chlorobactane (**VI**) in this system as the optimal pigment for chemocline depths between 5-20m in the green strain of GSB. The absence of chlorobactane (**VI**), a green pigment produced by GSB, could be explained by the replacement of this pigment with paleorenieratane (**II**) in the green strain of Devonian sulfur oxidizing bacteria in the Woodford Sea. Devonian oil derived from the Canning Basin in Australia exhibits a significant predominance of paleorenieratane (**II**) relative to chlorobactane (**VI**) (French et al., 2015), tentatively supporting this claim. In the analyzed samples, paleorenieratane (**II**) is the most dominant aromatic carotenoid present, indicating a competitive advantage over the bGSB (isorenieratane **I**). This could, and is proposed, to be a product of the shallower depths this pigment was at its optimum absorption. If a shallower depth is assumed, then a massive population was necessary to produce greater amounts of paleorenieratane (**II**) relative to isorenieratane (**I**) due to the relationship between residency depth and pigment production as

previously outlined (deeper = greater pigment production). Alternatively, greater concentrations of paleorenieratane (**II**) may indicate an even deeper depth than bGSB, sourced from extremophiles. Paleorenieratane (**II**) may have been synthesized by bGSB and isorenieratane (**I**) was synthesized as a secondary pigment, but there is no evidence currently to support these claims. A shallower position in the chemocline is more likely, granting better quality light than greater depths characterized by poor light intensity and irradiance. Numerous studies on GSB note the positive relationship between light availability and growth rate (Guerrero et al., 1985; Overmann et al., 1992; Borrego et al., 1997), citing exponential increases in growth rates when light is non-limiting. Therefore, paleorenieratane (**II**) is tentatively proposed to replace chlorobactane (**VI**) as the dominant pigment in the green strain of sulfur oxidizing bacteria in the Devonian, explained by the predominance over chlorobactane (**VI**) (not detected in measurable concentrations) and isorenieratane (**I**) due to its shallower position in the chemocline. Alternatively, separate strains of *Chlorobiaceae* generating paleorenieratane (**II**) and chlorobactane (**VI**) may have occupied similar depths of the chemocline, with GSB-producing paleorenieratane (**II**) outmaneuvering chlorobactane-producing bacteria for environmental resources in the Woodford paleoenvironment. Regardless, the position of the GSB synthesizing paleorenieratane (**II**) remains unchanged. This claim is based on the evidence outlined above, and is proposed to assist in guiding future work. Even if correct, the lack of detection post-Triassic (French et al., 2015) may indicate extinction of the extant *Chlorobiaceae* in the early Mesozoic (possibly the P-T extinction?) and render modern detection impossible. Similar source specificity challenges are encountered when attempting to decipher the

origin of two rare carotenoids detected in this study, renieratane (**III**) and renierapurpurane (**IV**).

Renieratane (**III**) is difficult to assess due to coelution on the flank of the isorenieratane (**I**) peak making quantification of this less abundant carotenoid questionable (Figure 44). Renierapurpurane (**IV**), eluting immediately after isorenieratane (**I**) and renieratane (**III**), is possibly derived from multiple sources in this study. Renierapurpurane (**IV**) was initially linked to marine sponges via isolation experiments (Yamaguchi, 1960; Schaefle et al., 1977; Liasaen-Jensen et al., 1982), but sponges are not able to synthesize carotenoids *de novo*. Either renierapurapurane[8] (**IV**) is synthesized by an unrecognized bacteria symbiotically related to sponges or is produced from dietary modification of ingested carotenoids (Liaaen Jensen et al., 1982). Cyanobacteria provide an alternative route for renierapurpurane (**IV**) synthesis via synechoxanthin (**IX**), but observation of decarboxylation products 2,3-dimethylaryl isoprenoids in the m/z 119 is pending. Decarboxylation of synechoxanthin (**IX**) is assumed because this carotenoid, with the renierapurpurane (**IV**) skeleton, is a dicarboxylic acid (Brocks and Summons, 2013). Other studies suggest a PSB (*Chromatiaceae)* origin of renierapurpurane (**IV**), but the lack of okenane (**V**) in the samples makes this interpretation unlikely. However, okenane (**V**) production may have diminished in the Devonian, with a noticeable gap between the Silurian and the Triassic (French et al., 2015; Figure 56). During this interval PSB may have resorted to alternative carotenoids, such as renierapurpurane (**IV**), causing misinterpretation of chemocline evolution. This is unlikely due to the C_{40} aromatic carotenoid distribution,

[8] Renierapurpurin is the actual pigment synthesized by the sponges, and renierapurpurane is the geological fossil (biomarker).

with key absences of okenane (**V**) and chlorobactane (**VI**) coupled with elevated concentrations of isorenieratane (**I**) suggesting an absence of PSB from the system, or PSB that do not synthesize okenone as only 11 PSB species are known to produce this okenane precursor (Smith et al., 2011). The bGSB are typically not found in environments characterized by proliferate populations of PSB (Overmann et al., 1992) and without PSB controlling the light spectra to lower depths, green pigmented strains

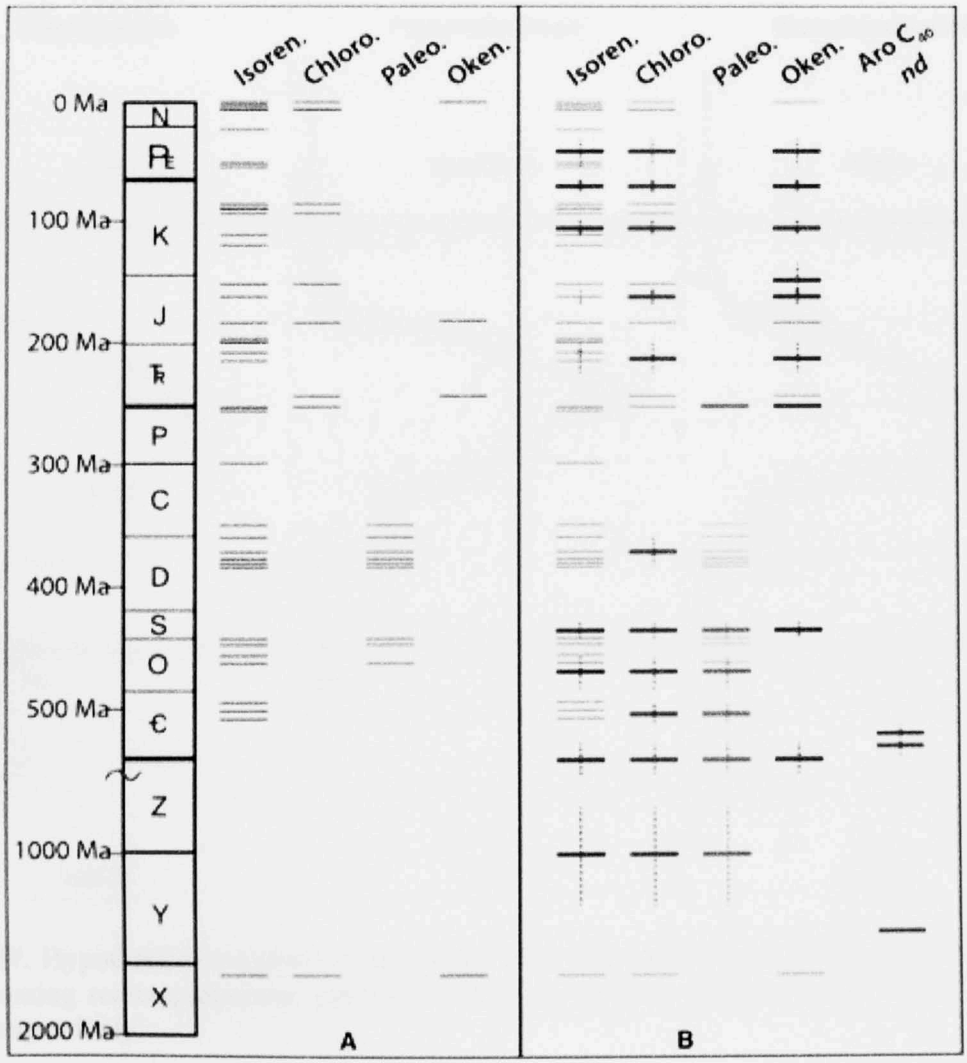

Figure 56. Temporal occurrence and distribution of C_{40} aromatic carotenoids (French et al., 2015). **A** represents stratigraphic distribution of C_{40} aromatic carotenoids according to current literature and **B** represents the updated temporal occurrence of these compounds from French et al. (2015).

are often outcompeted by brown (Montesinos et al., 1983). This lowers the probability of PSB as a possible source of renierapurpurane (**IV**) in the Woodford, and challenges the former theory of paleorenieratane (**II**). However, an interesting observation emerges if renierapurpurane (**IV**) is presumably produced by PSB, paleorenieratane (**II**) by GSB, and isorenieratane (**I**) by bGSB (Figure 57). Isorenieratane (**I**) exhibits the most intense relative increase in biomass in the LW, which is likely a result of low light

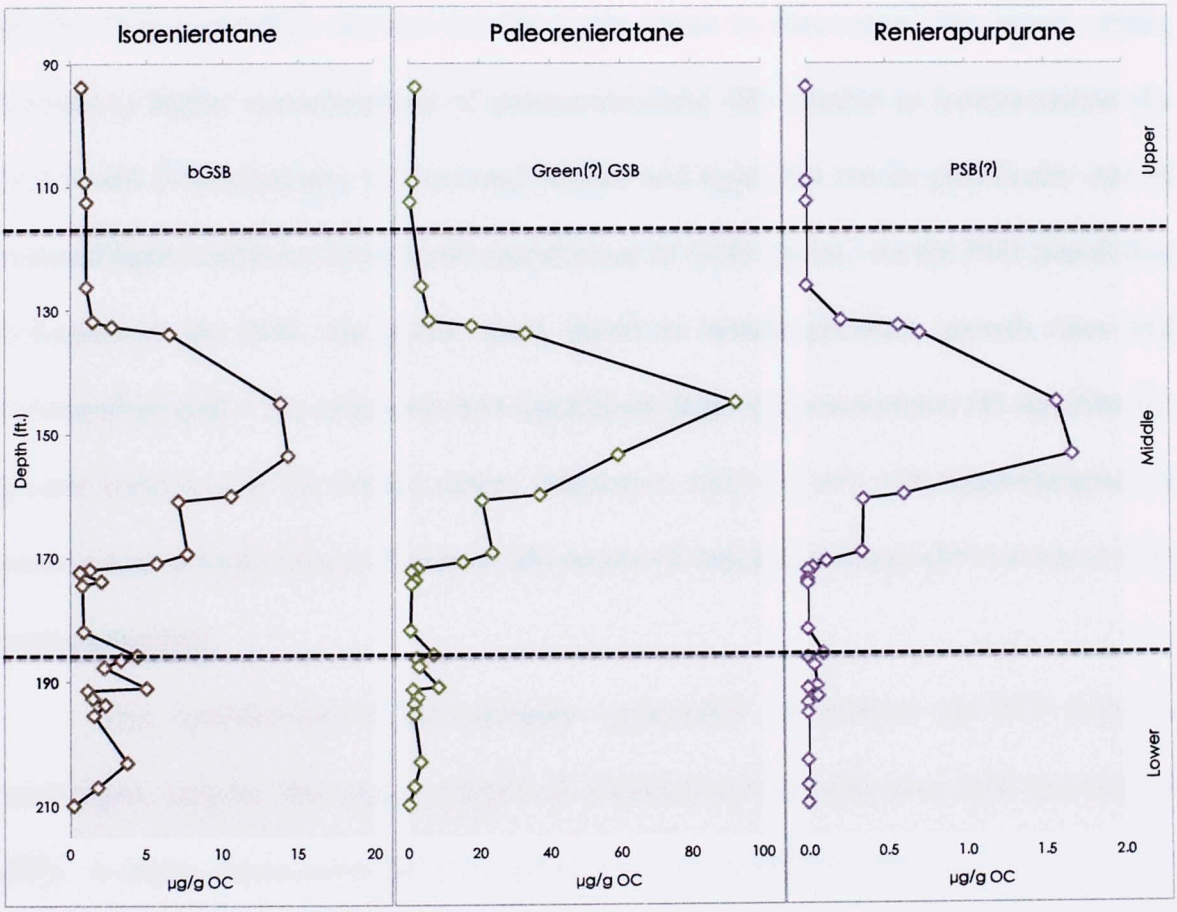

Figure 57. Hypothetical evolution of the sulfur oxidizing bacteria population in the Woodford Sea, assuming renierapurpurane, paleorenieratane and isorenieratane represent PSB, GSB and bGSB; respectively.

conditions in the shallowest extent of the chemocline at this time. Paleorenieratane (**II**) and renierapurpurane (**IV**) only display significant relative increases in the MW, where PZE is known to be much shallower and extensive relative to the LW episodes.

Renierapurpurane (**IV**), albeit low in concentration, could reflect a small population of PSB in the MW. This is inferred from the lack of detection in other regions of the core (trace amounts in the LW), with renierapurpurane (**IV**) only rising to prominence (relative to other Woodford members) in the MW. The chemocline was at the proper depth for PSB formation, and the selective enrichment of light passing through PSB populations is reflected by the overwhelming paleorenieratane (**II**) dominance. Shading by the PSB population allowed for the green strain to outcompete the brown strain, leading to higher concentrations of paleorenieratane (**II**) relative to isorenieratane (**I**). bGSB still flourished due to increased sulfide and light, but not as prolifically due to reduced light irradiance from dense populations of GSB above. As the PSB population collapsed in the MW, the green strain failed to sustain previous growth rates and collapsed as well. The relatively less significant drop of isorenieratane (**I**) signifies the greater resilience of the brown strain. However, until the m/z 119 fragmentogram is analyzed or isotopic data is obtained, the source of renierapurpurane (**IV**) in this system remains unclear.

The significance of the aromatic carotenoids as proxies for PZE remains unchanged, despite the vague origins of paleorenieratane (**II**) and renierapurpurane (**IV**). A strong relationship between gammacerane (**XXXVII**) and the C_{40} carotenoids (Figure 51) supports the utility of gammacerane (**XXXVII**) as a stratification indicator, and evinces its origin from bacterial ciliates grazing the chemocline (Harvey and McManus, 1991). The postulated precursor of gammacerane (**XXXVII**), tetrahymanol (**XXXVI**), undergoes dehydration and hydrogenation to form gammacer-2-ene and gammacerane, respectively (Venkatesan, 1989; ten Haven et al., 1989). Tetrahymanol

(**XXXVI**) is sourced by multiple organisms including ferns (Zander et al., 1969), photosynthetic nonsulfur purple bacteria (Kleemann et al., 1990) and bacterial ciliates (Harvey and McManus, 1991). These predatory organisms are documented in both oxic and anoxic settings, feeding on bacterial populations at the oxic-anoxic boundary. Isotopic geochemical analyses yield information of the diet, and have been found to be similarly enriched in carbon as the GSB previously discussed (Sinninghe Damste et al., 1995b). The gammacerane (**XXXVII**) in the Woodford is likely a product of bacterivorous ciliates grazing the chemocline, feeding on populations of *Chlorobiaceae*. Due to lack of isotopic data, this is based on consistently similar behaviors of the gammacerane index and carotenoid concentrations throughout the entire Wyche-1 core (Figure 49). If CSIA were conducted on gammacerane, it would be expected to exhibit enrichment in carbon-13 acquired from its primary energy source, the *Chlorbiaceae.*

The 28,30-Dinorhopane (**XXXVIII**; DNH) has been correlated with the development of euxinic conditions in this study (Figure 49 and 51) and previous works (Grantham et al., 1980; Schoell et al., 1992). Comparison of isotopic data derived from DNH (**XXXVIII**) reveals carbon depletion relative to other hopanes, indicating derivation from chemoautotrophic bacteria utilizing substrates depleted in ^{13}C for chemosynthesis (Schoell et al., 1992). Currently, there is no known biological source of DNH (**XXXVIII**), but the organism prefers conditions similar to those in which GSB are found. The decrease of the DNHI after 153.58ft. precedes and attenuates more quickly than the carotenoid diminishment which begins at 145.17ft. (Figure 49). There appears to be a slight relationship between the DNHI and GI, but this is likely a product of the similar conditions (PZE) controlling the indices. The DNHI demonstrates

variable behavior, contrasting with carotenoid logs as well. This evidence challenges the direct control of DNH (**XXXVIII**) by PZE alone, with secondary processes contributing to its abundance. Neither the 3rd or 2nd order cycles exhibit any correlation to this biomarker, with the chemoautrophs potentially more sensitive to variations in the water chemistry. The concomitant rise of DNH (**XXXVIII**) and aromatic carotenoids indicates a similar set of conditions is required for GSB and chemoautotrophs to flourish, such as increased sulfide production from benthic sulfur reducing bacteria. If DNH (**XXXVIII**) is synthesized from chemoautotrophs, then these organisms likely competed with the sulfur oxidizing bacteria for sulfur substrates. This explains the link between DNH (**XXXVIII**) and PZE, and the premature collapse of this population relative to the GSB. GSB biomass is an order to two orders of magnitude greater than DNH (**XXXVIII**) biomass, suggesting chemoautotrophs were outcompeted by GSB for available sulfur species. However, the source of DNH (**XXXVIII**) remains unclear without isotopic data to substantiate any evidence of a source organism. The origins of other compounds, such as the cheilanthanes (**XXXIII**), will be discussed during the following discussion on the temporal variations of the microbial community in the Woodford.

Understanding the changing composition of the local biosphere will allow environmental fluctuations to be better explained, building upon previous explanations of the overall environment and chemocline. Biomarkers with questionable origins, such as reneirapurpurane (**IV**) and DNH (**XXXVIII**), and correlation to sequence stratigraphy will be excluded from the following discussion. The biomarker isorenieratane (**I**) will represent the GSB community reliant on anoxic, H_2S-rich waters.

The sterane/hopane ratio (S/H) indicates the composition of aerobic primary producers with eukaryotes (algal)/prokaryotes (bacterial), and will partially reflect water column oxicity and the extent of PZE. Cheilanthanes (**XXXIII**) may be derived from multiple sources of prokaryotes or eukaryotes (Dutta et al., 2006), ranging from terrigenous plants to algae and bacteria. The abundance of the cheilanthanes relative to the 17α-hopanes (C/H) is similar to the S/H, suggesting a significant derivation from eukaryotic organisms (algae) in the Wyche-1 core and will be employed similarly as the S/H. Biomarkers for the heterotrophic community are limited, but gammacerane (**XXXVII**) will be utilized for this sect of life. It is expected the gammacerane (**XXXVII**) will loosely correlate with the periods of greatest disparity between the oxic and sulfidic communities (see Appendix **II** for all formulae, Appendix **III** for identification and Table 11 for all ratios used in the following discussion).

Overall, the S/H and C/H ratios are inversely proportional to the aromatic carotenoid abundances (Figure 58). Only between 185.92-174.42ft. and following the collapse of the GSB community do these ratios not maintain this relationship. The increase of all parameters preceding the GSB rise at 174.42 ft. and a decrease in all parameters following the GSB apex at 145.17 ft. indicates a significant environmental shift capable of affecting the entire biosphere. Enhanced nutrient contents from continental runoff may explain the rapid increase in algal and GSB communities at 174.42, with a rapid temperature change, reduction of nutrient input or excessive amounts of H_2S imposing great amounts of stress on the aerobic microbial community from 145.17-131.75ft. Typically, a S/H ratio >1 signifies appreciable contributions from planktonic and/or benthic algae and a ratio <1 indicates greater terrigenous input or

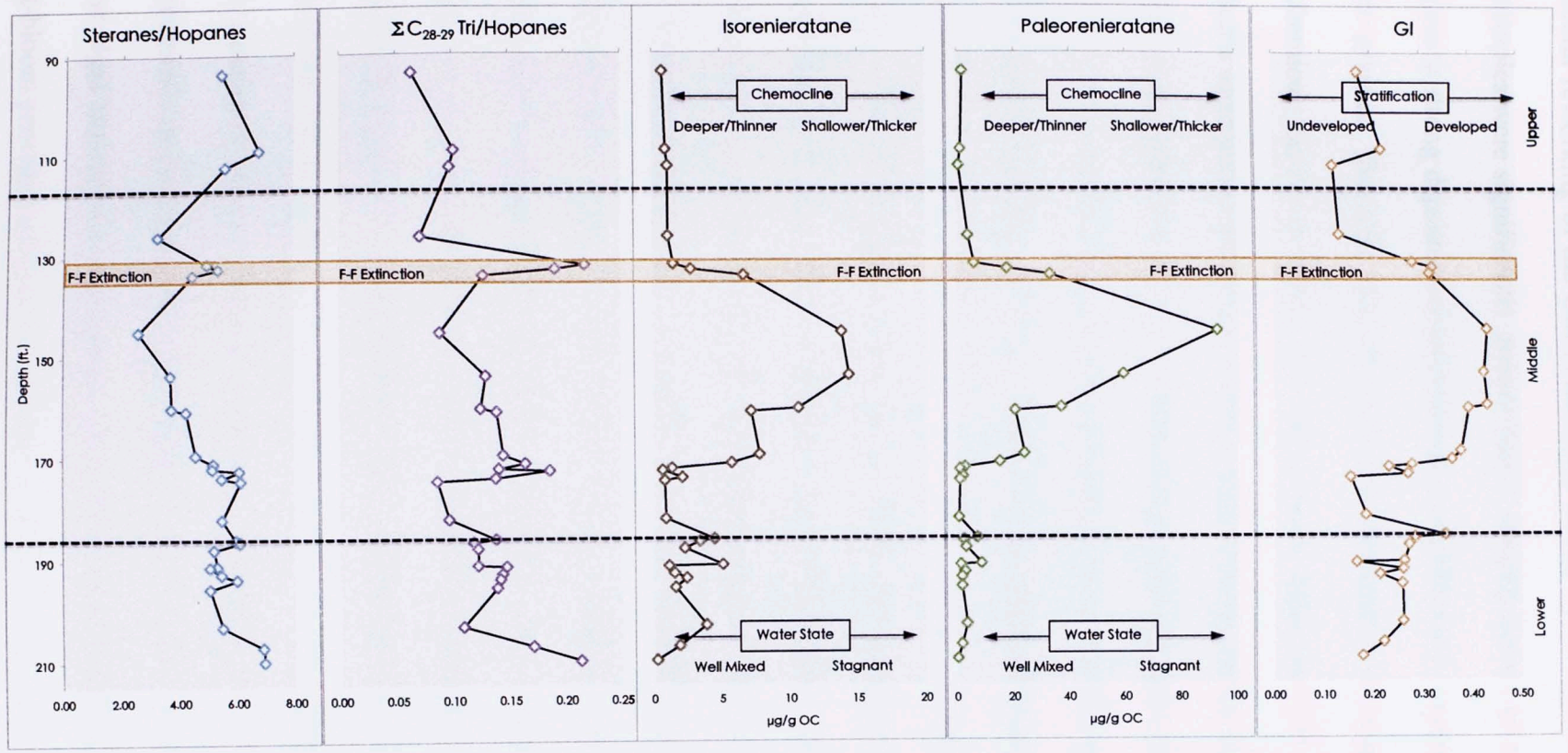

Figure 58. Biomarker parameters chosen to represent the various microbial communities in marine environments. Changes throughout Woodford deposition are evaluated, with aromatic carotenoids used as proxies for chemocline thickness and depth, as well as qualitatively measuring water ventilation. The GI was used to depict the temporal extent of stratification.

microbial reworking of the OM (Tissot and Welte, 1984; Moldowan et al., 1985). All the samples were significantly greater than 1, ranging from 2.63-6.95 (Table 11), which suggests a strong depositional predominance of eukaryotic, marine biomass (e.g. algae) in the system. The C/H ratio, as previously mentioned, is loosely similar to the S/H geochemical log (as a result, S/H will refer to both the S/H and C/H ratio unless explicitly mentioned otherwise). Smaller concentrations of the cheilanthanes (**XXXIII**) relative to the steranes explain the more exaggerated imitation of the S/H log in Figure 58. The LW is characterized by inverse fluctuations of the S/H and the C_{40} carotenoids, with interpreted periods of PZE impinging on the algal communities poisoned by H_2S. At the lower-middle boundary, the S/H, C/H, aromatic carotenoids and GI sharply increase. This was likely caused by an influx of terrigenous nutrients initializing eutrophication during a time of intense water stratification. Elevated *Chlorobiaceae* and algal biomass preserved in the sediments implies a stable chemocline and dense algal blooms, respectively. The rapid fall following this boundary in the C/H, C_{40} carotenoids and GI could reflect severe anoxia caused by large amounts of oxidized biomass precipitating to the sea floor. Algal blooms, a product of eutrophication, eventually collapse and introduce massive amounts of organic material into the water column. This material would become rapidly oxidized and lead to anoxia if unchecked. Prior to the rise in carotenoid abundance in the MW, the C/H (and to a lesser extent, S/H) exhibits a severe positive excursion. Eutrophication caused by an influx of continentally derived material or upwelling of nutrient-rich water led to a brief period of dense algal blooms near the surface. Increased sulfide production coupled with anoxia post-bloom provided adequate conditions for GSB to begin dominating the Woodford

Table 11. Biomarker parameters utilized to assess the temporal variance of the microbial community of the Woodford paleoenvironment in the Wyche-1 core.

Sample	Isorenieratane (µg/g OC)	Paleorenieratane (µg/g OC)	Renieratane (µg/g OC)	Renierapurpurane (µg/g OC)	Sterane/ Hopane	Cheilanthanes/ Hopanes	Gammacerane Index
WSLU-1	0.70	1.77	0.65	0.00	5.45	0.06	0.18
WSLU-2	0.97	1.08	0.29	0.00	6.78	0.10	0.22
WSLU-3	1.08	0.58	1.02	0.00	5.61	0.10	0.12
WSLU-4	1.10	3.79	1.09	0.00	3.28	0.07	0.13
WSLU-5	1.47	5.76	1.53	0.21	4.99	0.22	0.28
WSLU-6	2.76	17.72	2.81	0.58	5.40	0.19	0.32
WSLU-7	6.60	33.09	6.04	0.72	4.49	0.13	0.32
WSLU-8	13.82	92.84	12.69	1.58	2.63	0.09	0.43
WSLU-9	14.37	59.28	13.18	1.68	3.73	0.13	0.43
WSLU-10	10.63	37.07	10.13	0.61	3.76	0.13	0.43
WSLU-11	7.17	20.66	7.08	0.35	4.29	0.14	0.39
WSLU-12	7.76	23.71	7.82	0.35	4.62	0.14	0.38
WSLU-13	5.69	15.16	5.77	0.11	5.20	0.16	0.36
WSLU-14	1.32	2.68	1.40	0.03	5.18	0.14	0.28
WSLU-15	0.63	0.97	0.14	0.00	6.10	0.19	0.23
WSLU-16	2.09	1.76	2.29	0.00	5.49	0.14	0.27
WSLU-17	0.81	0.82	0.87	0.00	6.15	0.09	0.15
WSLU-18	0.88	0.57	0.89	0.00	5.51	0.10	0.18
WSLU-19	4.47	7.05	4.12	0.09	5.96	0.14	0.35
WSLU-20	3.35	2.35	3.05	0.00	6.11	0.12	0.28
WSLU-21	2.25	2.96	2.07	0.04	5.23	0.12	0.27
WSLU-22	5.06	8.32	4.41	0.05	5.31	0.12	0.26
WSLU-23	1.13	1.13	1.30	0.00	5.08	0.15	0.16
WSLU-24	1.45	2.59	0.54	0.06	5.47	0.14	0.26
WSLU-25	2.37	1.49	2.16	0.00	6.02	0.14	0.21
WSLU-26	1.60	1.43	1.40	0.00	5.08	0.14	0.26
WSLU-27	3.81	3.40	4.21	0.00	5.49	0.11	0.26
WSLU-28	1.84	1.52	2.05	0.00	6.91	0.17	0.22
WSLU-29	0.20	0.12	0.10	0.00	6.95	0.21	0.18
Average	3.70	12.13	3.49	0.22	5.25	0.13	0.27

paleoenvironment at 160.83ft. A step-wise decline in the S/H ratio suggests significant, isolated events resulted in rapid decreases in the algal community followed by a prolonged period of relative stability. The PZE pulses in the LW hint at potential environmental destabilization that is interpreted to occur at 160.83ft. Some event began to exert control on the LW periodically, causing the minor disturbances observed. In the MW, the carotenoids begin to increase following the final increase in the S/H before all parameters stabilize from 169.33-160.83ft. This depth is important because it marks the divergence of the environment from a moderately mixed, poorly stratified system to a stagnant system characterized by extremely stratified waters and a very shallow chemocline. Water exchange between the epicontinental Woodford Sea and the open ocean was restricted, resulting in sluggish ventilation, permitting GSB proliferation. The increase in the GSB concentration coincides with a steady decrease in the S/H ratio until the paleorenieratane (**II**) peak at 145.17ft. The highest concentrations of the aromatic carotenoids and lowest ratios of S/H occur at this depth, reflecting the shallowest extent of the chemocline. Eukaryotes were restricted from the water-atmosphere interface to possibly 10m, as the H_2S penetrated the shallowest portions of the photic zone. Cessation of sulfide production, reestablishment of vertical mixing, or increased ventilation due to improved communication with the open ocean may be responsible for the GSB decline after 145.17ft. The decrease in the GSB occurs simultaneously with an increase in algae and other eukaryotic organisms. A diminishing GI reflects degradation of the chemocline, with enhanced circulation reoxygenating significant portions of the previously anoxic water column. Habitat expansion via reoxygentation of previously H_2S-saturated waters resulted in the

increased aerobic eukaryote concentrations observed, but this prolific period was brief. Immediately following this rise to dominance over the GSB, the community was reduced to levels of the same magnitude during GSB dominance (132.75ft.). This period is characterized by abrupt changes in many biomarker ratios, signaling a rapid, ubiquitous alteration to the biosphere tentatively defined as the Frasnian-Famennian biotic crisis (Over, 2002; Marynowski et al., 2011). Rapid changes in the C_{27}/C_{29} and C_{28}/C_{29} sterane ratios imply a temporary change in the composition of the algal community (Figure 59). The sharp increase indicates a shift from primitive green algae assemblages to red and brown (modern) assemblages, which may have been better adapted to environmental stressors. The C_{40} aromatic carotenoids rapidly decrease during this same interval, suggesting degradation of stratified waters. More research is needed to correctly identify this biological shift as the F-F (Frasian-Famennian) biotic crisis, with additional notable changes occurring in sterane composition (e.g. 174.42ft., Upper Kacak Event?) and other biomarkers in the analyzed samples. Interpretations of this study's data and comparison with previous studies assisted in identifying the F-F. The F-F is proposed to be preceded by extensive euxinia (high concentrations of GSB in this study; Caplan and Bustin, 1999; Formolo et al., 2014) potentially fueled by increased volcanism (Chen et al., 2005) resulting in the mass deposition of biomass following a rapid drop in temperature (Formolo et al., 2014) creating the hot shales characteristic of the F-F (mfs in Wyche-1 core; Vleeschouwer et al., 2013). Eukaryotic communities recovered well from this event, but the GSB never returned to the previous levels reported in the LW and MW. This is likely controlled by nutrients and circulation, with the correlation between HSTs and GSB not observed in the UW. A

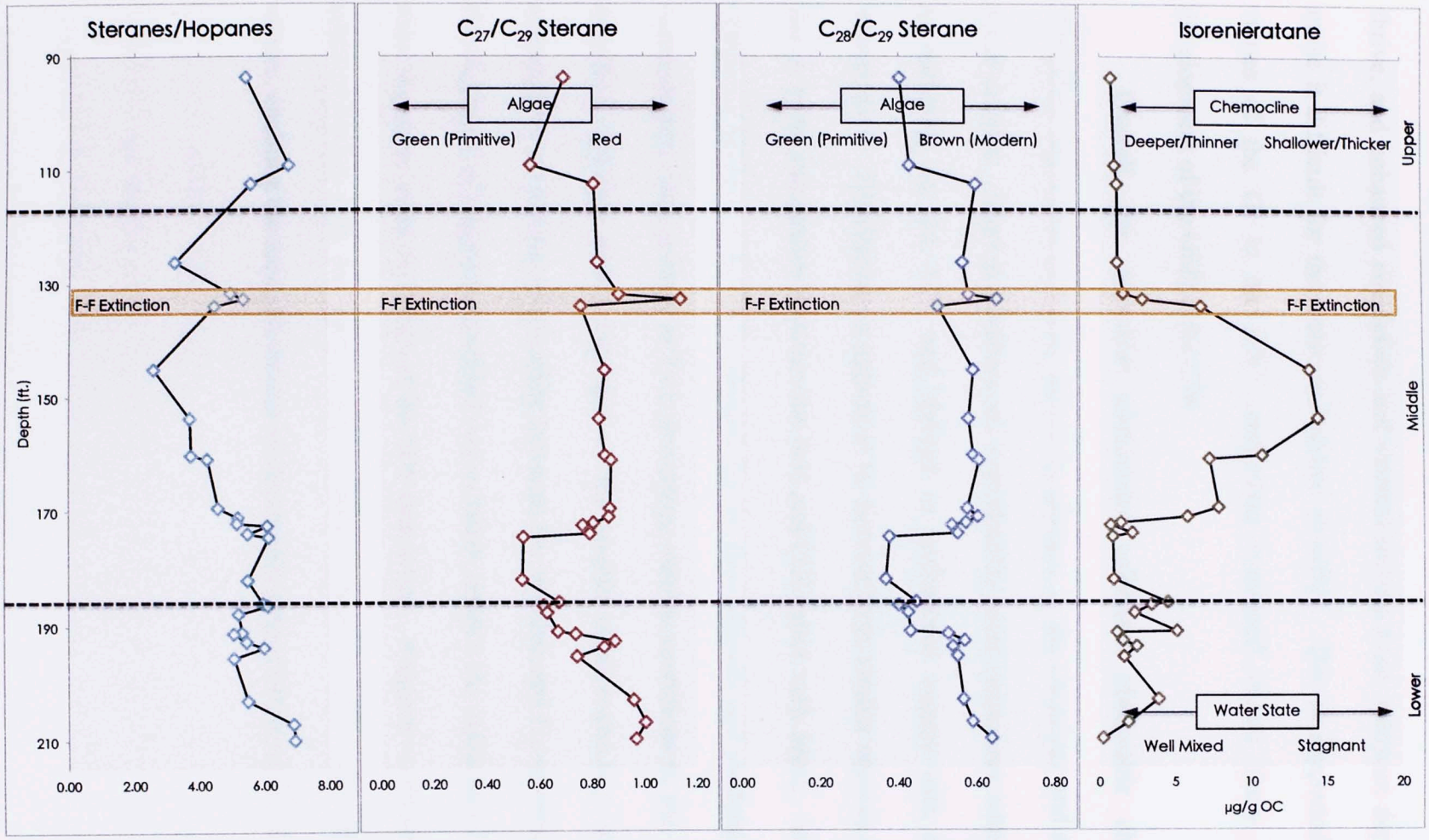

Figure 59. Assessment of biological changes during the Frasnian-Famennian biotic crisis. Sterane/hopanes depict the eukaryotic vs. prokaryotic communities, C_{27}/C_{29} and C_{28}/C_{29} illustrate changes in algal populations and isorenieratane represents the bGSB.

lack of sulfide production would limit the ability for sulfur dependent organisms to thrive, and enhanced circulation and vertical mixing from sediment deposition would make it difficult for the water to become stratified. This is supported by the lower values of the GI in the UW, confirming ventilated waters likely prevented the development of the GSB in the UW.

Overall, the microbial community exhibited observable changes during Woodford deposition primarily driven by changes in the chemistry and structure of the water column. Algal populations are considerably more prominent relative to bacteria as indicated by the S/H, and thrived in well-mixed waters with little chemical stratification. Cheilanthanes appear to be derived from similar sources as the steranes due to loose similarities between the S/H and C/H ratios with depth. Stagnant, poorly ventilated periods in the MW allowed for the development and predominance of GSB communities, with periods of PZE permitting similar conditions in the LW. Strongly stratified, H_2S-rich waters impinged on the aerobic phototrophs (e.g. algae), which is reflected by an inverse relationship between the steranes and C_{40} aromatic carotenoids. Development of stagnant, stratified waters likely reflects the isolation of the epeiric sea from the open ocean for much of the MW deposition. Sluggish ventiliation subsided as communication with the open ocean enabled currents to mix and ventilate stratified waters, enabling the reestablishment of the aerobic communities in the late MW.

CONCLUSIONS

The Woodford Shale in the Wyche Farm Shale Pit, Pontotoc County, Arkoma Basin, OK is a very good-excellent source rock comprised of predominantly immature Type II kerogen. Biomarker maturation proxies supported T_{max} data, indicating a thermally immature source rock with minimal depth variation.

The immature nature of the Wyche-1 core permitted direct interpretation of genetic environmental artifacts without excessive concern for secondary diagenetic and catagenetic effects that may adversely affect interpretations. Rearranged biomarkers (diasterenes, diahopane, and neohop-13(18)-enes) and benzohopanes were initially assessed as lithologic indicators constrained to the sequence stratigraphic framework developed by Molinares (2013). In certain members, such as the upper Woodford, these proxies aligned nicely with alternating system tracts, but in other sections of the core alternative processes, like pH, were proposed to partially govern the distribution and concentration of these compounds. Acid catalyzed backbone rearrangement is suggested to be inversely proportional to depositional rates in shales, with elevated concentrations of the diasterenes, C_{30} diahopane, and C_{27}, C_{28} and C_{30} neohop-13(18)-enes observed at the maximum flooding surface and condensed section characterized by low rates of deposition.

Utilization of geochemical clocks placed the samples in this study in the Devonian period. The C_{28}/C_{29} steranes established a general age range; with a Paleozoic age confirmed by the absence of triaromatic 23,24-dimethylcholesteroids and triaromatic dinosteroids. The C_{40} aromatic carotenoid distribution, particularly the high concentration of paleorenieratane, constrained the age to the Devonian period.

A general geochemical characterization of the depositional environment was conducted prior to water column structural analysis that found the Woodford samples in this study to be composed of a mixture of carbonaceous marine and terrestrial organic matter. Identification of MATH and isorenieratane suggests a shallow shelf setting less than 300m deep, but MATH is proposed to be dually controlled by source input and water acidity due to relatively high concentrations found at the maximum flooding surface.

The lower Woodford was deposited in anoxic waters, intermittently stratified with isolated periods of photic zone euxinia evinced by elevated concentrations of C_{40} aromatic carotenoids coinciding with 3rd order HSTs. Upwelling and circulation likely subsided during these restricted periods on the shelf, with GSB requiring stagnant, well-stratified waters to proliferate and contribute large amounts of *Chlorobiaceae* biomass to the settling organic matter. The middle Woodford was deposited during a relatively long 3rd order parasequence, with the rise and fall of *Chlorobiaceae* geological fossils corresponding with the HST and TST of the parasequence. As the HST formed, progradation to the south may have isolated the Woodford Sea from the open ocean, disrupting circulation and forming a restricted basin. The cessation of upwelling is probable, with no GSB species found in marine sulfidic upwelling zones or in non-restrictive settings. As vertical mixing gave way to sluggish ventilation, stagnant waters allowed for the development of a thick and shallow chemocline that continued to expand until the TST. The inflation of the OMZ and H_2S-saturated/stratified waters began to impinge upon the aerobic algae and bacteria by constricting habitable space and cutting off nutrient supply from upwelling, resulting in an overall decrease in

productivity in the oxic zone, increasing the light availability at greater depths that allowed for proliferation of sulfur oxidizing bacteria. Thick planktonic mats of *Chlorbiaceae* likely developed, reflected by the high concentrations of paleorenieratane, which was isotopically enriched relative to algal biomass ($\delta^{13}C$=-12$^{o}/_{oo}$ ± 1.5$^{o}/_{oo}$) suggesting carbon was fixed via the reverse TCA cycle. This indicates derivation from an extinct or uncharacterized species of extant *Chlorobiaceae*, with the potential source organism proposed to occupy a slightly shallower region of the chemocline relative to the bGSB. The 3rd order TST in the middle Woodford is marked by the concomitant decrease in C_{40} aromatic carotenoid and gammacerane concentrations and increases in biomarkers utilized to infer the composition of the aerobic community. This implies reoxygenation of the previously H_2S-saturated waters and reestablishment of circulation patterns as communication with the open ocean is achieved. Upwelling was probably a factor, with algal blooms inferred from a rising sterane/hopane ratio as nutrient-rich waters provided essential nutrients to the aerobic community. The upper Woodford was marked by a deep, if present, chemocline and increasing anoxia that coincides with the development of both 2nd and 3rd order HSTs.

FUTURE WORK

1. Correlate biomarker distributions and occurrences, particular the C_{40} aromatic carotenoids, with depositional models of the Woodford Shale to enhance the current understanding of circulation in the Woodford Sea during the late Devonian-early Mississippian.
2. Identify the Frasnian-Famennian biotic crisis and other extinction events in the Woodford to provide further insight into the global, regional and local processes affecting microbial communities in the Woodford Sea and attempt to correlate changes in the Woodford paleoenvironment with other North American epicontinental seas from the same time period.
3. Assess the relationship between potential C_{40} aromatic carotenoid derivatives, (with guidance from Koopmans et al., 1996b), and C_{40} aromatic carotenoids to develop a better understanding of diagenetic and catagenetic effects on these novel compounds.
4. Develop an integrated sequence stratigraphic framework using organic geochemical data to evaluate the impact of different organofacies (need to be characterized) on biomarker distributions during 3rd and 2nd order cycles. This needs to be done before integrated models are applied to unconventional source rocks, specifically shales, in basins with varying depositional histories.
5. Integrate trace element data from Turner et al. (2015) with organic data to address conflicting trends (e.g. Mo and V contrasting elevated concentrations of *Chlorobiaceae* biomass) as observed in this study, identifying the pitfalls and strengths of both proxy methods.

BIBLIOGRAPHY

Abousleiman Y., Tran M., Hoang S., Bobko C., Ortega A., Ulm F. J. (2007) Geomechanics field and lab characterization of Woodford Shale: The next gas play. *Society of Petroleum Engineers Paper* **110120**, 11-14.

Aguilera R., Aguilera R. F. and Ripple R. D. (2014) Link between endowments, economics and environment in conventional and unconventional gas reservoirs. *Fuel* **126**, 224–238.

Algeo T.J., Maynard J.B. (1997) Cyclic Sedimentation of Appalachian Devonian and Midcontinent Pennsylvanian Black Shales: Analysis of Ancient Anoxic Marine Systems—A Combined Core and Field Workshop: Joint Meeting of Eastern Section AAPG and The Society for Organic Petrography (TSOP), Lexington, Kentucky. Univ. of Cincinnati, Dept. of Geology, Cincinnati, Ohio. Sept. 27–28, 147.

Algeo T. A., Lyons T. W., Blakey R. C., Over J. D. (2007) Hydrographic conditions of the Devono=Carboniferous North American Seaway inferred from sedimentary Mo-TOC relationships. *Palaeogeography, Palaeoclimatology, Palaeoecology* **256,** 204-230.

Aquino Neto F. R. A., Cardoso J. N., Rodrigues R. and Trindade L. a. F. (1986) Evolution of tricyclic alkanes in the Espirito Santo Basin, Brazil. *Geochim. Cosmochim. Acta* **50**, 2069–2072.

Barbanti S. M., Moldowan J. M., Watt D. S. and Kolaczkowska E. (2011) New triaromatic steroids distinguish Paleozoic from Mesozoic oil. *Org. Geochem.* **42**, 409–424.

Barrick J. E., Haywa-Branch J. N., Over D. J. (1990) Stop 6: Woodford Shale, pre-Welden Shale, Weldon Limestone, and basal Caney Shale; Hass G section, In: *OGS Guidebook* **27**, 23-25.

Baskin D. K. (1997) Atomic H/C ratio of kerogen as an estimate of thermal maturity and organic matter conversion. *AAPG Bulletin* **81**, 1437-1450.

Behar F., Beaumont V. and De B. Penteado H. L. (2001) Rock-Eval 6 Technology: Performances and Developments. *Oil Gas Sci. Technol.* **56**, 111–134.

Berti G. and Bottari F. (1968) Constituents of ferns. In: *Progress in Phytochemistry* **1**, 589-685.

Biebl H. and Pfennig N. (1978) Growth yields of green sulfur bacteria in mixed culture with sulfur and sulfate-reducing bacteria. *Arch Mikrobiol.* **117**, 9-16.

Binet S., Pfohl-Leszkowicz A., Brandt H., Lafontaine M., and Castegnario M. (2002) Bitumen fumes: review of work on potential risk to workers and the present knowledge on its origin. *Science Total Environment* **300**, 37-49.

Bishop A.N. and Farrimond, P. (1995) A new method of comparing extended hopane distributions *Organic Geochemistry* **23**, 987-990.

Borrego, C. M. Garcia-Gil L. J., Vila X., Cristina J. B., Figueras J. B., Abella C. A. (1977) Distribution of bacteriochlorophyll homologs in natural populations of brown-colored phototrophic sulfur bacteria. *FEMS Microbiology Ecology* **24**, 301-309.

Brincat D. and Abbott G. (2001) Some aspects of the molecular biogeochemistry of laminated and massive rocks from the Naples Beach Section (Santa Barbara-Ventura Basin). In: *The Monterey Formation: From Rocks to Molecules* 140-149.

Brocks J. J. and Schaeffer P. (2008) Okenane, a biomarker for purple sulfur bacteria (Chromatiaceae), and other new carotenoid derivatives from the 1640 Ma Barney Creek Formation. *Geochim. Cosmochim. Acta* **72**, 1396–1414.

Brocks J. J. and Summons. R. E. (2013) Sedimentary Hydrocarbons, Biomarkers for Early Life. *2nd ed., Elsevier Ltd* **8,** 63-115.

Brown T. C. and Kenig F. (2004) Water column structure during deposition of Middle Devonian-Lower Mississippian black and green/gray shales of the Illinois and Michigan Basins: a biomarker approach. *Palaeogeography, Palaeoclimatology, Palaeoecology* **215,** 59-85.

Brune, D.C. (1989) Sulfur oxidation by phototrophic bacteria. *Biochim. Biophys. Acta* **975**, 189–221.

Bryant D. A. and Dahl N. U. (2006) Prokaryotic photosynthesis and phototrophy illuminated. *Trends in Microbiology* **14**, 488-496.

Buckner T. N., Slatt R. M., Coffey B. and Davis R. J. (2009) Stratigraphy of the Woodford Shale from behind-outcrop drilling, logging, and coring. In AAPG Annual Convention, San Antonio, TX. *AAPG Search and Discovery, article #50147*

Caplan M. L. and Bustin R. M. (1999) Devonian-Carboniferous Hangenberg mass extinction event, widespread organic-rich mudrock and anoxia: Causes and consequences. *Palaeogeogr. Palaeoclimatol. Palaeoecol.* **148**, 187–207.

Cardott, B. J. (2005) Overview of unconventional energy resources of Oklahoma. *In* B. J. Cardott, ed., Unconventional energy resources in the southern mid-continent: 2004 Symposium *Oklahoma Geological Survey Circular* **110**, 7-18.

Cardott B. J. and Geological O. (2007) Overview of Woodford Gas - Shale Play in Oklahoma.

Cardott B. J. (2012) Thermal maturity of Woodford Shale gas and oil plays, Oklahoma, USA. *Int. J. Coal Geol.* **103**, 109–119.

Chen D., Qing H., Li R. (2005) The late Devonian Frasnian-Famennian (F/F) biotic crisis: Insights from $\delta^{13}C_{carb}$, $\delta^{13}C_{org}$ and $^{87}Sr/^{86}Sr$ isotopic systematics. *Earth and Planetary Scientific Letters* **235,** 151-166.

Clifford D. J., Clayton J. L. and Sinninghe Damsté J. S. (1998) 2,3,6-/3,4,5-Trimethyl substituted diaryl carotenoid derivatives (Chlorobiaceae) in petroleums of the Belarussian Pripyat River Basin. *Org. Geochem.* **29**, 1253–1267.

Coleman J. I., (2004) Petroleum Systems of the Ouachita Thrust Belt and foreland basins (with emphasis on the Arkoma Basin). In: *Oklahoma Geological Survey* **112B**, 1-17.

Comer J. B. (1991) Stratigraphic Analysis of the Upper Devonian Woodford Formation, Permian Basin, West Texas and Southeastern New Mexico. *Bureau of Economic Geology Report of Investigations No. 201* 1-61.

Comer J. B. (2005) Facies distributions and hydrocarbon production potential of Woodford Shale in the Southern Midcontinent. In Cardott B. J. (ed.) Unconventional energy resources in the Southern Midcontinent, 2004 symposium. *Oklahoma Geological Survey Circular* **110,** 51-62.

Comer J. B. (2008a) Reservoir characteristics and production potential of the Woodford Shale. WorldOil Magazine 229 August 2008, http://petesplace-peter.blogspot.com/2008/08/woodford-shale-major-new-unconventional.html; accessed on January , 2009.

Comer J. B. (2008b) Woodford Shale in southern Midcontinent, USA – Transgressive system tract marine source rocks on an arid passive continental margin with persistent ocean upwelling. American Association of Petroleum Geologists Annual Convention, San Antonio, Texas. Poster presentation.

Comer J. B. (2012) Woodford shale and the evaporite connection- the significance of aridity and hypersalinity in organic matter productivity and preservation. *Geological Society of America Abstracts with Programs* **44/45**, 6.

Connan J. and Dessort D. (1987) Novel family of hexacyclic hopanoid alkanes occurring in sediments and oils from anoxic paleoenvironments. *Org. Geochem.* **11**, 103–113.

Connan J. (1999) Use and trade of bitumens in antiquity and prehistory: molecular archaeology reveals secrets of past civilizations. *Biological Science* **354**, 33-50.

Corbett R. E. and Smith R. A. (1969) Lichens and fungi. Part IV. Dehydration rearrangements of 15-hydroxyhopanes. *Journal of Chemical Society* 44-47.

Cornford C., Gardner P. and Burgess C. (1998) Geochemical truths in large data sets. I: Geochemical screening data. *Org. Geochem.* **29**, 519–530.

Curiale J. A. and Odermatt J. R. (1989) Short-term biomarker variability in the Monterey Formation, Santa Maria Basin. *Organic Geochemistry* **14**, 1-13.

Dahl B. (2004) The use of bisnorhopane as a stratigraphic marker in the Oseberg Back Basin, North Viking Graben, Norwegian North Sea. *Org. Geochem.* **35**, 1551–1571.

Dahl B., Bojesen-Koefoed J., Holm A., Justwan H., Rasmussen E. and Thomsen E. (2004) A new approach to interpreting Rock-Eval S 2 and TOC data for kerogen quality assessment. *Org. Geochem.* **35**, 1461–1477.

DeGarmo D. C. (2015) Geochemical Characterization of the Woodford Shale (Devonian-Mississippian), McAlister Cemetery Quarry, Criner Hills Uplift, Ardmore Basin, Oklahoma. *University of Oklahoma M.S. Thesis.*

Didyk B. M., Simoneit B. R. T., Brassel S. C., Eglinton G. (1978) Organic geochemical indicators of paleoenvironmental conditions of sedimentation. *Nature* **272**, 216-222.

Drews G. and Golecki J. R. (1995) Structure, molecular organization and biosynthesis of membranes of purple sulfur bacteria. In: *Anoxygenic Photosynthesis* **2**, 231-257.

Dutta S., Greenwood P.F., Brocke R., Schaefer R.G., Mann U., 2006. New insights into the relationship of Tasmanites and tricyclic terpenoids. *Organic Geochemistry* **37**, 117-127.

Dzou B. C., Choppin de Janvry G., Heidmann J. C., Pition J. L., ten Haven H. L. (1995) A hybrid petroleum system on the Western African Margin, an example in offshore Anghola. Presented at the Annual Meeting of the American Association of Petroleum Geologists, May 3-5, San Francisco.

Eglinton G. and Calvin M. (1967) Chemical fossils. *Scientific American* **261**, 32-43.

Ensminger A., Albrecht P., Ourisson G., Tissot B. (1977) Evolution of polycyclic alkanes under the effect of burial (Early Toarcian shales, Paris Basin). In: *Advances in Geochemistry 1975 Madrid* 45-52.

Eriksson P., Banerjee S., Catuneanu O., Corcoran P., Eriksson L., Hiatt E., Laflamme M., Lenhardt N., Long D., Miall A., Mints M., Pufahl P., Sarkar S., Simpson S., Williams E. (2013). Secular changes in sedimentation systems and sequence stratigraphy. *Gondwana Research* **24**, 468-489.

Espitalie J., Laporte J.L., Madec M., Marquis F., Leplat P., Paulet J., Boutefeu A. (1977) Rapid method for source rock characterization, and for determination of their petroleum potential and degree of evolution. *Revue de l'Institut Francais du Petrole et Annales des Combustibles Liquides* **32**, 23-42.

Fang H., Jianyu C., Yongchuan S. and Yaozong L. (1993) Application of organic facies studies to sedimentary basin analysis: a case study from the Yitong Graben, China. *Organic Geochemistry* **20**(1), 27-42.

Farrimond P. and Telnæs N. (1996) Three series of rearranged hopanes in Toarcian sediments (northern Italy). *Org. Geochem.* **25**, 165–177.

Farrimond P., Taylor A. and TelnÆs N. (1998) Biomarker maturity parameters: The role of generation and thermal degradation. *Org. Geochem.* **29**, 1181–1197.

Fleck S., Michels R., Ferry S., Malartre F., Elion P., Landais P. (2002) Organic geochemistry in a sequence stratigraphic framework. The siliciclastic shelf environment of Cretaceous series, SE France. *Organic Geochemistry* **33**, 1533-1557.

Formolo M. J., Riedinger N. and Gill B. C. (2014) Geochemical evidence for euxinia during the Late Devonian extinction events in the Michigan Basin (U . S . A .). *Palaeogeogr. Palaeoclimatol. Palaeoecol.* **414**, 146–154.

Fowler M. G. (1992) The influence of *Gloeocapsomorpha prisca* on the organic geochemistry of oils and organic-rich rocks of Late Ordovician age from Canada. In: *Early Organic Evolution: Implications for Mineral and Energy Resources* 336-356.

French K. L., Sepúlveda J., Trabucho-Alexandre J., Gröcke D. R. and Summons R. E. (2014) Organic geochemistry of the early Toarcian oceanic anoxic event in Hawsker Bottoms, Yorkshire, England. *Earth Planet. Sci. Lett.* **390**, 116–127.

French K. L., Rocher D., Zumberge J. E. and Summons R. E. (2015) Assessing the distribution of sedimentary C 40 carotenoids through time. *Geobiology* **13**, 139–151.

Frigaard N.U., Chew A.G.M., Li H., Maresca J.A. and Bryant D.A. (2003) Chlorobium tepidum: Insights into the structure, physiology, and metabolism of a green sulfur bacterium derived from the complete genome sequence. *Photosyn. Res.* **78**, 93–117.

Frigaard N. U. and Dahl C. (2008) *Sulfur Metabolism in Phototrophic Sulfur Bacteria.*, Elsevier Masson SAS. Available at: http://dx.doi.org/10.1016/S0065-2911(08)00002-7.

Fu J., Sheng G., Peng P., et al. (1986) Peculiarities of salt lake sediments as potential source rocks in China. *Organic Geochemistry* **10**, 119-126.

Ge S., Dilcher D. L., Shaoling Z. and Zhekun Z. (1998) In search of the first flower: a Jurassic angiosperm, *Archaefructus*, from Northeast China. *Science* **282,** 1692-1695.

Gorlenko V. M. (1988) Ecological niches of green sulfur and gliding bacteria. In: *Green Photosynthetic Bacteria* 257-267.

Grabowski G.J. (1984) Generation and migration of hydrocarbons in Upper Cretaceous Austin Chalk, south-central Texas. *Petroleum geochemistry and source rock potential of carbonate rocks: AAPG studies in Geology* **18**, 97-115.

Grantham P. J., Posthuma J., DeGroot K. (1980) Variation and significance of the C_{27} and C_{28} triterpane content of a North Sea core and various North Sea crude oils. In: *Advances in Organic Geochemistry 1981* 675-683.

Grantham P. J., Posthuma J. and Baak A. (1983) Triterpanes in a number of Far-Eastern crude oils. In: *Advances in Organic Geochemistry 1981* 675-683.

Grantham P. J. and Wakefield L. L. (1988) Variations in the sterane carbon number distributions of marine source rock derived crude oils through geological time. *Org. Geochem.* **12**, 61–73.

Greenwood P. F. and Summons R. E. (2003) GC-MS detection and significance of crocetane and pentamethylicosane in sediments and crude oils. *Org. Geochem.* **34**, 1211–1222.

Grice K., Schaeffer P., Schwark L. and Maxwell J. R. (1996) Molecular indicators of palaeoenvironmental conditions in an immature Permian shale (Kupferschiefer, Lower Rhine Basin, north-west Germany) from free and S-bound lipids. *Org. Geochem.* **25**, 131–147.

Grice K., Cao C., Love G.D., Bottcher M. E., Twitchett R. J., Grosjean E., Summons R. E., Turgeon S. C., Dunning W., Jin Y. (2005). Photic zone euxinia during the Permian-Triassic Superanoxic Event. *Science* **307**, 706-708.

Guerrero R., Montesinos E., Pedrós-Alió C., Esteve I., Mas J., Van Gemerden H., Hofman P. a. G. and Bakker J. F. (1985) Phototrophic sulfur bacteria in two Spanish lakes: Vertical distribution and limiting factors. *Limnol. Oceanogr.* **30**, 919–931.

Haines L. (2006) Activity Builds in the Woodford Shale. *Oil and Gas Investor* **17**.

Hartgers W., Sinninghe Damsté J. S., Requejo a G., Allan J., Hayes J. M., Ling Y., Xie T. M., Primack J. and De Leeuw J. W. (1994) A molecular and carbon isotopic study towards the origin and diagenetic fate of diaromatic carotenoids. *Org. Geochem.* **22**, 703–725.

Hartkopf-Fröder C., Kloppisch M., Mann U., Neumann-Mahlkau P., Schaefer R.G., Wilkes H. (2007) The end-Frasnian mass extinction in the Eifel Mountains, Germany: new insights from organic matter composition and preservation. In: *Becker, R.T., Kirchgasser, W.T. (Eds.), Devonian events and correlations: Geological Society, London, Special Publications* **278,** 173–196.

Harvey H. R. and McManus G. B. (1991) Marine ciliates as a widespread source of tetrahymanol and hopan-3b-ol in sediments. *Geochimica et Cosmochimica Acta* **55**, 3387–3390.

Hays, L. E., Grice K., Foster. C. B., Summons R. E. (2012) Biomarker and isotopic trends in a Permian-Triassic sedimentary section at Kap Stosch, Greenland. *Organic Geochemistry* **43**, 67-82.

Holba A.G., Dxou L.I.P., and Masterson W.D. (1998) Application of 24-norcholestanes for constraining source age of petroleum. *Organic Geochemistry* **29**, 1269-1283.

Huang K. and Armstrong D. W. (2009) GC-MS analysis of crocetane, phytane and some of their stereoisomers using cyclodextrin-based stationary phases. *Org. Geochem.* **40**, 283–286.

Hughes W. B., Holba A. G. and Dzou L. I. P. (1995) The ratios of dibenzothiophene to phenanthrene and pristane to phytane as indicators of depositional environment and lithology of petroleum source rocks. *Geochim. Cosmochim. Acta* **59**, 3581–3598.

Hunt, J.M. (1996) Petroleum geochemistry and geology. 2nd edition, 743.

Hussler G., Connan J. and Albrecht P. (1984) Novel families of tetra- and hexacyclic aromatic hopanoids predominant in carbonate rocks and crude oils. *Org. Geochem.* **6**, 39–49.

Imhoff J. F. (1995) Taxonomy and physiology of phototrophic purple bacteria and green sulfur bacteria. *Anoxygenic Photosynthetic Bacteria* 1-15.

Jaminski J., Algeo T. J., Maynard J. B., Hower J. C. (1998) Climatic origin of dm-scale compositional cyclicity in the Cleveland Member of the Ohio Shale (upper Devonian), central Appalachian basin, USA. *Shales and Mudstones* **1**, 217-242.

Jarvie D. M., Hill R. J., Ruble T. E., and Pollastro R. M. (2007) Unconventional shale-gas systems: the Mississippian Barnett Shale of north-central Texas as one model for thermogenic shale-gas assessment. *American Association of Petroleum Geologists Bulletin* **91**, 475-499.

Jerlov N. G. (1951) Optical studies of ocean water. In: *Reports of the Swedish deep-sea expedition 1947-1948* **3**, 1-59.

Johnson J. G., Klapper G. and Sandberg C. a (1985) Geological Society of America Bulletin Devonian eustatic fluctuations in Euramerica Devonian eustatic fluctuations in Euramerica.

Johnson K. S., Amsden T. W., Denison R. E., Dutton S. P., Goldstein A. G., Rascoe Jr. B., Sutherland P. K. and Thompson D. M. (1989) Geology of the southern Midcontinent. *Oklahoma Geological Survey Special Publication* **89-2,** 1-53.

Johnson K. S. and Cardott B. J. (1992) Geologic framework and hydrocarbon source rocks of Oklahoma. *Oklahoma Geological Survey Circular* **93,** 21-37.

Jones R. W. (1987) Organic Facies. *Advances in Petroleum Geochemistry* 1-90.

Jorgensen B. B. (1989) Biogeochemistry of chemoautotrophic bacteria. In: *Autotrophic Bacteria* 117-146.

Kannenberg E.L and Paralla K. (1999) Hopanoid biosynthesis and function in bacteria. *Naturwissenschaften* **86**, 168-176.

Katz B. J. (1983) Limitations of "Rock-Eval" pyrolysis for typing organic matter. *Org. Geochem.* **4**, 195–199.

Katz B. J. and Elrod L. W. (1983) Organic geochemistry of DSDP Site 467, offshore California, Middle Miocene to Lower Pliocene strata. *Geochimica et Cosmochimica Acta* **47**, 389-396.

Kirkland D. W., Denison R. E., Summers D. M., and Gormly J. R. (1992) Geology and organic geochemistry of the Woodford Shale in the Criner Hills and western Arbuckle Mountains, Oklahoma. In Johnson K. S. and Cardott B. J. (eds.) Source rocks in the Southern Midcontinent, 1990 symposium. *Oklahoma Geological Survey Circular* **93,** 38-69.

Kleemann G., Poralla K., Englert G., et al. (1990) Tetrahymanol from the phototrophic bacterium *Rhodopseudomonas palustris:* first report of a gammacerane triterpane from a prokaryote. *Journal of General Microbiology* **136**, 2551-2553.

Kolaczkowska E., Slougui N.E., Watt D.S., Marcura R.E. and Moldowan J.M. (1990) Thermodynamic stability of various alkylated, dealkylatd, and rearranged 17α – and 17β-hopane isomers using molecular mechanics calculations. *Organic Geochemistry* **16**, 1033-1038.

Kohnen M. E. L., Schouten S., Sinninghe Damste J. S., de Leeuw J. W., Merritt D. a and Hayes J. M. (1992) Recognition by. *Science (80-.).* **256**, 358–362.

Koopmans M. P., Schouten S., Kohnen M. E. L. and Sinninghe Damsté J. S. (1996a) Restricted utility of aryl isoprenoids as indicators for photic zone anoxia. *Geochim. Cosmochim. Acta* **60**, 4873–4876.

Koopmans M. P., Köster J., Van Kaam-Peters H. M. E., Kenig F., Schouten S., Hartgers W. a., De Leeuw J. W. and Sinninghe Damsté J. S. (1996b) Diagenetic and catagenetic products of isorenieratene: Molecular indicators for photic zone anoxia. *Geochim. Cosmochim. Acta* **60**, 4467–4496.

Koster J., Rospondek M., Schouten S., Kotarba M., Zubrzycki A., Sinninghe Damste J. S. (1998) Artificial maturation of an immature sulphur- and organic matter-rich limestone from the Ghareb Formation. *Jordan Organic Geochemistry* **28**, 503-521.

Kulkarni P. (2011) Complex geology requires the Woodford Shale operators to apply traditional methods to explore for and produce shale oil, gas and condensates. *World Oil*, 93-98.

Kuuskraa, V.A. (2011) Worldwide assessment underscores vast potential of gas shale resources. *American Oil & Gas Reporter* **54**, 40–46.

Kuypers M. M. M., Pancost R. D., Nijenhuis I. A. and Sinninghe Damste´ J. S. (2002) Enhanced productivity led to increased organic carbon burial in the euxinic North Atlantic basin during the late Cenomanian oceanic anoxic event. *Paleoceanography* **17**.

Lambert M. W. (1993) Internal stratigraphy and organic facies of the Devonian-Mississippian Chatanooga (Woodford) Shale in Oklahoma and Kansas. In Katz B. J. and Pratt L. M. (eds.) Source rocks in a sequence stratigraphic framework. *American Association of Petroleum Geologists Studies in Geology* **37,** 163-176.

Liaeen-Jensen S. (1979) Marine Carotenoids. In: *Marine Natural Products, Chemical and Biological Perspectives* **2**, 1-73.

Liaaen-Jensen S., Renstrøm B., Ramdahl T., Hallenstvet M. and Bergquist P. (1982) Carotenoids of marine sponges. *Biochem. Syst. Ecol.* **10**, 167–174.

Mackenzie A. S., Patience R. L., Maxwell J. J., Vandenbroucke M., Durand B. (1980) Molecular parameters of maturation in the Toarcian shales, Paris Basin, France- I. Changes in the configuration of acyclic isoprenoid alkanes, steranes, and triterpanes. *Geochimica et Cosmochimica Acta* **44**, 1709-1721.

Mackenzie A. S. (1984) Application of biological markers in petroleum geochemistry. *In: Advances in Petroleum Geochemistry* **1**, 115-214.

Mackenzie a S. and Province S. (1986) marker compounds in the Linyi Basin. *Org. Geochem.* **10**.

Madigan M. T. (2002) Anoxygenic phototrophic bacteria from extreme environmnets. *Photosynthesis Research* **76**, 157-171.

Maloof A. C., Porter S. M., Moore J. L., Dudas F. O., Bowring S. A., Higgins J. A., Fike D. A., Eddy M. P. (2010) The earliest Cambrian record of animals and ocean geochemical change. *Geological Society of America Bulletin* **122**, 1731-1774.

Maresca J., Romberger S. P. and Bryant D. a. (2008) Isorenieratene biosynthesis in green sulfur bacteria requires the cooperative actions of two carotenoid cyclases. *J. Bacteriol.* **190**, 6384–6391.

Marynowski L., Narkiewicz M., Grelowski C. (2000) Biomarkers as environmental indicators in a carbonate complex, examples from the Middle Devonian, the Holy Cross Mountains, Poland. *Sedimentary Geology* **137,** 187–212.

Marynowski L., Rakociński M., Borcuch E., Kremer B., Schubert B. a. and Jahren a. H. (2011) Molecular and petrographic indicators of redox conditions and bacterial communities after the F/F mass extinction (Kowala, Holy Cross Mountains, Poland). *Palaeogeogr. Palaeoclimatol. Palaeoecol.* **306**, 1–14.

Maslen E., Grice K., Gale J. D., Hallmann C. and Horsfield B. (2009) Crocetane: A potential marker of photic zone euxinia in thermally mature sediments and crude oils of Devonian age. *Org. Geochem.* **40**, 1–11.

McCarthy K., Rojas K., Niemann M., Palmowski D., Peters K. and Stankiewicz A. (2011) Basic Petroleum Geochemistry for Source Rock Evaluation. *Oilf. Rev.* **23**, 32–43.

McGhee, G. R. (1996) The Late Devonian mass extinction. *Columbia University Press*, New York.

Melendez I., Grice K., Trinajstic K., Ladjavardi M., Greenwood P. and Thompson K. (2013) Biomarkers reveal the role of photic zone euxinia in exceptional fossil preservation: An organic geochemical perspective. *Geology* **41**, 123–126.

Meyer K. M. and Kump L. R. (2008) Oceanic euxinia in Earth history: causes and consequences. *Annual Review of Earth and Planetary Sciences* **36**, 747-750.

Meyer K., Kump L., Ridgwell A. (2008) Biogeochemical controls on photic-zone euxinia during the end-Permian mass extinction. *Geology* **36,** 747–750.

Mille G., Munoz D., Jacquot F., Rivet L. And Bertrand J. C. (1998) The Amoco Cadiz oil spill-evolution of petroleum hydrocarbons in the Ile Grande salt marshes (Brittany) after a 13-year period. *Estuarine, Coastal and Shelf Science* **47,** 547-559.

Moldowan J. M., Seifert W. F., Arnold E., Clardy J. (1984) Structure proof and significance of stereoisomeric 28,30-bisnorhopanes in petroleum and petroleum source rocks. *Geochimica et Cosmochimica Acta* **48**, 1651-1661.

Moldowan J. M., Seifert W. K., Gallegos E. J. (1985) Relationship between petroleum composition and depositional environment of petroleum source rocks. *American Association of Petroleum Geologists Bulletin* **69**, 1255-1268.

Moldowan J. M., Sundararaman P., Schoell M. (1986) Sensitivity of biomarker properties to depositional environment and/or source input in the Lower Toarcian of S.W. Germany. *Organic Geochemistry* **10**, 915-926.

Moldowan J. M., Fago F. J., Lee C. Y., et al. (1990) Sedimentary 24-*n*-propylcholestanes, molecular fossils diagnostic of marine algae. *Science* **247**, 309-312.

Moldowan J. M., Fago F. J., Carlson R. M. K., Young D. C., an Duvne G., Clardy J., Schoell M., Pillinger C. T. and Watt D. S. (1991) Rearranged hopanes in sediments and petroleum. *Geochim. Cosmochim. Acta* **55**, 3333–3353.

Moldowan J.M. and McCaffrey M. A. (1995). A novel microbial hydrocarbon degradation pathway revealed by hopane demthylation in a petroleum reservoir. *Geochimica et Cosmochimica Acta* **59**, 1891-1894.

Moldowan J. M. (2000) Trails of Life. *Chemistry in Britain* **36**, 34-37.

Molinares, C. (2013) Stratigraphy and palynomorphs composition of the Woodford Shale in the Wyche Farm Shale Pit, Pontotoc County, Oklahoma. University of Oklahoma M.S. Thesis.

Monteiro F. M., Pancost RD., Ridgewell A., Donnadieu Y. (2012) Nutrients as the dominant control on the spread of anoxia and euxinia across the Cenomanian-Turonian oceanic anoxic event (OAE2): model-data comparison. Paleoceanography **27,** 59-85.

Montesinos E., Guerrero R., Abella` C. and Esteve I. (1983) Ecology and physiology of the competition for light between *Chlorobium limicola* and *Chlorobium phaeobacteroides* in natu- ral habitats. *Appl. Environ. Microbiol.* **46**, 1007–1016.

Moore J., and Stanitski C., Jurs P. (2008) Chemistry: The Molecular Science. 3rd edition. *Thompson Brooks/Cole* 546-547.

Noble R., Alexander R., Kagi R. I. (1985) The occurrence of bisnorhopane, trisnohopane, and 25-norhopanes as free hydrocarbons in some Australian shales. *Organic Geochemistry* **10**, 825-829.

Northcutt R. A., Johnson K. S., and Hinshaw G. C. (2001) Geology and petroleum reservoirs in Silurian, Devonian, and Mississippian rocks in Oklahoma. In Johnson K. S. (ed.) Silurian, Devonian, and Mississippian geology and petroleum in the southern Midcontinent, 1999 symposium. *Oklahoma Geological Survey Circular* **105,** 1-29.

Nowaczewski V. (2011) Biomarker and paleontological investigations of the late Devonian extinctions, Woodford Shale, Southern Oklahoma. *University of Kansas M.S. Thesis.*

Orr W.L. (1981) Comments on pyrolytic hydrocarbon yields in source-rock evaluation. *Advances in Organic Geochemistry* 775-787.

Ourisson G., Rohmer M., and Poralla K. (1987) Prokaryotic hopanoids and other polyterpenoid sterol surrogates. *Annual Review of Microbiology* **41**, 301-333.

Ourisson G. and Albrecht P. (1992) Hopanoids: 1. Geohopanoids: The most abundant natural products on Earth? *Accounts of Chemical Research* **25**, 398-402.

Over D. J. (2002) The Frasnian / Famennian boundary in central and eastern United States. *Palaeogeogr. Palaeoclimatol. Palaeoecol.* **181**, 153–169.

Overmann J. (2008) Ecology of phototrophic sulfur bacteria. In: *Sulfur Metabolism in Phototrophic Organisms* **2**, 375–396.

Overmann J., Cypionka H. and Pfennig N. (1992) An extremely low-light adapted phototrophic sulfur bacterium from the Black Sea. *Limnol. Oceanogr.* **37**, 150–155.

Ozaki K., Tajima S., Tajika E. (2011) Conditions required for oceanic anoxia/euxinia: constraints from a one-dimensional ocean biogeochemical cycle model. *Earth and Planetary Science Letters* **304,** 270–279.

Parkin T.B. and Brock T.D. (1980) The effects of light quality on the growth of phototropic bacteria in lakes. *Arch. Microbiol.* **125**, 19–27.

Paxton S.T., Cruse, A.M., Krystyniak, A.M. (2006) Fingerprints of Global Sea-level Change Revealed in Upper Devonian/Lower Mississippian Woodford Shale of South-central Oklahoma. *AAPG Search and Discovery Article* #4021.

Paxton S. T., Cruse A., Krystyniak A. (2007) Fingerprints of global sea level revealed in hydrocarbon source rock. *AAPG Search and Discovery* ref in: Molinares 2013, 86.

Peters K. E. (1986) Guidelines for Evaluating Petroleum Source Rock Using Programmed Pyrolysis. *Am. Assoc. Pet. Geol. Bull.* **70**, 318–329.

Peters K. E., Moldowan J. M., Schoell M., Hempkins W. B. (1986) Petroleum isotopic and biomarker composition related to source rock organic matter and depositional environment. *Organic Geochemistry* **10**, 17-27.

Peters K. E., Moldowan J. M. and Sundararaman P. (1990) Effects of hydrous pyrolysis on biomarker thermal maturity parameters: Monterey Phosphatic and Siliceous members. *Org. Geochem.* **15**, 249–265.

Peters K. E. and Moldowan J. M. (1991) Effects of source, thermal maturity, and biodegradation on the distribution and isomerization of homohopanes in petroleum. *Org. Geochem.* **17**, 47–61.

Peters K.E. and Cassa M. R. (1994) Applied source rock geochemistry. In: *The Petroleum System-from source to trap, AAPG Memoir* **60**, 93-117.

Peters K. E., Walters C. C. and Moldowan J. M. (2005) *The biomarker guide, Volume 2: biomarkers and isotopes in petroleum exploration and earth history.* Second Edition, p. 1155. Cambridge University Press. USA.

Pfennig N. and Truper H. G. (1989) Anoxygenic phototrophic bacteria. *Systematic Bacteriology* 1635-1709.

Philp R.P. (1986) Geochemistry in the Search for Oil. *University of Oklahoma/C&EN* 28-43.

Philp R. P. and Gilbert T. D. (1986) Biomarker distributions in Australia oils predominantly derived from terrigenous source material. *Organic Geochemistry* **10**, 73-84.

Philp R. P. and Mansuy L. (1997) Petroleum geochemistry: concepts, applications, and results. *Energy and Fuels* **11**, 749–760.

Philp R. P. (2013) *Formation and Geochemistry of Oil and Gas*. 2nd ed., Elsevier Ltd. Available at: http://dx.doi.org/10.1016/B978-0-08-095975-7.00709-9.

Portas R. (2009) Characterization and origin of fracture patterns int eh Woodford Shale in southeastern Oklahoma for application to exploration and development. *University of Oklahoma M.S. Thesis*.

Potter P. E., Maynard J. B., Pryor W. A. (1982) Appalachian gas-bearing Devonian shales: Statements and discussion. *Oil and Gas Journal* **80**, 290-318.

Quandt, L., Gottschalk, G., Ziegler, H., and Stichler W. (1977) Isotope Discrimination by Photosynthetic Bacteria. *FEMS Microbiol. Lett.* **1**, 125–128.

Raederstorff D. and Rohmer M. (1984) Sterols of the unicellular algae *Nematochrysopsis reoscoffensis* and *Chrysotila lamellose*: isolation of (24E)-24-*n*-propylidenecholesterol and 24-*n*-propylcholesterol. *Phytochemistry* **23**, 2835-2838.

Rampen, S.W., Schouten, S., Abbas, B., Panoto, F.E., Muyzer, G., Campbell, C.N., Fehling, J., and Sinninghe Damsté, J.S. (2007) On the origin of 24-norcholestanes and their use as age-diagnostic biomarkers. *Geology* **35**, 419–422.

Reed J. D., Illich H. a. and Horsfield B. (1986) Biochemical evolutionary significance of Ordovician oils and their sources. *Org. Geochem.* **10**, 347–358.

Requejo a. G., Allan J., Creaney S., Gray N. R. and Cole K. S. (1992) Aryl isoprenoids and diaromatic carotenoids in Paleozoic source rocks and oils from the Western Canada and Williston Basins. *Org. Geochem.* **19**, 245–264.

Requejo A. G. (1994) Maturation of petroleum source rocks-II. Quantitative changes in extractable hydrocarbon content and composition associated with hydrocarbon generation. *Organic Geochemistry* **21**, 91-105.

Rinaldi G. G. L., Leopold V. M., Koons C. B., (1988) Presence of benzohopanes, monoaromatic secohopanes, and saturate hexacyclic hydrocarbons in petroleum from carbonate environments. In: *Geochemical Biomarkers* 331-353.

Roberts C.T., and Mitterer R. M. (1992) Laminated black shale-bedded chert cyclicity in the Woodford Formation, southern Oklahoma, In: *K.S. Johnson and B.J. Cardott, eds., Source rocks in the southern Midcontinent, 1990 symposium: OGS Circular* **93**, 330-336

Rohmer M., Bouvier P., Ourisson G. (1979) Molecular evolution of biomembranes: structural equivalents and phylogenetic precursors of sterols. *Proceedings of the National Academy of Sciences of the United States of America* **76**, 847-851.

Rohmer M., Bouvier-Nave P., Ourisson G. (1984) Distribution of hopanoid triterpenes in prokaryotes. *Journal of General Microbiology* **130**, 1137-1150.

Romero A. M. (2008). Geochemical characterization of the Woodford Shale, Central and Southeastern Oklahoma. . University of Oklahoma M.S. Thesis.

Romero A. M. and Philp R. P. (2012) Organic geochemistry of the Woodford Shale, southeastern Oklahoma: How variable can shales be? *Am. Assoc. Pet. Geol. Bull.* **96**, 493–517.

Rubinstein I., Sieskind O., Albrecht P. (1975) Rearranged sterenes in shale: occurrence and simulated formation. *Journal of Chemical Society, Perkin Transaction* I, 1833-1836.

Sagemen B. B., Murphy A. E., Werne J. P., ver Straeten C. A., Hollander D. J., Lyons T. W. (2003) A tale of shales: the relative roles of production, decomposition, and dilution in the accumulation of organic-rich strata, Middle-Upper Devonian, Appalachian basin. *Chemical Geology* **195**, 229-273.

Sahai S. and Çemen I. (2008) Enhanced structural interpreatation in the Arkoma Basin with Seismic Attributes. In: *Suneson, N. H., Slatt, R.,and Ç emen, I., (eds.) Stratigraphic and structural evolution of the Ouachita Mountains and Arkoma Basin, southeastern Oklahoma and west-central Arkansas: Applications to petroleum exploration: 2004 field symposium. Technical papers: Oklahoma Geological Survey Circular 112B,* p. 25-30.

Schaefle J., Ludwig B., Albrecht P. and Ourisson G. (1977) Hydrocarbures aromatiques d'origine geologique. II. *Tetrahedron Lett.* **18**, 3673–3676.

Schoell M., McCaffrey M. A., Fago F. J., Moldowan J. M. (1992) Carbon isotopic compositions of 23,30-bisnorhopanes and other biological markers in a Monterey crude oil. *Geochimica et Cosmochimica Acta* **56**, 1391-1399.

Schwark L. and Frimmel A. (2004) Chemostratigraphy of the Posidonia Black Shale, SW-Germany II. Assessment of extent and persistence of photic-zone anoxia using aryl isoprenoid distributions. *Chem. Geol.* **206**, 231–248.

Schwark L. and Empt P. (2006) Sterane biomarkers as indicators of palaeozoic algal evolution and extinction events. *Palaeogeogr. Palaeoclimatol. Palaeoecol.* **240**, 225–236.

Seifert W. K., and Moldowan J. M. (1979) The effect of biodegradation on steranes and terpanes in crude oils. *Geochimica et Cosmochimica Acta* **43**, 111-126.

Seifert W. K., and Moldowan J. M. (1980) The effect of thermal stress on source-rock quality as measured by hopane stereochemistry. *Physics and Chemistry of Earth* **12**, 229-237.

Seifert W. K. and Moldowan J. M. (1981) Paleoreconstruction by biological markers. *Geochim. Cosmochim. Acta* **45**, 783–794.

Seifert W. K., Carlson R. M. K., and Moldowan J. M. (1983) Geomimetic synthesis, structure assignment, and geochemical correlation application of monoaromatized petroleum steranes. *In: Advances in Organic Geochemistry 1981* 710-724.

Seifert W. K. and Moldowan J. M. (1986) Use of biological markers in petroleum exploration. In*: Methods in Geochemistry and Geophysics* **24**, 261-290.

Shaw A. B. (1964) Time in stratigraphy. *McGraw-Hill, New York* 1-365.

Sierra R., Tran M. H., Abousleiman Y., Slatt R. M. (2010) Woodford Shale mechanical properties and impacts of lithofacies. *44th U.S. Rock Mechanics Symposium* (ARMA 10-461).

Sieskind O., Joly G., Albrecht P. (1979) Simulation of the geochemical transformation of sterols: superacid effects on clay minerals. *Geochimica et Cosmochimica Acta* **43**, 1675-1679.

Sinninghe Damste J. S. S., Keely B. J., Betts S. E., Baas M., Maxwell J. R. and Deleeuw J. W. (1993) Variations in Abundances and Distributions of Isoprenoid Chromans and Long-Chain Alkylbenzenes in Sediments of the Mulhouse Basin - a Molecular Sedimentary Record of Paleosalinity. **20**, 1201–1215.

Sinninghe Damsté J. S., Van Duin A. C. T., Hollander D., Kohnen M. E. L. and De Leeuw J. W. (1995a) Early diagenesis of bacteriohopanepolyol derivatives: Formation of fossil homohopanoids. *Geochim. Cosmochim. Acta* **59**, 5141–5157.

Sinninghe Damste J. S., Kenig F., Koopmans M. P., Koster J., Schouten S., Hayes J. M. and de Leeuw J. W. (1995b) Evidence for gammacerane as an indicator of water column stratification. *Geochim. Cosmochim. Acta* **59**, 1895–1900.

Sinninghe Damsté J. S., Schouten S. and Van Duin A. C. T. (2001) Isorenieratene derivatives in sediments: Possible controls on their distribution. *Geochim. Cosmochim. Acta* **65**, 1557–1571.

Sinninghe Damsté J. S., Kuypers M. M. M., Schouten S., Schulte S. and Rullkötter J. (2003) The lycopane/C31 n-alkane ratio as a proxy to assess palaeoxicity during sediment deposition. *Earth Planet. Sci. Lett.* **209**, 215–226.

Sinninghe Damsté J. S., Schouten S. and Volkman J. K. (2014) C27-C30 neohop-13(18)-enes and their saturated and aromatic derivatives in sediments: Indicators for diagenesis and water column stratification. *Geochim. Cosmochim. Acta* **133**, 402–421.

Sirevåg R. and Ormerod J. G. (1970) Carbon dioxide fixation in green sulphur bacteria. *Biochem. J.* **120**, 399–408.

Sirevåg R., Buchanan B. B., Berry J. a. and Troughton J. H. (1977) Mechanisms of CO2 fixation in bacterial photosynthesis studied by the carbon isotope fractionation technique. *Arch. Microbiol.* **112**, 35–38.

Slatt, R. M., et al., (2011) Outcrop/behind outcrop (quarry), multiscale characterization of the Woodford Gas Shale, Oklahoma (abs.): *AAPG Search and Discovery article 80138.*

Slatt R. M. and Rodriguez N. D. (2012) Comparative sequence stratigraphy and organic geochemistry of gas shales: Commonality or coincidence? *J. Nat. Gas Sci. Eng.* **8**, 68–84.

Slatt, R. M., N. Buckner, Y. Abousleiman, R. Sierra, P. Philp, A. Miceli-Romero, R. Portas, N.O'Brien, M. Tran, R. Davis, and T. Wawrzyniec (2012) Outcrop/behind outcrop (quarry), multiscale characterization of the Woodford Gas Shale, Oklahoma. *in* J. Breyer, eds., Shale reservoirs—Giant resources for the 21st century: AAPG Memoir **97**, 382-402.

Slatt R. (2013). Reservoir Characterization Lecture. *Reservoir Characterization I, University of Oklahoma.*

Slowakiewicz M., Tucker M., Perri E., Pancost R. D. (2015) Nearshore euxinia in the photic zone of an ancient sea. *Palaeogeography, Palaeoclimatology, Palaeoecology* **426,** 242-259.

Smil V. (1994) Energy in World History. *Westwood Press, Boulder CO.*

Smith D., Scott J. H., Steele A., Cody G., Ohara S., Bowden R., Fogel M. (2011) Biosynthesis and isotopic composition of bacteriochlorophyll and okenone in purple sulfur bacteria. *American Geophysical Union* Abstract # B53B-03.

Strachan M. G., Alexander R., van B. W., Kagi R. I. (1989) Source and heating rate effects upon maturity parameters based on ratios of 24-ethylcholestane diastereomers. *Journal of Geochemical Exploration* **31**, 285-294.

Sousa Júnior G. R., Santos A. L. S., De Lima S. G., Lopes J. a D., Reis F. a M., Santos Neto E. V. and Chang H. K. (2013) Evidence for euphotic zone anoxia during the deposition of Aptian source rocks based on aryl isoprenoids in petroleum, Sergipe-Alagoas Basin, northeastern Brazil. *Org. Geochem.* **63**, 94–104.

Suneson, N. H., C. Ibrahim., K. Dennis., S. Roberts., T. Michael., R. M. Slatt, and C. G. Stone. (2005) Stratigraphic and structural evolution of the Ouachita Mountains and Arkoma Basin, southeastern Oklahoma and west-central Arkansas: applications to petroleum exploration: *Oklahoma Geological Survey Guidebook* **34** 128-134.

Summons R. E. and Powell T. G. (1987) Identification of aryl isoprenoids in source rocks and crude oils: Biological markers for the green sulphur bacteria. *Geochim. Cosmochim. Acta* **51**, 557–566.

Takahashi S., Shin-ichi Y., Ogawa Y., Kimura K., Kaiho K., Yoshida T., Tsuchiya N. (2014) Bioessential element-depleted ocean following the euxinic maximum of the end-Permian mass extinction. *Earth and Planetary Science Letters* **393**, 94-104.

Tannenbaum E., Ruth E., Huizinga B. J., Kaplan I. R. (1986) Biological marker distribution in coexisting kerogen, bitumen and asphaltenes in Monterey Formation diatomite, California. *Organic Geochemistry* **10**, 531-536.

ten Haven H. L., De Leeuw J. W. and Schenck P. a. (1985) Organic geochemical studies of a Messinian evaporitic basin, northern Apennines (Italy) I: Hydrocarbon biological markers for a hypersaline environment. *Geochim. Cosmochim. Acta* **49**, 2181–2191.

ten Haven H. L., Leeuw J. W., Peakman T. M., Maxwell J. R. (1986) Anomalies in steroid and hopanoid maturity indices. *Geochimica et Cosmochimica Acta* **50**, 853-855.

ten Haven H.L., de Leeuw, J.W., Rullkotter, J. Sinninghe-Damsté, J. (1987) Restricted utility of the pristane/phytane ratio as a palaeoenvironmental indicator. *Nature* **330**, 641-643.

ten Haven H. L. and Rullkotter J. (1988) The diagenetic fate of taraxer-14-ene and oleanane isomers. *Geochimica et Cosmochimica Acta* **52**, 2543-2548.

ten Haven H. L., de Leeuw J. W., Sinninghe Damste J. S., Schenck P. A., Palmer S. E. and Zumberge J. E. (1988) Application of biological markers in the recognition of paleohypersaline environments. *Lacustrine Petroleum Source Rocks* **40**, 123-130.

ten Haven H. L., Rohmer M., Rullkotter J., Bisseret P. (1989) Tetrahymanol, the most likely precursor of gammacerane, occurs ubiquitously in marine sediments. *Geochimica et Cosmochimica Acta* **53**, 3073-3079.

Tissot B. P. and Welte D. H. (1984) Petroleum Formation and Occurrence. *Springer-Verlag, New York.*

Totten G. E. (2007) A timeline of highlights from the histories of ASTM Committee D02 and the Petroleum Industry. *ASTM.*

Treibs A. (1936) Chlorophyll and hemin derivatives in organic mineral substances. *Angewandte Chemie* **49**, 682-686.

Truper H. G. and Genovese S. (1968) Characterization of photosynthetic sulfur bacteria causing red water in Lake Faro. *Woods Hole Oceanographic Institution* 225-232.

Tulipani S., Grice K., Greenwood P., Haines P. W., Summons R. E., Bottcher M. E., Foster C. B., Woltering M. and Playton T. (2013) Changes in palaeoenvironmental conditions in Late Devonian reef systems from the Canning Basin, WA: a biomarker and stable isotope approach. *Wabs 2013*, 1.

Turner B. W., Molinares-blanco C. E. and Slatt R. M. (2015) Special section : Shale paleoenvironments stratigraphic analysis of the Woodford Shale , Wyche Farm Quarry , Pontotoc County , Oklahoma. **3**, 1–9.

Urban J. B. (1960) Microfossils of the Woodford Shale of Oklahoma. *University of Oklahoma M.S. Thesis.*

Vandenbroucke M. and Largeau C. (2007) Kerogen origin, evolution and structure. *Organic Geochemistry* **38**, 719-833.

van der Meer M.T.J., Schouten S., van Dongen B.E. (2001) Biosynthetic controls on the ^{13}C contents of organic components in photoautotrophic bacterium *Chloroflexus aurantiacus. The Journal of Biological Chemistry* **276,** 10971-10976.

van Gemerden H. (1983) Physiological ecology of purple and green bacteria. *Ann. Microbiol.* **134**, 73-92.

van Kaam-Peters H. M. E., Köster J., Van Der Gaast S. J., Dekker M., De Leeuw J. W. and Sinninghe Damsté J. S. (1998) The effect of clay minerals on diasterane/sterane ratios. *Geochim. Cosmochim. Acta* **62**, 2923–2929.

van Krevelen D.W. (1950) Graphical-statistical method for the study of structure and reaction processes of coal. *Fuel* **29**, 269-283.

van Krevelen D. W. (1984) Organic geochemistry—old and new. *Org. Geochem.* **6**, 1–10.

Venkatesan M. I. (1989) Tetrahymanol: its widespread occurrence and geochemical significance. *Geochimica et Cosmochimica Acta* **53**, 3095-3101.

Vila X. and Abella C. (1994) Effects of light quality on the physiology and the ecology of planktonic green sulfur bacteria in lakes. *Photosynth. Res.* **41**, 53–65.

Vleeshouwer D. D., Rakocinski M., Racki G., Bond D., Sobien K., Claeys P. (2013). The astronomical rhythm of late-Devonian climate change (Kowala section, Holy Cross Mountains, Poland). *Earth and Planetary Science Letters* **365**, 25-37.

Vliex M., Hagemann H. . and Püttmann W. (1994) Aromatized arborane/fernane hydrocarbons as molecular indicators of floral changes in Upper Carboniferous/Lower Permian strata of the Saar-Nahe Basin, southwestern Germany. *Geochim. Cosmochim. Acta* **58**, 4689–4702.

Volkman J. K (1986) A review of sterol markers for marine and terrigenous organic matter. *Organic Geochemistry* **9**, 83-99.

Volkman, J.K. (2005) Sterols and other triterpenoids: Source specificity and evolution of biosynthetic pathways. *Organic Geochemistry* **36**, 139-159.

Vulgamore T., Clawson T. and Pope C. (2007) Applying Hydraulic Fracture Diagnostics to Optimize Stimulations in the Woodford Shale. *SPE Annu. Tech. ....* Available at: http://www.onepetro.org/mslib/servlet/onepetropreview?id=SPE-110029-MS.

Waples D. (1981) Organic geochemistry for exploration geologists. *Minneapolis, Burgess Publishing,* 151.

Werne, J. P., Sagemen B. B., Lyons T. W., Hollander D. J. (2002). An integrated assessment of a "type euxinic" deposit: evidence for multiple controls on black shale deposition in the middle Devonian Oatka Creek Formation. *American Journal of Science* **302**, 110-143.

Whitehead E. V. (1973) Molecular evidence for the biogenesis of petroleum and natural gas. *In*: Ingerson E (ed.) *Proceedings of Symposium on Hydrogeochemistry and Biogeochemistry* **2**, 158-211.

Whitehead E. V. (1974) The structure of petroleum pentacyclanes. *In: Advances in Organic Geochemistry 1973* 225-243.

Yamaguchi M. (1960) Total synthesis of renieratene and renierapurpurin. *Bull. Chem. Soc. Japan* **33**, 1560–1562.

Yentsch C. S. (1962) Marine plankton. In: *Physiology and biochemistry of algae* 771-797.

Zander J. M., Caspi E., Pandey G. N., Mitra C. R. (1969) The presence of tetrahymanol in *Oleandra wallichii. Phytochemistry* **8**, 2265-2267.

Zuber,H. and Cogdell R.J. (1995) Structure and organization of purple bacterial antenna complexes. In: *Anoxygenic Photosynthetic Bacteria* **2,** 315–348.

Zumberge J, E, (1987) Prediction of source rock characteristics based on terpane biomarkers in crude oils: a multivariate statistical approach. *Geochimica et Cosmochimica Acta* **51**, 1625-1637.

APPENDIX I: STRUCTURES

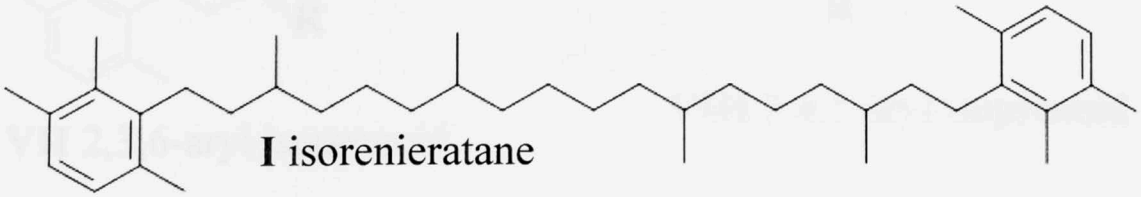

I isorenieratane

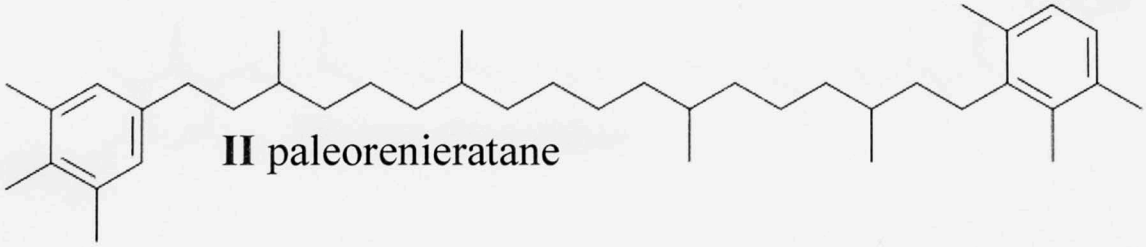

II paleorenieratane

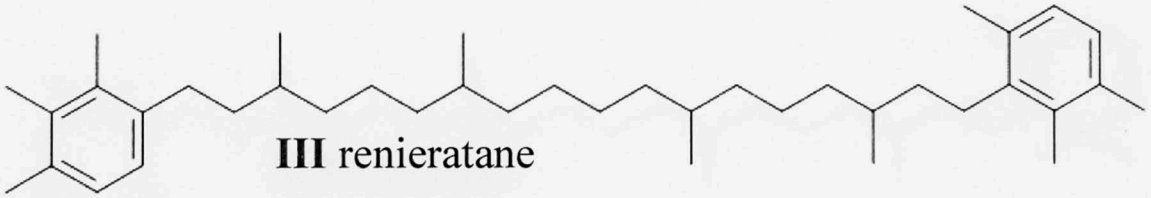

III renieratane

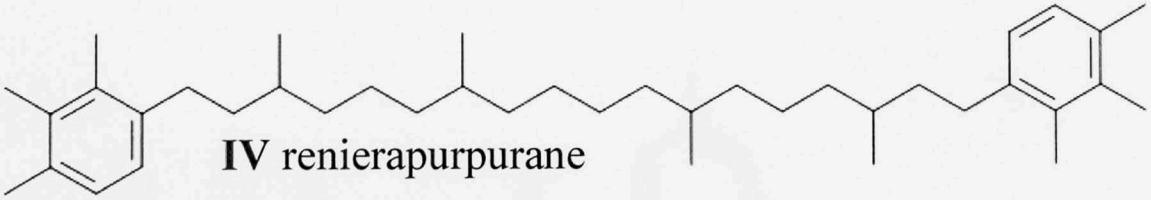

IV renierapurpurane

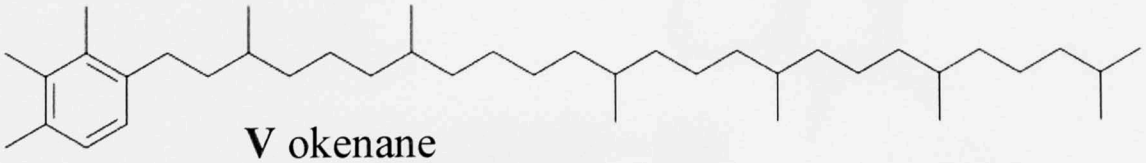

V okenane

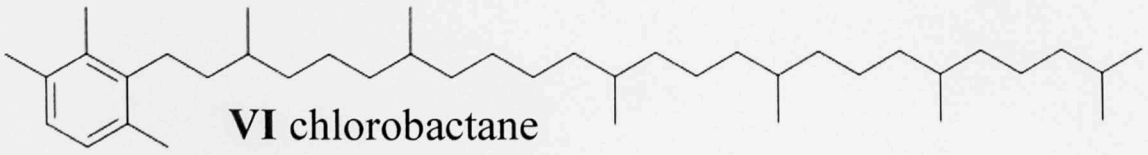

VI chlorobactane

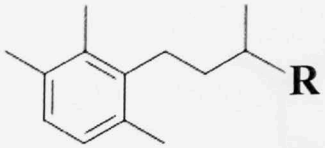

VII 2,3,6-aryl isoprenoid

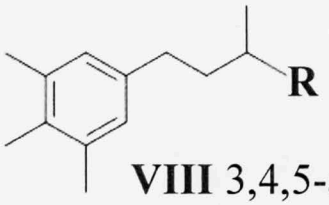

VIII 3,4,5-aryl isoprenoid

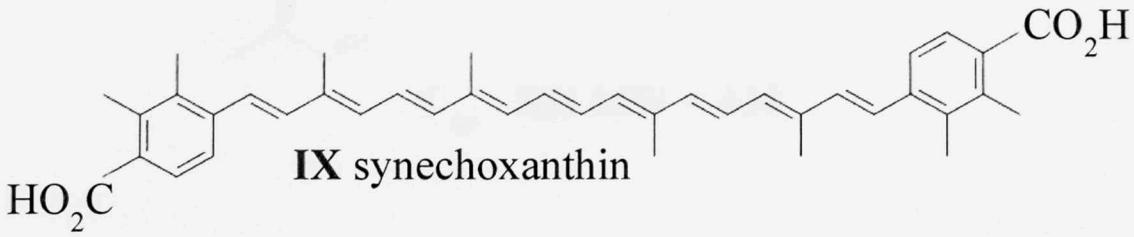

IX synechoxanthin

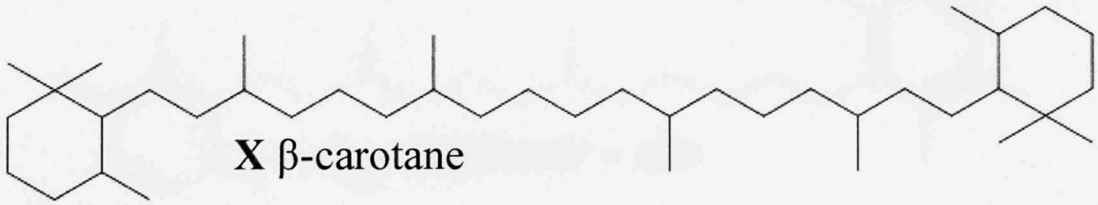

X β-carotane

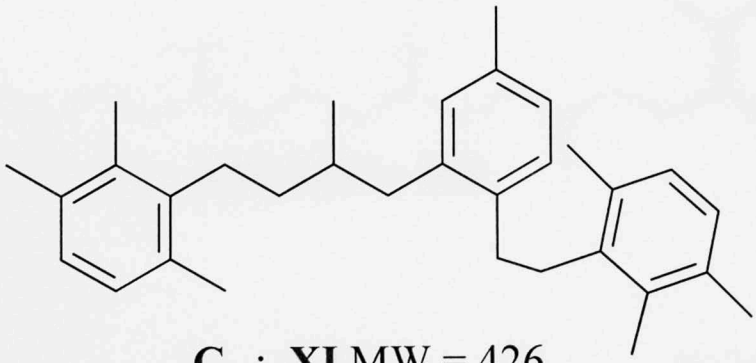

C_{32}: **XI** MW = 426

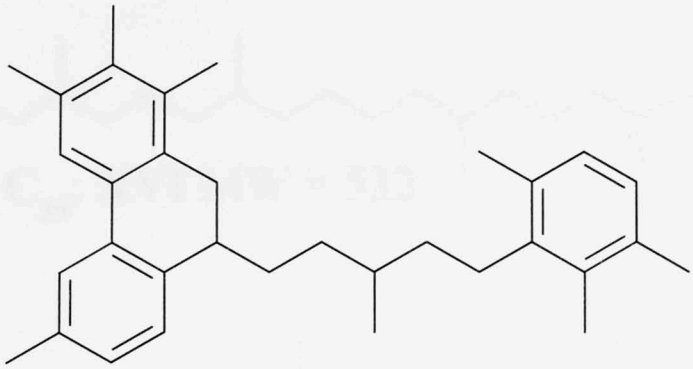

C_{33}: **XII** MW = 438

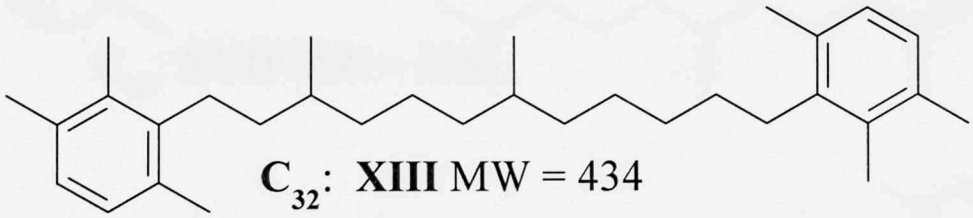

C_{32}: **XIII** MW = 434

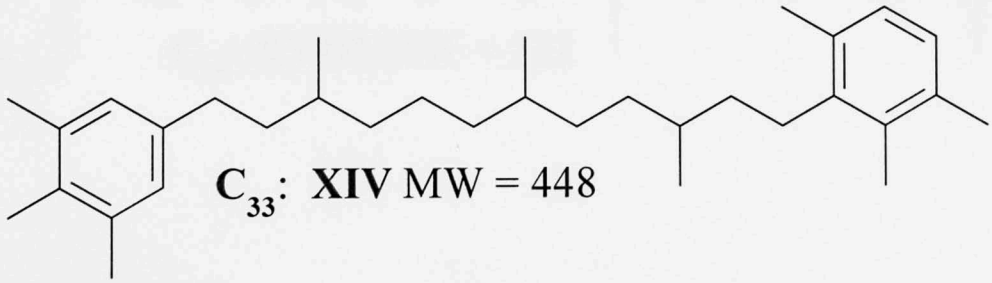

C_{33}: **XIV** MW = 448

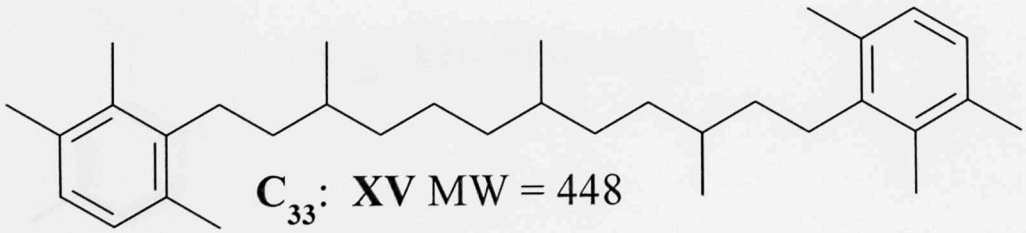

C_{33}: **XV** MW = 448

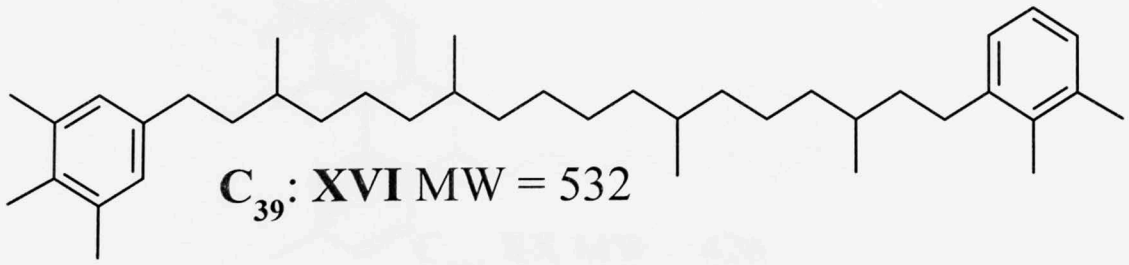

C_{39}: **XVI** MW = 532

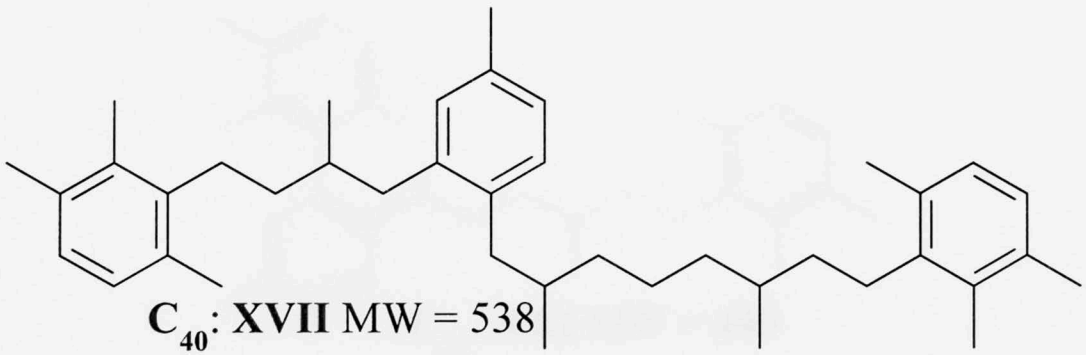

C_{40}: **XVII** MW = 538

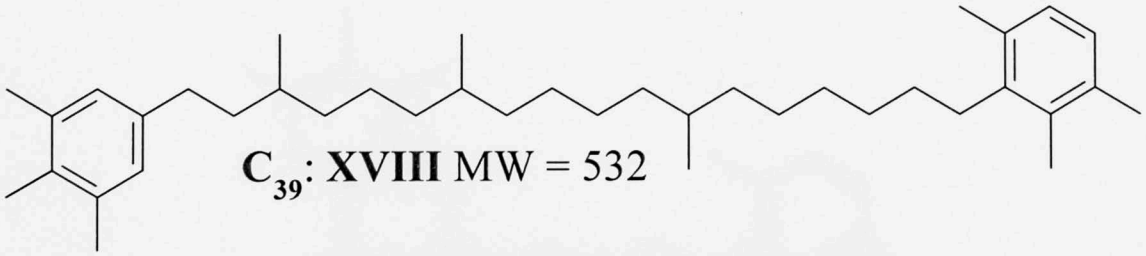

C_{39}: **XVIII** MW = 532

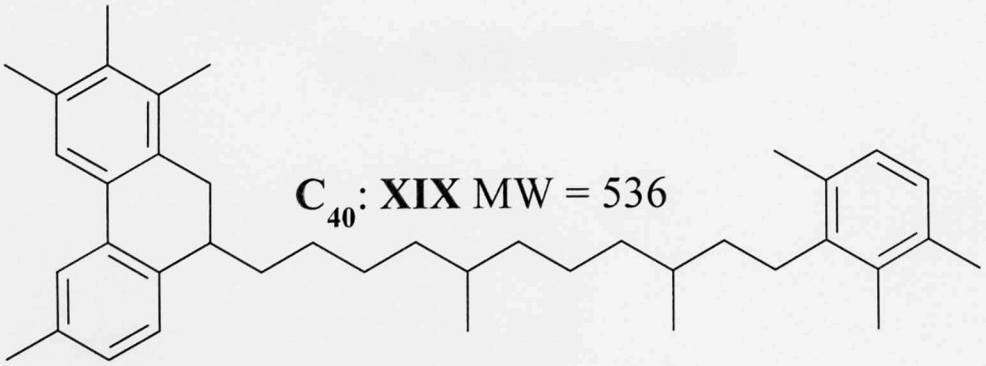

C_{40}: **XIX** MW = 536

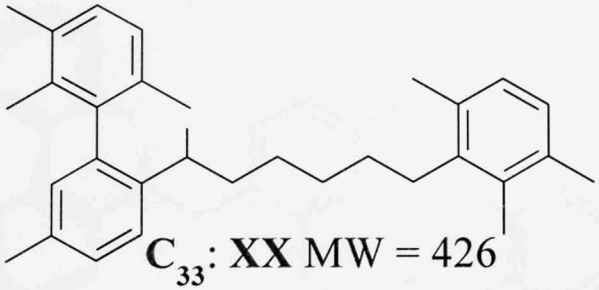

C_{33}: **XX** MW = 426

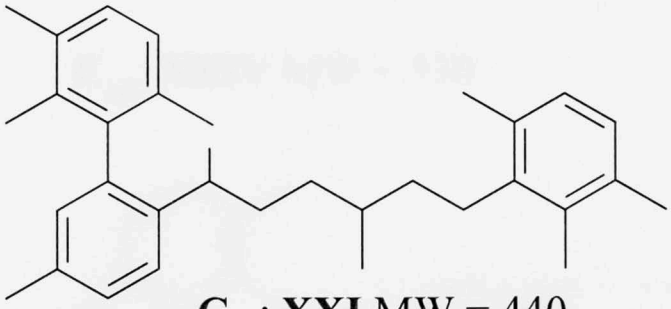

C_{33}: **XXI** MW = 440

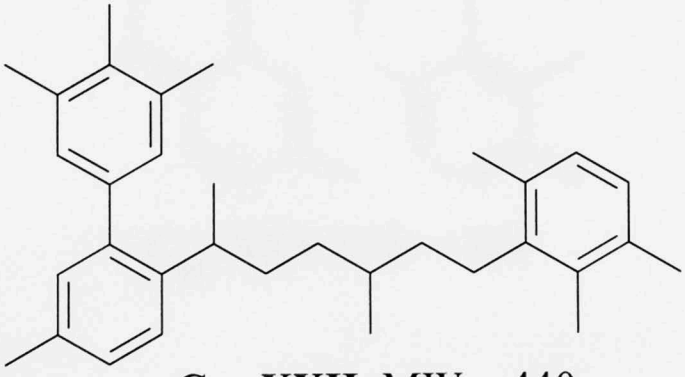

C_{33}: **XXII** MW = 440

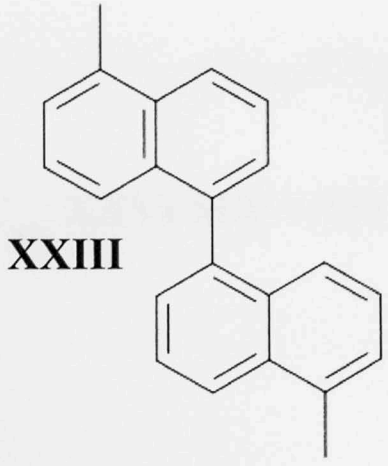

XXIII

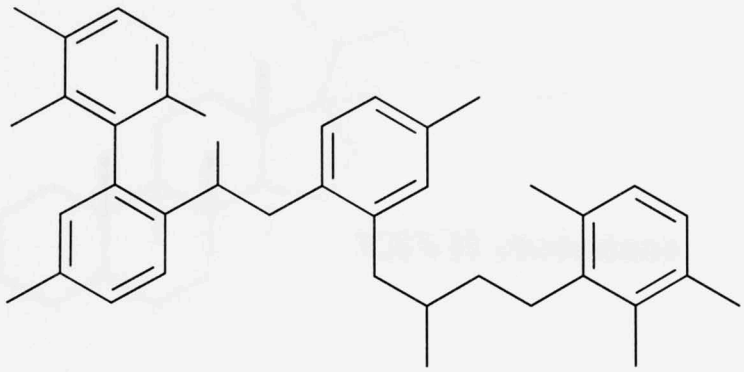

C_{40}: XXIV MW = 530

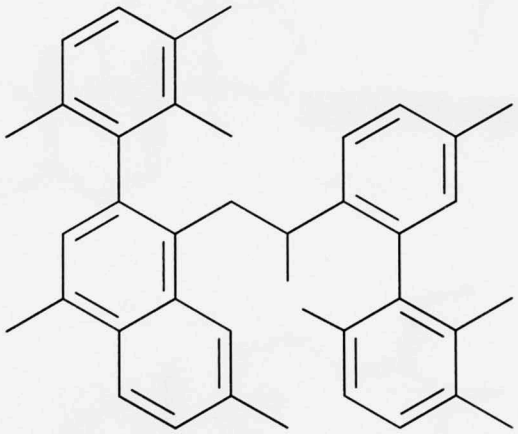

C_{40}: XXV MW = 524

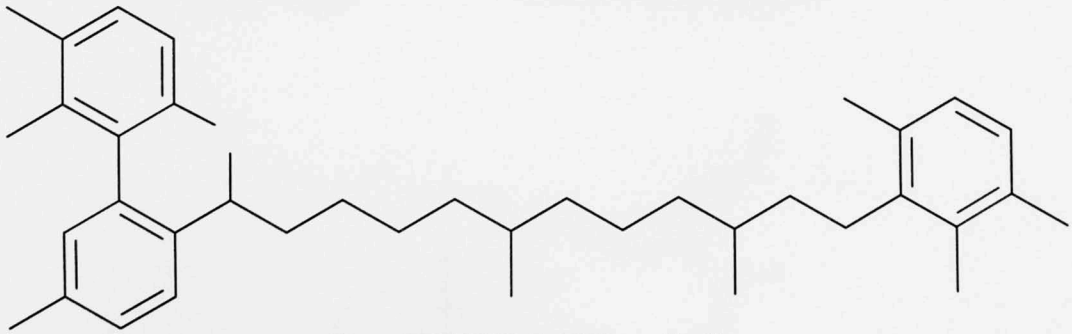

C_{40}: XXVI MW = 538

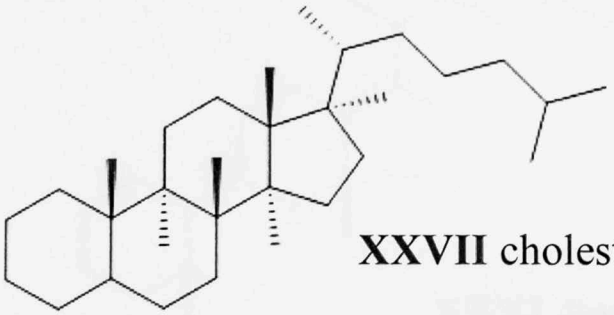

XXVII cholestane

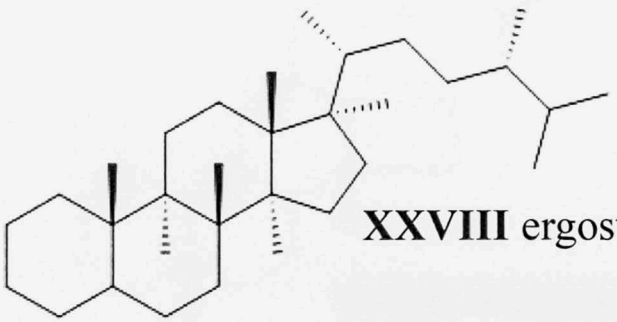

XXVIII ergostane

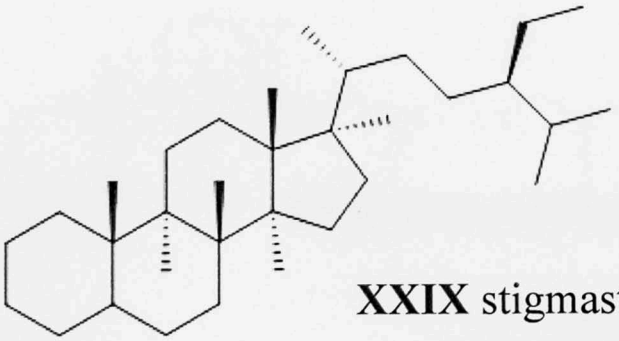

XXIX stigmastane

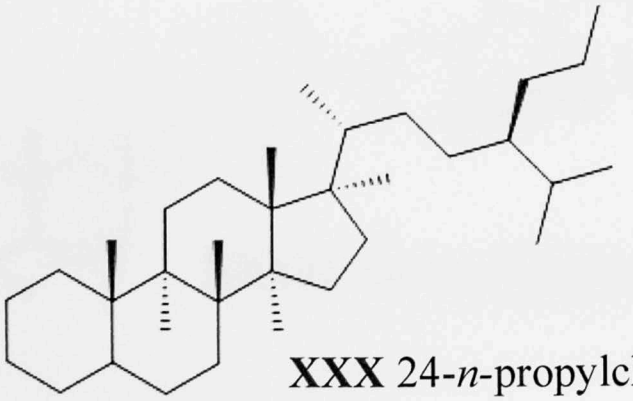

XXX 24-*n*-propylcholestane

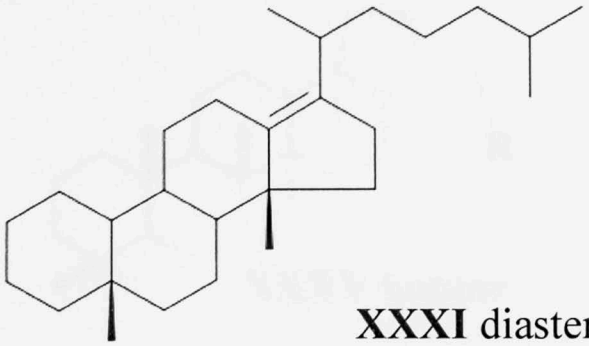

XXXI diasterene

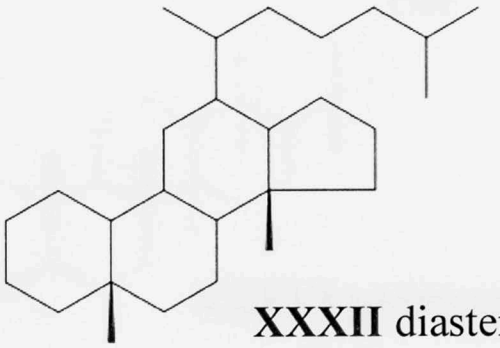

XXXII diasterane

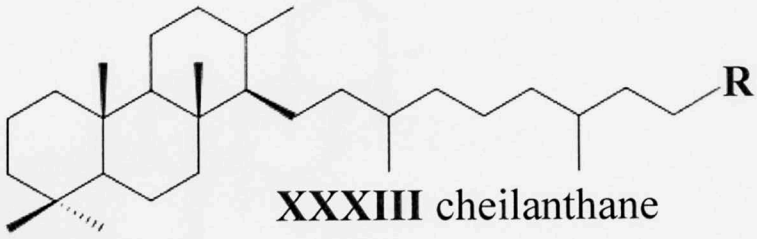

XXXIII cheilanthane

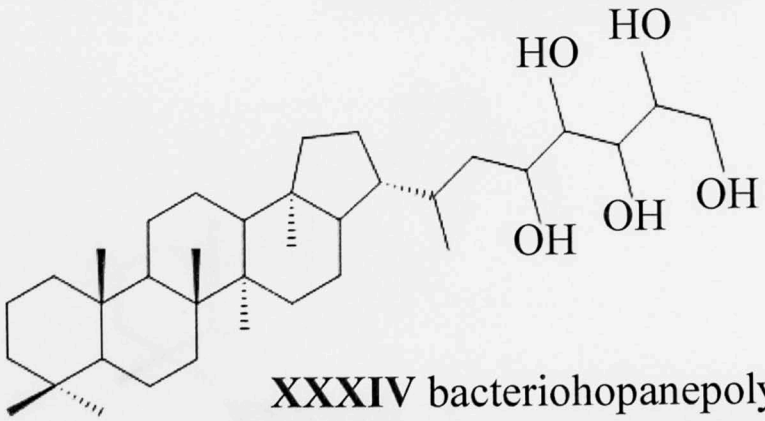

XXXIV bacteriohopanepolyol

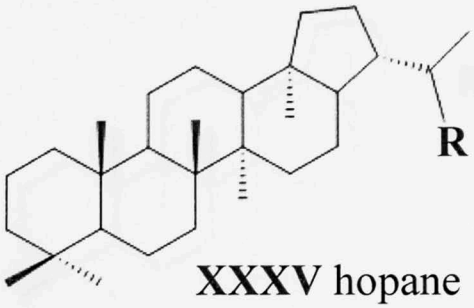

XXXV hopane

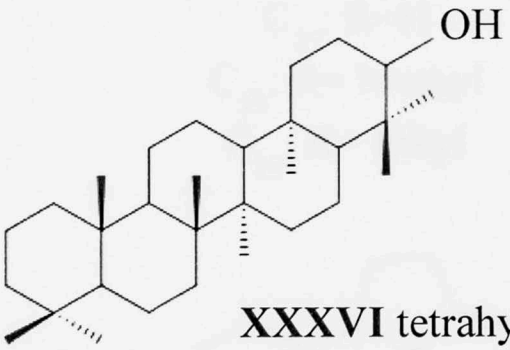

XXXVI tetrahymanol

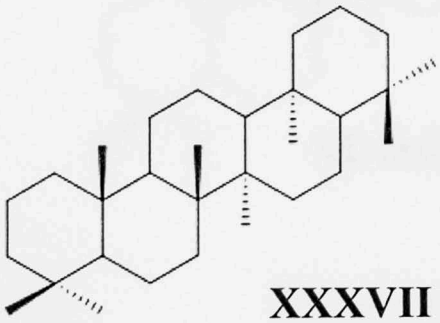

XXXVII gammacerane

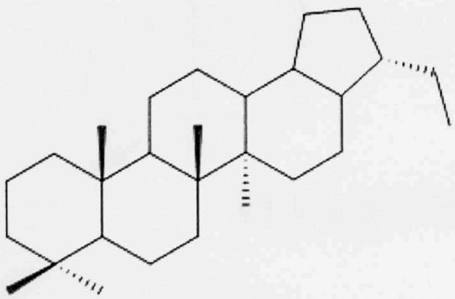

XXXVIII 28, 30-dinorhopane

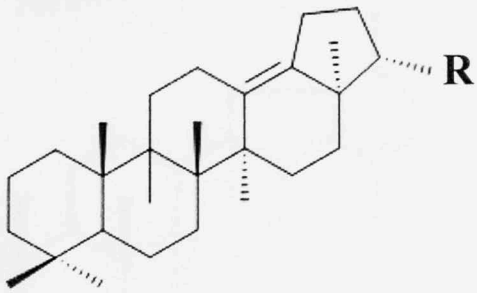

XXXIX neohop-13(18)-enes

C_{27}: R=H

C_{29}: R= Methyl

C_{30}: R= Ethyl

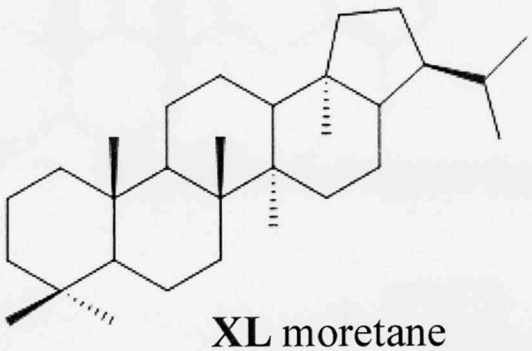

XL moretane

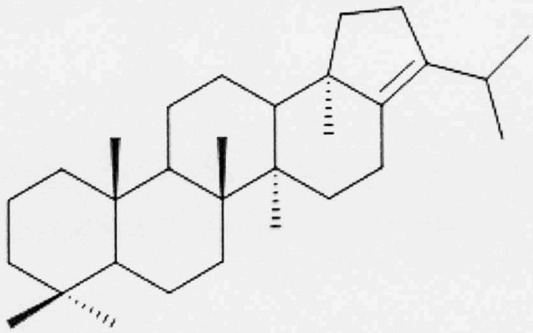

XLI hop-17(21)-ene

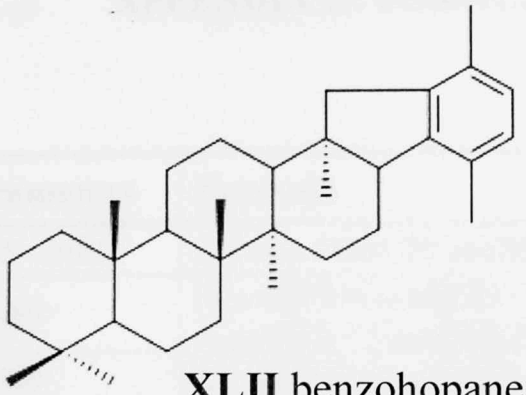

XLII benzohopane (m/z 191)

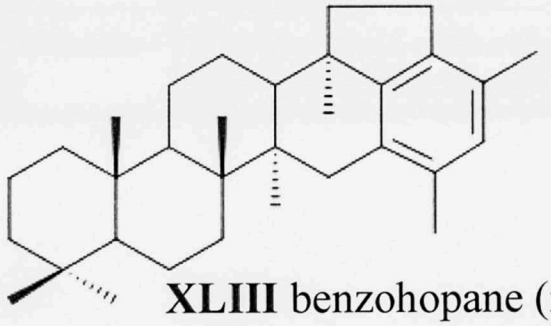

XLIII benzohopane (m/z 197)

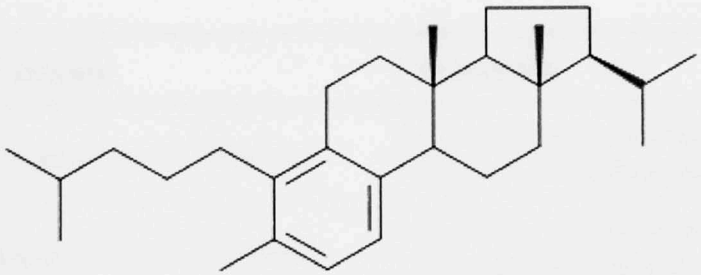

XLIV 5-methyl-10-(4-methylpentyl)-des-*A*-25-norabora(ferna)-5,7,9-triene

APPENDIX II: FORMULAE

Maturity Parameters	Formula
C_{29} *ααα 20S/(20S+20R)*	C_{29} ααα 20S/(C29 ααα20S+C29 ααα20R)
C_{29} *αββ/(ααα+αββ)*	(C_{29} αββ S+C_{29} αββ R) / (C_{29} ααα S + C_{29} ααα R)+ (C_{29} αββ S + C_{29} αββ R)
C_{31} *22S/(22S+22R)*	C_{31} αβ 22S/ (C_{31} αβ 22S + C_{31} αβ 22R)
C_{30} *Moretane/*C_{30} *Hopane*	C_{30} βα moretane / C_{30} αβ hopane
C_{21} *Tri ββ/(βα+αα)*	C_{21} ββ/(C_{21} βα+ C_{21} αα)
Σ C_{30}-C_{35} *Hop-(17)21-enes / Σ*C_{30}-C_{35} *Hopanes*	(C_{30}+C_{31}+C_{32}+C_{33}+C_{34}+C_{35} Hop-17(21)-enes)/ (C_{30}+C_{31}+C_{32}+C_{33}+C_{34}+C_{35} Hopanes

Lithology Proxies	Formula
C_{27}-C_{29} *Diasteranes/*C_{27}-C_{29} *Steranes*	(C_{27}+C_{28}+C_{29} βα Diasteranes) / (C_{27}+C_{28}+C_{29} Regular Steranes)
C_{27}-C_{29} *Diasterene/* C_{27}-C_{29} *Steranes*	(C_{27}+C_{28}+C_{29} βα Diasterenes) / (C_{27}+C_{28}+C_{29} Regular Steranes)
C_{27}-C_{30} *Diasterenes/*C_{27}-C_{30} *Diasteranes*	(C_{27}+C_{28}+C_{29} βα Diasterenes) / (C_{27}+C_{28}+C_{29} βα Diasteranes)
C_{30}*Diahopane/*C_{30}*Hopane*	C_{30} 17α diahopane/ C_{30} 17α,21β hopane
C_{32}-C_{35} *Benzohopanes/* C_{32}-C_{35} *Homohopanes*	(C_{32}+C_{33}+C_{34}+C_{35} Benzohopanes)/ (C_{32}+C_{33}+C_{34}+C_{35} Hopanes)
C_{27}, $C_{29\text{-}30}$ *Neohopenes/*C_{30}*Hopane*	(C_{27}+C_{29}+C_{30} neohop-13(18)-enes) / (C_{30} Hopane)

Environmental Indicators	Formula
Pr/Ph	C_{19} Pristane/ C_{20} Phytane
Sterane Index (%)	(24-*n*-propylcholestane)/(C_{27}+C_{28}+C_{29}+C_{30} steranes)*100
C_{27}/C_{29} Steranes	(C_{27} ααα S+R + C_{27} αββ S+R)/ (C_{28} ααα S+R + C_{28} αββ S+R)
C_{26}/C_{25} Cheilanthanes	C_{26} βα Cheilanthane /C_{25} βα Cheilanthane
C_{31}R/C_{30}Hopane	C_{31} 22R Hopane/ C_{30} Hopane
C_{29} Norhopane/C_{30} Hopane	C_{29} Hopane/ C_{30} Hopane
C_{30} TPP/C_{30} Sterane	C_{30} Tetracyclic Polyprenoid/ C_{30} Sterane
MATH (µg/g OC)	Absolute Concentration of MATH

Water Chemistry	Formula
Paleorenieratane (µg/g OC)	Absolute Concentration of Paleorenieratane
Isorenieratane (µg/g OC)	Absolute Concentration of Isorenieratane
Σ C_{15}-C_{31} 2,3,6 Aryl Isoprenoids (µg/g OC)	Absolute Concentration of 2,3,6-aryl isoprenoids
Σ C_{15}-C_{31} 3,4,5 Aryl Isoprenoids (µg/g OC)	Absolute concentration of 3,4,5-aryl isoprenoids
28, 30 Dinhorhopane/C_{30} Hopane (DNH Index)	28, 30 Dinorhopane/ C30 Hopane
Gammacerane Index	Gammacerane/ C30 Hopane
Homohopane Index (%)	(C_{35} S+R Homohopane) / (C_{31}+C_{32}+C_{33}+C_{34}+C_{35} S+R homohopanes)*100
C_{35}/C_{34} Homohopanes	C_{35} S+R Homohopane/ C_{34} S+R Homohopane
Pr/Ph	C_{19} Pristane / C_{20} Phytane

Microbial Community	Formula
Paleorenieratane (μg/g OC)	Absolute Concnetration of Paleorenieratane
Isorenieratane (μg/g OC)	Absolute Concentration of Isorenieratane
Renieratane (μg/g OC)	Absolute Concentration of Renieratane
Renierapurpurane (μg/g OC)	Absolute Concentration of Renierapurpurane
Gammacerane Index	Gammacerane/ C30 Hopane
Sterane/Hopane	(C_{27}+C_{28}+C_{29} regular steranes)/ (C_{29}+C_{30}+C_{31}+C_{32}+C_{33} hopanes)
Σ C_{28-29} Tri/Hopanes	(C_{28}+C_{29} cheilanthanes) / (C_{29}+C_{30}+C_{31}+C_{32}+C_{33} hopanes)
C_{27}/C_{29} Steranes	(C_{27} ααα S+R + C_{27} αββ S+R)/ (C_{29} ααα S+R + C_{29} αββ S+R)
C_{28}/C_{29} Steranes	(C_{28} ααα S+R + C_{28} αββ S+R)/ (C_{29} ααα S+R + C_{29} αββ S+R)

AIII.I. Wyche-1 core m/z 191

***samples arranged by increasing depth on following page

m/z 191

WSLU-8 SATURATE

Peak No.	Compound
1	C_{20} cheilanthane
2a	C_{21} ββ cheilanthane
2b	C_{21} βα cheilanthane
2c	C_{21} αα cheilanthane
3a	C_{23} βα cheilanthane
3b	C_{23} αα cheilanthane
4a	C_{24} βα cheilanthane
4b	C_{24} αα cheilanthane
5a	C_{25} βα cheilanthane
5b	C_{25} αα cheilanthane
6a	C_{26} βα cheilanthane
6b	C_{26} αα cheilanthane
7	C_{24} tetracyclic terpane
8a	C_{28} βα cheilanthane
8b	C_{28} αα cheilanthane
9a	C_{29} βα cheilanthane
9b	C_{29} αα cheilanthane
10	C_{27} neohop-13(18)-ene
11	C_{27} 18α trisnorhopane
12	C_{27} 17α trisnorhopane
13	28, 30-dinorhopane
14	C_{29} neohop-13(18)-ene
15	C_{30} norhopane
16	C_{30} diahopane
17	C_{30} hop-17(21)-ene

Peak No.	Compound
18	C_{29} 17α21β Moretane
19	C_{30} 17β21α Hopane
20	C_{30} neohop-13(18)-ene
21	C_{30} 17α21β Moretane
22	C_{31} hop-17(21)-ene
23a	C_{33} βα cheilanthane
23b	C_{33} αα cheilanthane
24a	C_{31} 17β21α 22S Hopane
24b	C_{31} 17β21α 22R Hopane
25	C_{32} hop-17(21)-ene
26	gammacerane
27	C_{31} 17α21β Moretane
28a	C_{32} 17β21α 22S Hopane
28b	C_{32} 17β21α 22R Hopane
29	C_{33} hop-17(21)-ene
30	C_{32} 17α21β Moretane
31a	C_{33} 17β21α 22S Hopane
31b	C_{33} 17β21α 22R Hopane
32	C_{34} hop-17(21)-ene
33	C_{33} 17α21β Moretane
34a	C_{34} 17β21α 22S Hopane
34b	C_{34} 17β21α 22R Hopane
35	C_{34} 17α21β Moretane
36a	C_{35} 17β21α 22S Hopane
36b	C_{35} 17β21α 22R Hopane
37	C_{35} 17α21β Moretane

WSLU-1 SATURATE

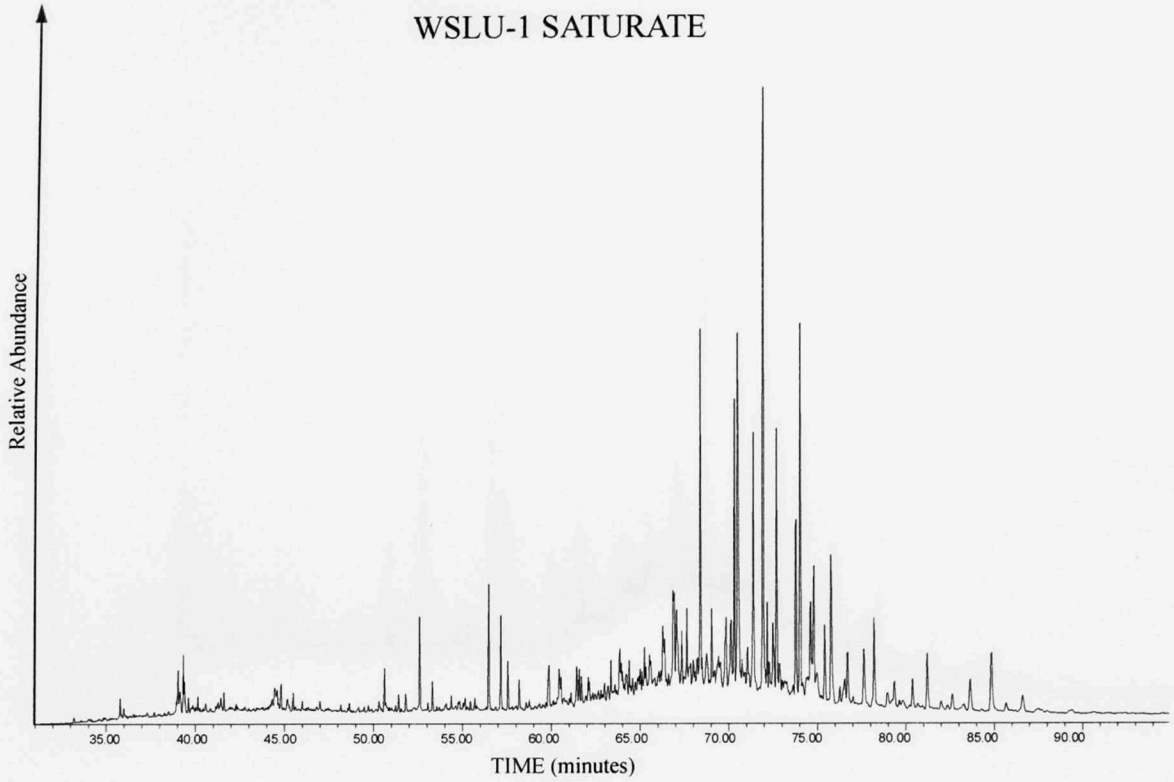

WSLU-2 SATURATE

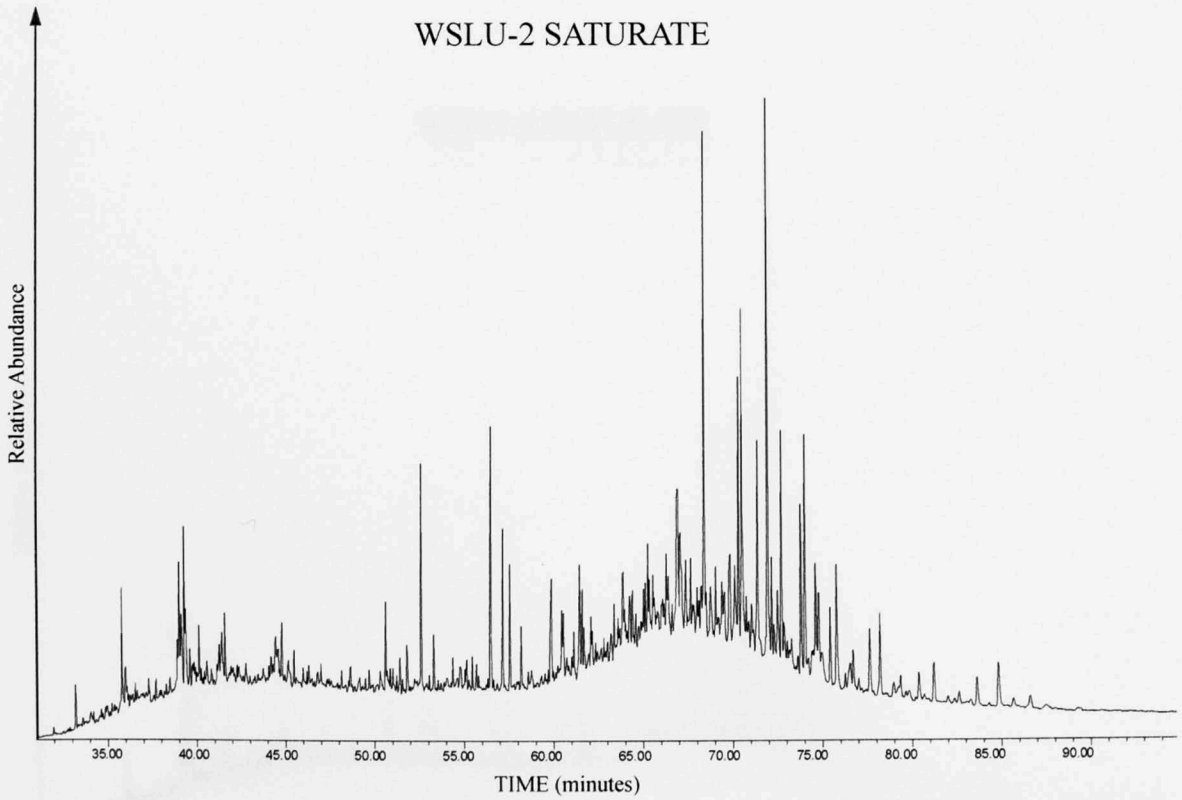

WSLU-3 SATURATE

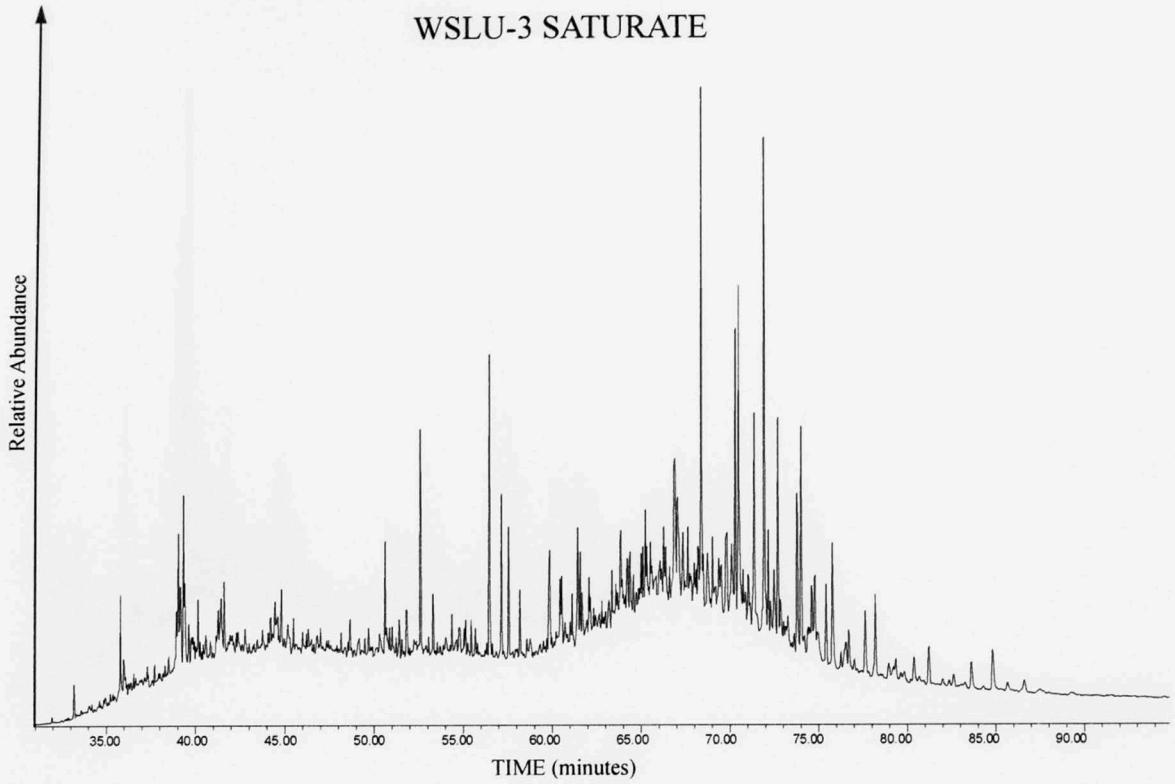

WSLU-4 SATURATE

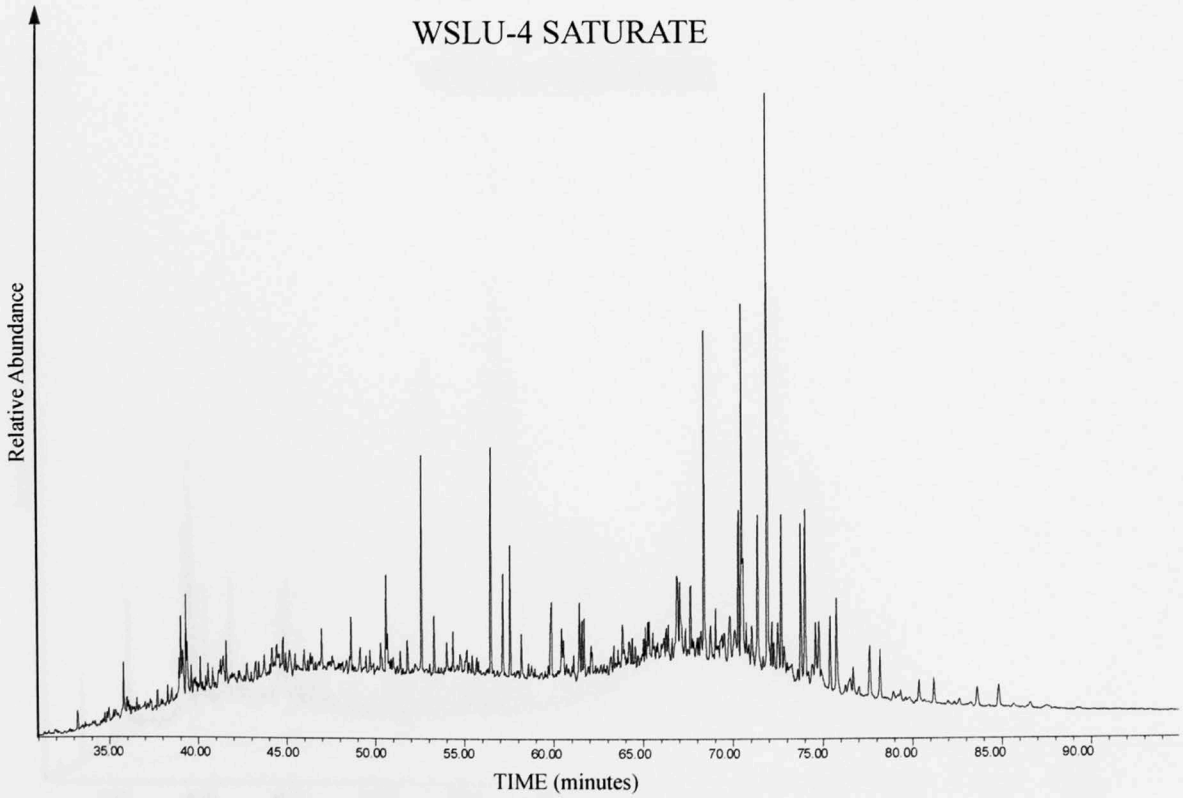

WSLU-5 SATURATE

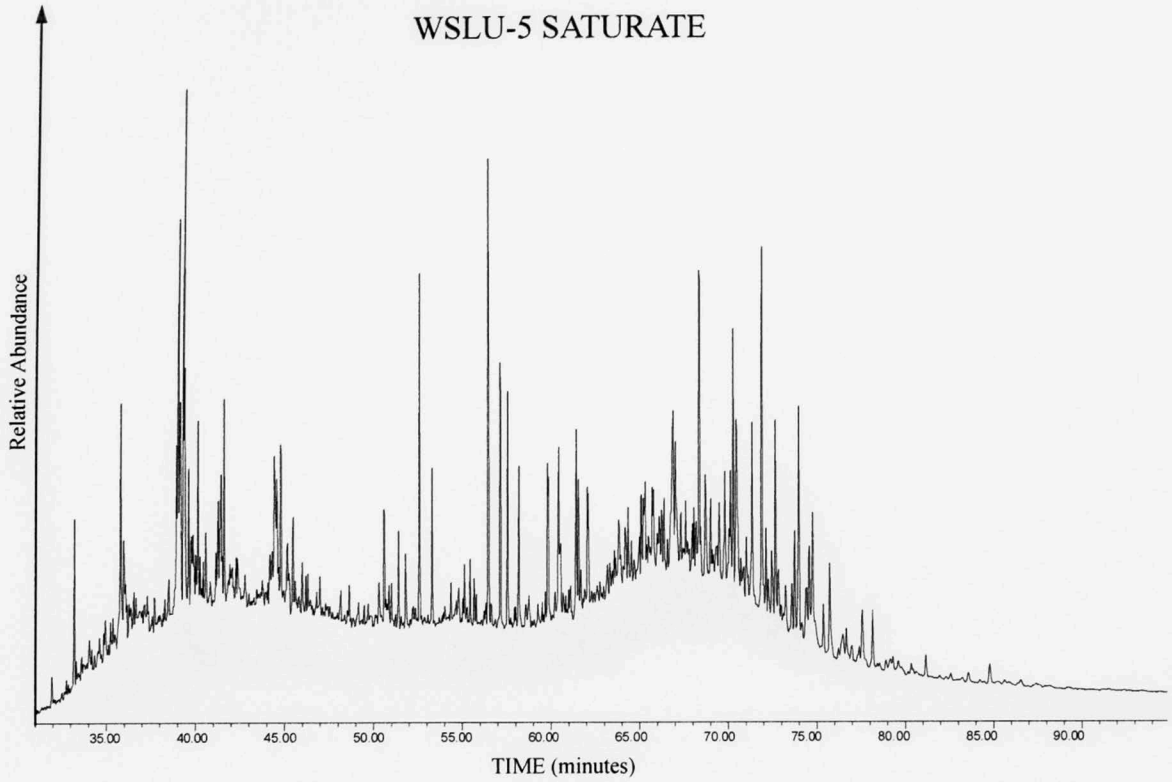

WSLU-6 SATURATE

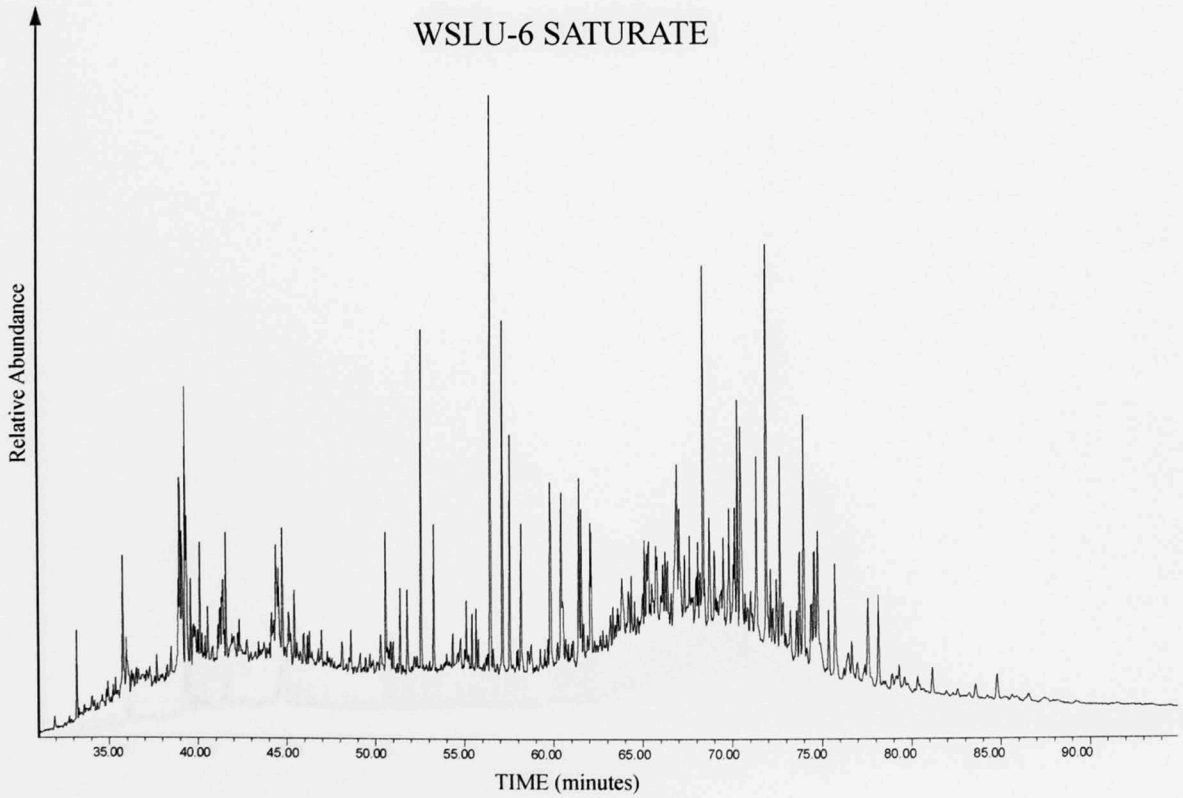

WSLU-7 SATURATE

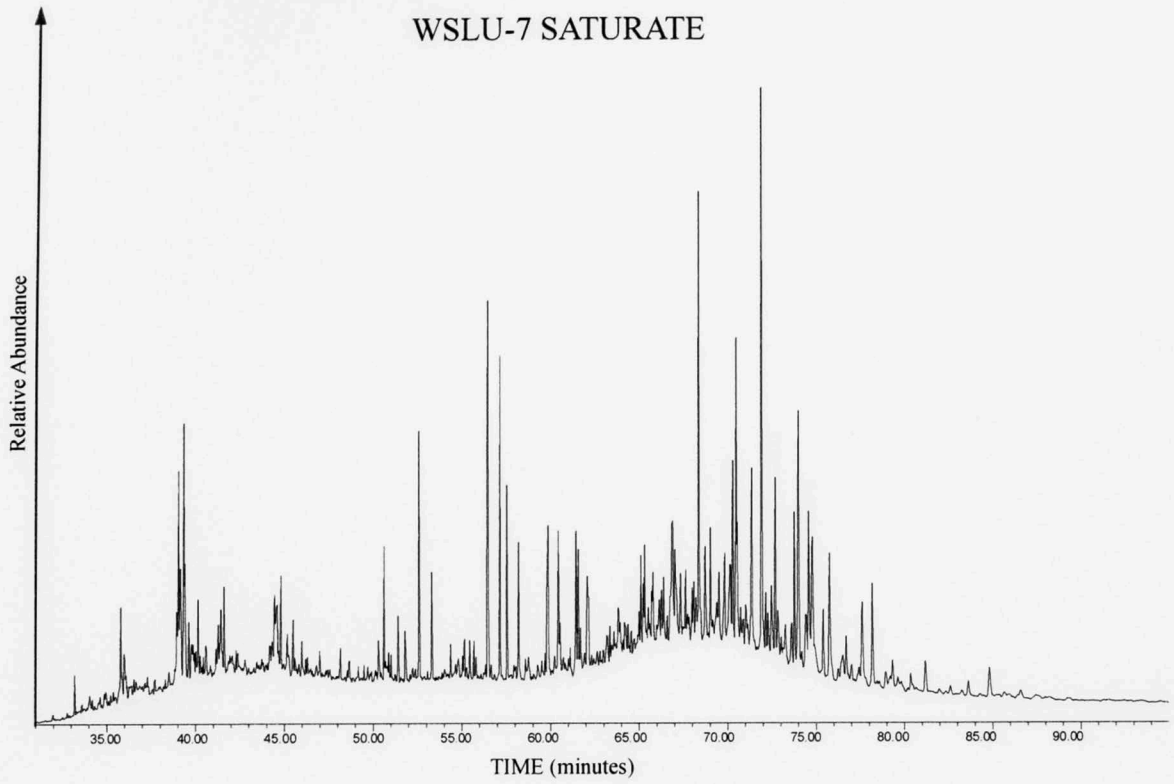

WSLU-8 SATURATE

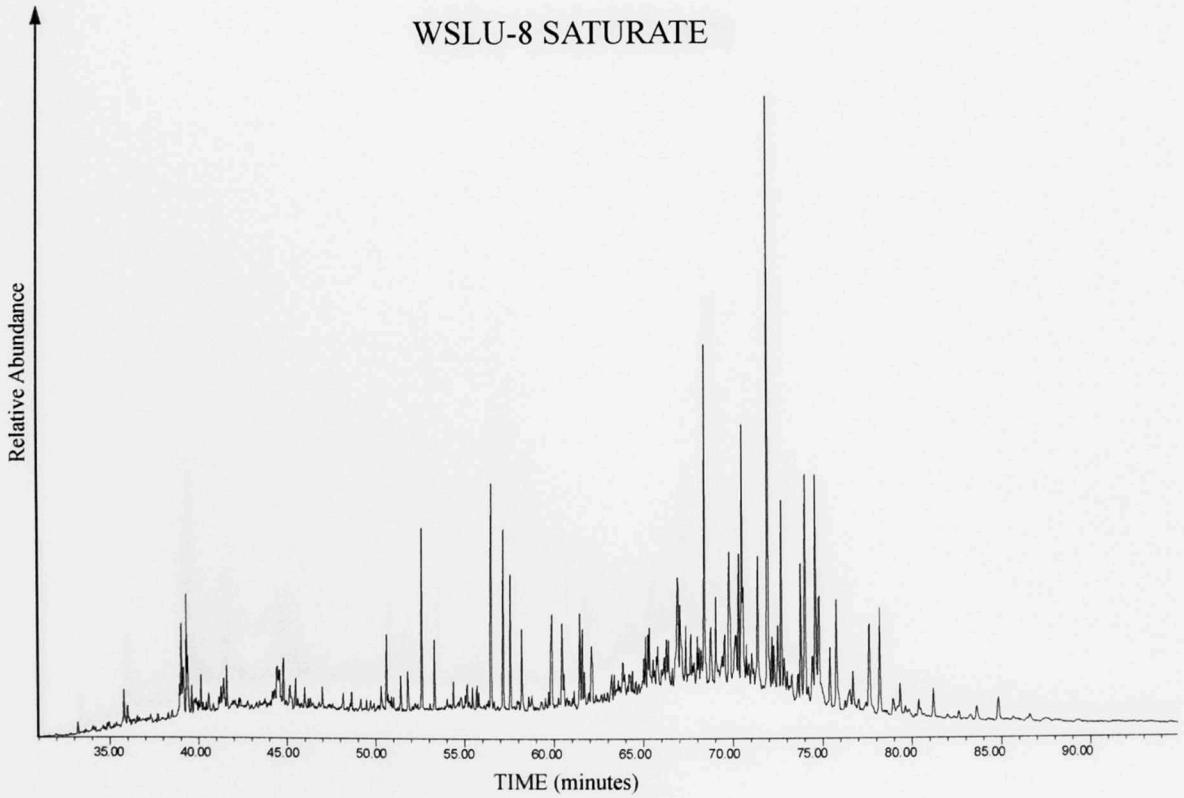

WSLU-9 SATURATE

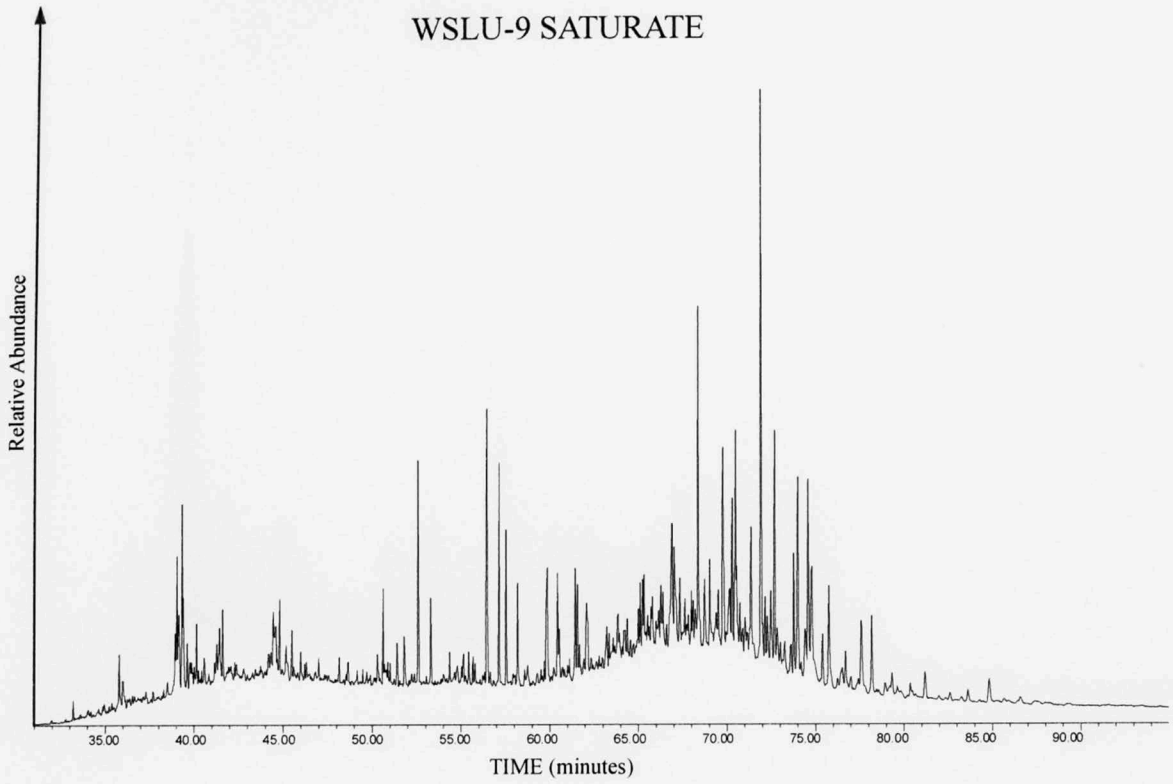

WSLU-10 SATURATE

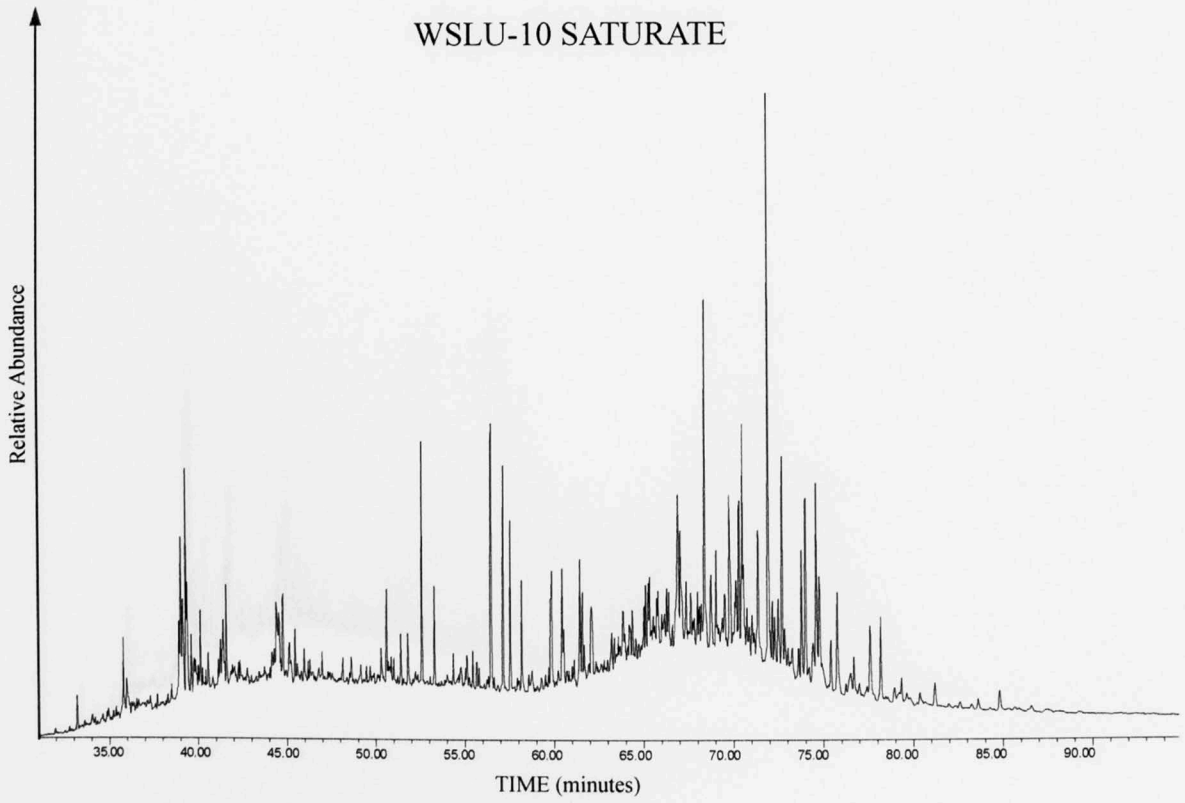

WSLU-11 SATURATE

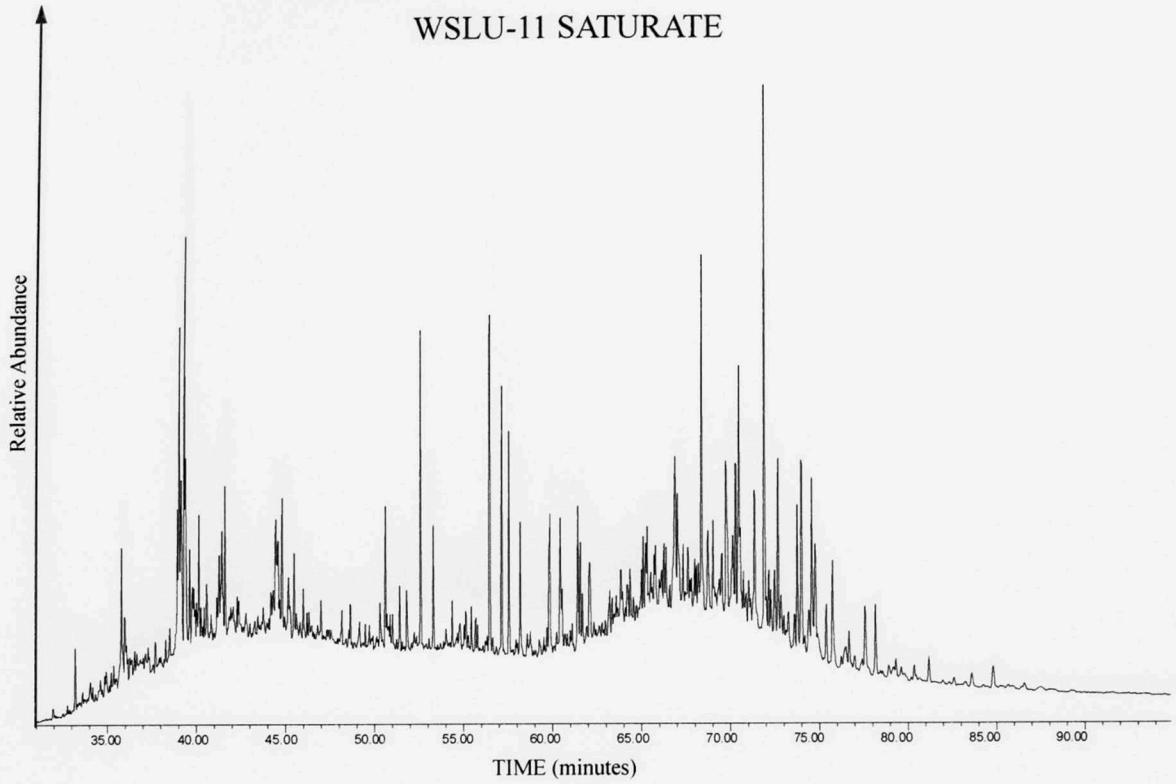

WSLU-12 SATURATE

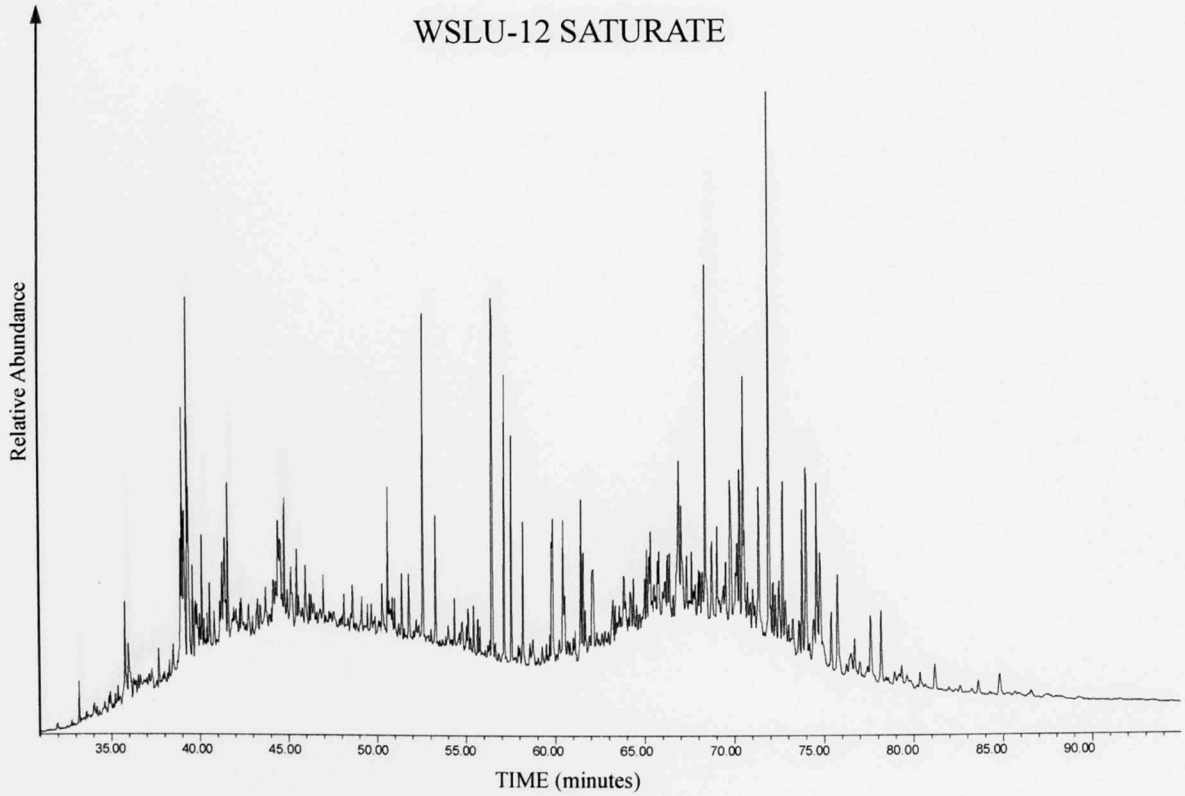

WSLU-13 SATURATE

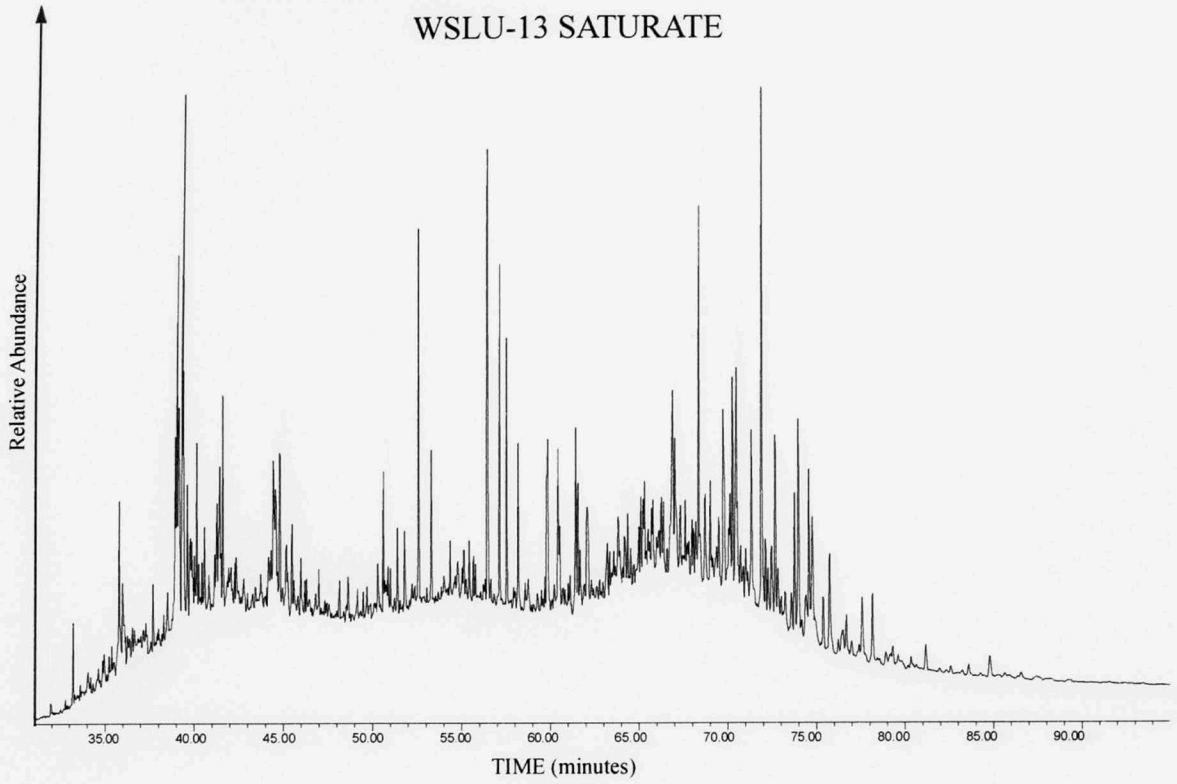

WSLU-14 SATURATE

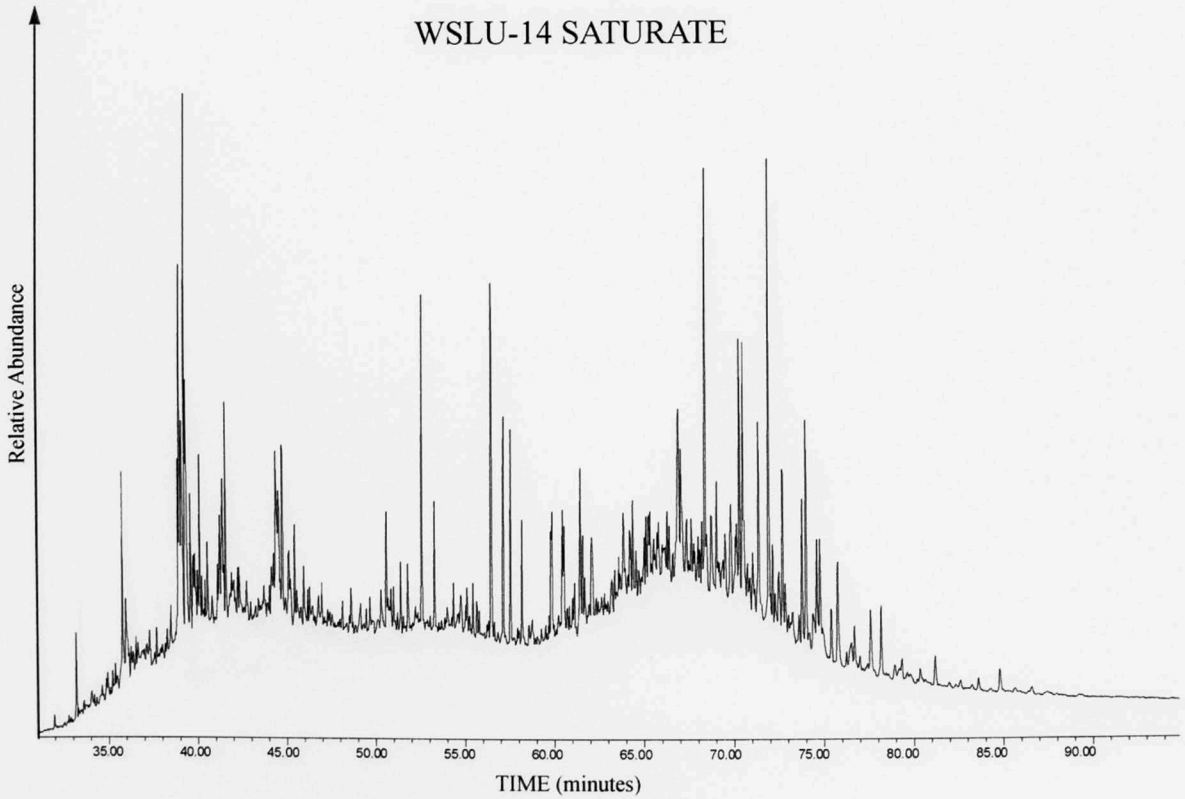

WSLU-15 SATURATE

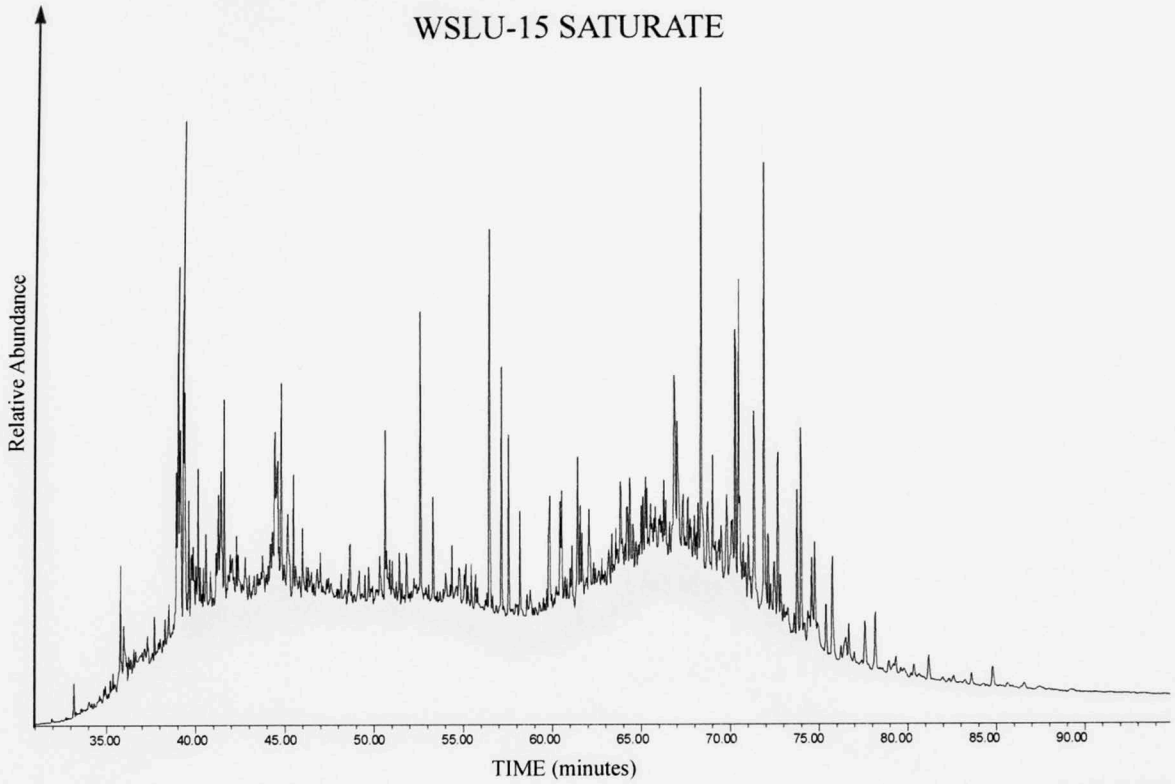

WSLU-16 SATURATE

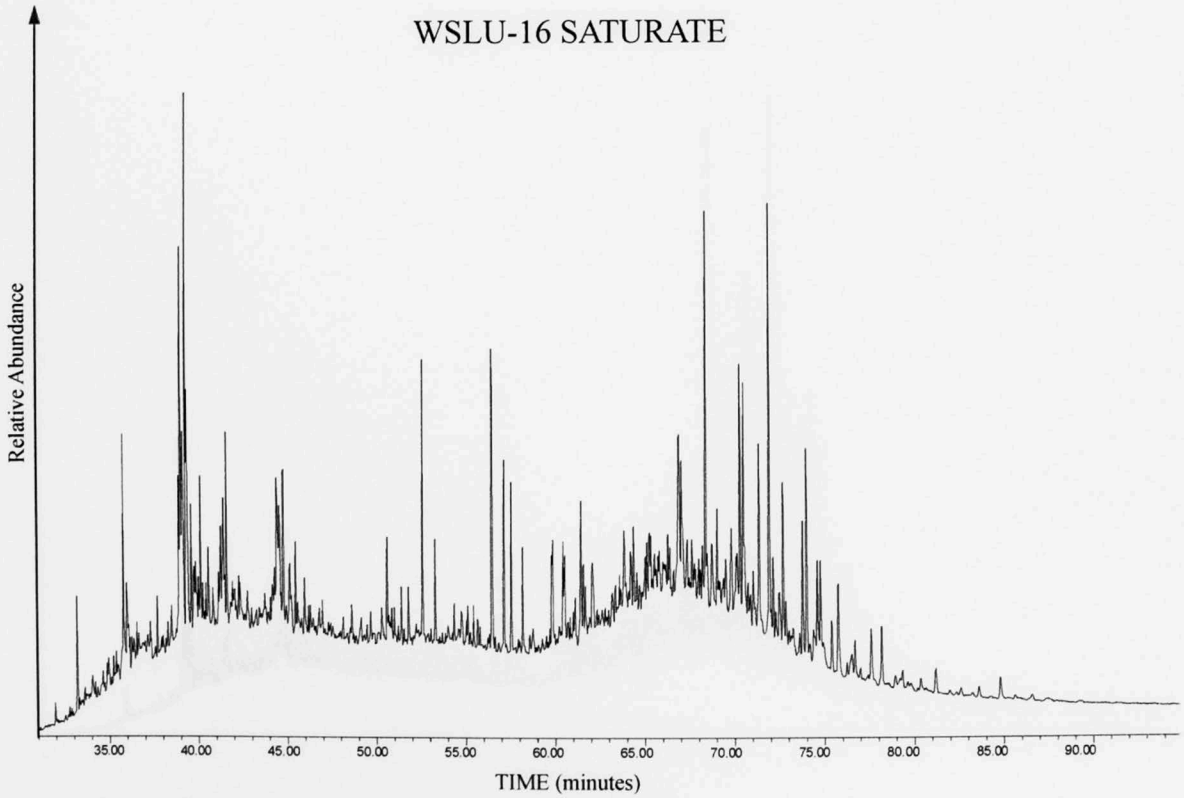

WSLU-17 SATURATE

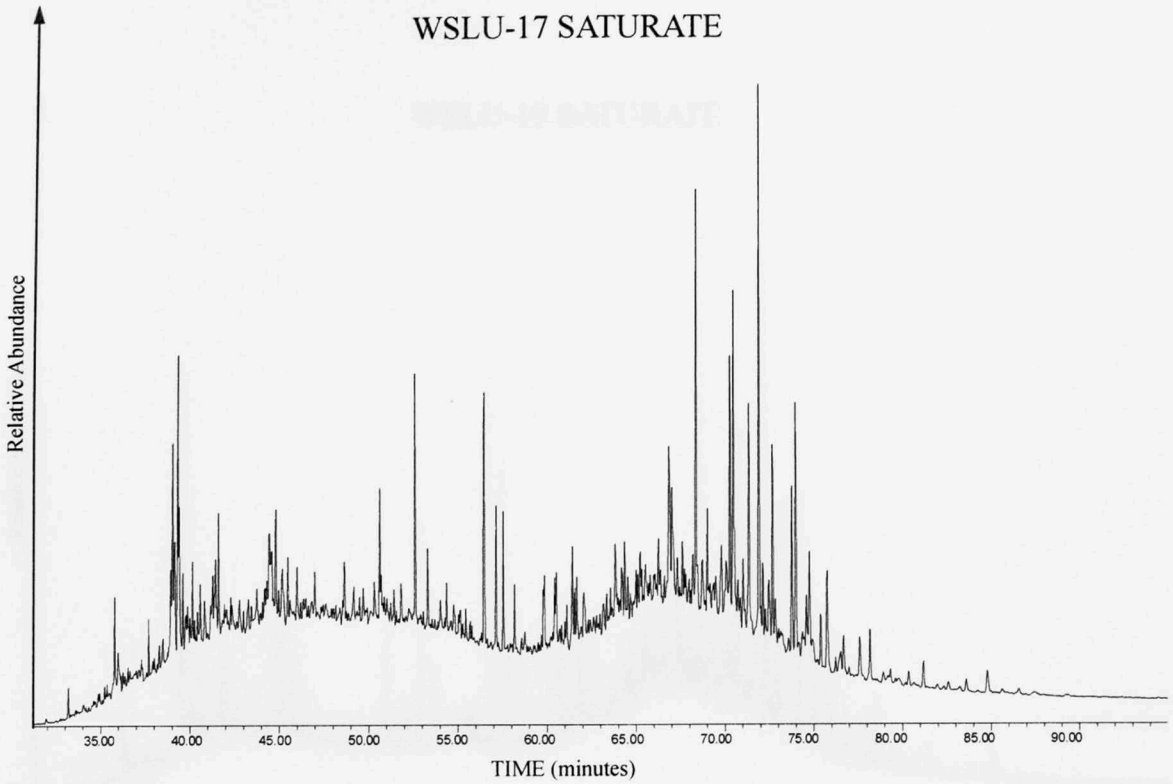

WSLU-18 SATURATE

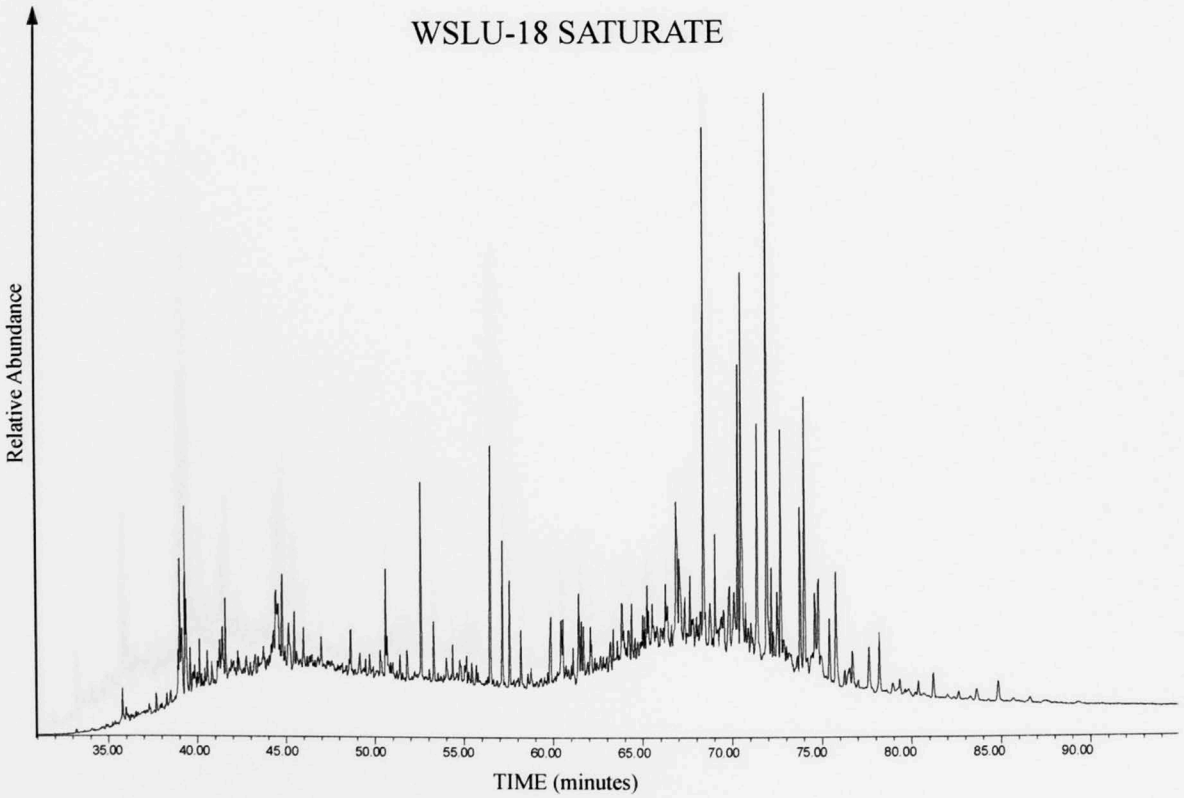

WSLU-19 SATURATE

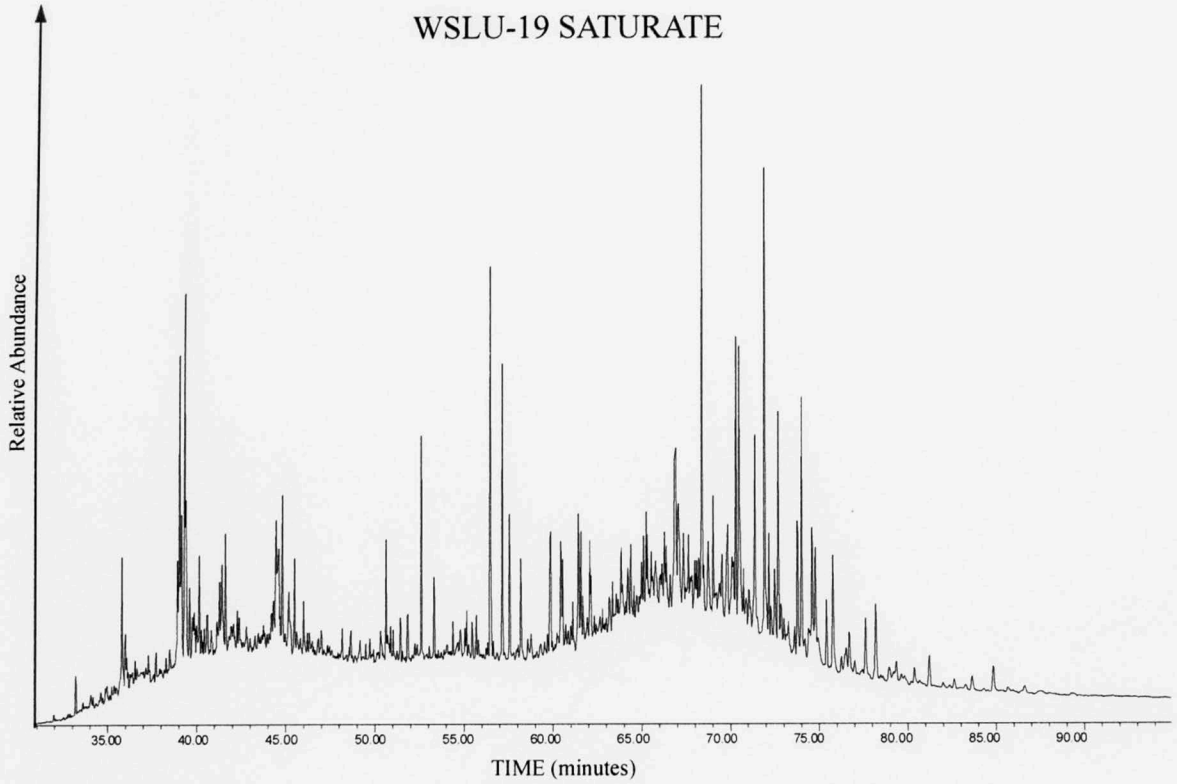

WSLU-20 SATURATE

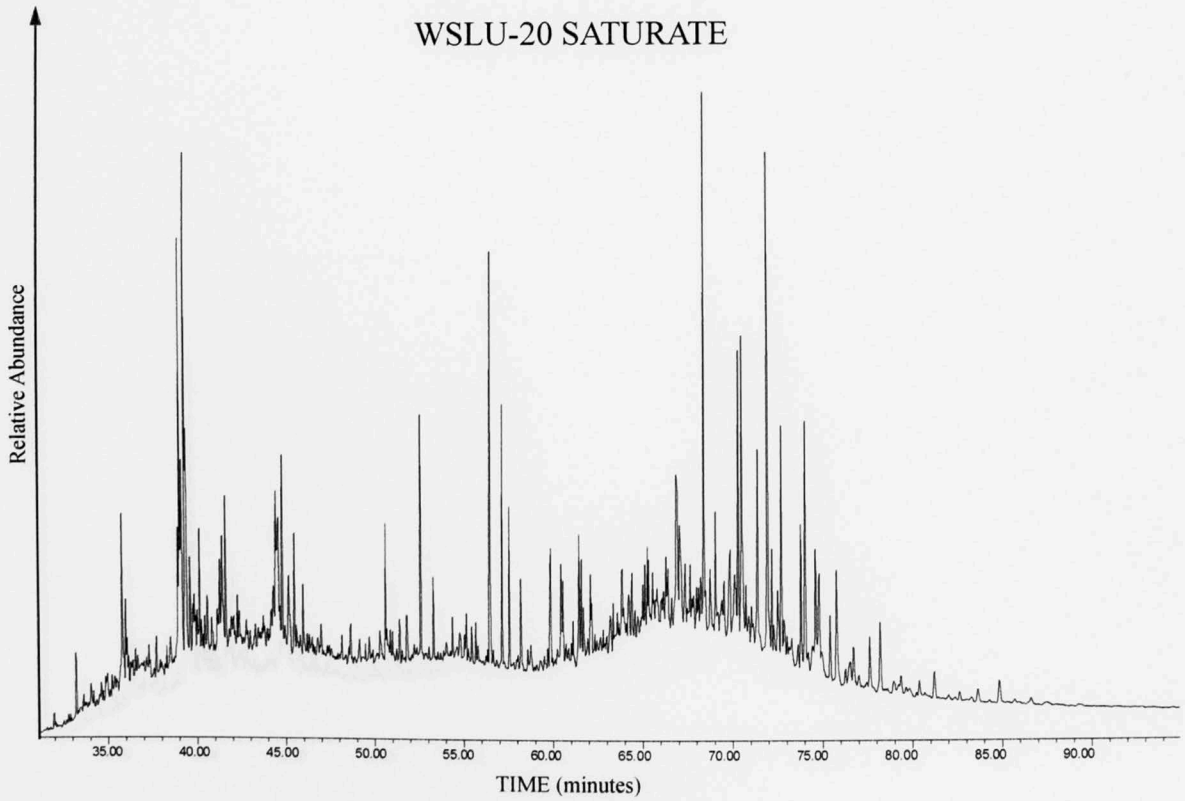

WSLU-21 SATURATE

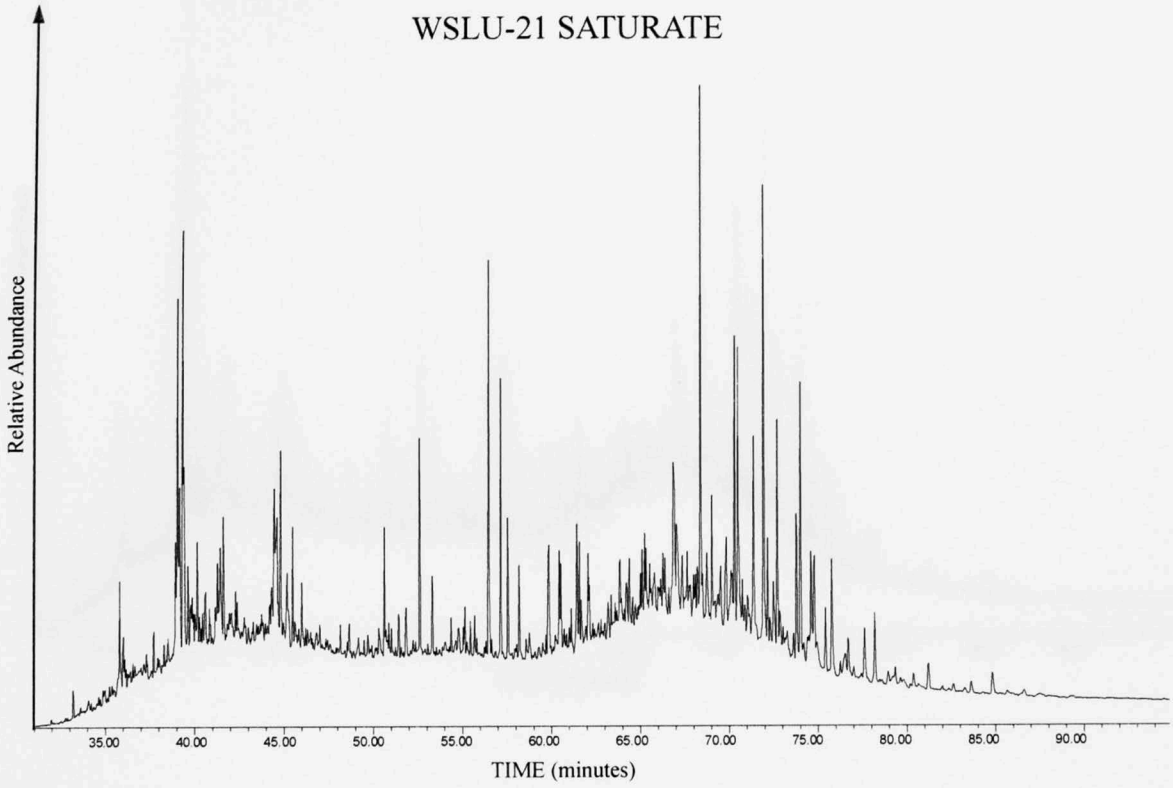

WSLU-22 SATURATE

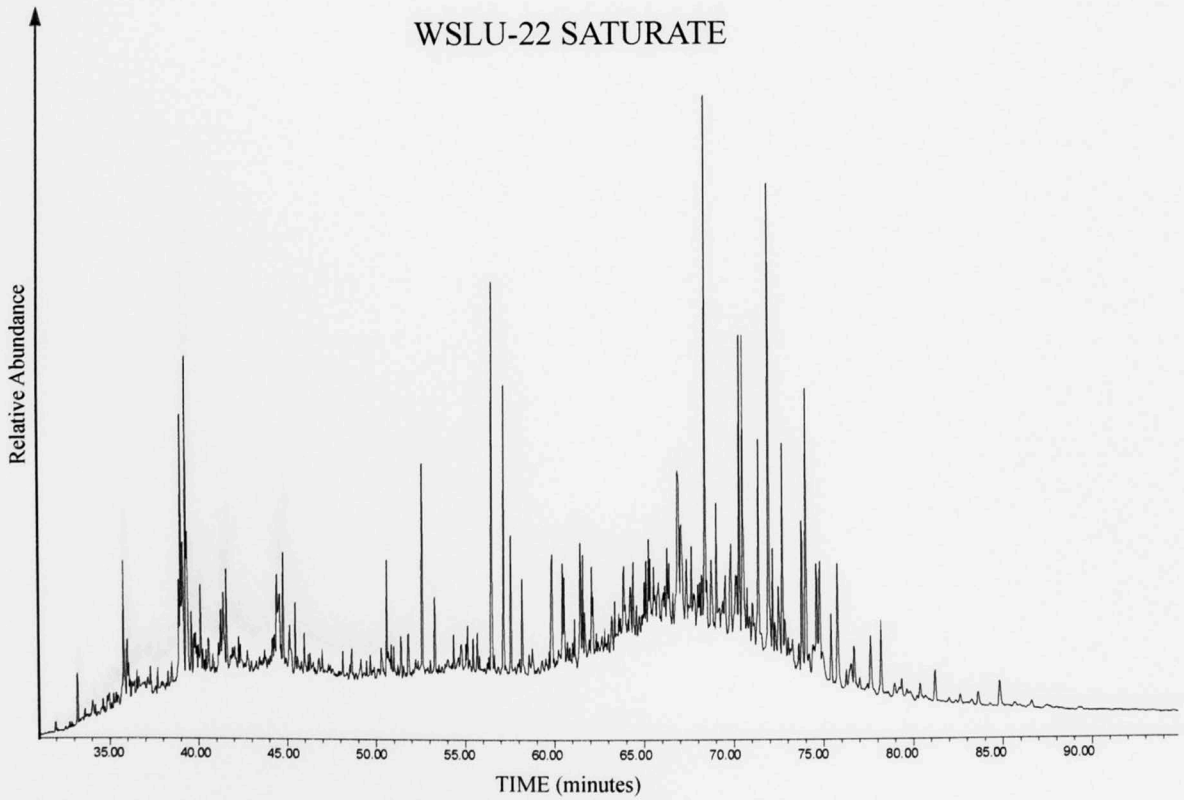

WSLU-23 SATURATE

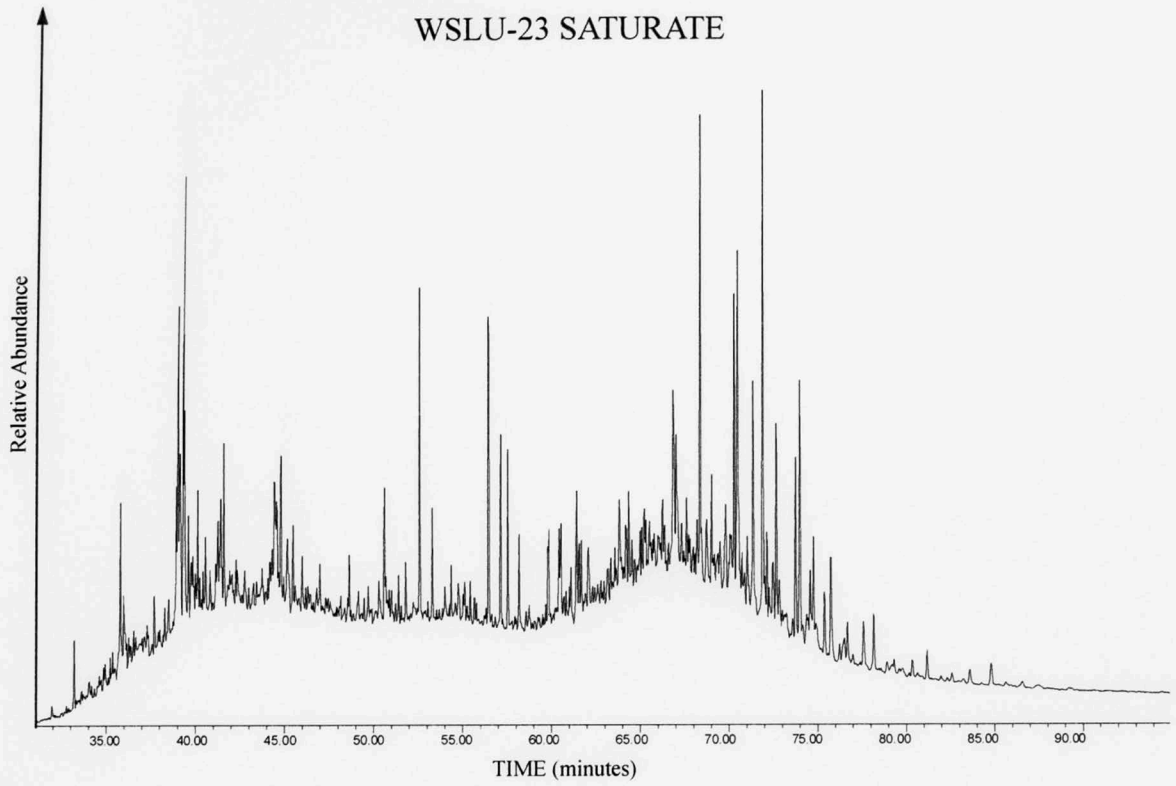

WSLU-24 SATURATE

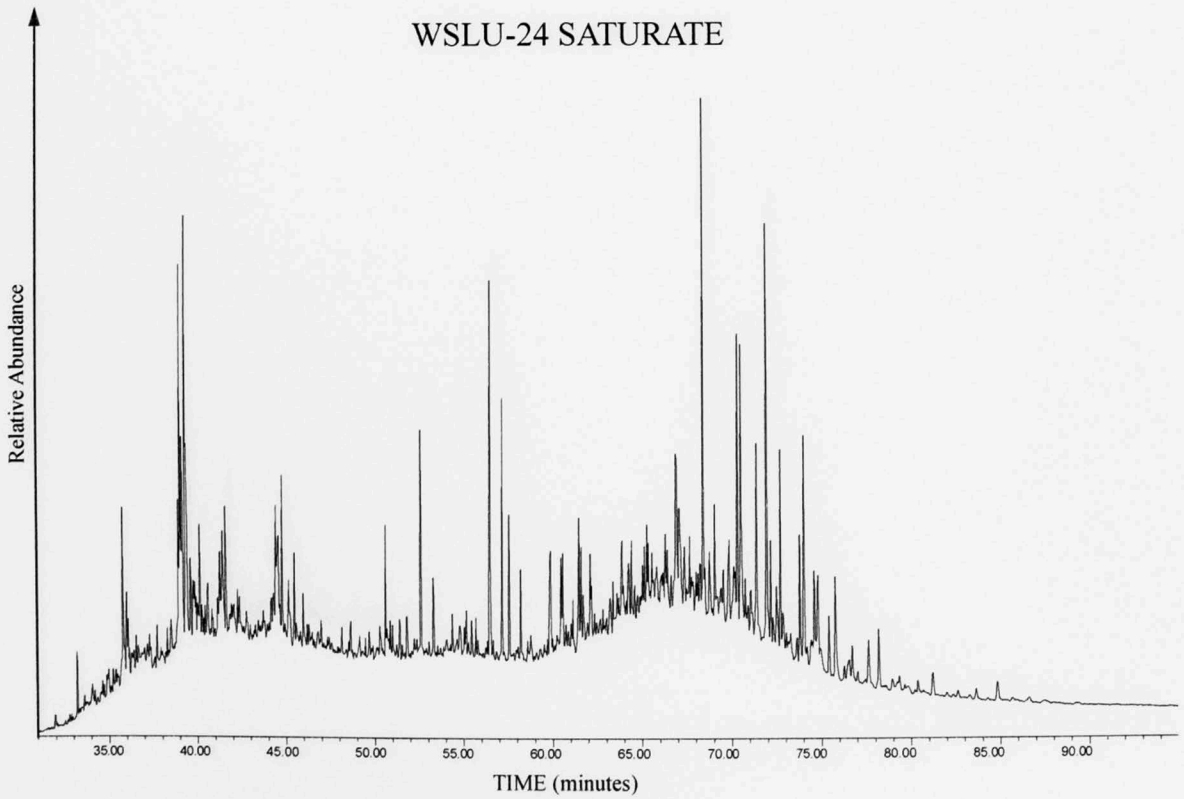

WSLU-25 SATURATE

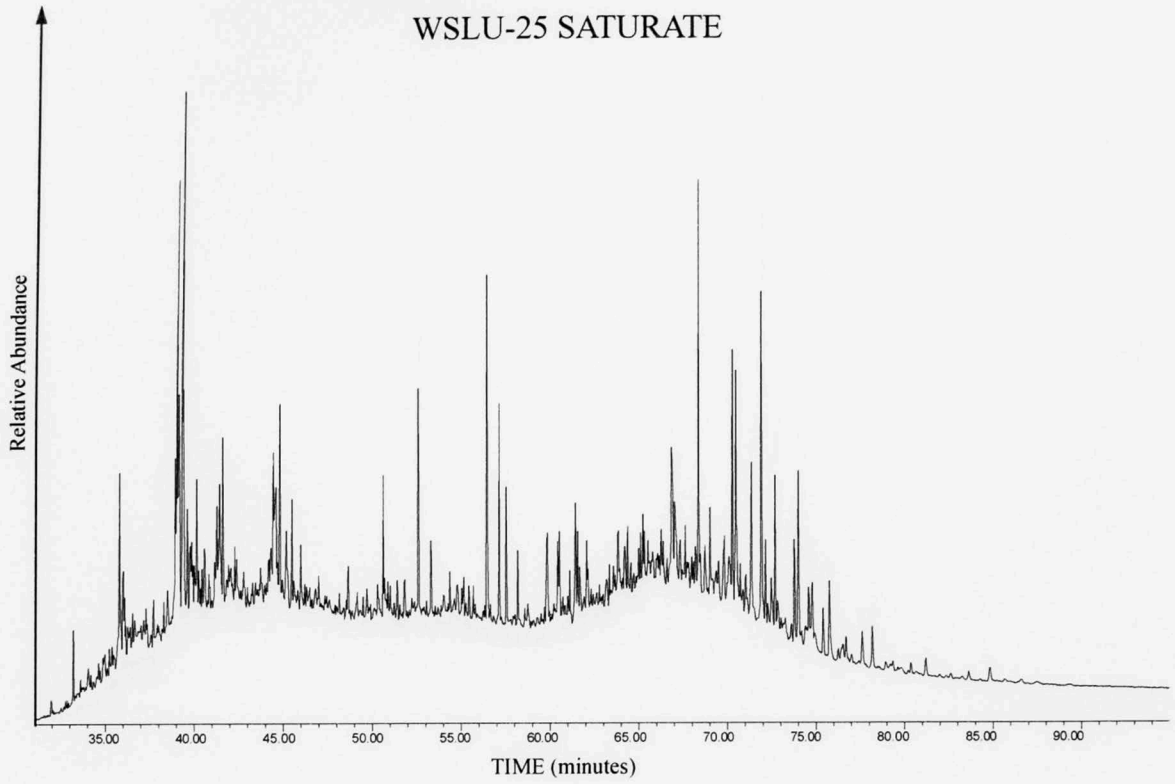

WSLU-26 SATURATE

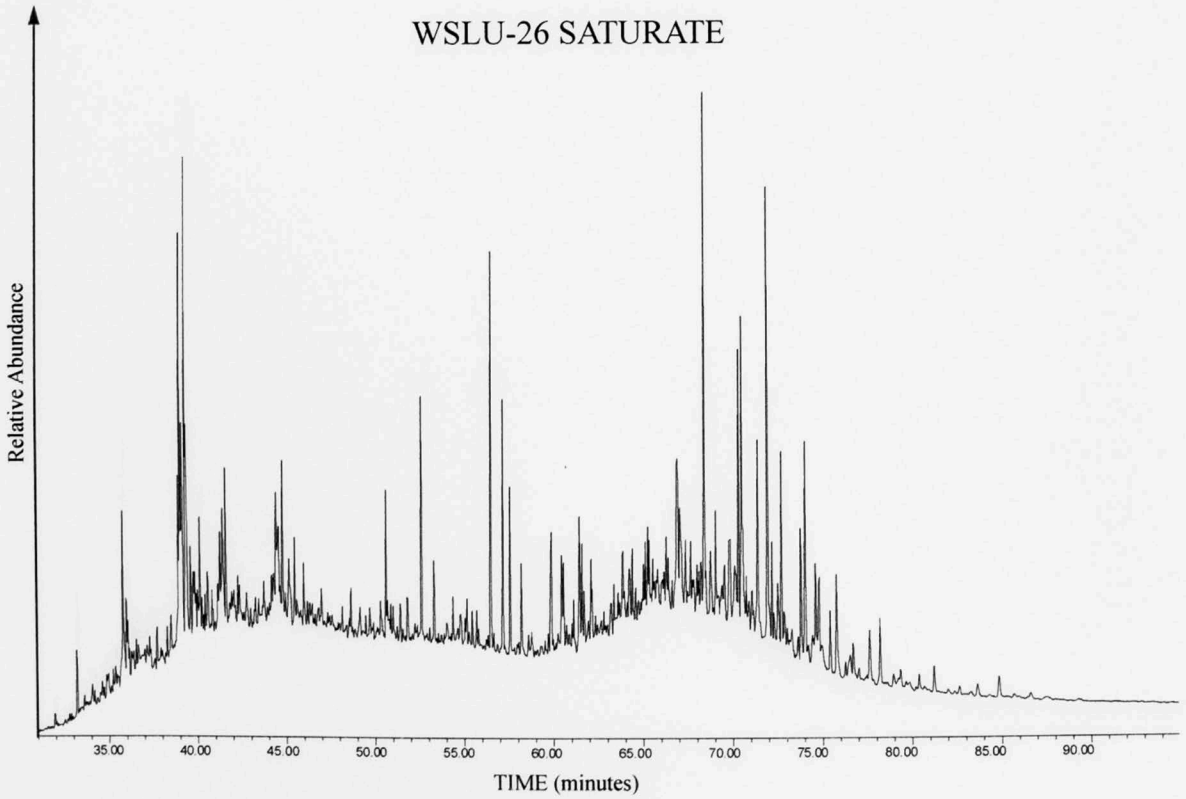

WSLU-27 SATURATE

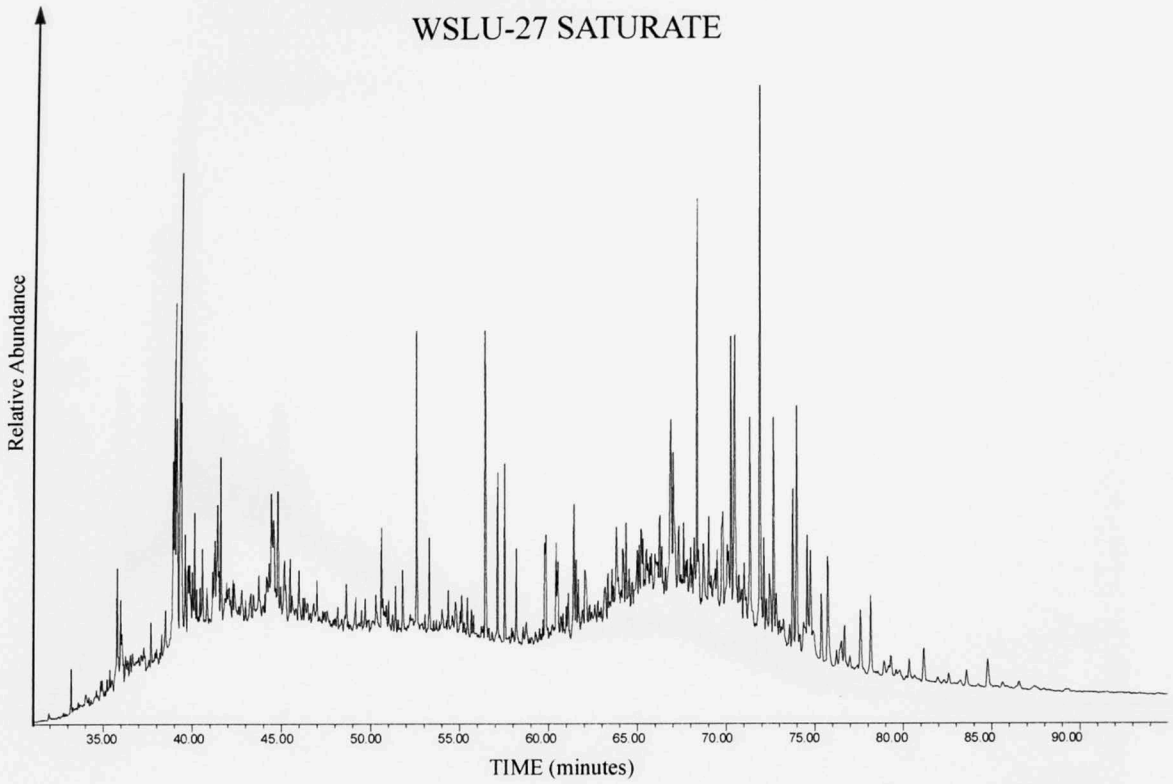

WSLU-28 SATURATE

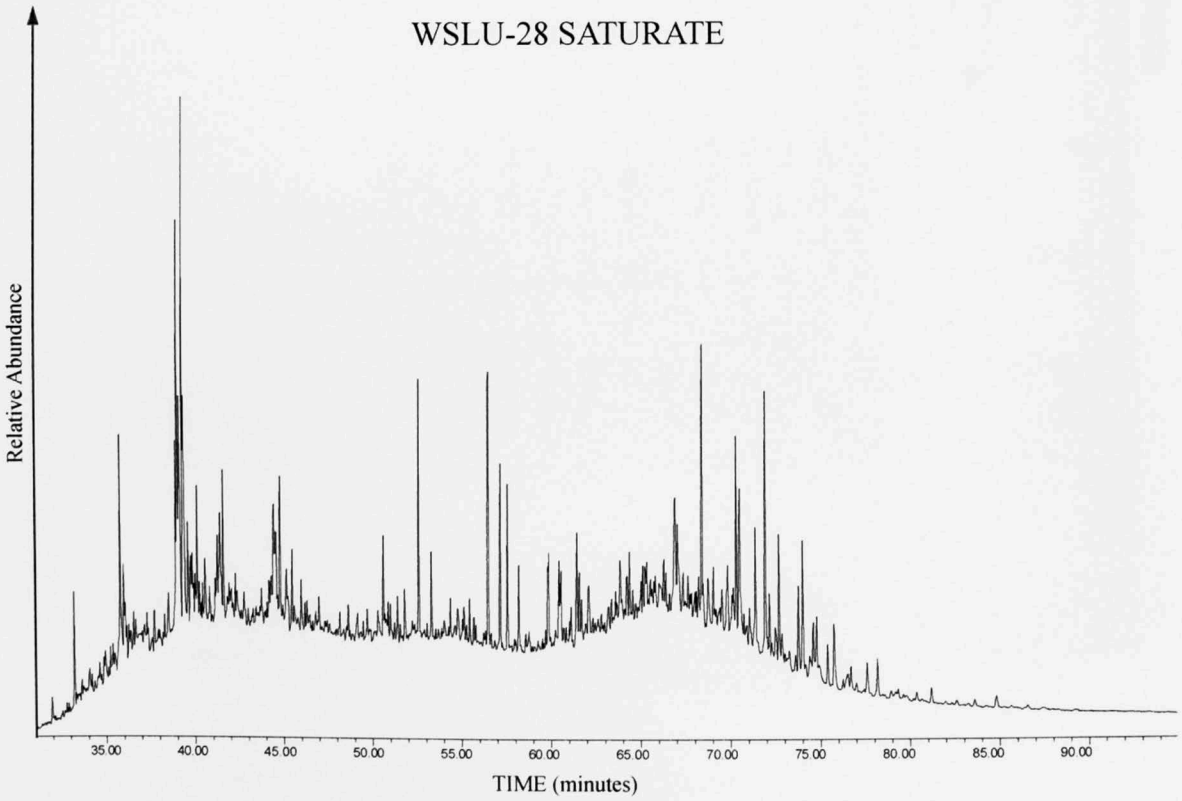

WSLU-29 SATURATE

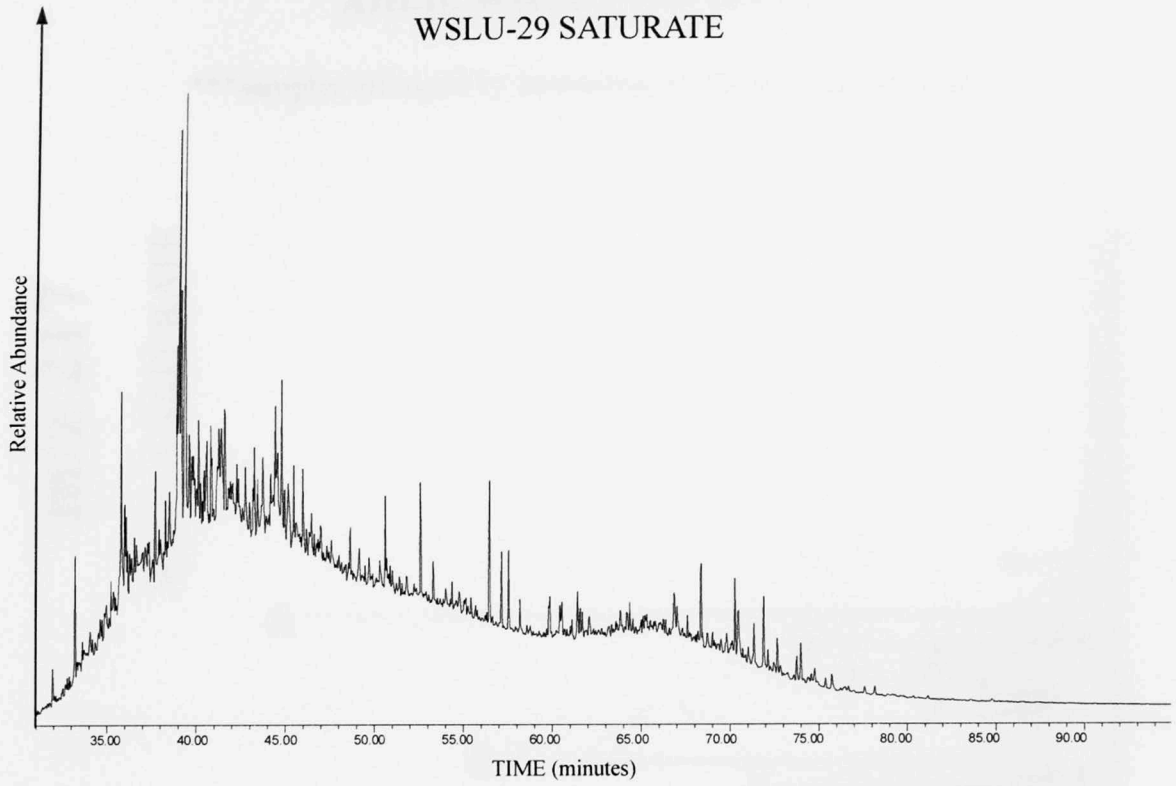

m/z 217

WSLU-8 SATURATE

Peak No.	Compound
1	pregnane
2	homopregnane
3a	C_{27} 13β17α diasterane S
3b	C_{27} 13β17α diasterane R
4a	C_{27} 13α17β diasterane S
4b	C_{27} 13α17β diasterane R
5a	C_{28} 13β17α diasterane S
5b	C_{28} 13β17α diasterane R
6a	C_{27} 5α14α17α 20S cholestane
6b	C_{27} 5α14α17α 20R cholestane
6c	C_{27} 5α14β17β 20R cholestane
6d	C_{27} 5α14β17β 20S cholestane
7a	C_{28} 5α14α17α 20S ergostane
7b	C_{28} 5α14α17α 20R ergostane
7c	C_{28} 5α14β17β 20R ergostane
7d	C_{28} 5α14β17β 20S ergostane
8a	C_{29} 5α14α17α 20S stigmastane
8b	C_{29} 5α14α17α 20R stigmastane
8c	C_{29} 5α14β17β 20R stigmastane
8d	C_{29} 5α14β17β 20S stigmastane
9	C_{30} 5α14α17α 20R 24-*n*-propylcholestane

***samples arranged by increasing depth on following page

WSLU-1 SATURATE

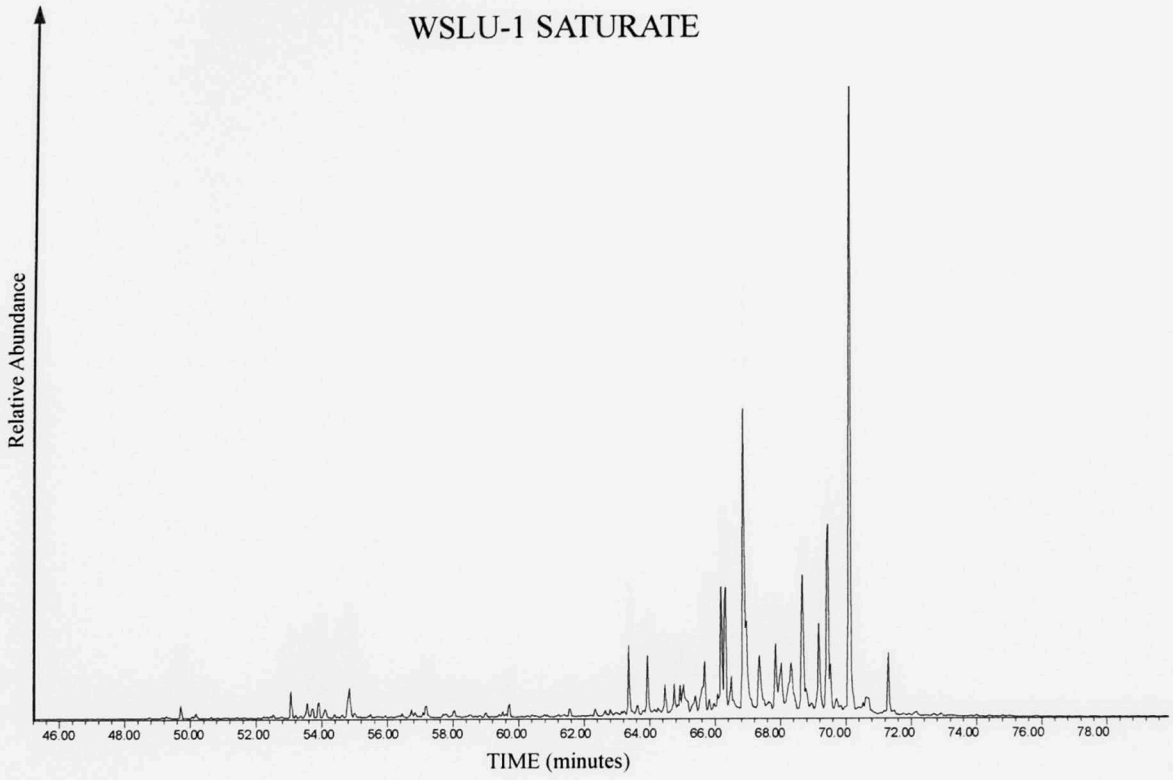

WSLU-2 SATURATE

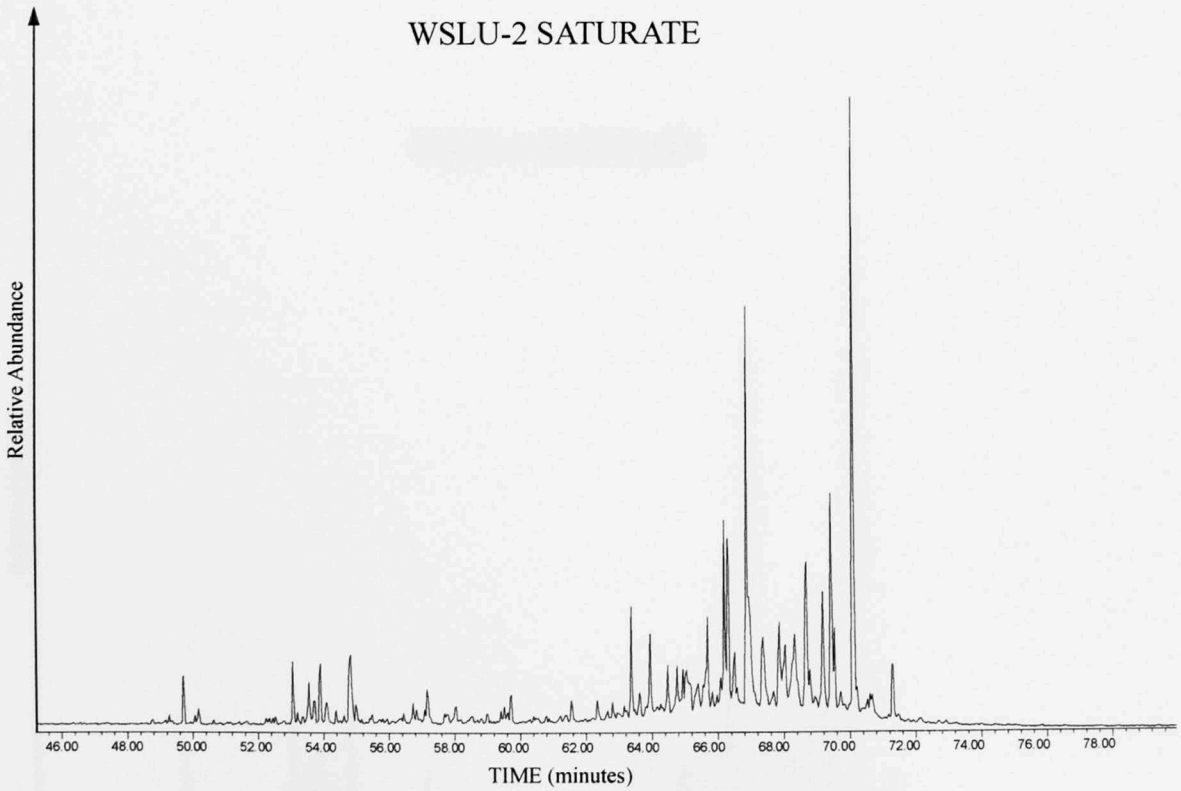

WSLU-3 SATURATE

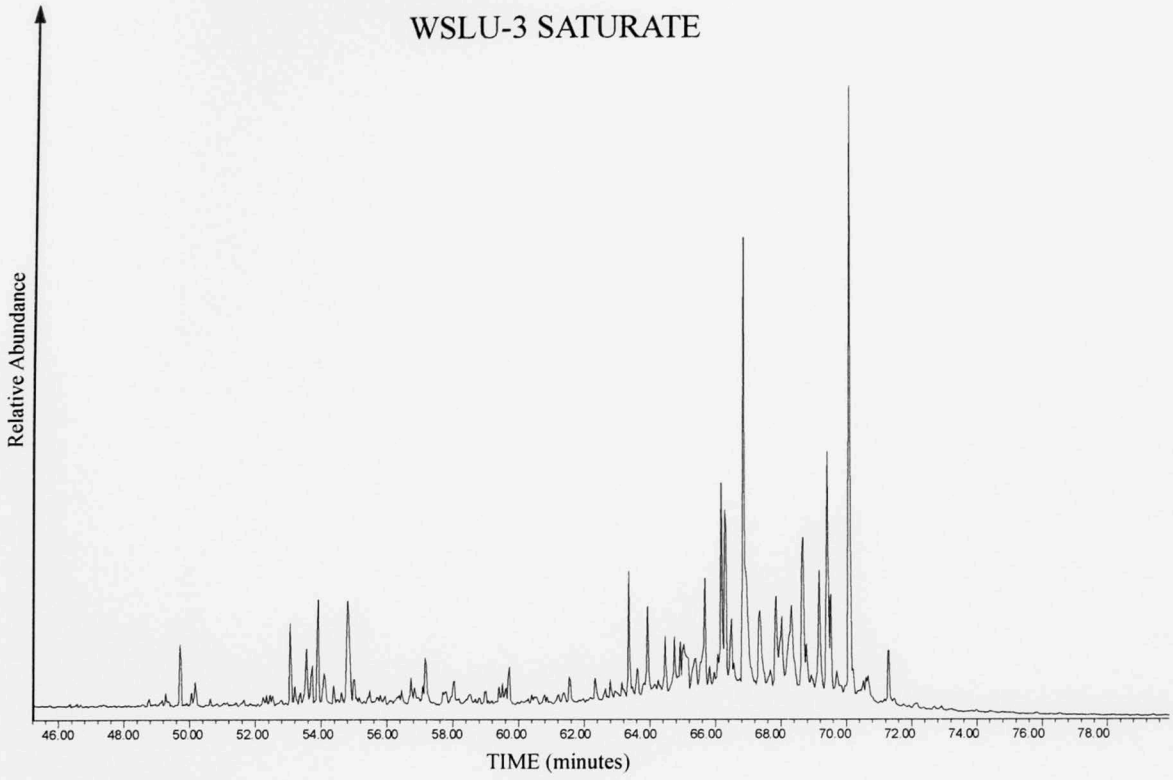

WSLU-4 SATURATE

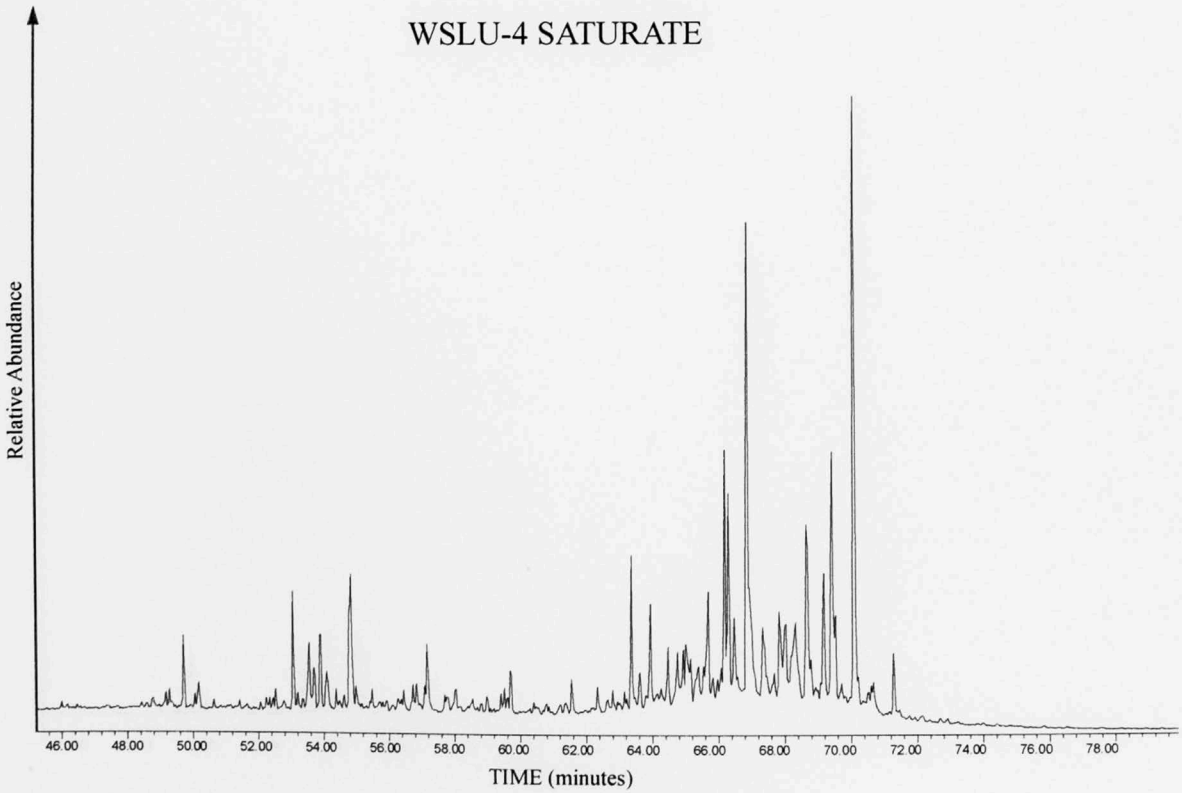

WSLU-5 SATURATE

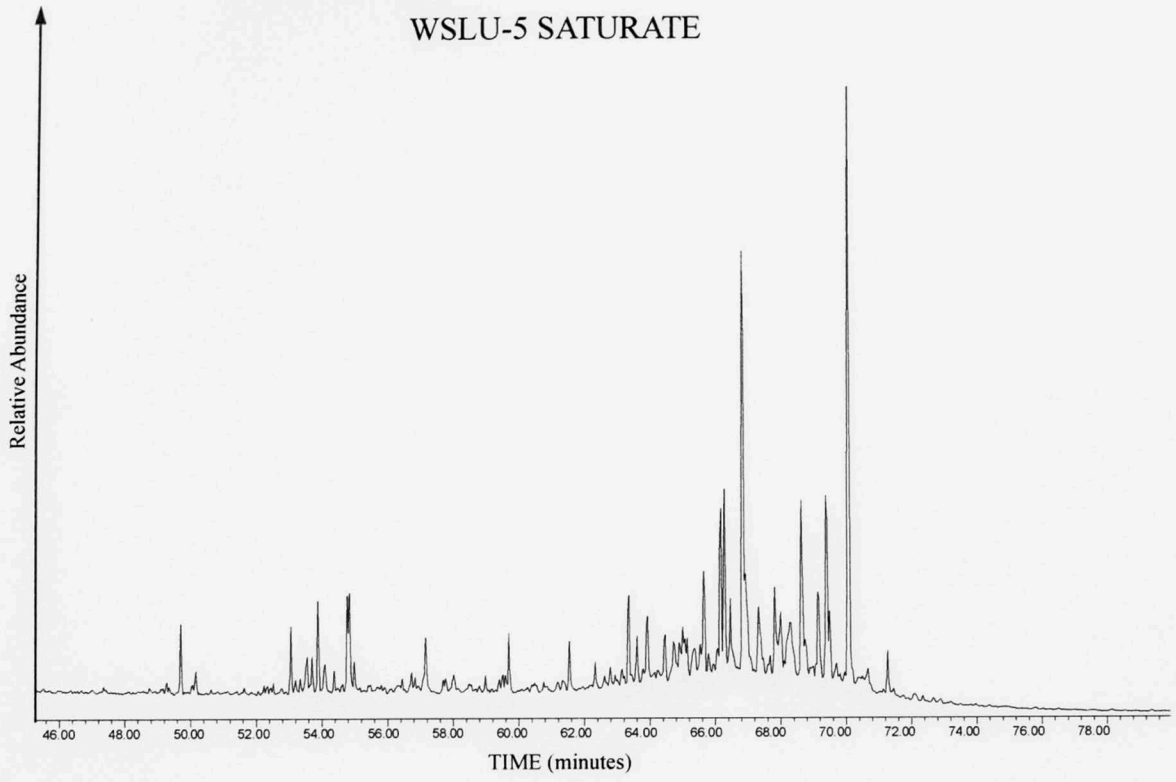

WSLU-6 SATURATE

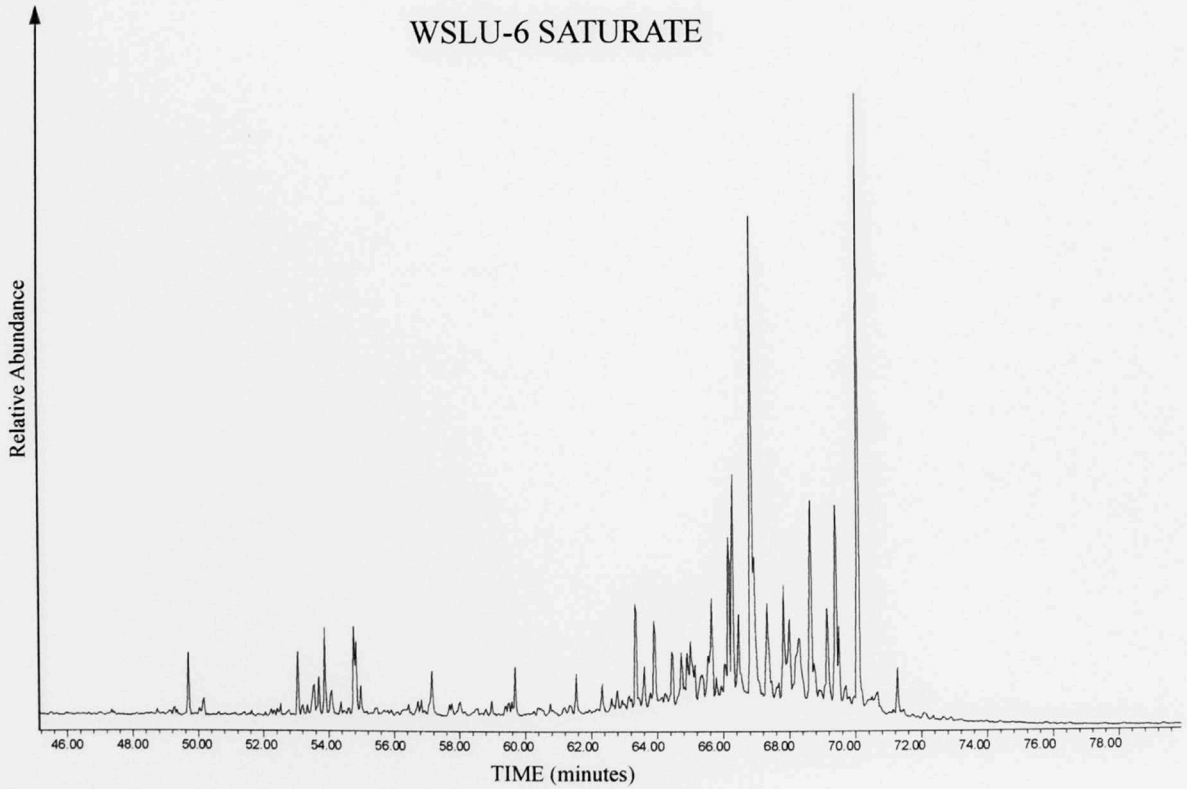

WSLU-7 SATURATE

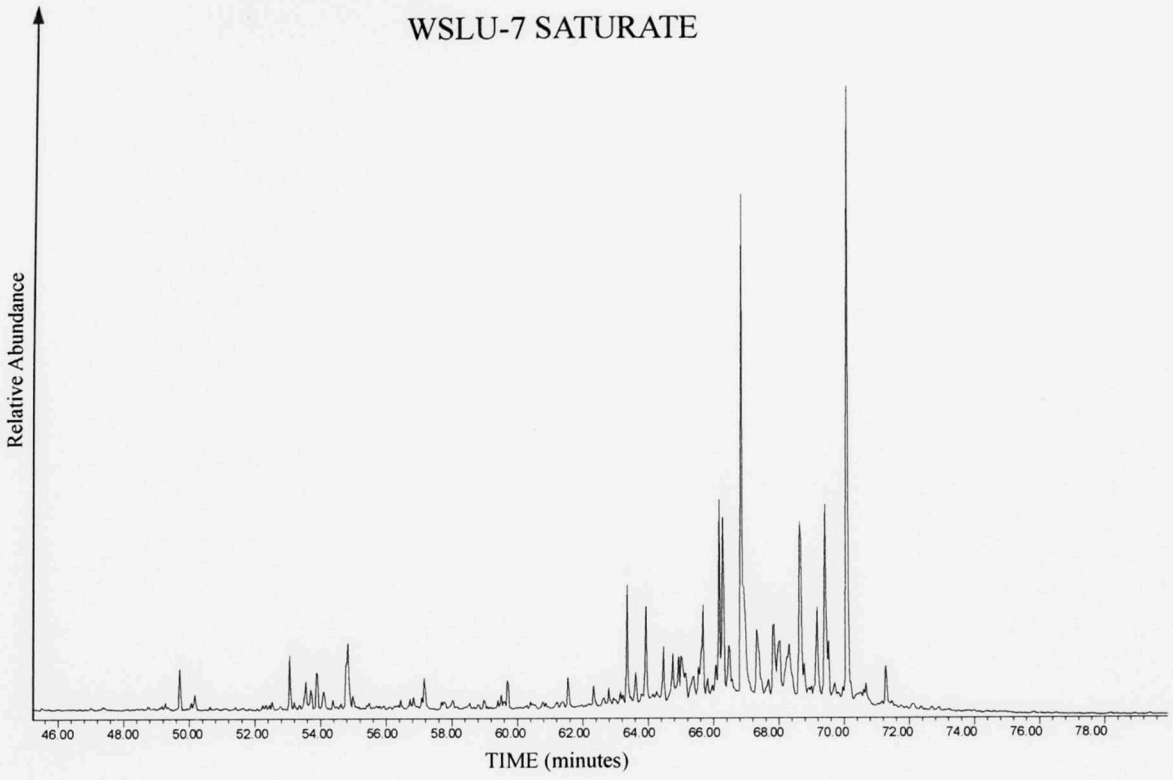

WSLU-8 SATURATE

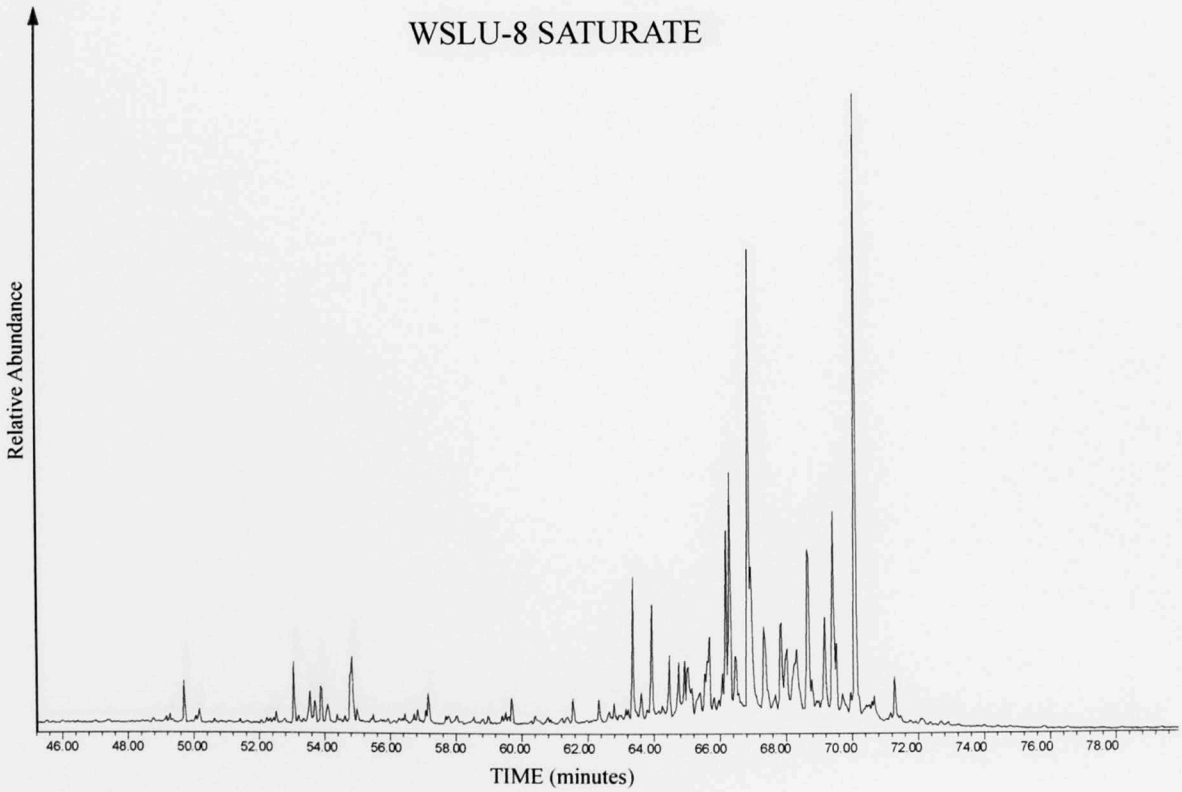

WSLU-9 SATURATE

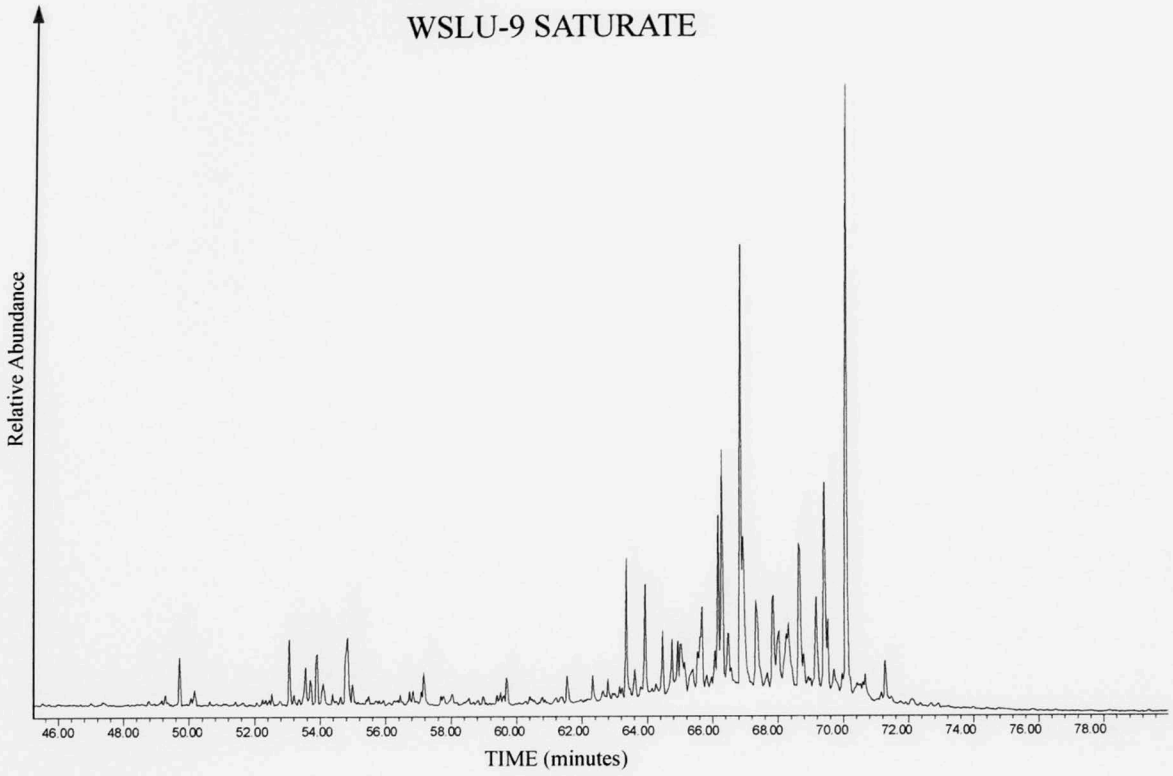

WSLU-10 SATURATE

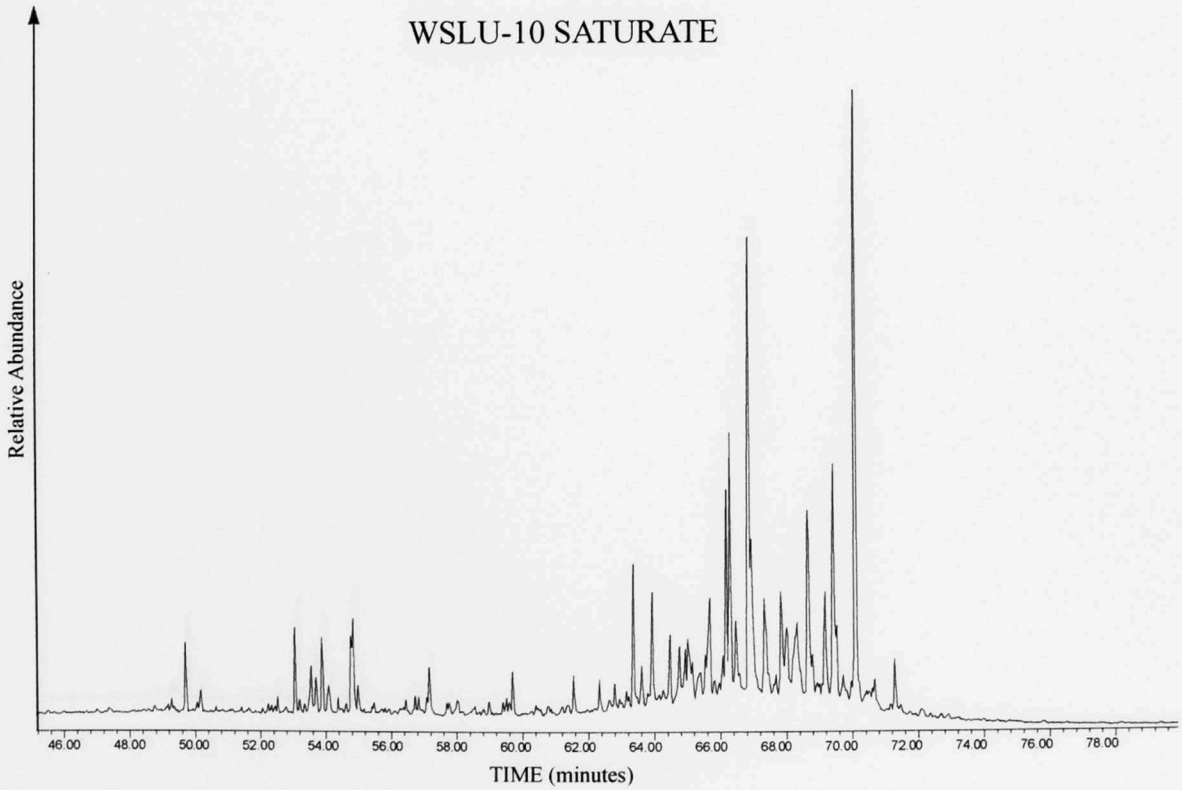

WSLU-11 SATURATE

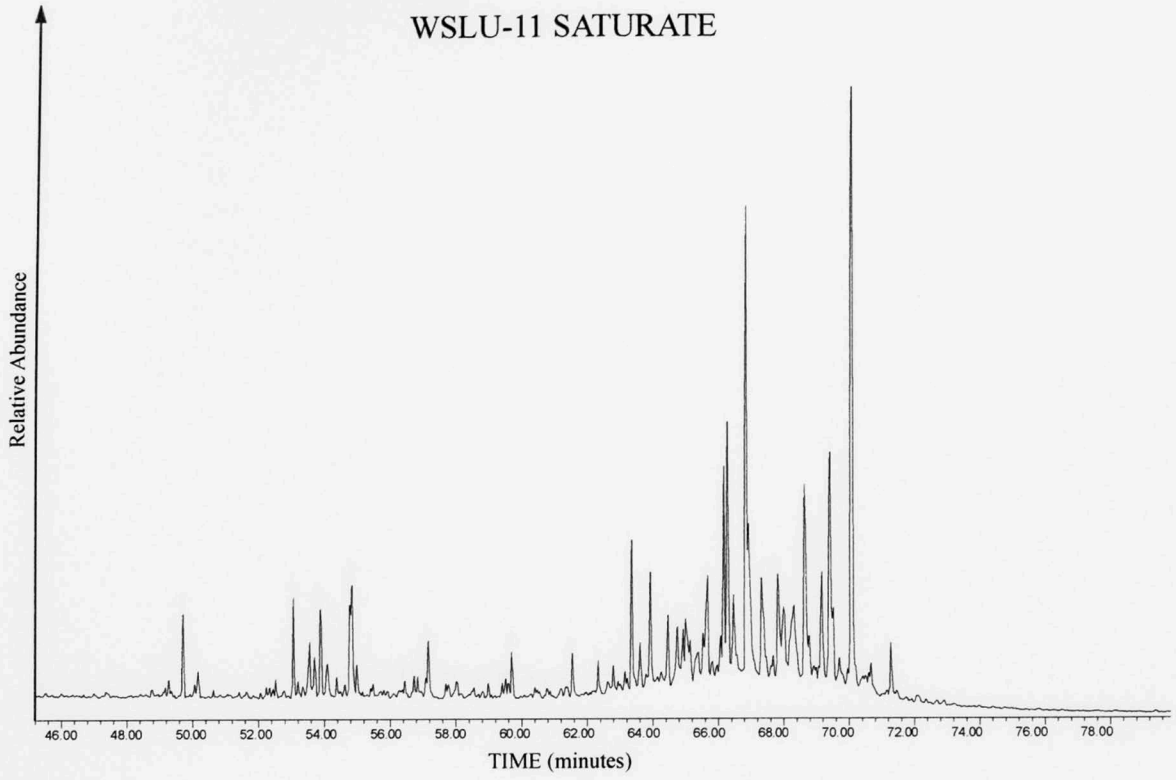

WSLU-12 SATURATE

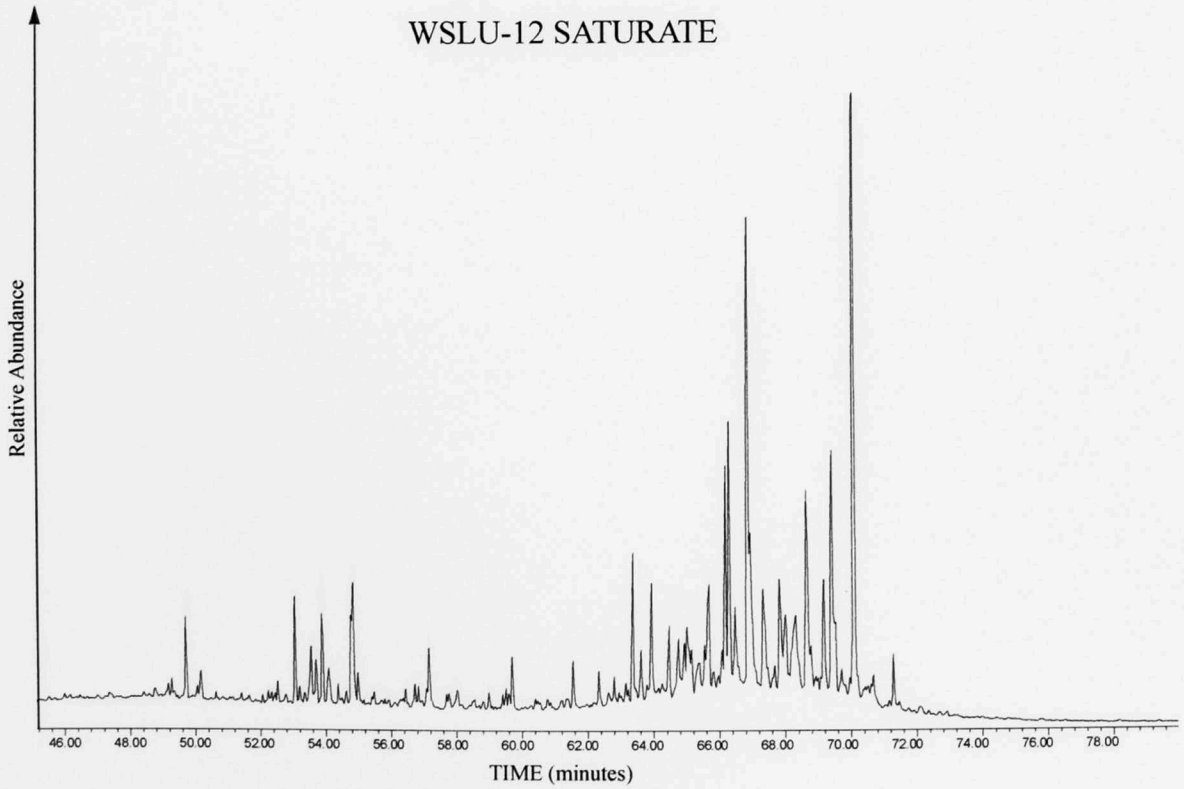

WSLU-13 SATURATE

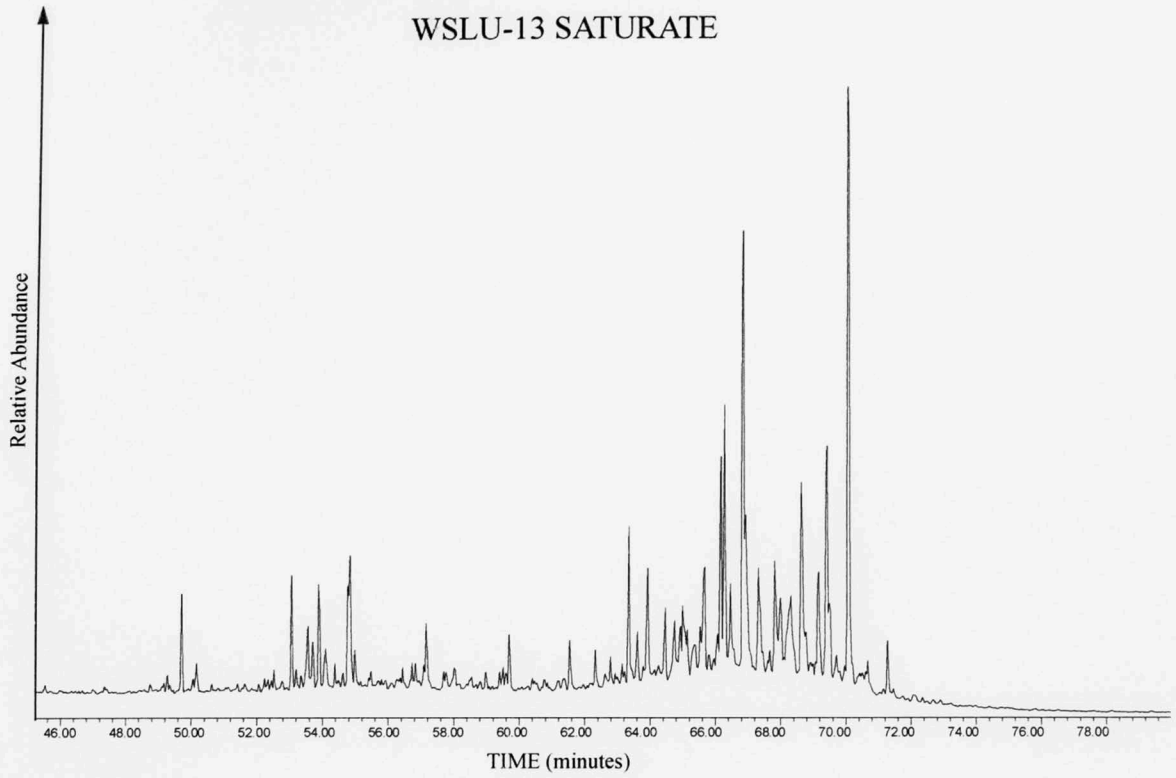

WSLU-14 SATURATE

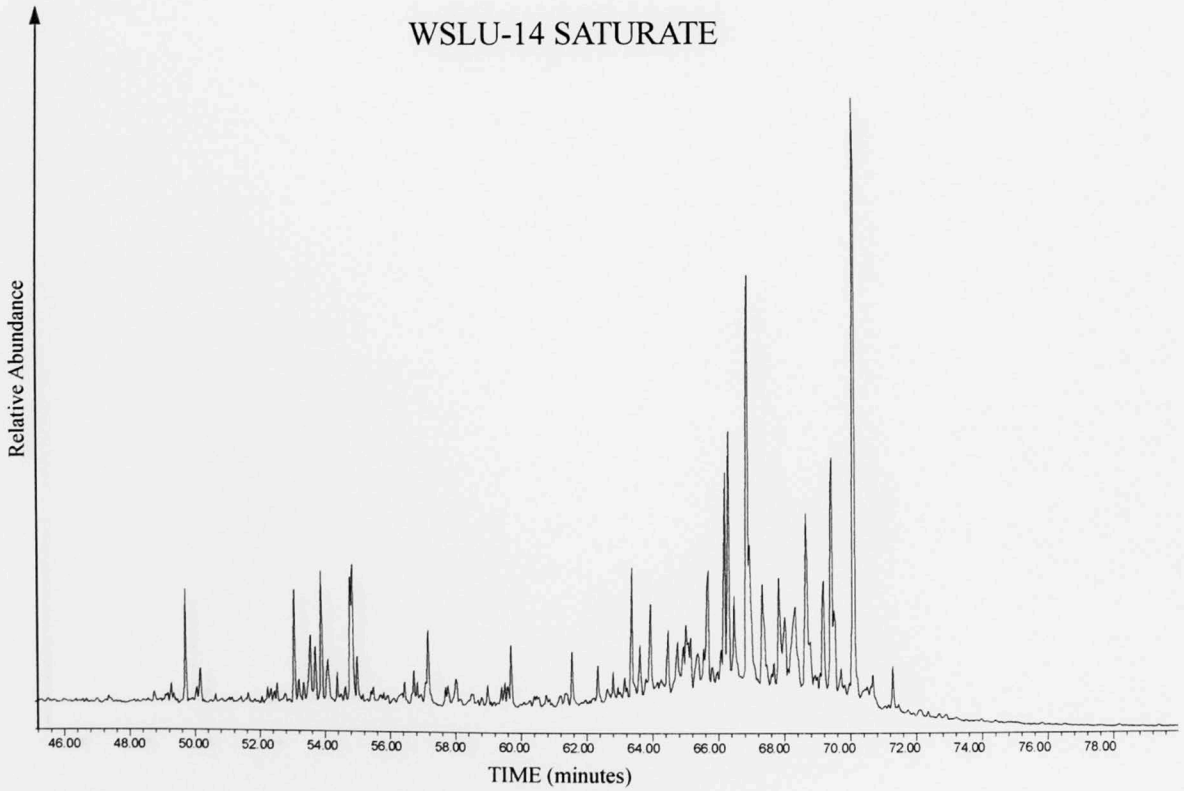

WSLU-15 SATURATE

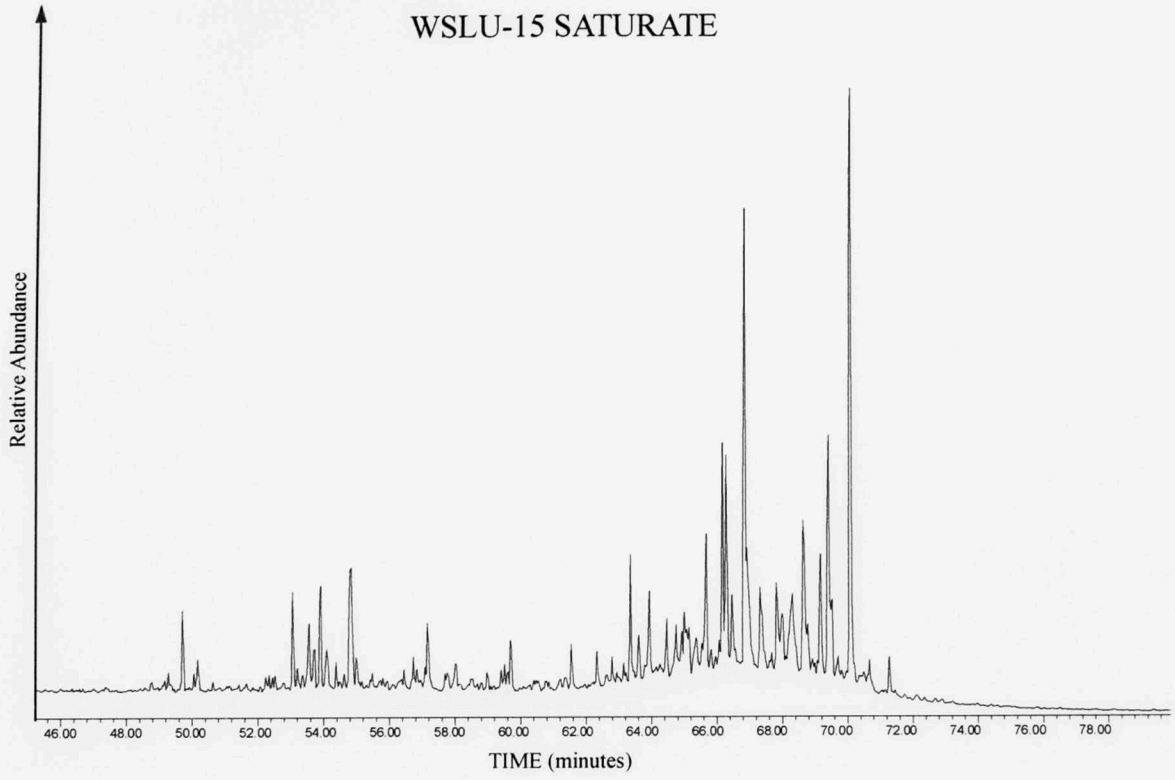

WSLU-16 SATURATE

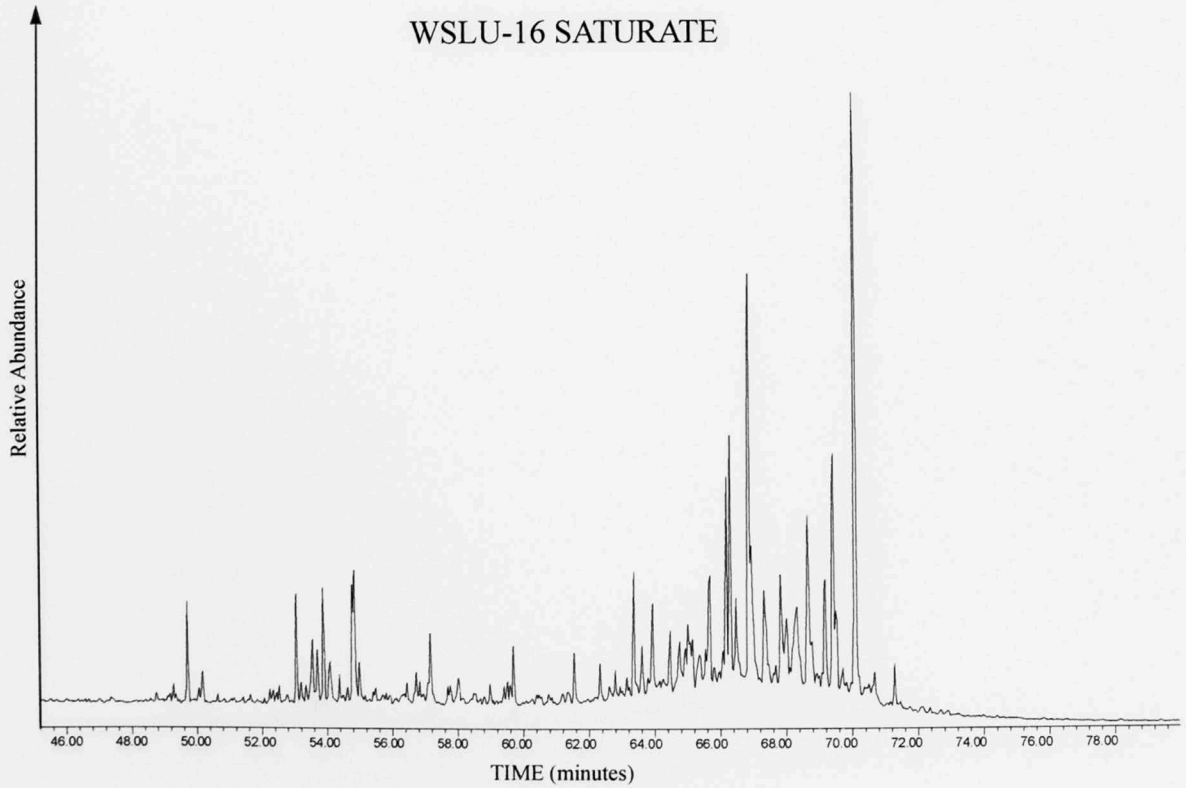

WSLU-17 SATURATE

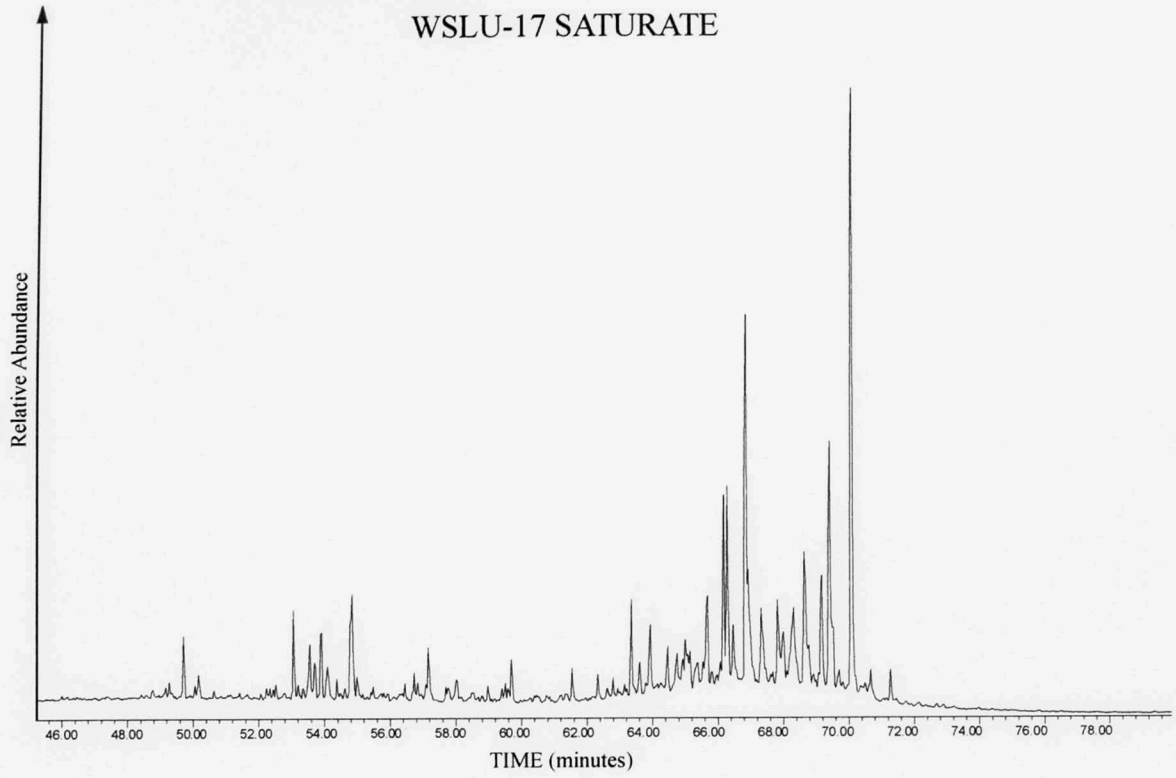

WSLU-18 SATURATE

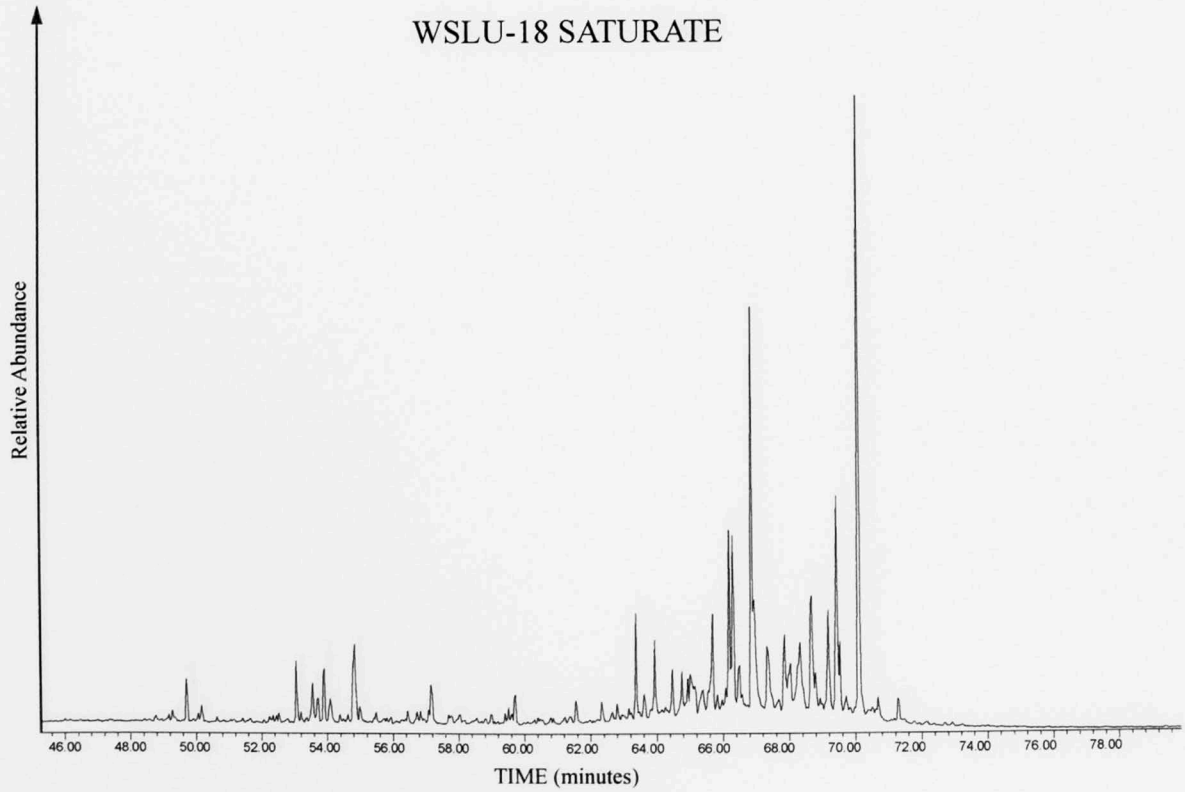

WSLU-19 SATURATE

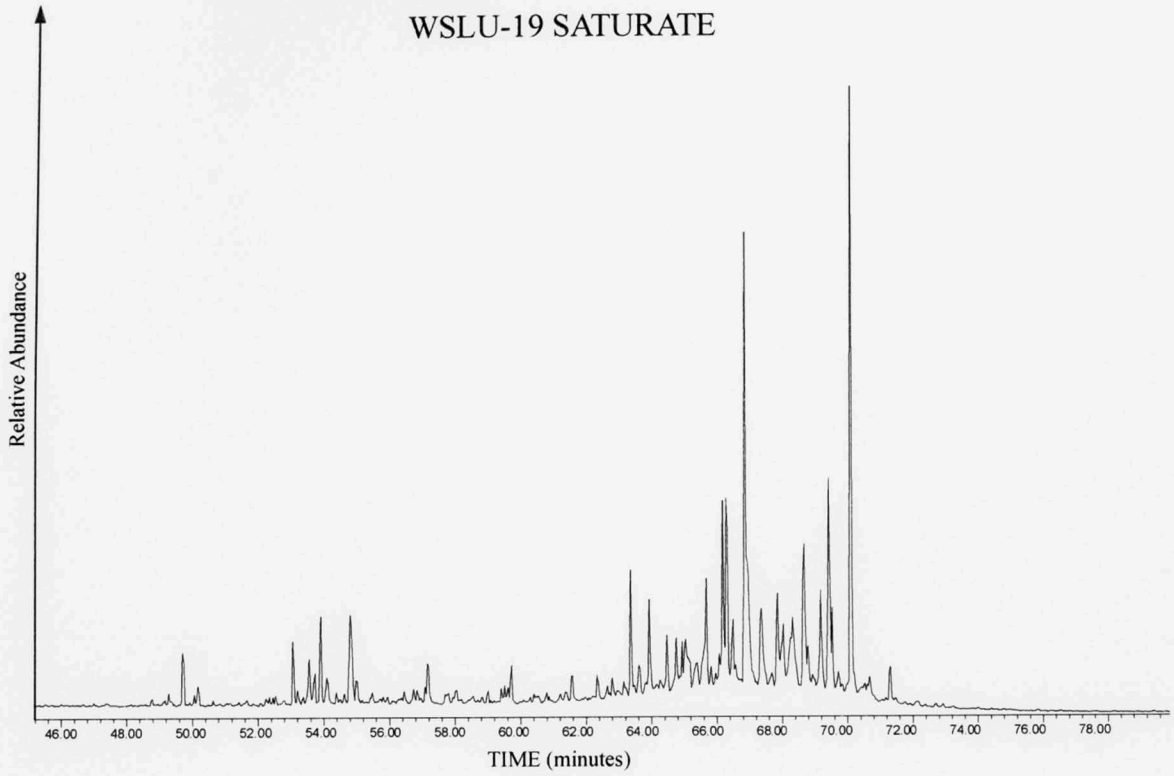

WSLU-20 SATURATE

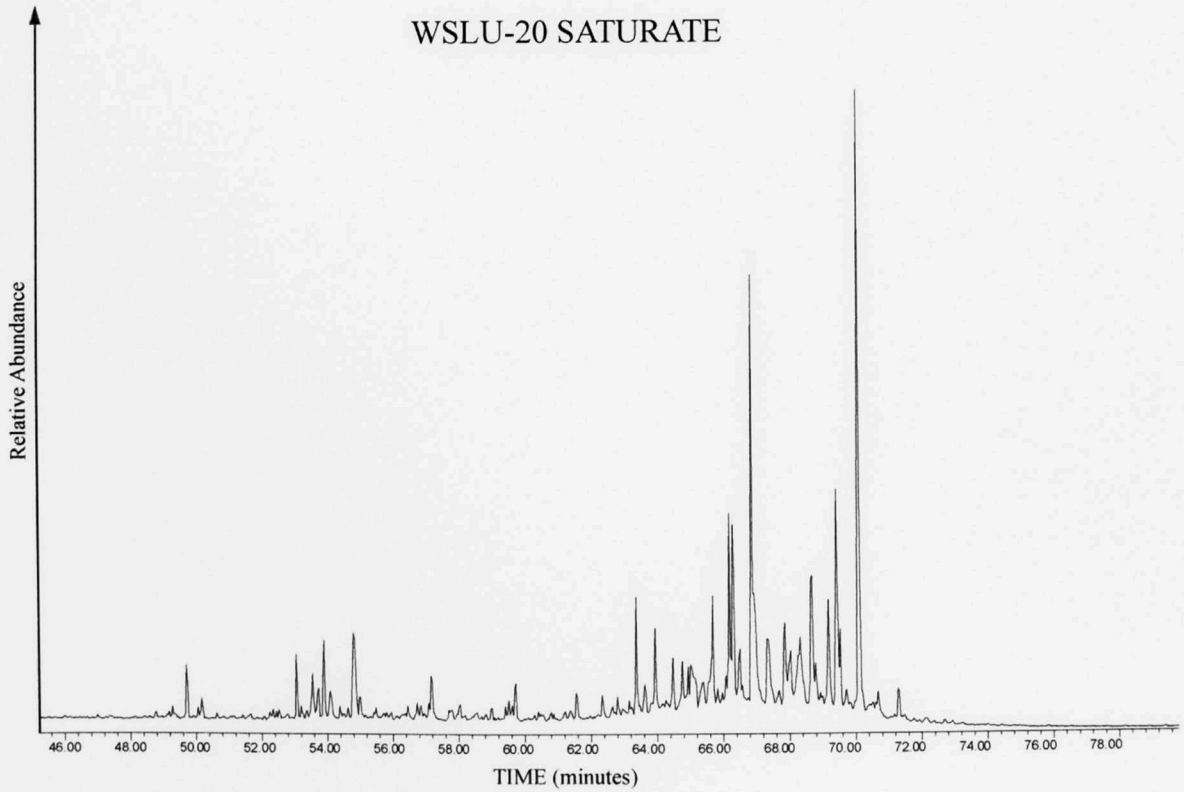

WSLU-21 SATURATE

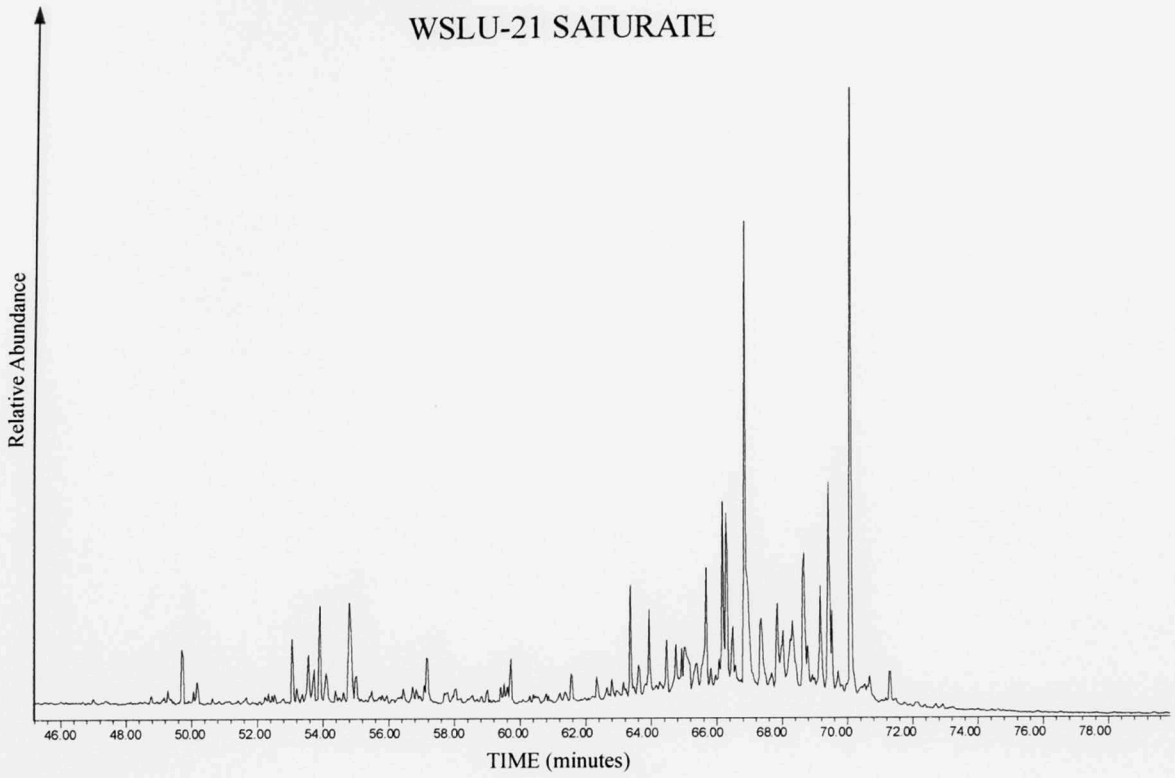

WSLU-22 SATURATE

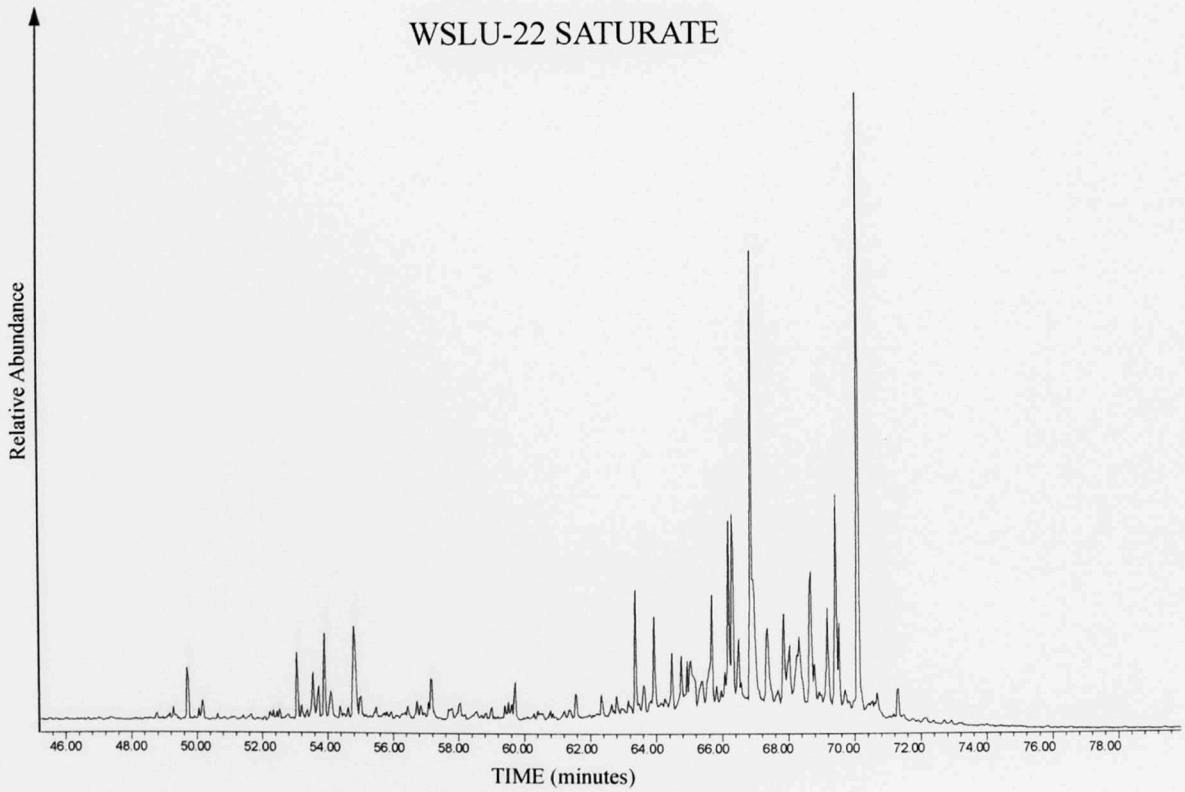

WSLU-23 SATURATE

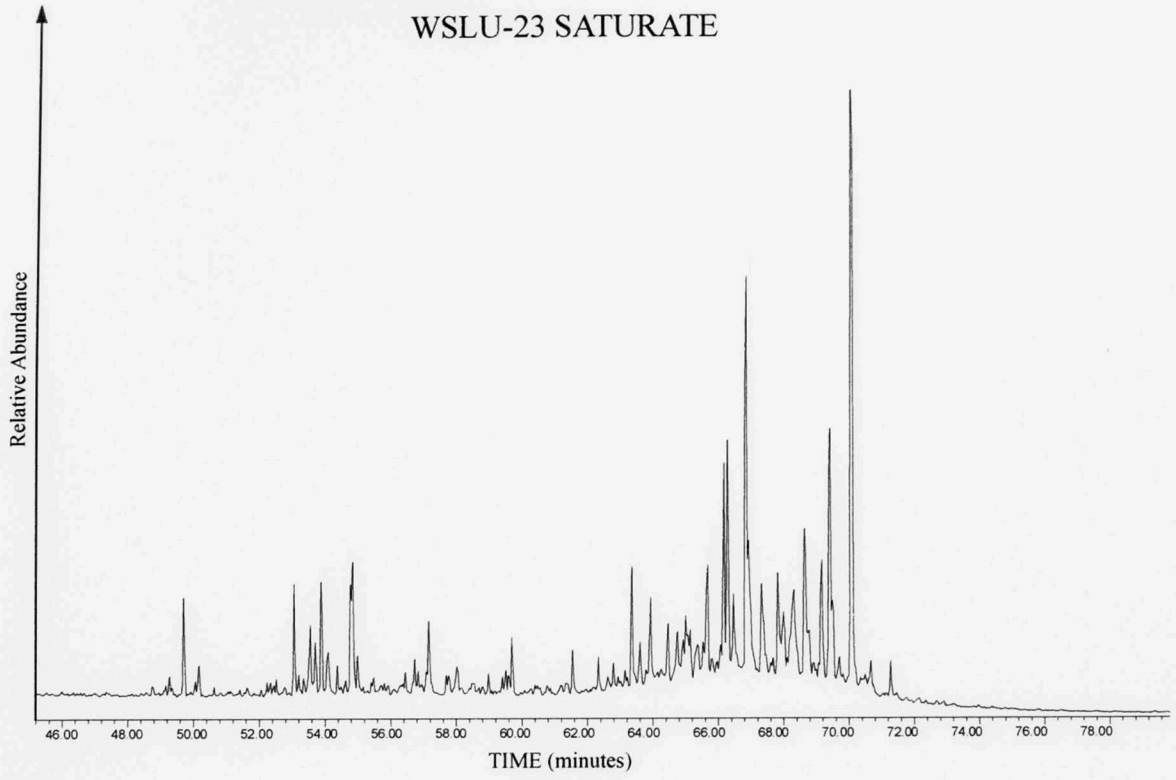

WSLU-24 SATURATE

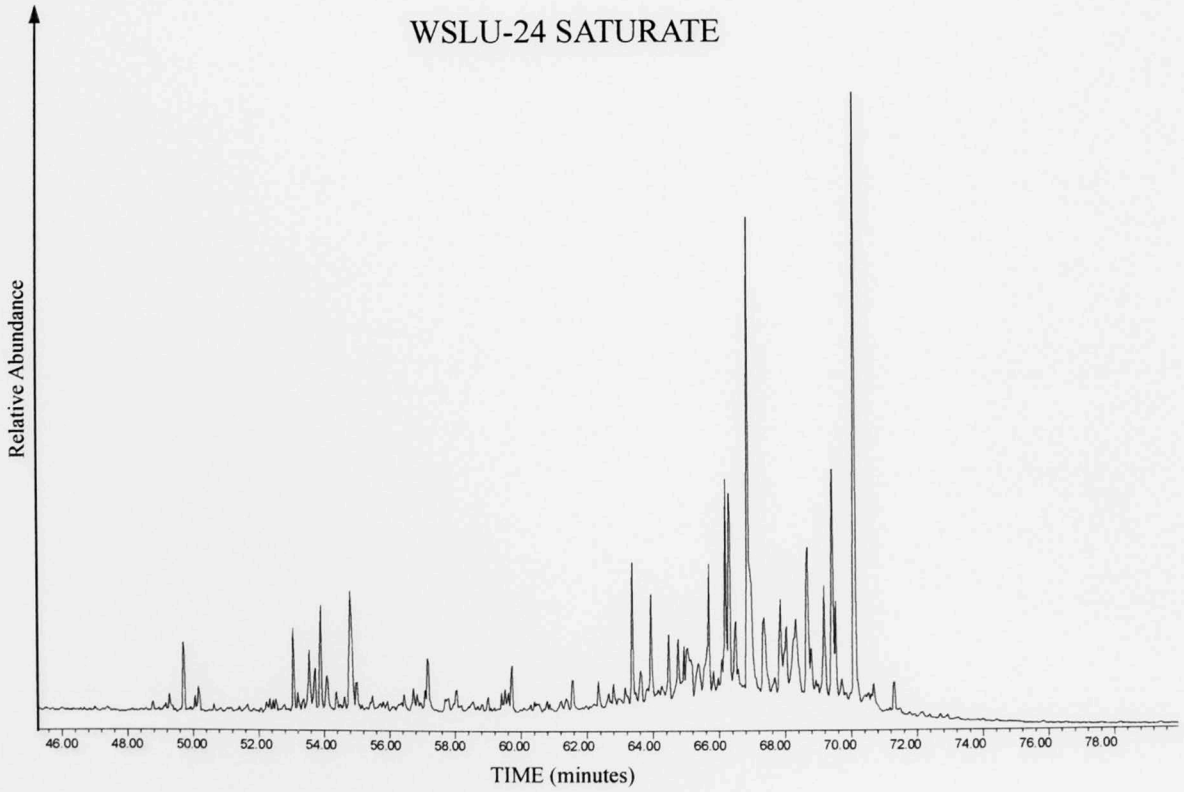

WSLU-25 SATURATE

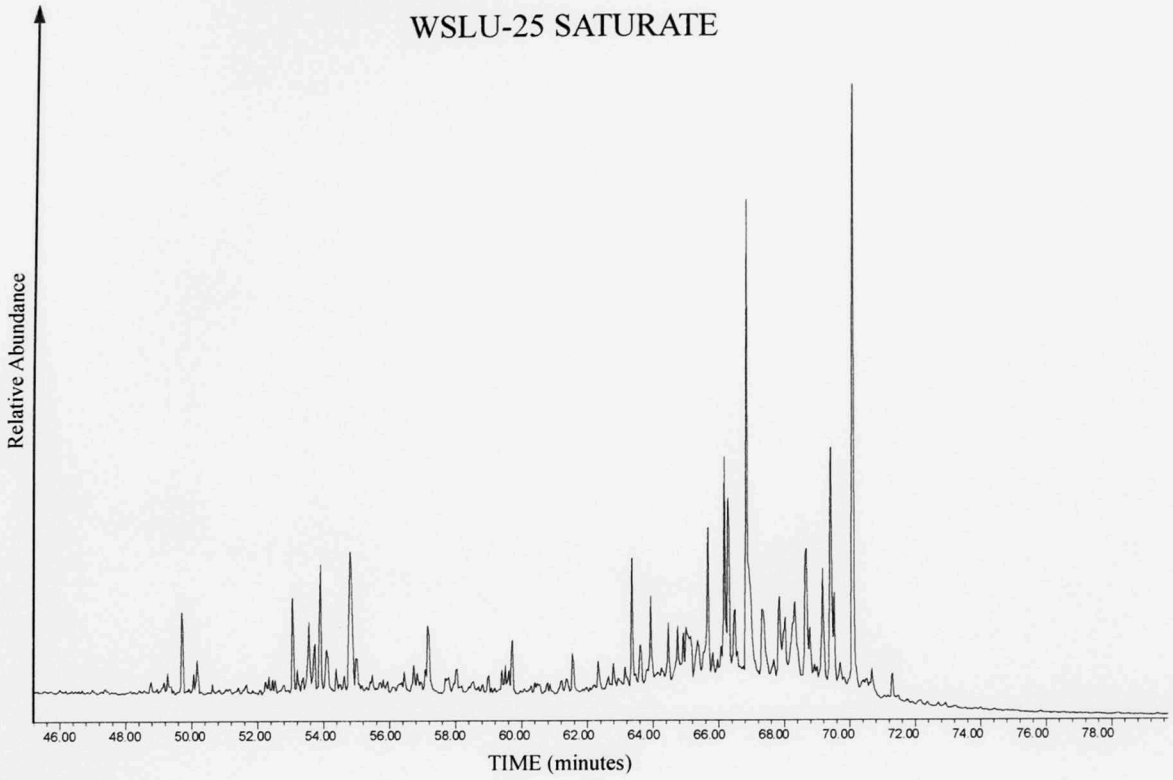

WSLU-26 SATURATE

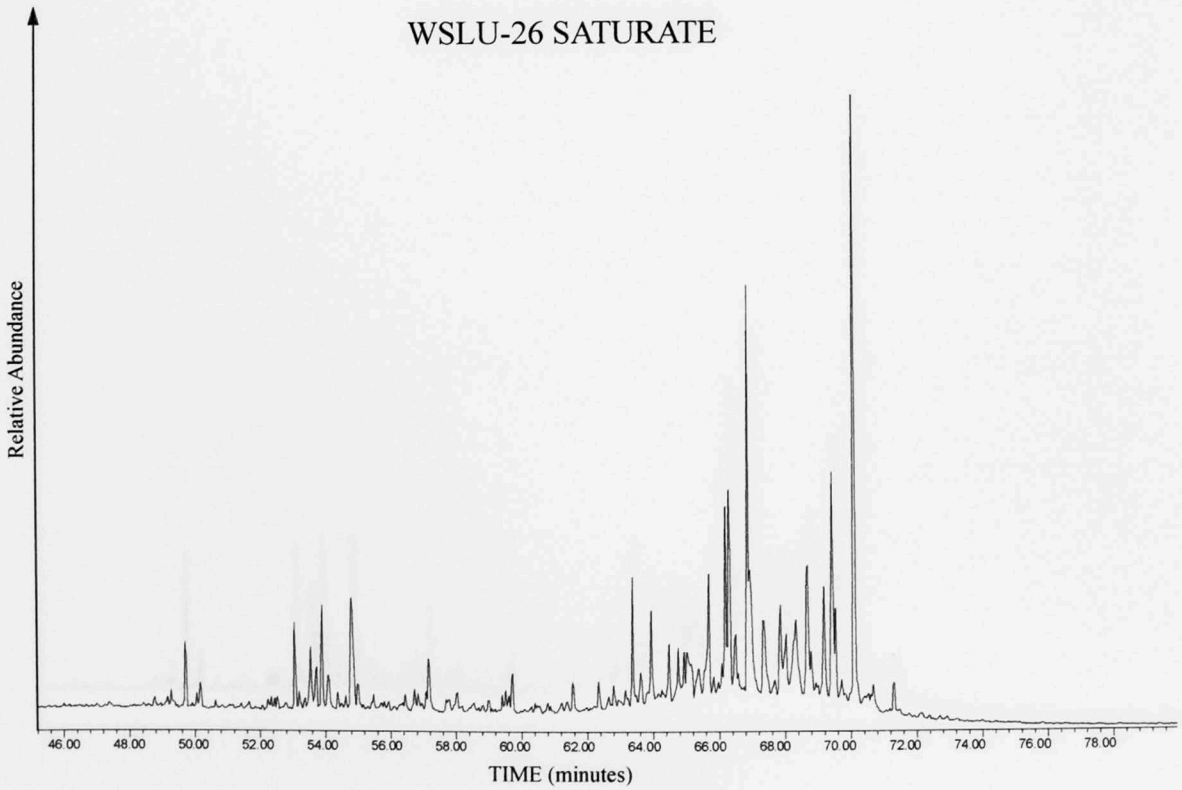

WSLU-27 SATURATE

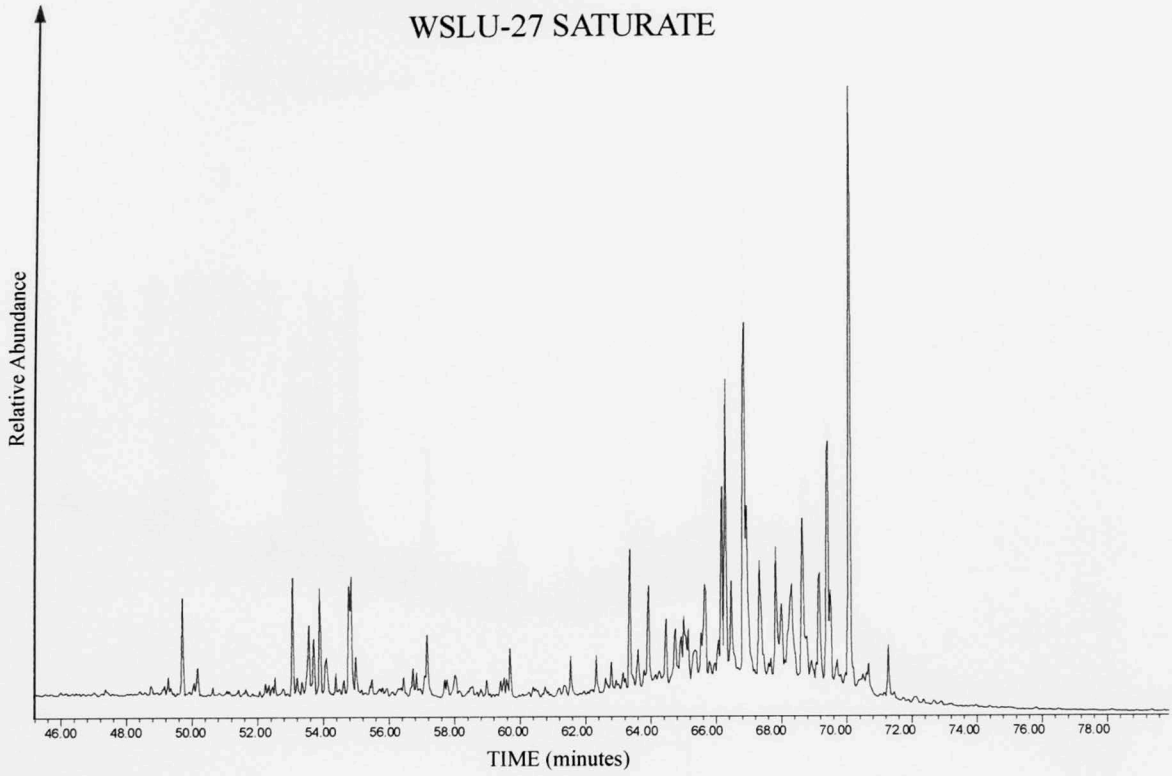

WSLU-28 SATURATE

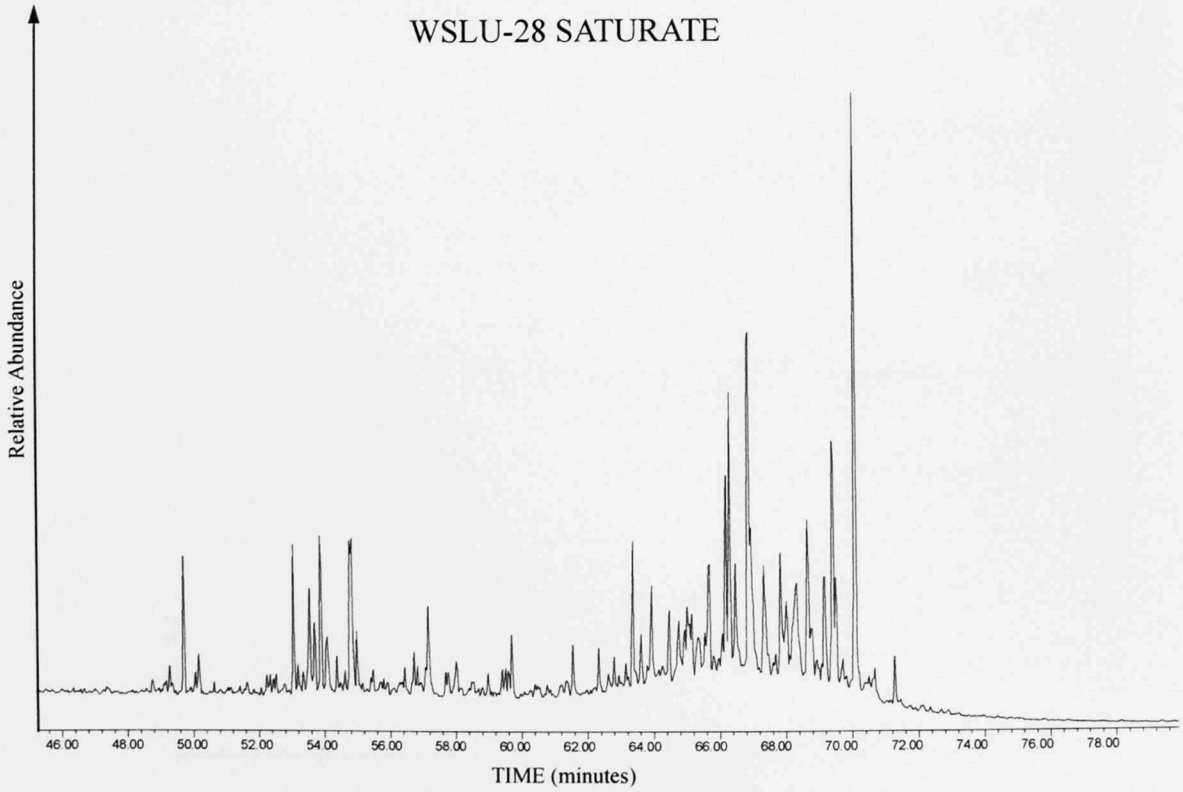

WSLU-29 SATURATE

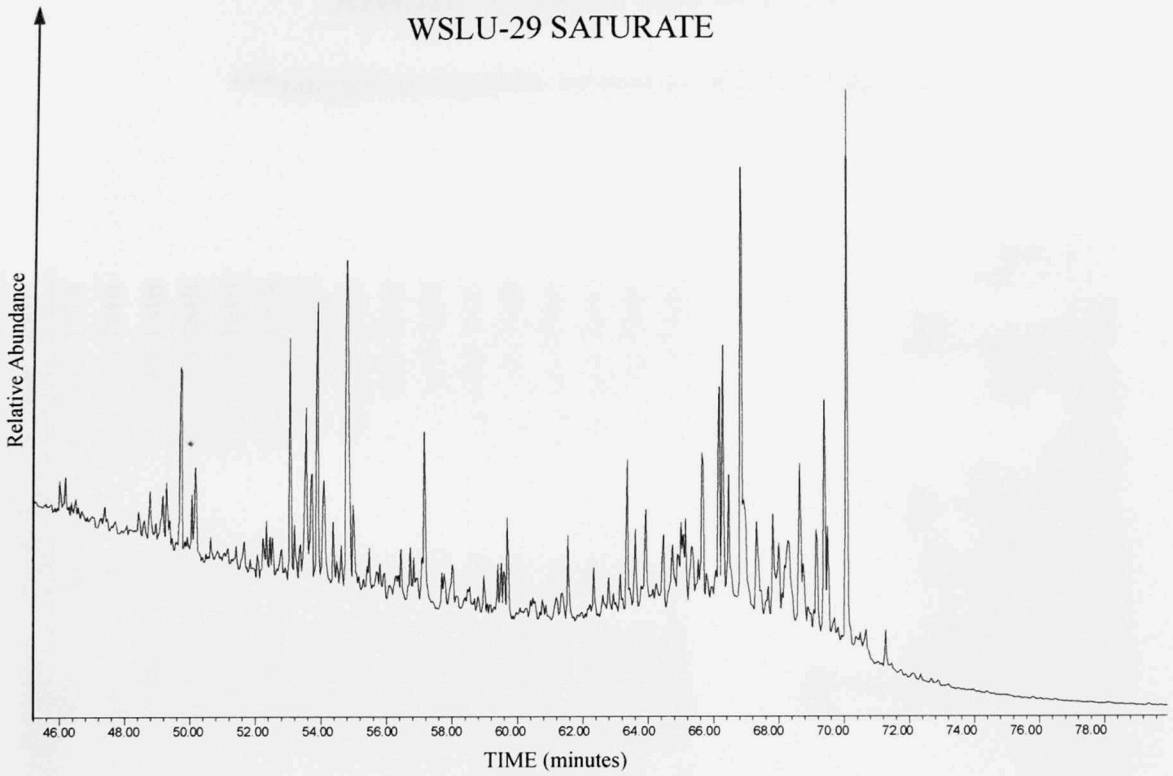

AIII.III. Wyche-1 core m/z 134

***samples arranged by increasing depth on page 231

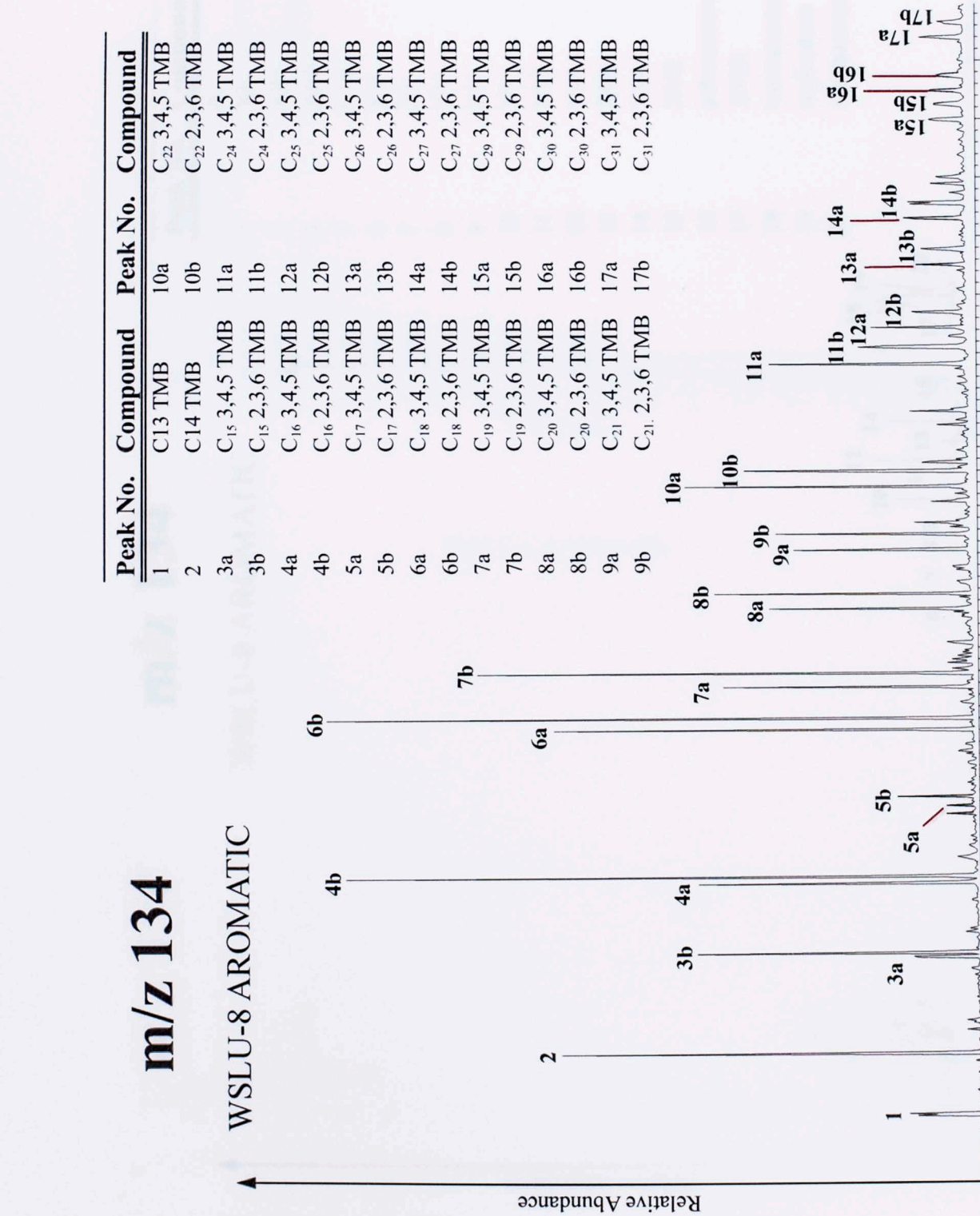

Peak No.	Compound	Peak No.	Compound
1	C13 TMB	10a	C_{22} 3,4,5 TMB
2	C14 TMB	10b	C_{22} 2,3,6 TMB
3a	C_{15} 3,4,5 TMB	11a	C_{24} 3,4,5 TMB
3b	C_{15} 2,3,6 TMB	11b	C_{24} 2,3,6 TMB
4a	C_{16} 3,4,5 TMB	12a	C_{25} 3,4,5 TMB
4b	C_{16} 2,3,6 TMB	12b	C_{25} 2,3,6 TMB
5a	C_{17} 3,4,5 TMB	13a	C_{26} 3,4,5 TMB
5b	C_{17} 2,3,6 TMB	13b	C_{26} 2,3,6 TMB
6a	C_{18} 3,4,5 TMB	14a	C_{27} 3,4,5 TMB
6b	C_{18} 2,3,6 TMB	14b	C_{27} 2,3,6 TMB
7a	C_{19} 3,4,5 TMB	15a	C_{29} 3,4,5 TMB
7b	C_{19} 2,3,6 TMB	15b	C_{29} 2,3,6 TMB
8a	C_{20} 3,4,5 TMB	16a	C_{30} 3,4,5 TMB
8b	C_{20} 2,3,6 TMB	16b	C_{30} 2,3,6 TMB
9a	C_{21} 3,4,5 TMB	17a	C_{31} 3,4,5 TMB
9b	C_{21} 2,3,6 TMB	17b	C_{31} 2,3,6 TMB

m/z 134

WSLU-8 AROMATIC

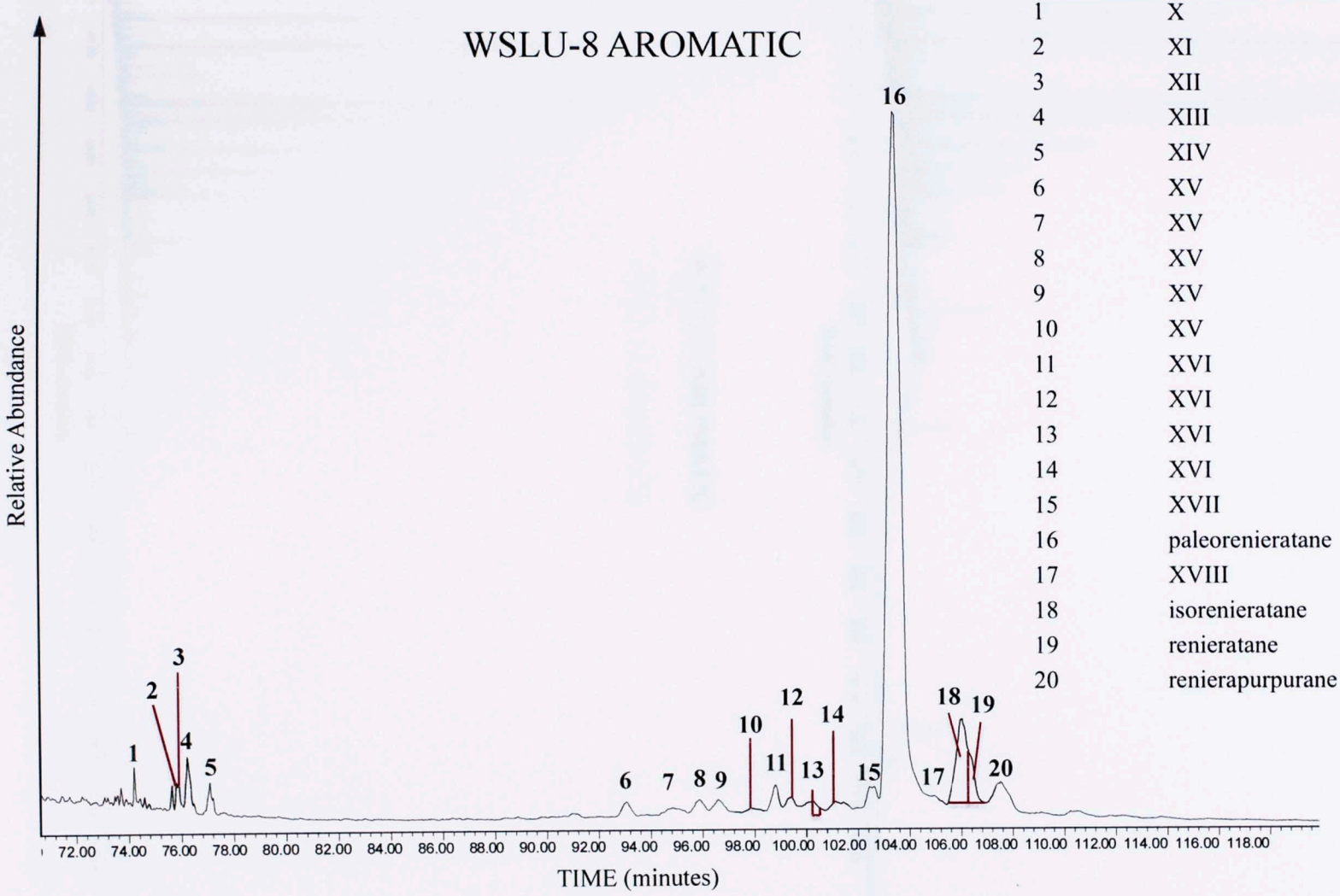

Peak No.	Compound
1	X
2	XI
3	XII
4	XIII
5	XIV
6	XV
7	XV
8	XV
9	XV
10	XV
11	XVI
12	XVI
13	XVI
14	XVI
15	XVII
16	paleorenieratane
17	XVIII
18	isorenieratane
19	renieratane
20	renierapurpurane

WSLU-1 AROMATIC

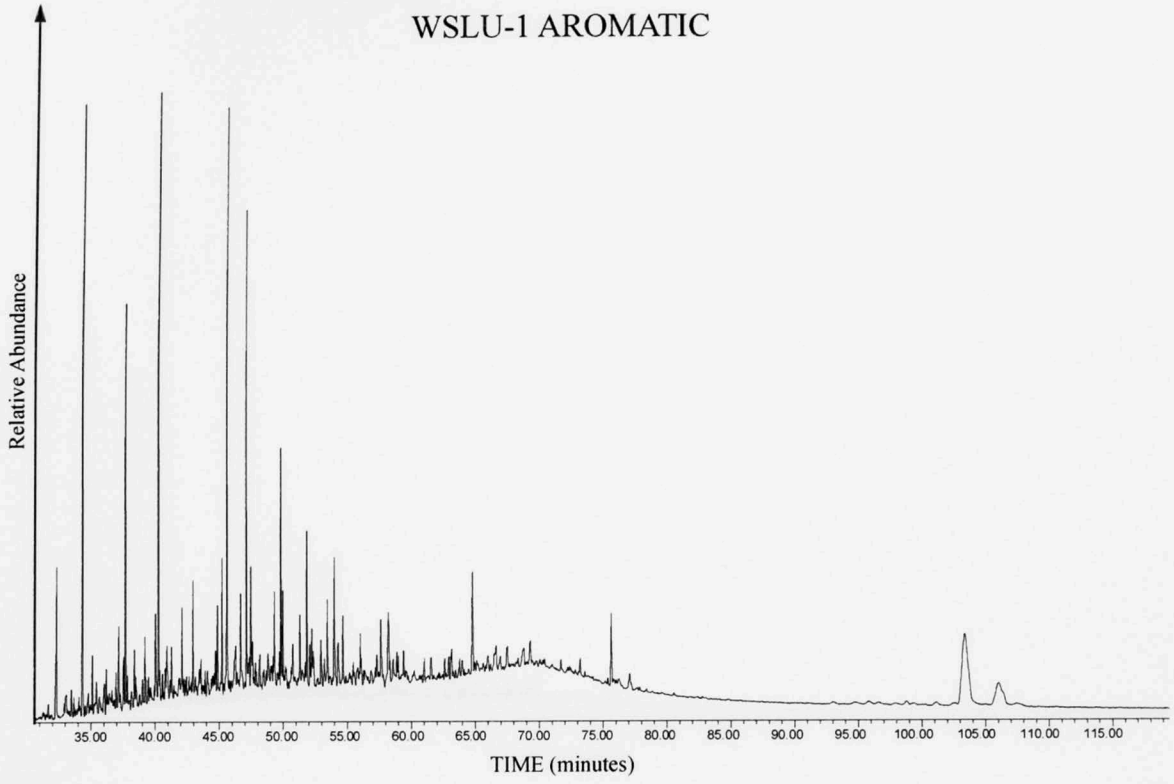

WSLU-2 AROMATIC

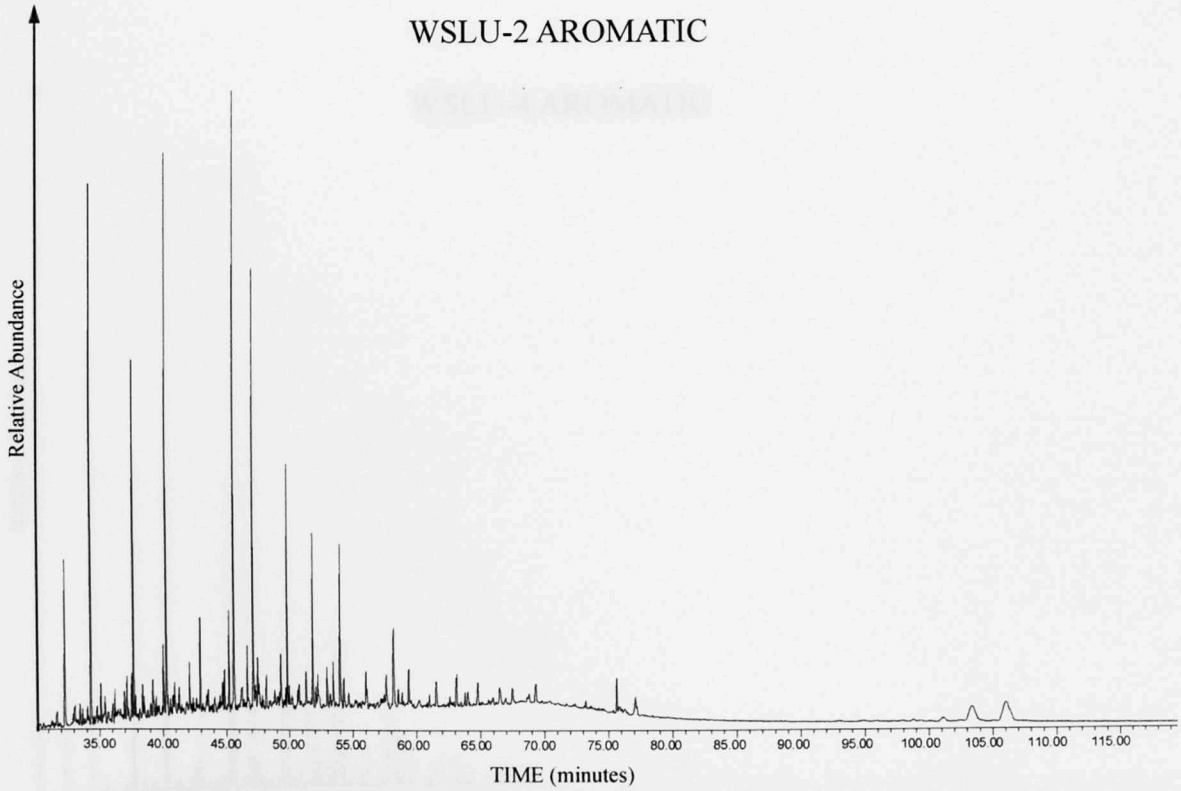

WSLU-3 AROMATIC

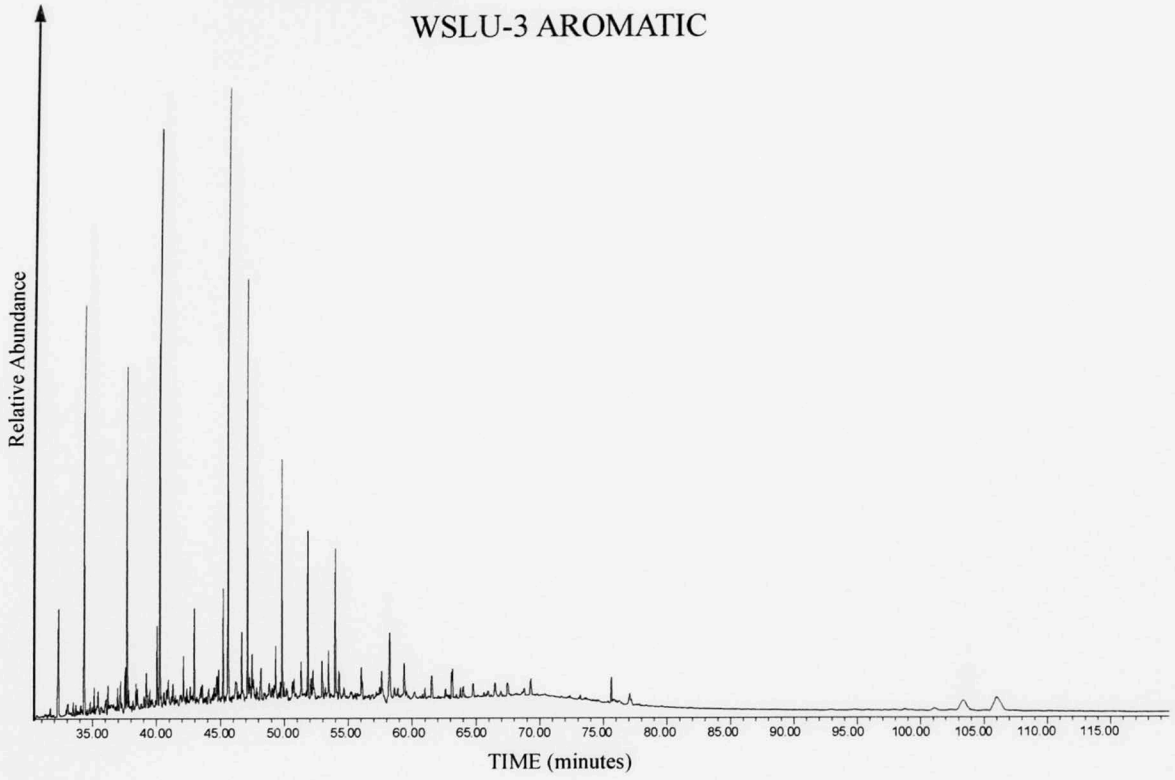

WSLU-4 AROMATIC

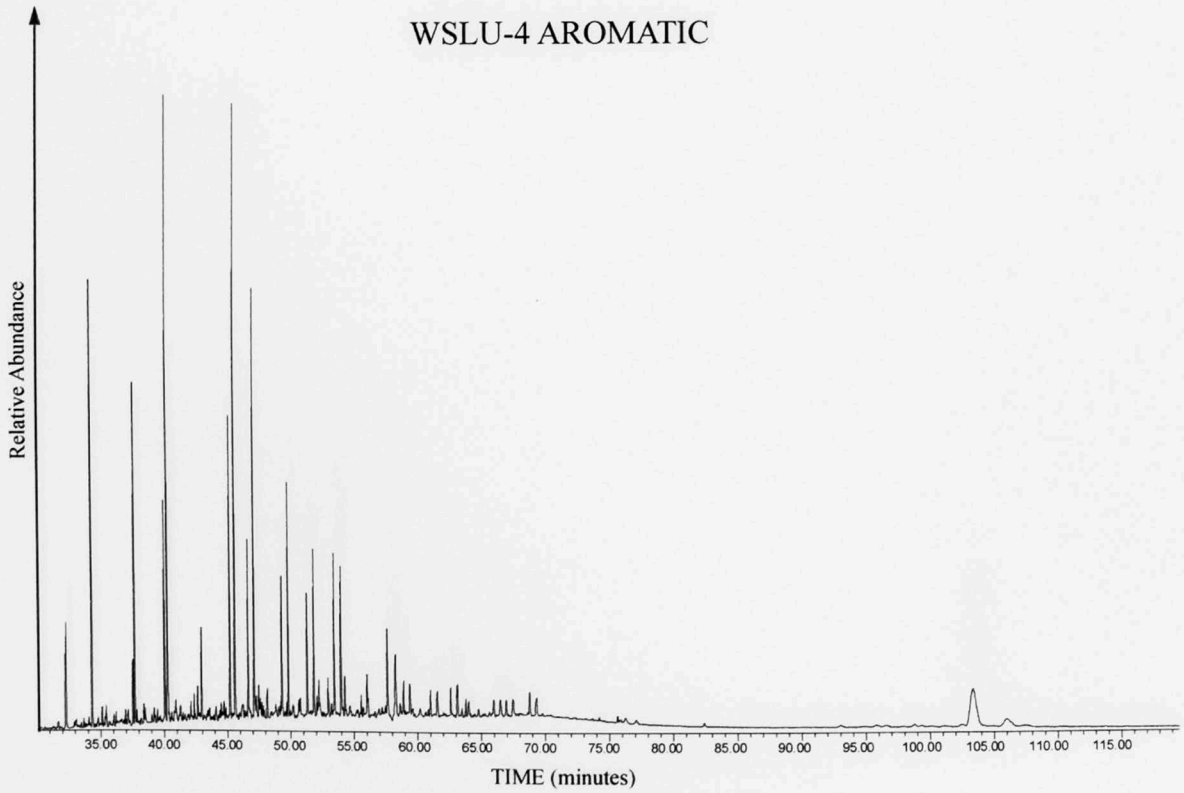

WSLU-5 AROMATIC

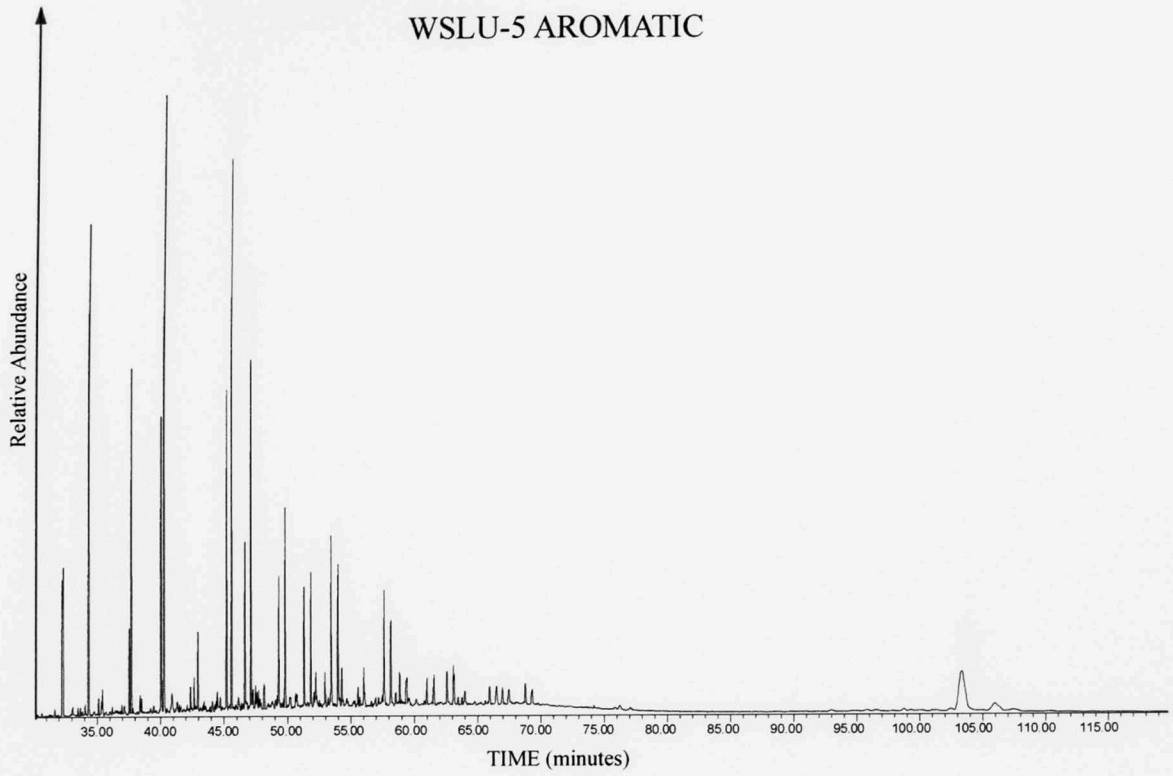

WSLU-6 AROMATIC

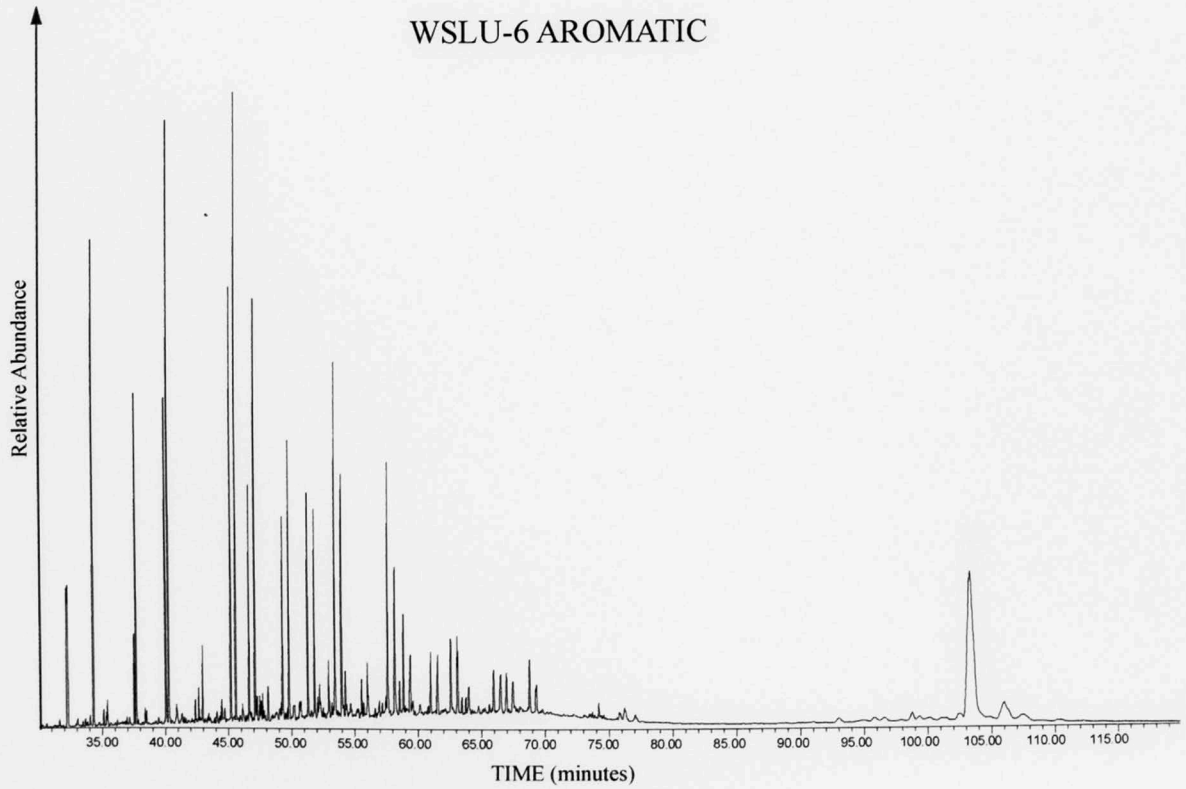

WSLU-7 AROMATIC

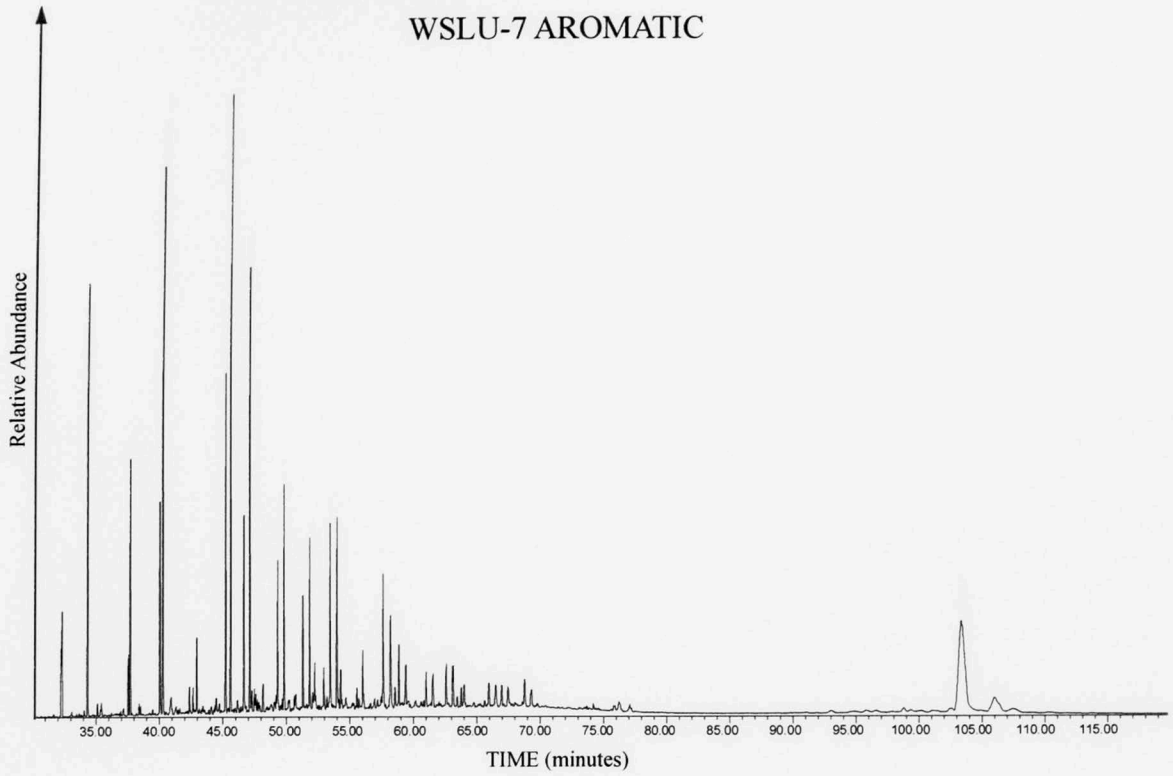

WSLU-8 AROMATIC

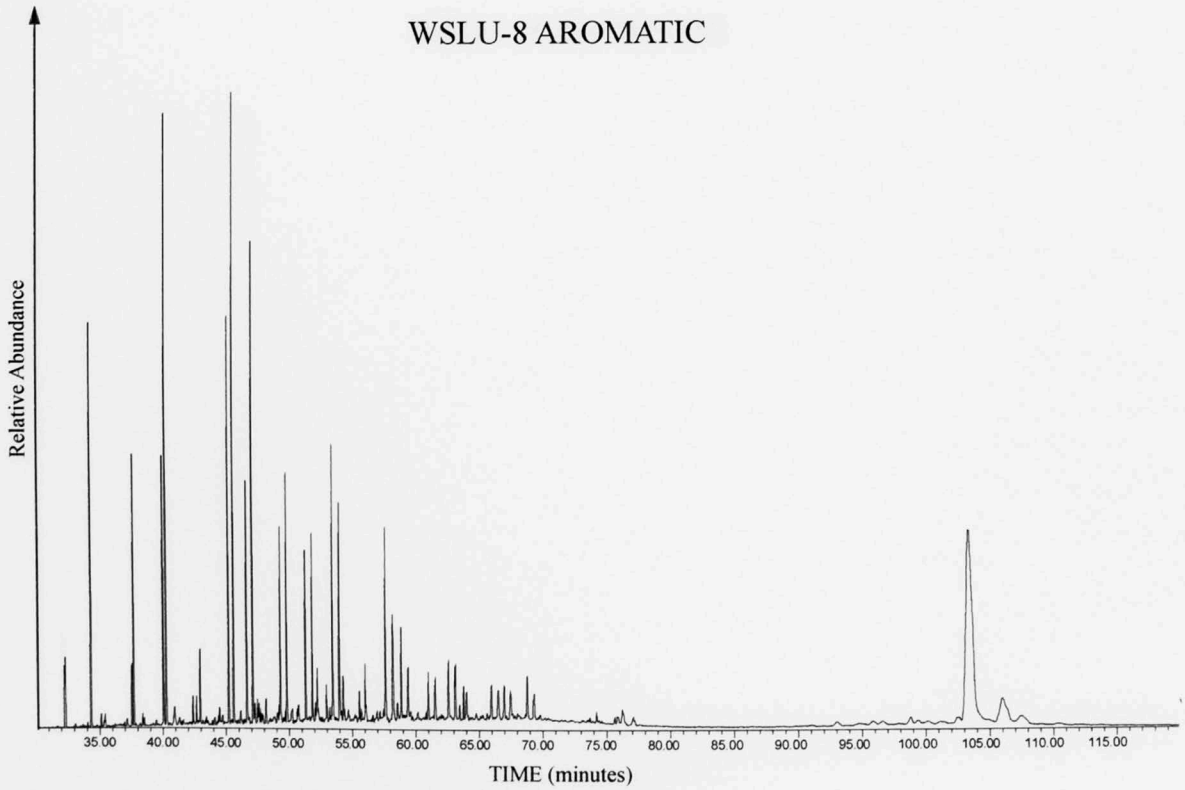

WSLU-9 AROMATIC

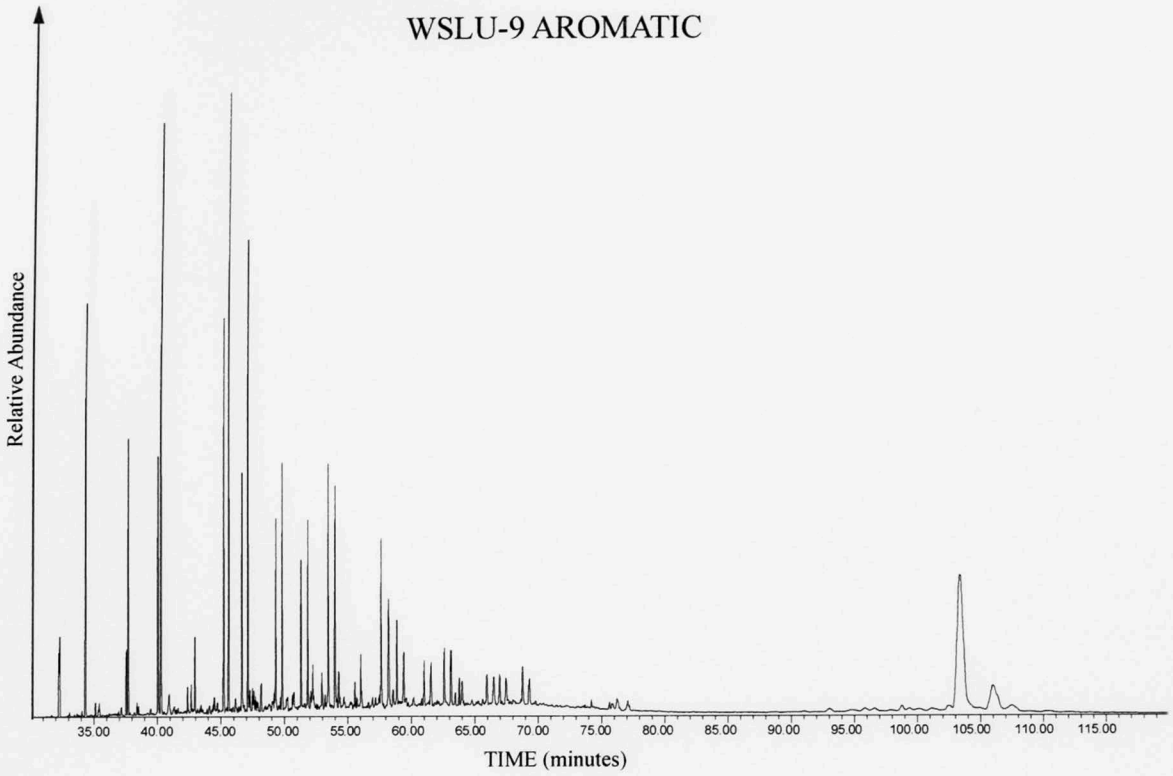

WSLU-10 AROMATIC

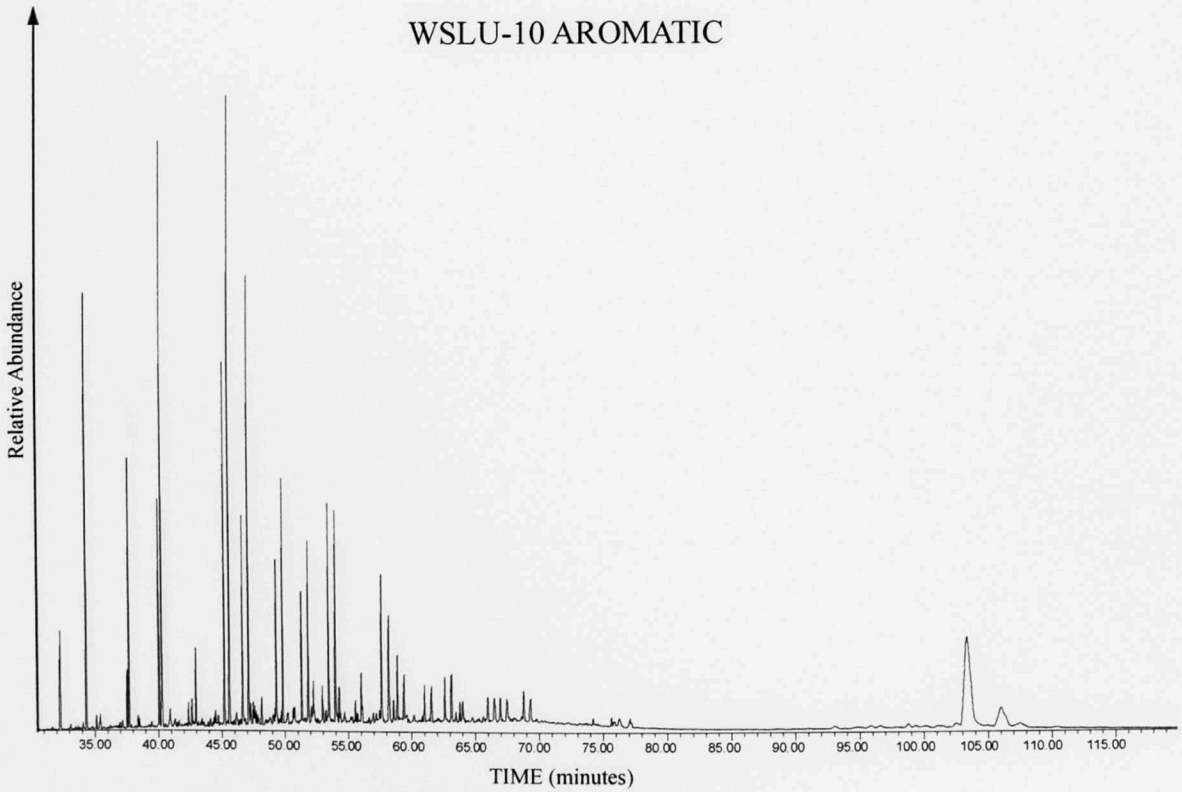

WSLU-11 AROMATIC

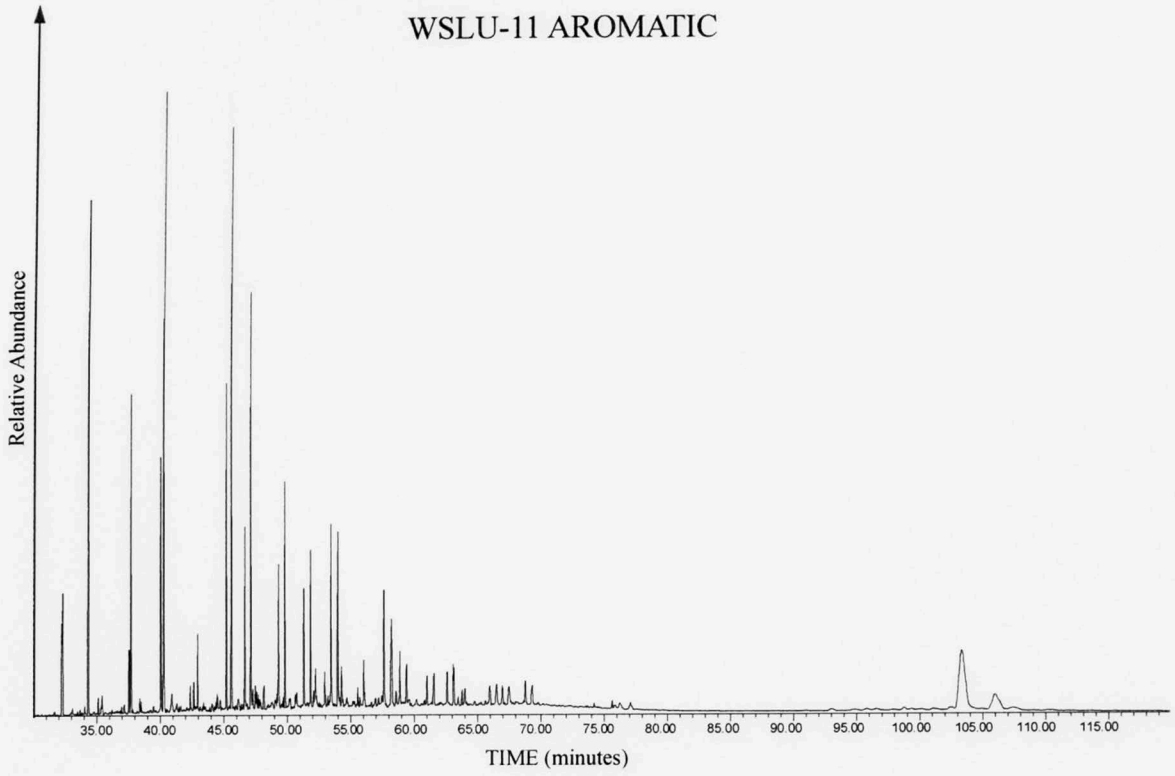

WSLU-12 AROMATIC

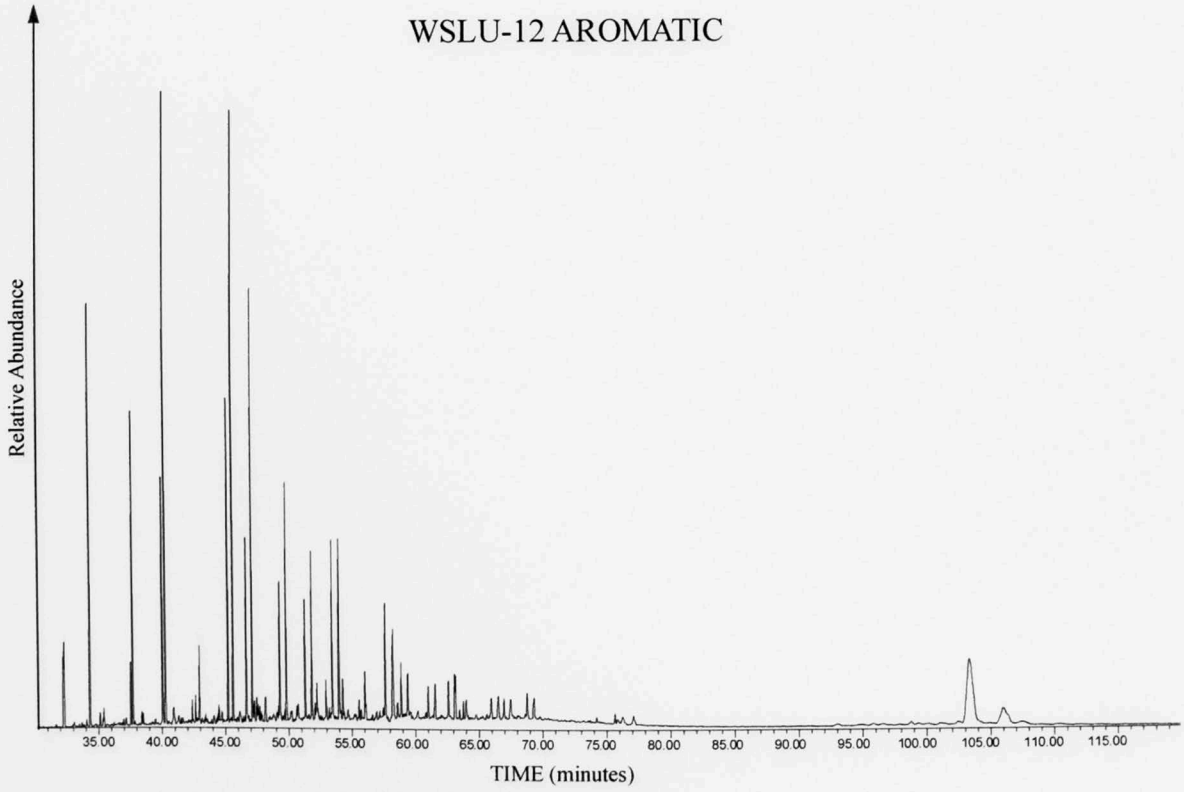

WSLU-13 AROMATIC

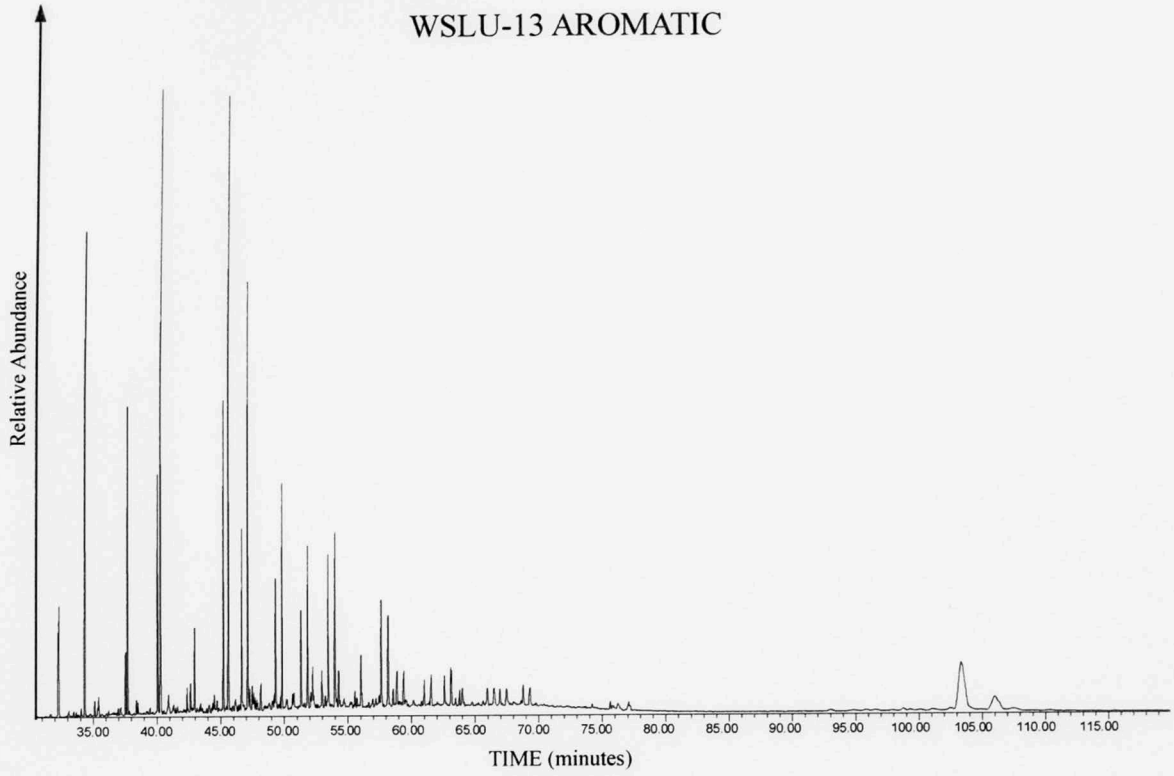

WSLU-14 AROMATIC

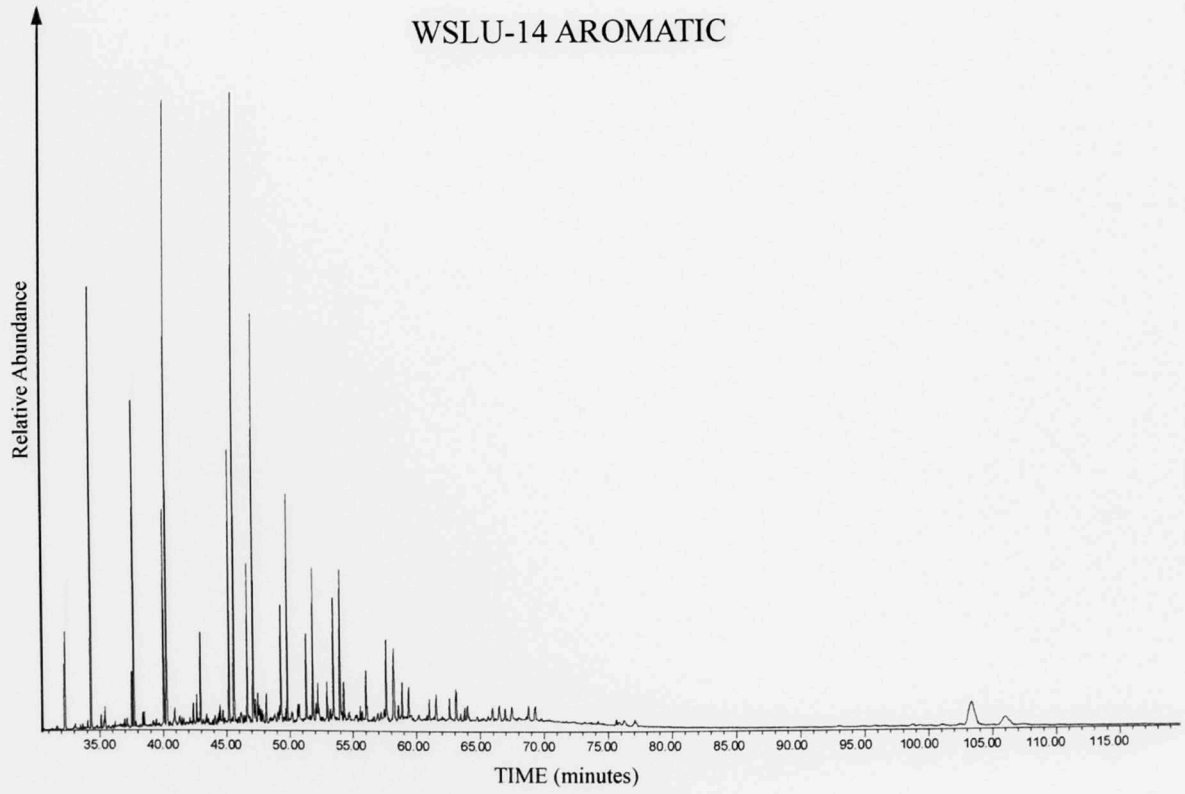

WSLU-15 AROMATIC

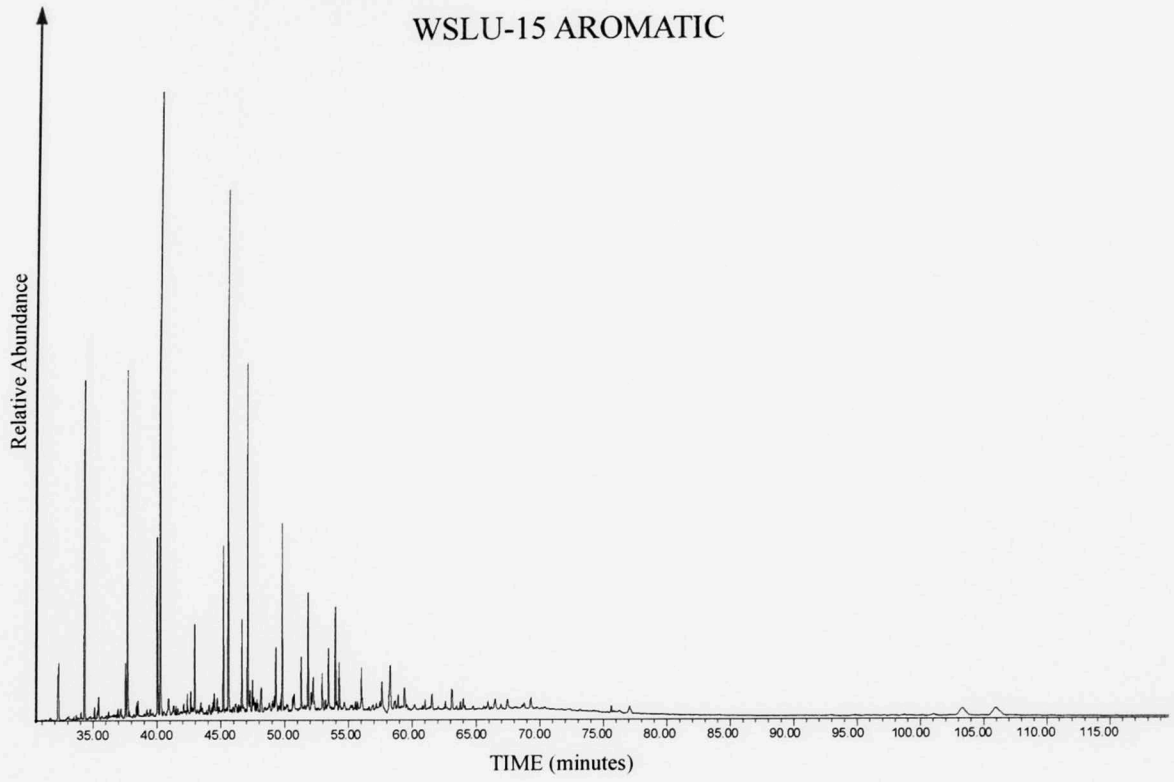

WSLU-16 AROMATIC

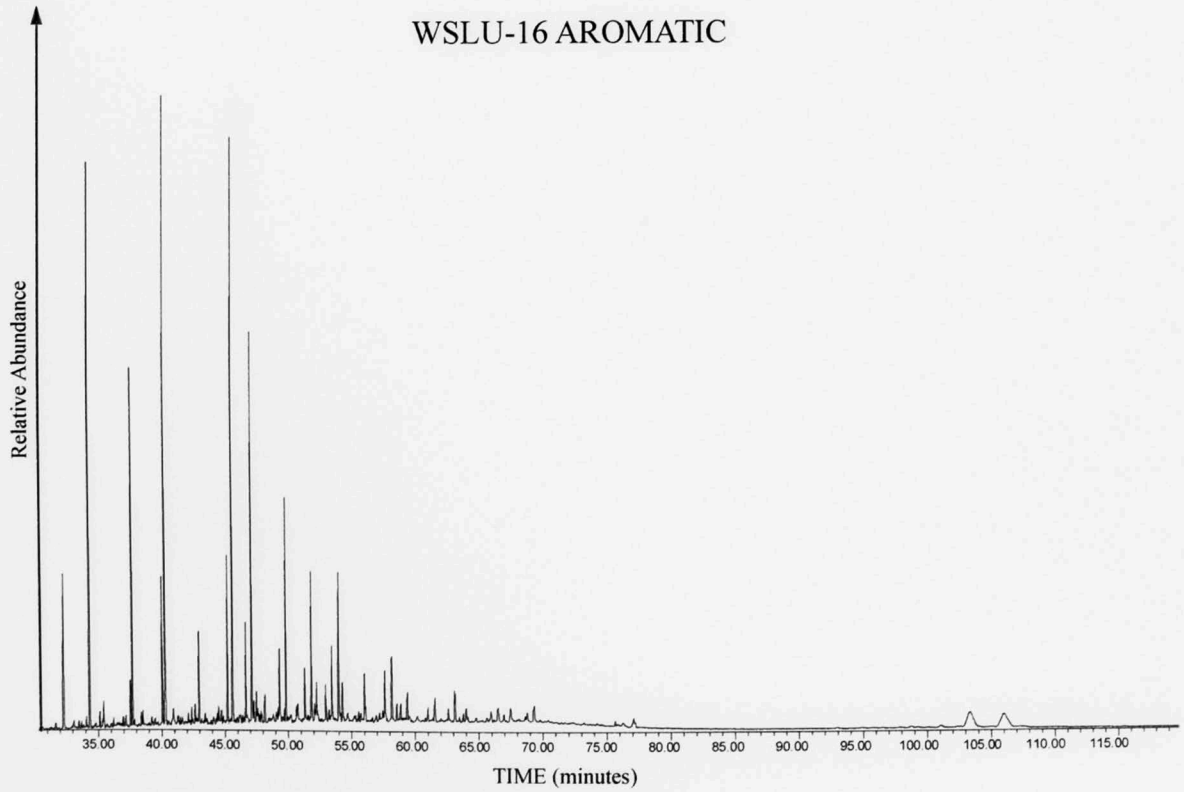

WSLU-17 AROMATIC

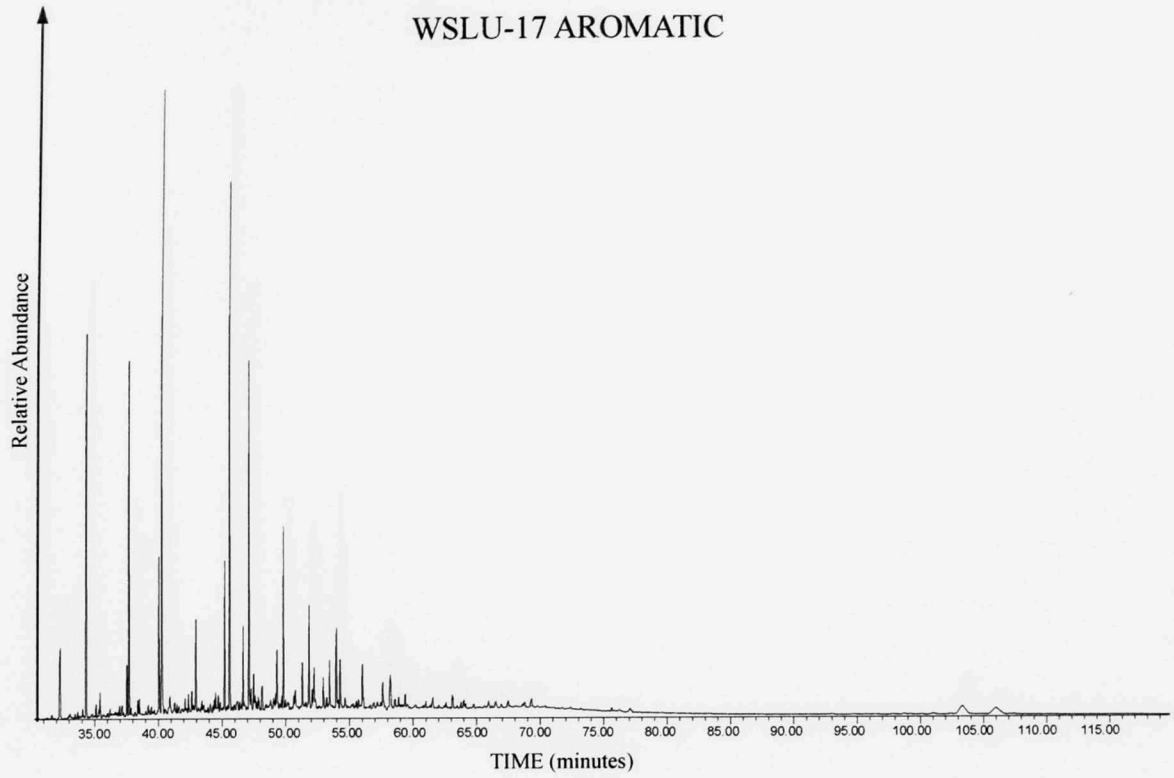

WSLU-18 AROMATIC

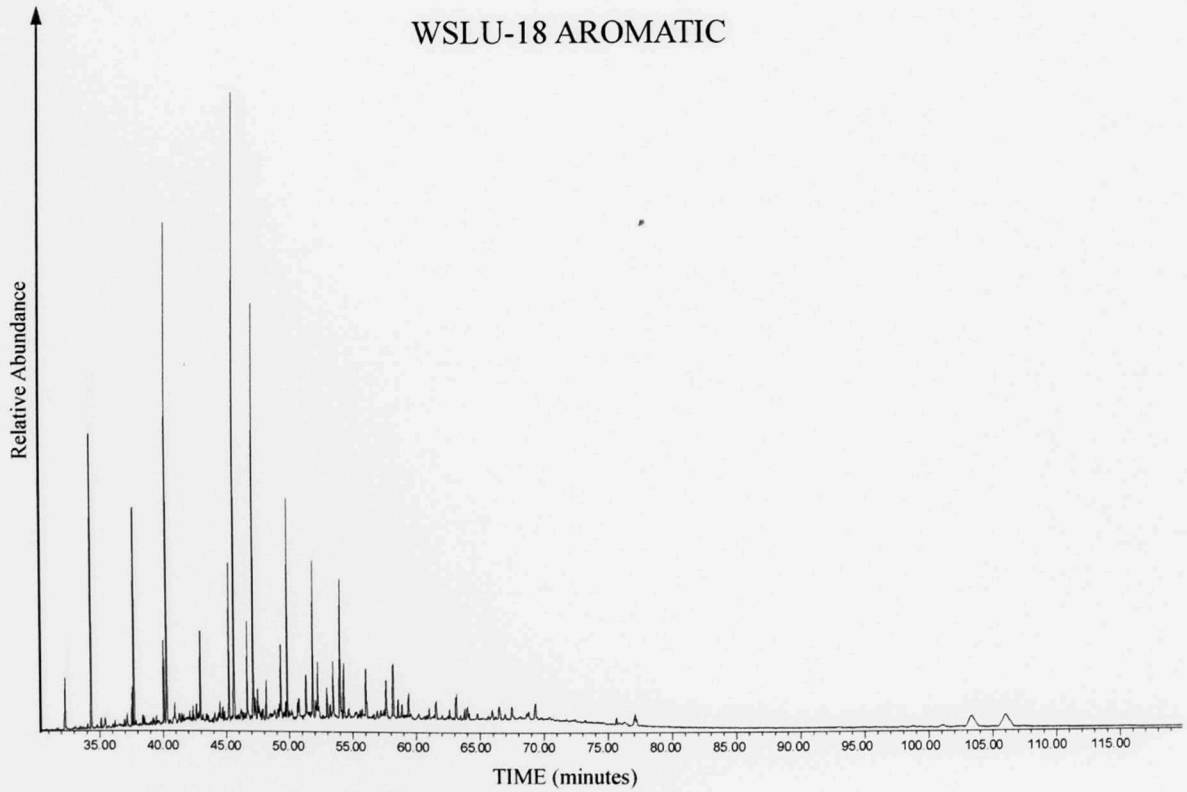

WSLU-19 AROMATIC

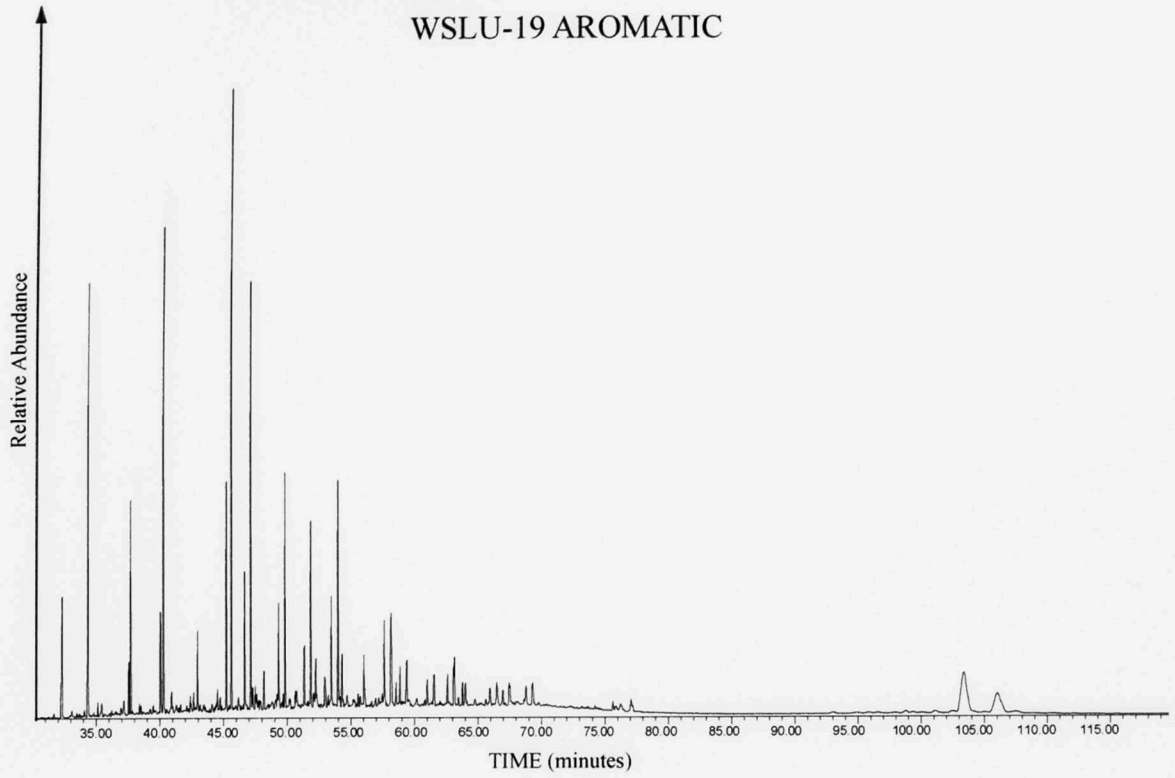

WSLU-20 AROMATIC

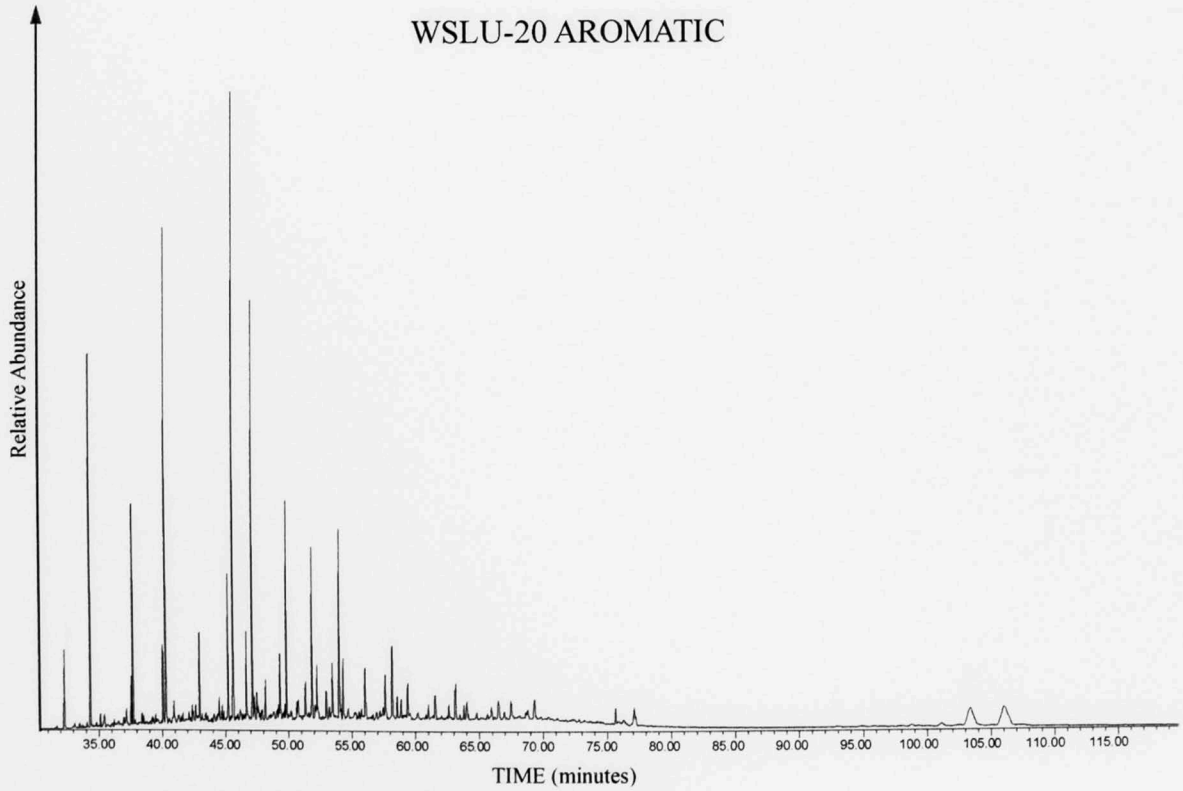

WSLU-21 AROMATIC

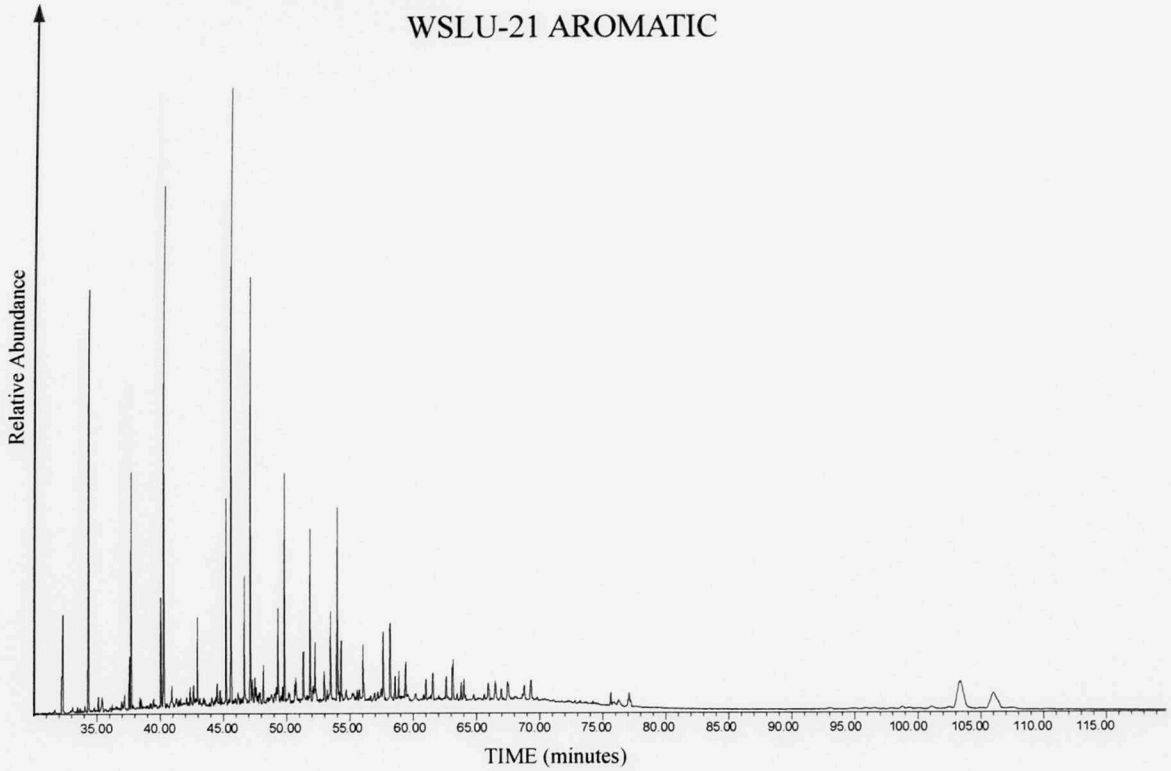

WSLU-22 AROMATIC

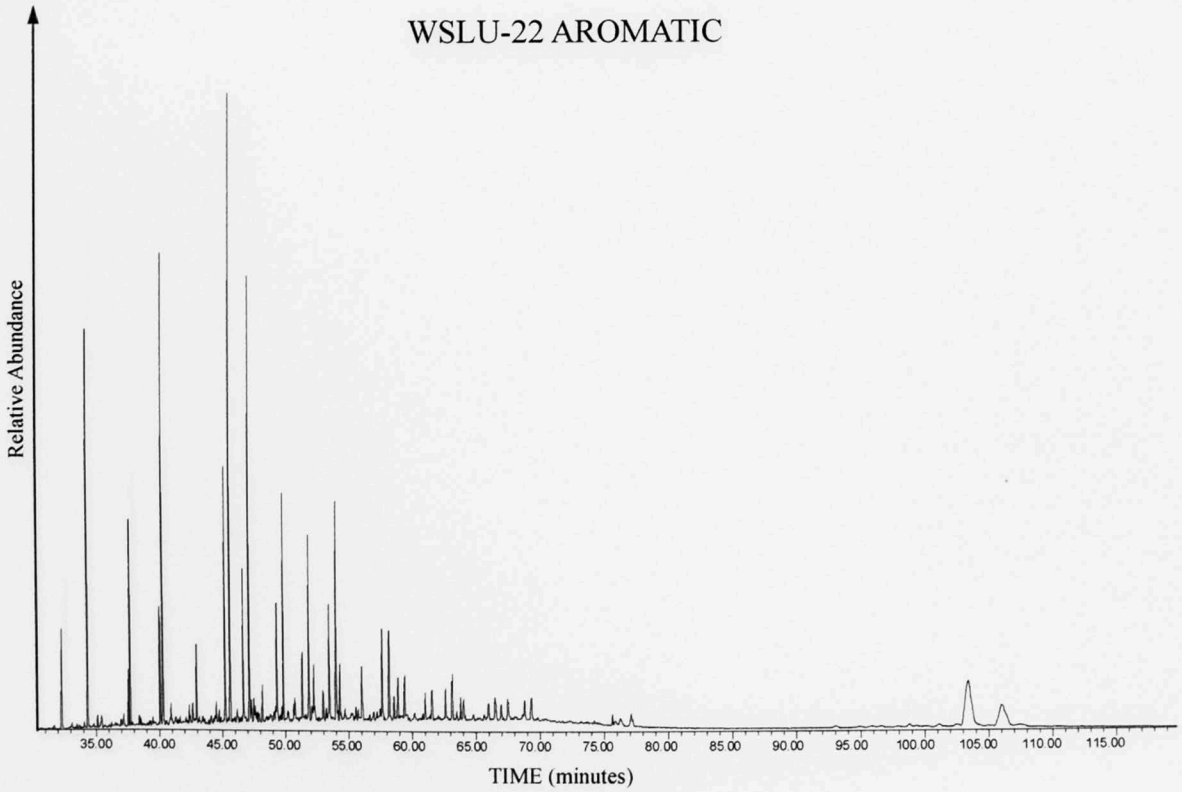

WSLU-23 AROMATIC

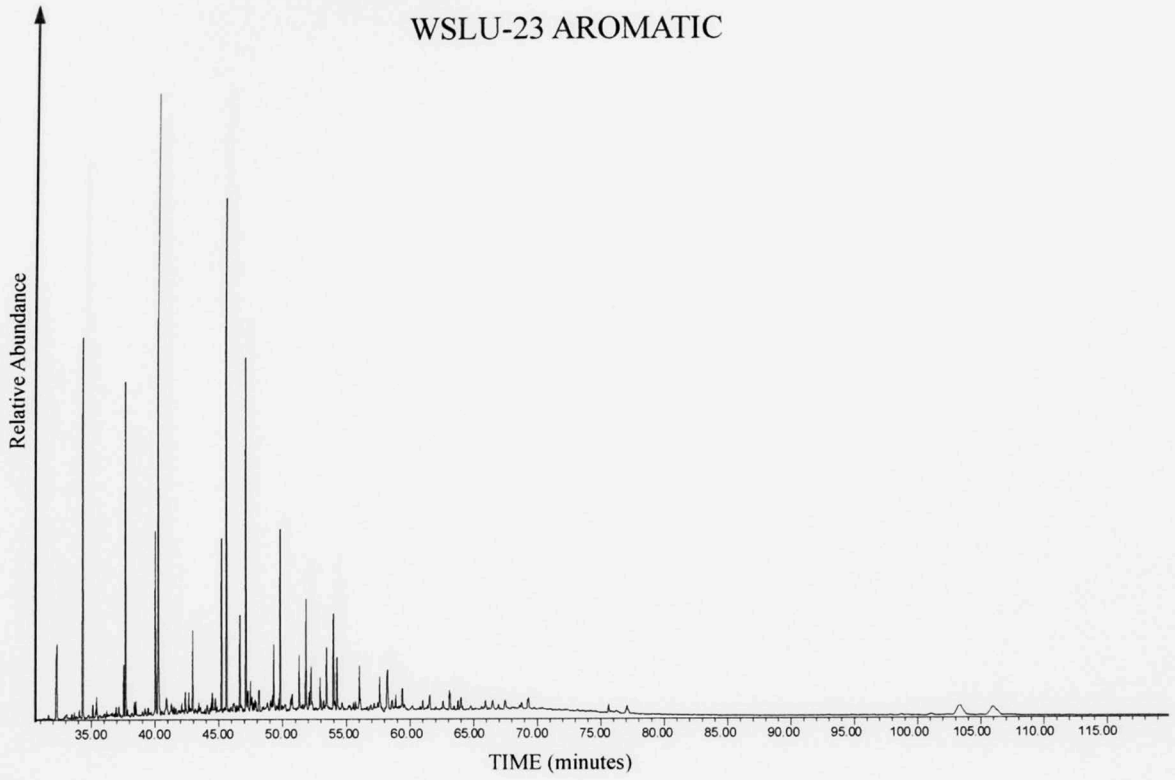

WSLU-24 AROMATIC

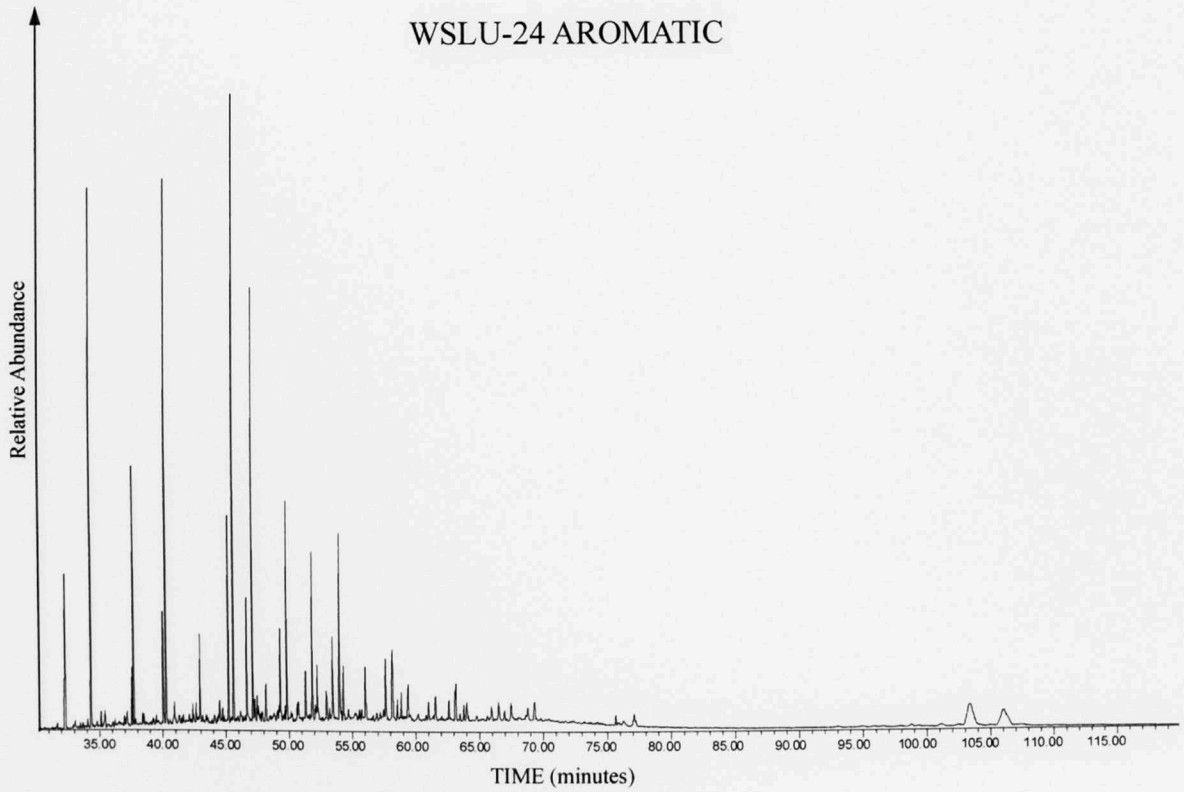

WSLU-25 AROMATIC

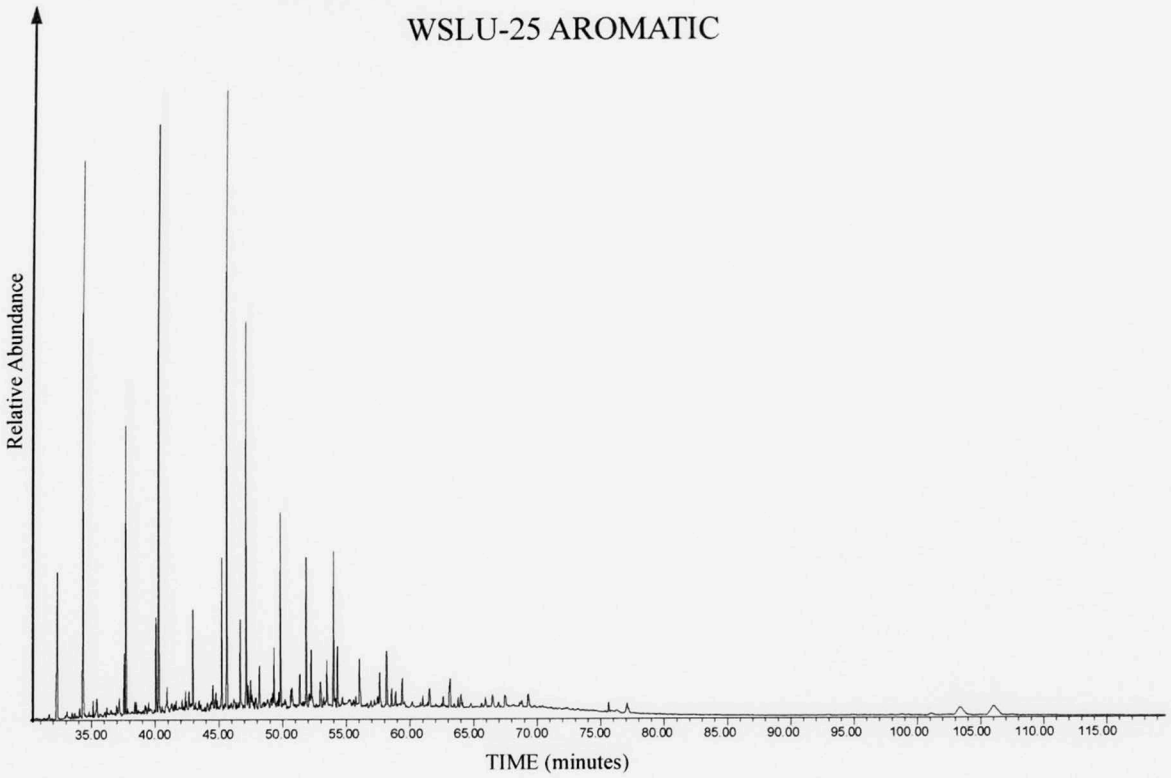

WSLU-26 AROMATIC

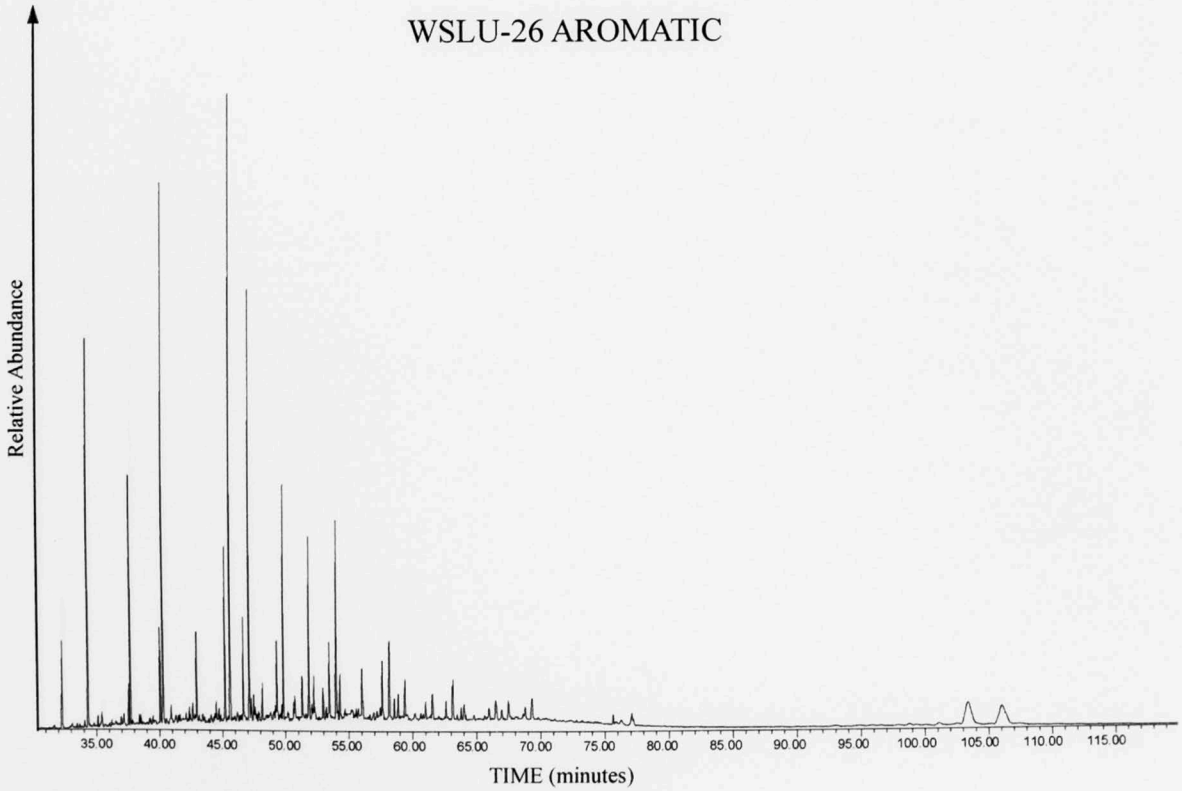

WSLU-27 AROMATIC

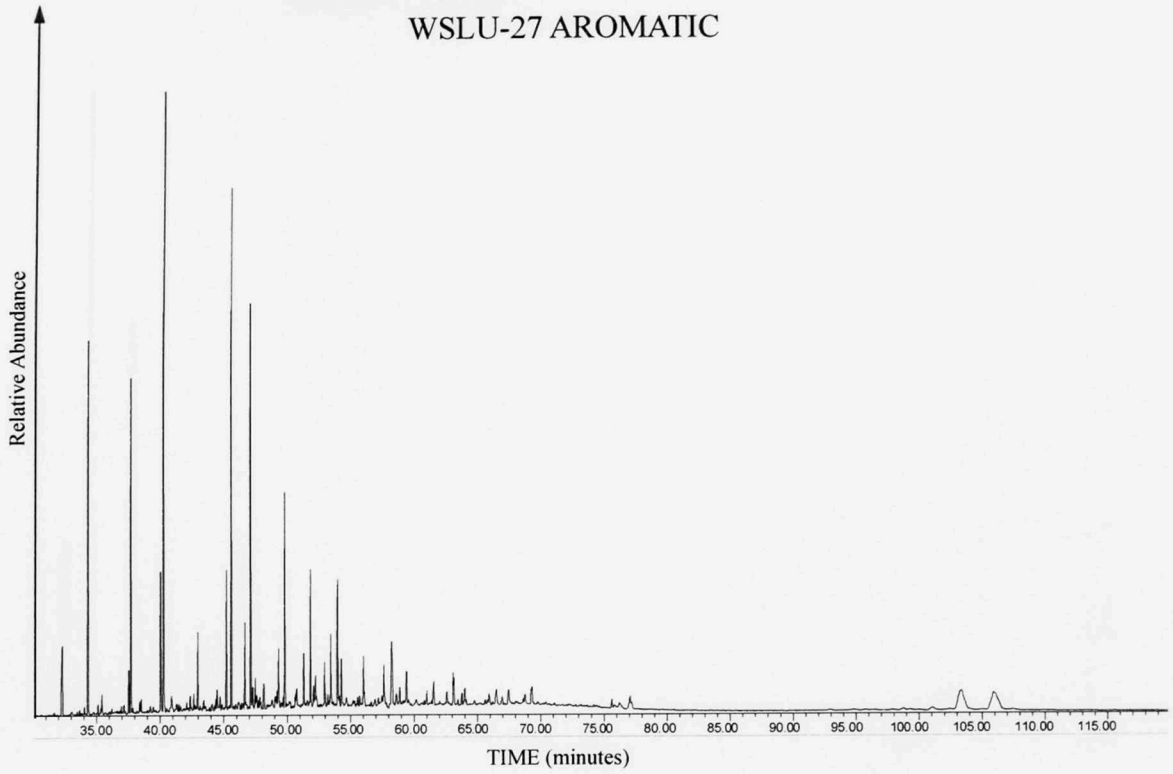

WSLU-28 AROMATIC

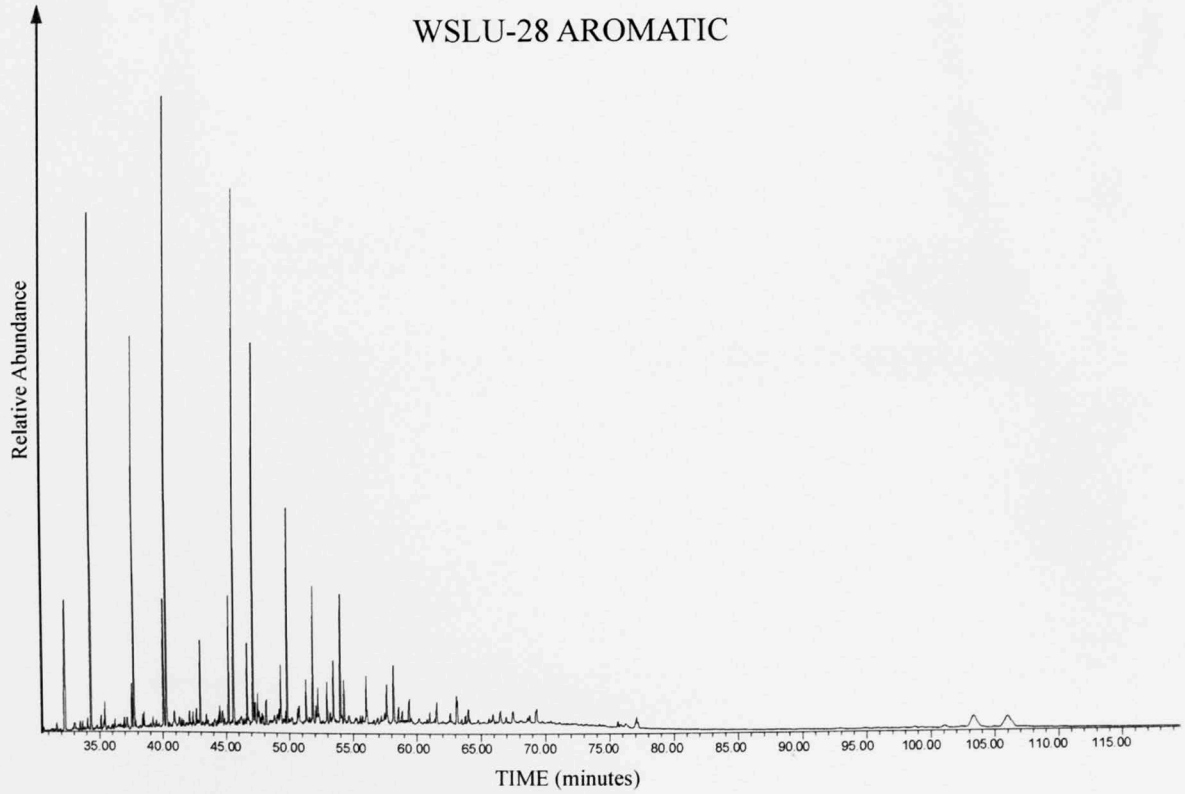

WSLU-29 AROMATIC

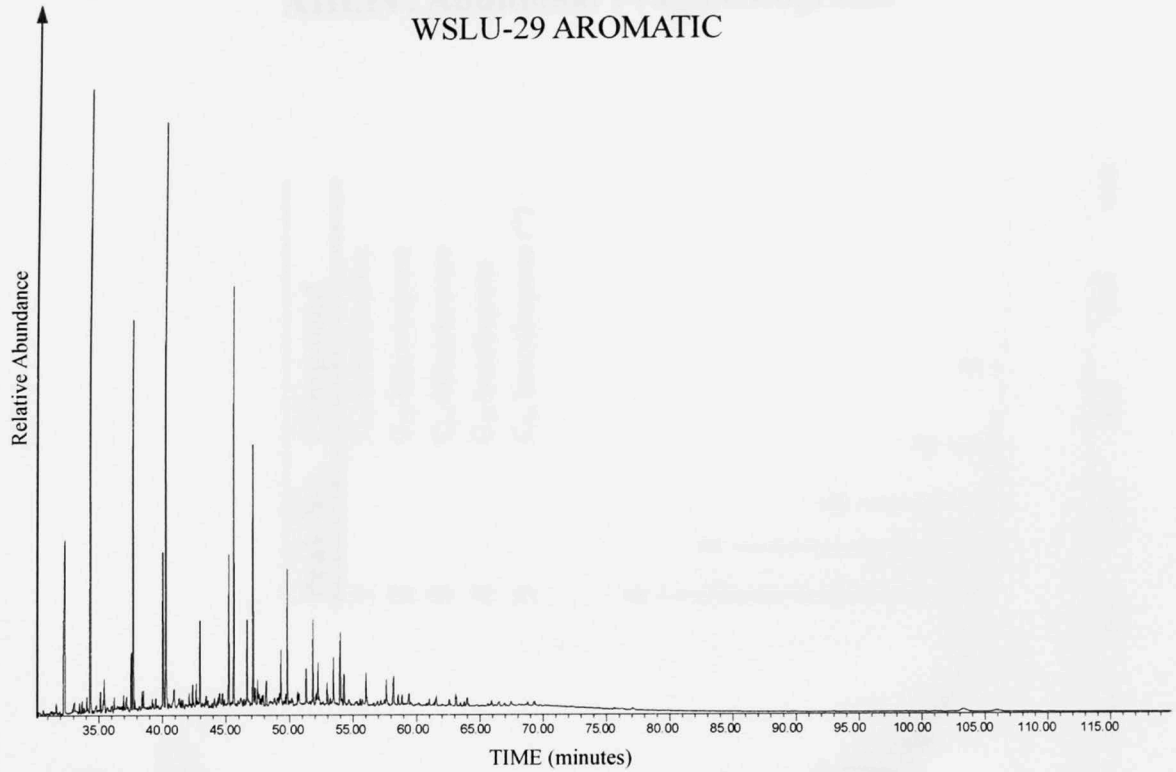

AIII.IV. Additional Fragmentograms

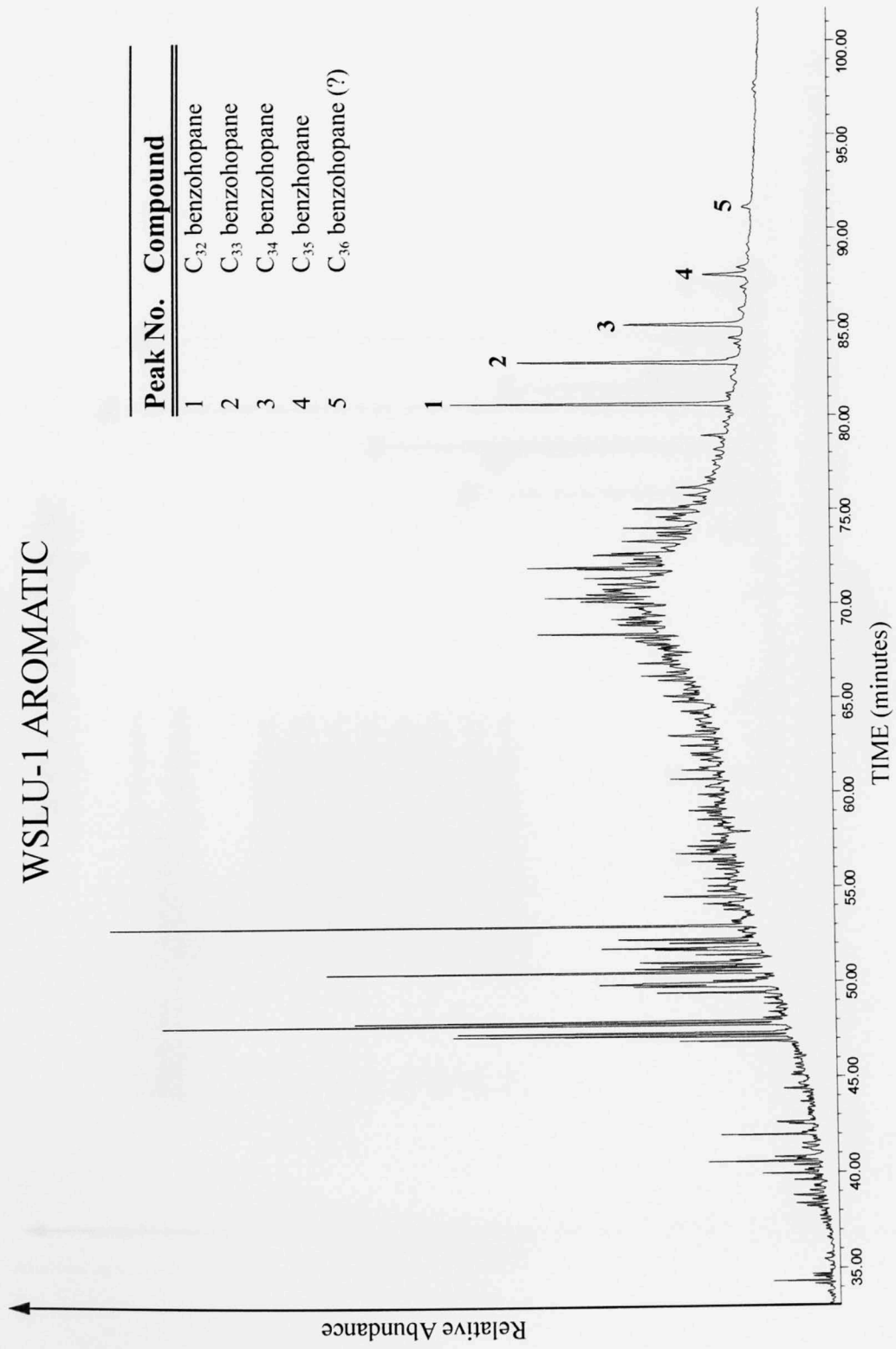

m/z 231

WSLU-8 AROMATIC

Peak No.	Compound
1	TAP
2	TAPH
3a	C26 triaromatic sterane S
3b	C26 triaromatic sterane R
4a	C27 triaromatic sterane S
4b	C27 triaromatic sterane R
5a	C28 triaromatic sterane S
5b	C28 triaromatic sterane R
6a	C29 triaromatic sterane S
6b	C29 triaromatic sterane R

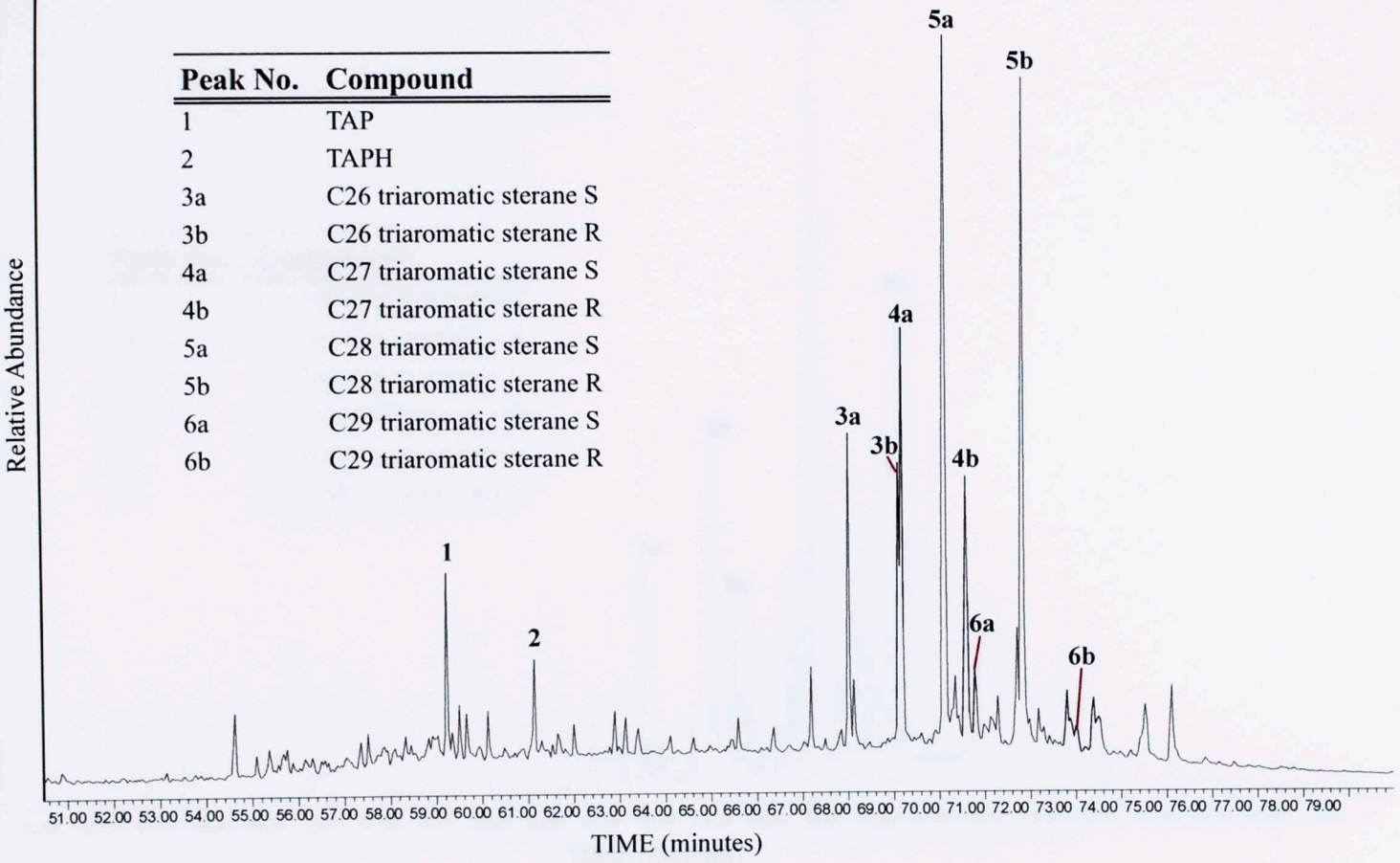

m/z 257

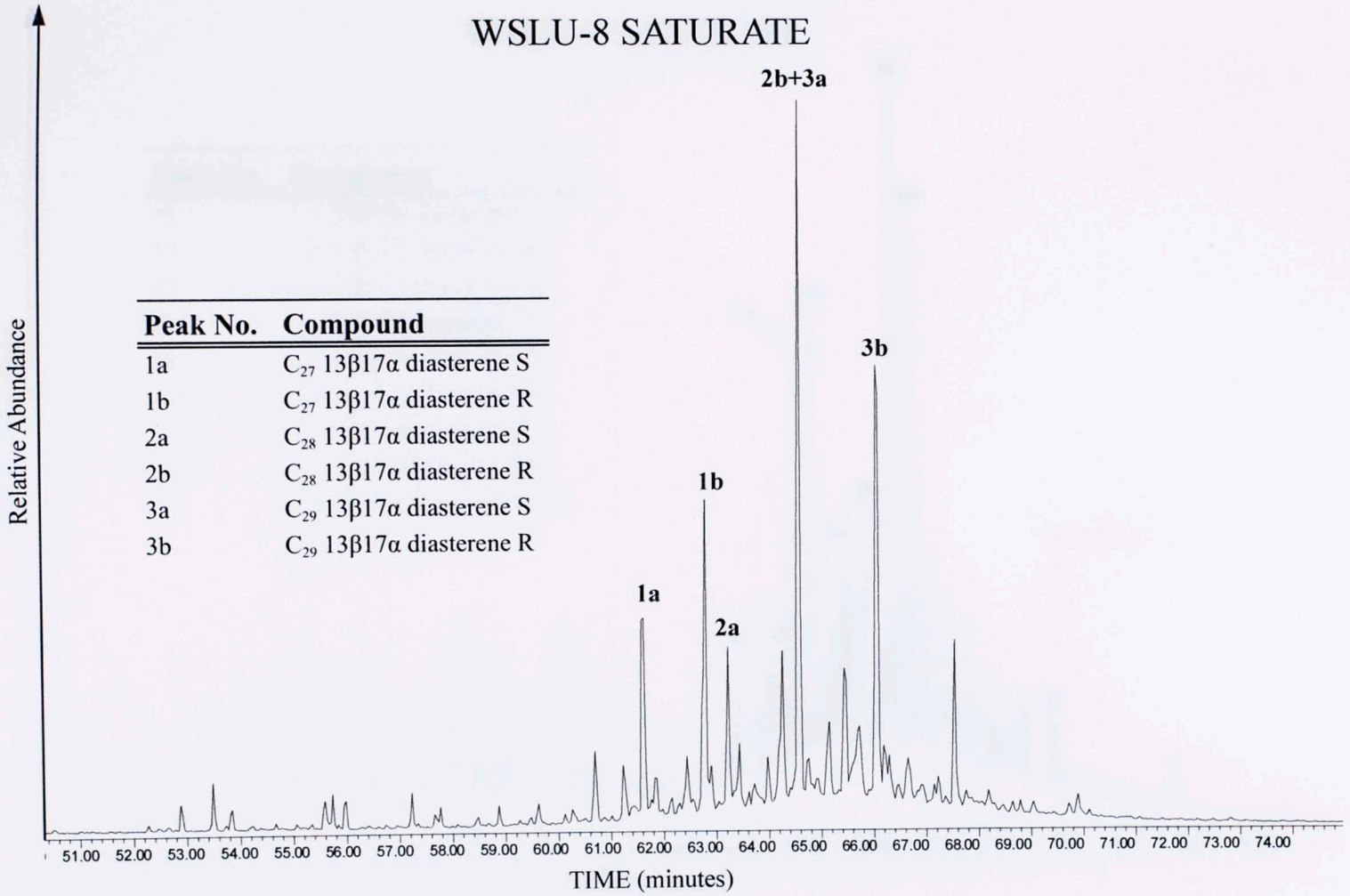

Peak No.	Compound
1a	C_{27} 13β17α diasterene S
1b	C_{27} 13β17α diasterene R
2a	C_{28} 13β17α diasterene S
2b	C_{28} 13β17α diasterene R
3a	C_{29} 13β17α diasterene S
3b	C_{29} 13β17α diasterene R

m/z 259

WSLU-8 SATURATE

Peak No.	Compound
1a	C_{26} 13β17α diasterane S
1b	C_{26} 13β17α diasterane R
2a	C_{27} 13β17α diasterane S
2b	C_{27} 13β17α diasterane R
3a	C_{28} 13β17α diasterane S
3b	C_{28} 13β17α diasterane R
4a	C_{29} 13β17α diasterane S
4b	C_{29} 13β17α diasterane R
5	C_{30} tetracyclic polyprenoid

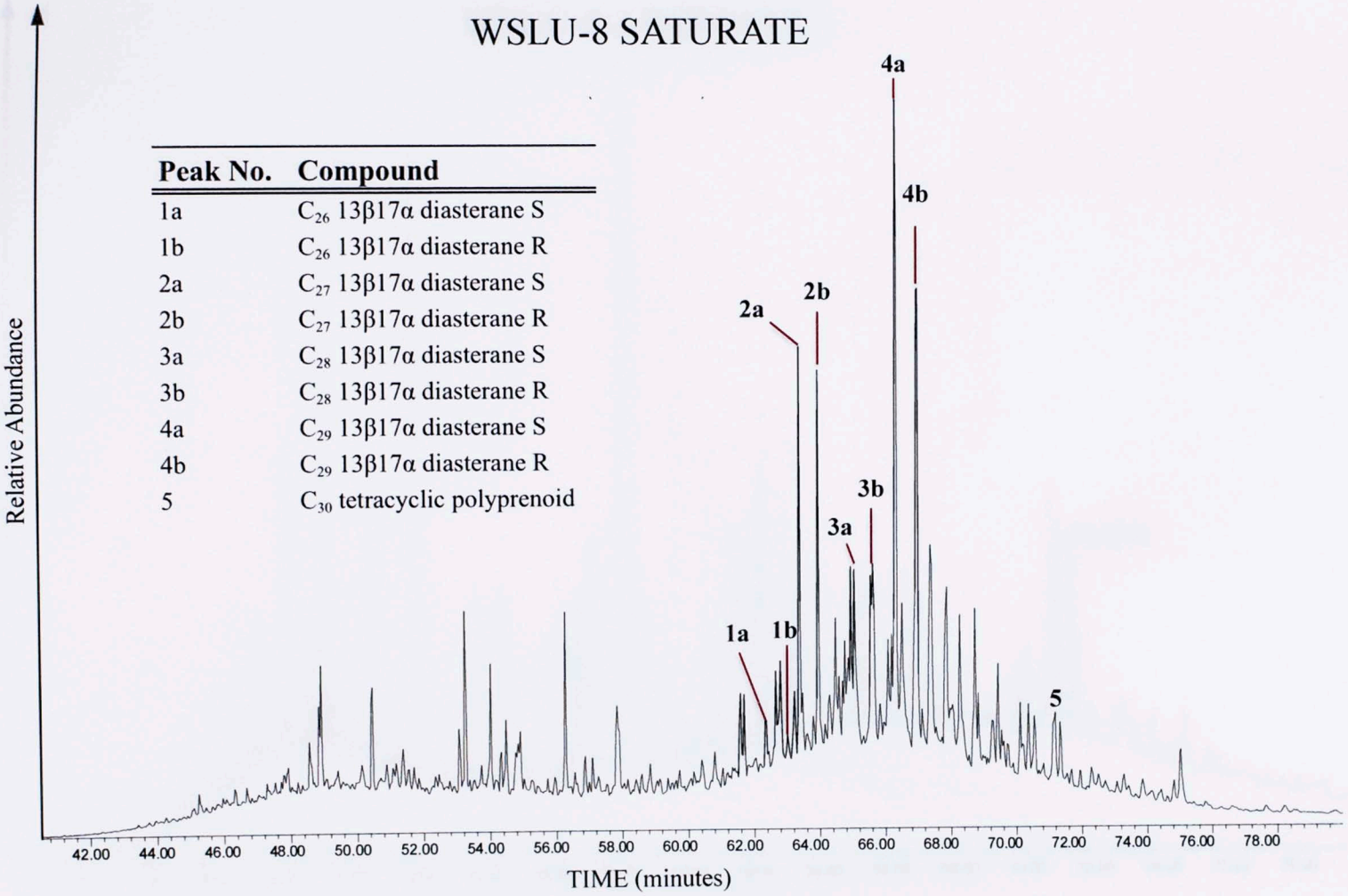

m/z 241

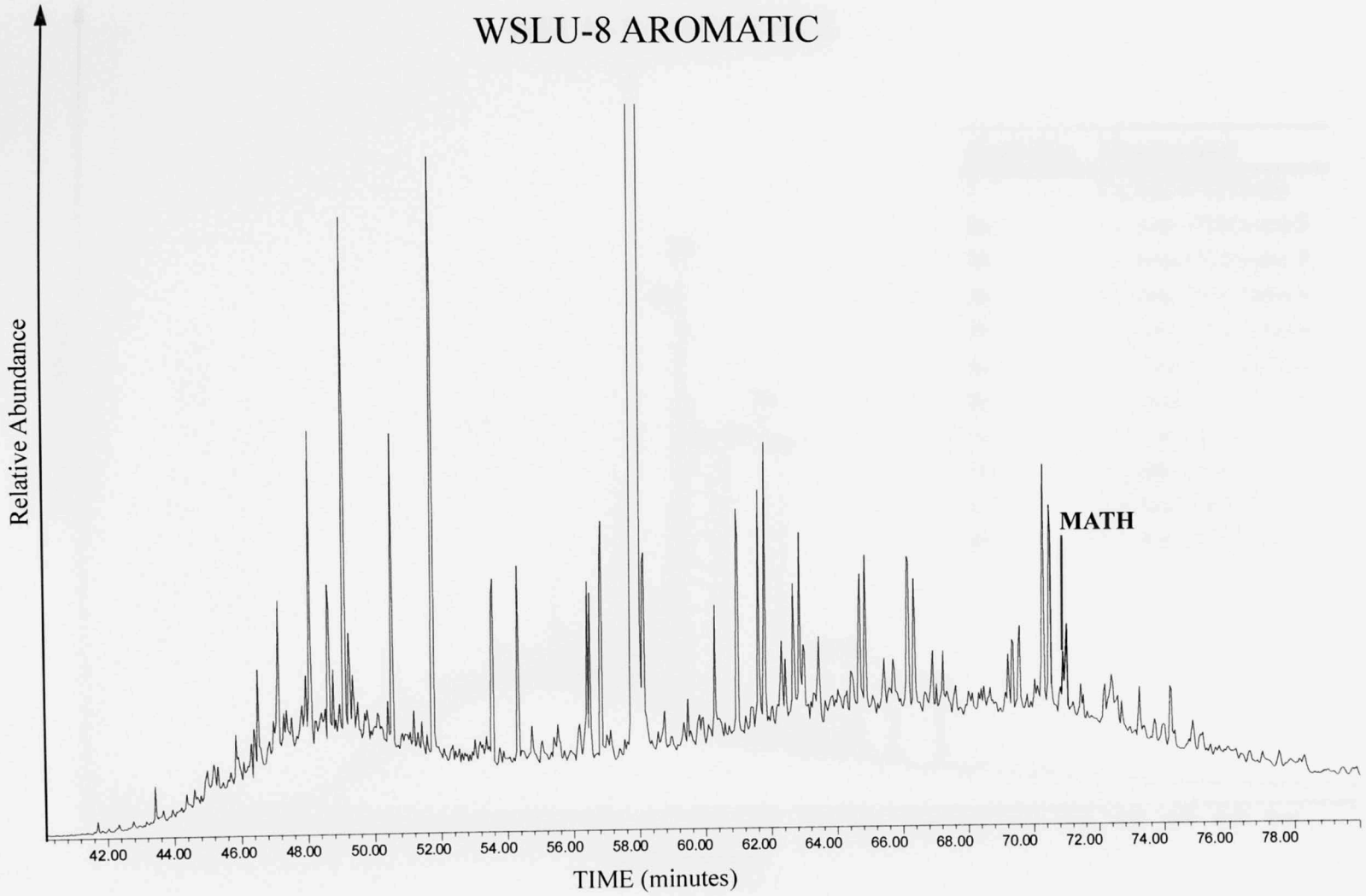
WSLU-8 AROMATIC
Relative Abundance
MATH
42.00
44.00
46.00
48.00
50.00
52.00
54.00
56.00
58.00
60.00
62.00
64.00
66.00
68.00
70.00
72.00
74.00
76.00
78.00
TIME (minutes)

m/z 367

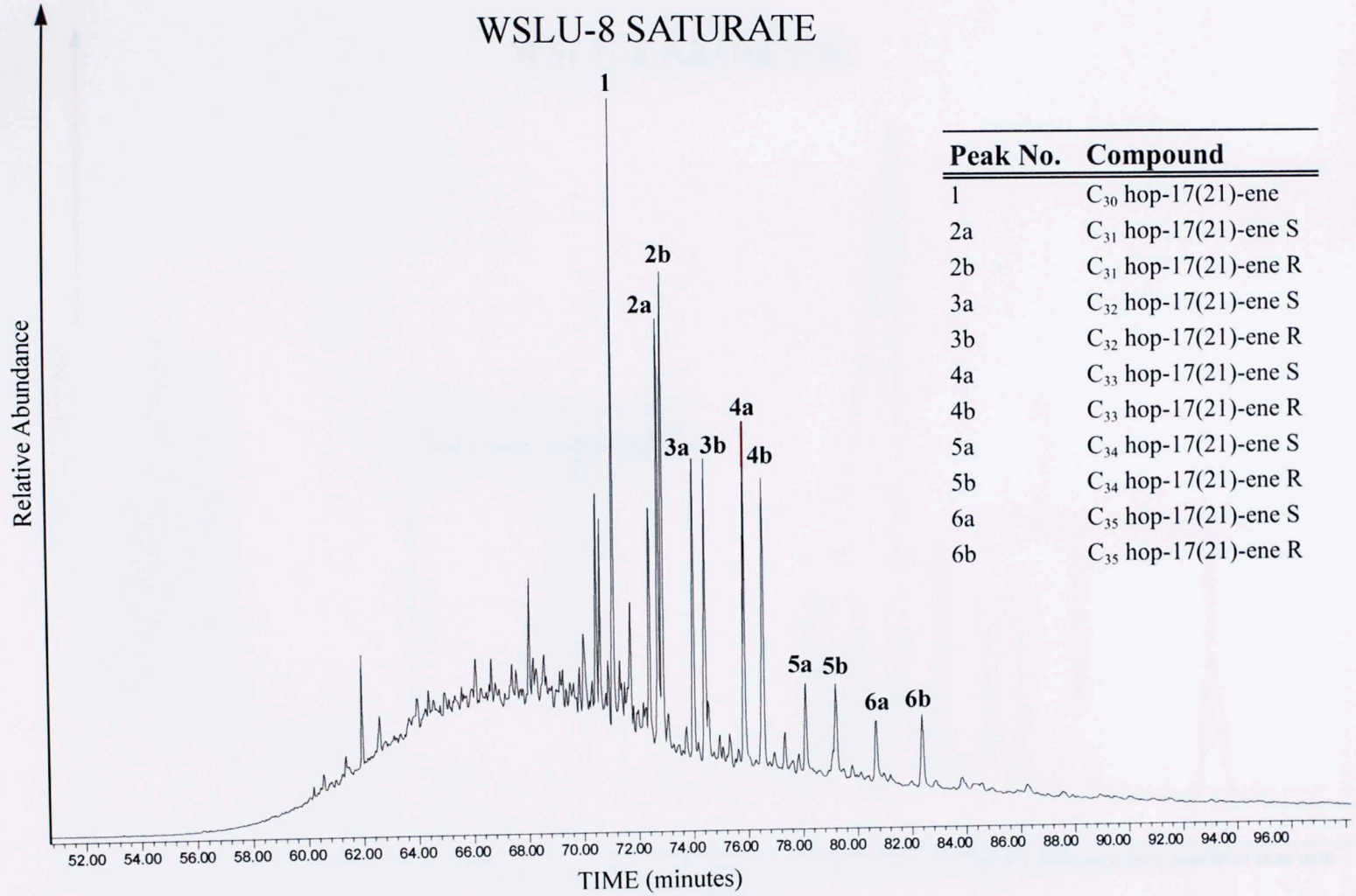

Peak No.	Compound
1	C_{30} hop-17(21)-ene
2a	C_{31} hop-17(21)-ene S
2b	C_{31} hop-17(21)-ene R
3a	C_{32} hop-17(21)-ene S
3b	C_{32} hop-17(21)-ene R
4a	C_{33} hop-17(21)-ene S
4b	C_{33} hop-17(21)-ene R
5a	C_{34} hop-17(21)-ene S
5b	C_{34} hop-17(21)-ene R
6a	C_{35} hop-17(21)-ene S
6b	C_{35} hop-17(21)-ene R

m/z 237

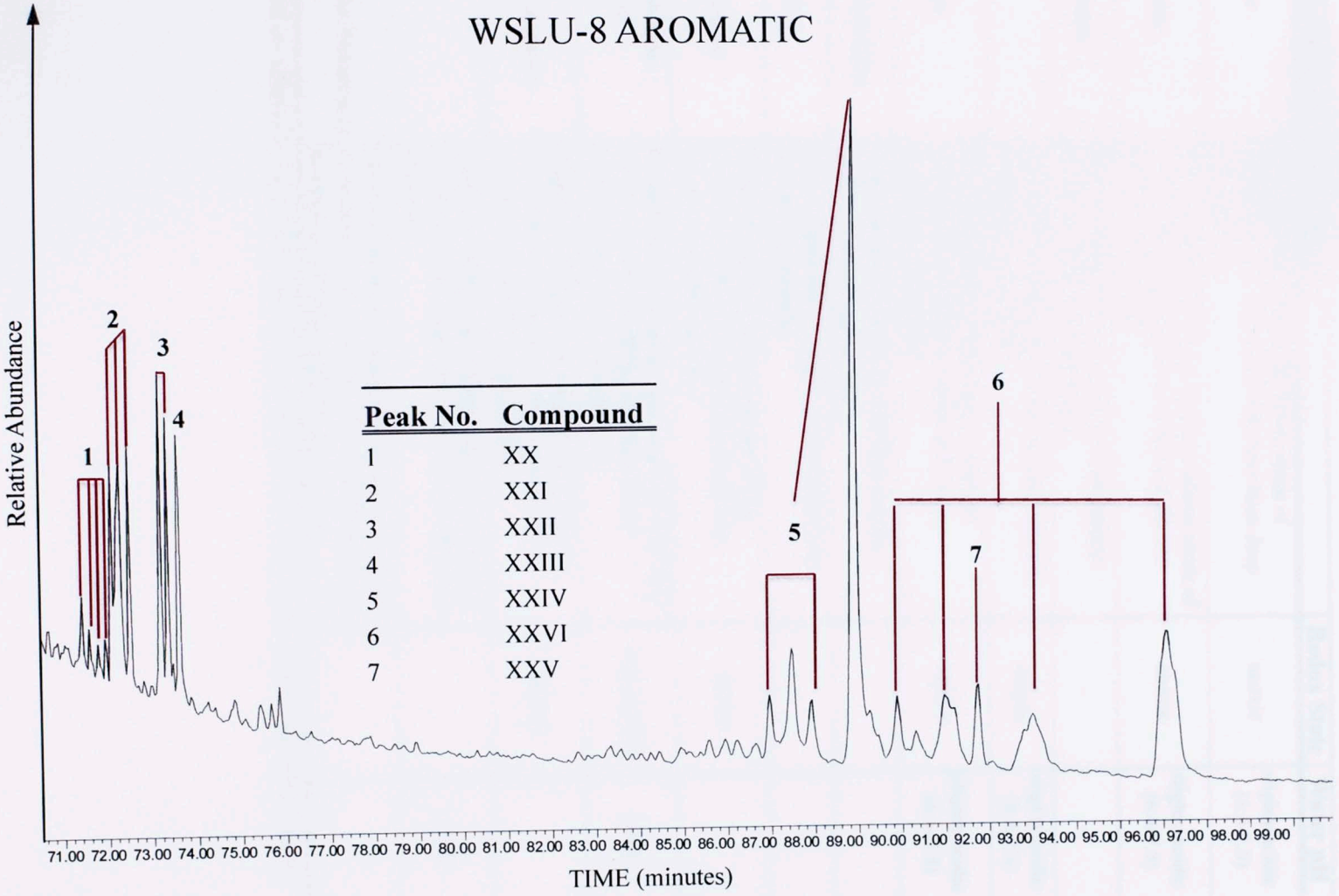
WSLU-8 AROMATIC
Relative Abundance
1
2
3
4
5
6
7
Peak No. Compound
1 XX
2 XXI
3 XXII
4 XXIII
5 XXIV
6 XXVI
7 XXV
71.00 72.00 73.00 74.00 75.00 76.00 77.00 78.00 79.00 80.00 81.00 82.00 83.00 84.00 85.00 86.00 87.00 88.00 89.00 90.00 91.00 92.00 93.00 94.00 95.00 96.00 97.00 98.00 99.00
TIME (minutes)

Appendix IV: BIOMARKER REFERENCE TABLE

Biogeochemical Fossil	Significance	Redox State	Water pH
Isorenieratane	PZE; biosynthesized by the brown strain of *Chlorobiaceae;* chemocline may have been deep (<80-100m)*	anoxic	slighty acidic (6.4-7.8)
Paloerenieratane	PZE; biosynthesized by an extant or extinct strain of *Chlorobiaceae*; proposed to occupy a shallower depth than the bGSB	anoxic	slighty acidic (6.4-7.8)
Renierapurpurane	PZE?; multiple origins including marine sponge symbionts, PSB or cyanobacteria	-	-
Okenane	PZE; sole biomarker for *Chromatiaceae*; shallow chemocline (<12-25m)*	anoxic	slighty acidic (6.4-7.8)
Chlorobactane	PZE; biosynthesized by the green strain of *Chlrobiaceae*, shallow to moderately deep chemocline (<20-50m)*	anoxic	slighty acidic (6.4-7.8)
24-*n*-propylcholestane	Strong marine indicator, derived from marine pelagophyte/chrysophyte algae	-	-
Gammacerane	Water stratification, in high concentrations may indicate hypersalinity	-	-
28,30-Dinorhopane	Primarily used as a redox indicator, strong correlation with PZE, supporting origin from chemoautotrophic bacteria	anoxic	-
Neohop-13(18)-enes Diaster(e/a)nes Diahopane	Dependent upon lithology and water pH, with clay-rich source rocks deposited in acidic waters facilitating backbone rearrangement	oxic-suboxic	acidic
C_{32}-C_{35} Benzohopanes	High concentrations associated with sulfur-rich carbonates and evaporites; ubiquitous in marine source rocks and oils in low amounts	anoxic	-
MATH	Marker for early gymnosperms and coniferophytes, formed in acidic conditions from fernane/arbornane precursors	-	acidic
C_{30} Tetracyclic Polyprenoid	High concentrations suggest deposition in freshwater or brackish water conditions; low concentrations can be detected in marine and coal source rocks	-	-

* PSB/GSB are affected by light , H_2S concentration, pH, and wind; may impact chemocline interpretations